Investigation of Highly Lewis Acidic Gold(III) Compounds Containing Fluorido and Pentafluoroorthotellurato Ligands

Inaugural-Dissertation
to obtain the academic degree
Doctor rerum naturalium (Dr. rer. nat.)

submitted to the Department of Biology, Chemistry, Pharmacy
of Freie Universität Berlin

by

Marlon Winter

2023

The work for this thesis has been conducted between April 2018 and August 2023 under the supervision of Prof. Dr. Sebastian Hasenstab-Riedel at the Institute of Chemistry and Biochemistry of Freie Universität Berlin.

1st reviewer: Prof. Dr. Sebastian Hasenstab-Riedel

2nd reviewer: Prof. Dr. Thomas Braun

Date of defense: 08.12.2023

Acknowledgment

First of all, I want to thank Prof. Dr. Sebastian Hasenstab-Riedel for giving me the opportunity to conduct my thesis in his group after I have already been in his group for the Bachelor's thesis and Master's thesis, and for the support. I am grateful for the possibility to have worked on this interesting topic.

I want to thank Prof. Dr. Thomas Braun for kindly accepting the role as the second reviewer.

For fruitful discussions and guidance on laboratory work, data analysis and scientific writing, I want to thank Dr. Simon Steinhauer, Dr. habil. Helmut Beckers, Dr. Julia Bader and Dr. Günther Thiele. I want to thank the whole *AC*, including the secretariats, the workshops, and the *Materialverwaltung*, as well as the BioSupraMol and ZEDAT for their work and support. The Dahlem Research School is acknowledged for a scholarship. A big thank you to Dr. Alberto Pérez-Bitrián, Dr. Julia Bader and Gene Senges for carefully proofreading this thesis in a very short amount of time, and to Jennifer Anders for help with the formalities. Prof. em. Dr. Antonio Togni is thanked for an inspiring talk and a stimulating discussion.

I am thankful to Dr. Mathias A. Ellwanger for introducing me into the fascinating chemistry of gold fluorides, for the numerous ideas and for being so passionate (*für das Thema brennend*) in the countless discussions we had. My deep gratitude is expressed to Dr. Alberto Pérez-Bitrián who willingly shared his expertise on organometallic gold chemistry with me in the extensive scientific discussions we had and for the numerous times he proofread manuscripts/slides/posters.

I am grateful to all the students that chose me as their supervisor during their Bachelor's theses or research internships, namely Lucia Anghileri, Rickesh Rajamenon, Niklas Limberg, Natallia Peshkur, and Samantha Frank. Thank you for your interest and hard work. I hope you learned from me as much as I learned from the experience of supervising you!

A special thanks to the whole AG Riedel for the nice atmosphere and the joyful coffee breaks and barbecues. Also to all the people whom I shared the lab with in U408 – Thomas Drews, Dr. Jan H. Nissen, Holger Pernice, Paul Golz, and Dr. Alberto-Pérez-Bitrián – for the great time we had and for not complaining about the music I played, which at times turned into karaoke.

I want to emphasize a few people that have become not only colleagues but dear friends. A big shout-out to Gene, Benny, Paul, Vossi, Helen, Luise, Niklas, Jonas, Tyler, Maite, Lili, Gesa, Alberto, Jan, and Karsten for the numerous evenings spent discussing chemistry, psychology, or politics, the squash, climbing, tennis, and bouldering and many other free time activities and even holidays spent together. You have made the last five and a half years less stress- and more joyful!

I really want to thank a few people that have been a part of my eleven-year journey at the Freie Universität. Thank you to Steffi, Jenni, Gene, Siri, HeRo, Lawrence, Simon, Anna, and Eva for the many evenings we spent studying and working, but also for the continuous support and cheerful evenings. A true oasis was the *OC-Café* with its familiar atmosphere and all the evenings playing *Doppelkopf* or *Skat* or just fooling around, especially in the time with Steffi and her natural authority at the helm!

My deep gratitude belongs to some truly beloved friends that have been supporting me even longer than this – at times seemingly endless – journey. Thank you to Jonas, Karo, Hanin, Ruffy, Asil, Holger, Jo, Jew, Panda, Janis, and all *Die üblichen Verdächtigen* for always being there for me.

My deepest thank you goes to my parents as well as my whole family, who have always supported me, believed in me and loved me for who I am; and to my beloved partner Alina, for loving and comforting me in the last year, making me feel at home and becoming my new family. I love you from the bottom of my heart!

Declaration of Independence

Herewith I certify that I have prepared and written my thesis independently and that I have not used any sources and aids other than those indicated by me. All intellectual property of other authors used as references has been marked accordingly. I also certify that I have not applied for an examination procedure at any other institution and that this dissertation has not been submitted in this or any other form to another faculty.

Berlin, 19.12.2023

Marlon Winter_____

List of Abbreviations

Ad	adamantyl
*a*HF	anhydrous hydrogen fluoride
BDE	bond dissociation energy
BP86	Becke 88, Perdew 86
Bu	butyl
CAAC	cyclic (alkyl)(amino)carbene
Cy	cyclohexyl
C^N^C	tridentate pincer ligand with C, N and C donor atoms
DCM	dichloromethane
def-SV(P)	split valence polarization (without hydrogens)
DME	1,2-dimethoxyethane
EDG	electron donating group
EWG	electron withdrawing group
Et	ethyl
FIA	fluoride ion affinity
G	Gibbs energy
H	enthalpy
h	Planck constant
HSAB	hard and soft acids and bases
H_0	Hammett acidity function
IAd	1,3-di(1-adamantyl)imidazol-2-ylidene
IMes	1,3-bis(2,4,6-trimethylphenyl)imidazol-2-ylidene
IPr	1,3-bis(2,6-diisopropylphenyl)imidazol-2-ylidene
IPr^{Cl}	1,3-bis(2,6-diisopropylphenyl)-4,5-dichloroimidazol-2-ylidene
IUPAC	International Union of Pure and Applied Chemistry
M	metal
Me	methyl
MIC	mesoionic carbene
Ng	noble gas
NHC	*N*-heterocyclic carbene
N^C	bidentate pincer ligand with N and C donor atoms
N^C^C	tridentate pincer ligand with N, C, and C donor atoms

N^P	bidentate pincer ligand with N and P donor atoms
v	frequency
PFA	perfluoroalkoxy alkanes
Ph	phenyl
pH_{abs}	absolute pH value
pip	piperidine
Pr	propyl
PTFE	polytetrafluoroethylene
PVPHF	poly[4-vinylpyridinium poly(hydrogen fluoride)]
py	pyridine
RI	resolution of identity
rt	room temperature
SARS-CoV-2	severe acute respiratory syndrome coronaviruses
Selectfluor®	1-chloromethyl-4-fluoro-1,4-diazoniabicyclo[2.2.2]octane bis(tetrafluoroborate)
SIPr	1,3-bis(2,6-diisopropylphenyl)-4,5-dihydroimidazol-2-ylidene
SIMes	1,3-bis(2,4,6-trimethylphenyl)-4,5-dihydroimidazol-2-ylidene
Teflate	pentafluoroorthotellurate, $OTeF_5$
THF	tetrahydrofuran
TM	transition metal
WCA	weakly coordinating anion

Table of Contents

Abstract

In this thesis, highly Lewis acidic gold(III) compounds were studied. In the first part, the reactivity of [AuF_3(SIMes)], the first trifluorido organo gold complex, was thoroughly investigated. Based on initial studies of a selective substitution of the *trans*-fluorido ligand by Cl or $OTeF_5$ groups, the trifluoromethyl group, alkynyls, cyanide, and azide were successfully introduced by using the respective trimethylsilyl compounds. Additionally, for the introduction of a variety of perfluorinated alkoxides a novel synthetic route based on the reaction of [AuF_3(SIMes)] with the corresponding perfluorinated ketones was developed. In most cases, a selective substitution to yield a product of the type *trans*-[AuF_2X(SIMes)] was observed. However, for the trifluoromethyl group, the whole series of [$Au(CF_3)_xF_{3-x}$(SIMes)] (x = 1–3) complexes was obtained by variation of the solvent and the stoichiometry of the reaction. In the case of cyanide and azide, a selective substitution of one or all fluorides was achieved, depending on the amount of trimethylsilyl reagent used. For all obtained complexes, a correlation between their calculated SIMes affinity and the chemical shift of the carbene carbon atom in the ^{13}C NMR spectra was found, leading to an order of the introduced ligands by their *trans*-influence and a tunable Lewis acidity of the gold center.

In the second part of this thesis, an improved synthetic route for the only known pentafluoroorthotellurate (teflate) of gold, $[Au(OTeF_5)_3]_2$, was developed. It is obtained quantitatively by the reaction of commercially available $AuCl_3$ with neat $ClOTeF_5$ at room temperature. Based on experimental and computational methods, the dimeric $Au(OTeF_5)_3$ was shown to exhibit a strikingly increased Lewis acidity compared to its fluoride analogue AuF_3. Hence, it was classified as a Lewis superacid in the first extensive Lewis acidity study of a transition metal teflate complex. Moreover, the first teflato gold complexes containing the monomeric $Au(OTeF_5)_3$ unit were obtained in the form of the acetonitrile and triphenylphosphane oxide adducts. The hitherto unknown $[Au(OTeF_5)_4]^-$ anion was successfully prepared in a quantitative yield with alkali metal or *N*-alkylammonium cations using the corresponding $[AuCl_4]^-$ salts and $ClOTeF_5$.

Kurzzusammenfassung

In dieser Arbeit wurden außergewöhnlich stark Lewis-azide Gold(III)-Verbindungen untersucht. Im ersten Teil wurde die Reaktivität von [AuF_3(SIMes)], dem ersten Trifluoridoorganogold-Komplex, eingehend erforscht. Basierend auf anfänglichen Studien einer selektiven Substitution des *trans*-Fluorido-Liganden durch Cl oder $OTeF_5$-Gruppen wurden die Trifluormethyl-Gruppe, Alkinyle, Cyanid und Azid unter Verwendung der jeweiligen Trimethylsilyl-Verbindungen erfolgreich eingeführt. Zusätzlich wurde für die Einführung von perfluorierten Alkoxiden eine neue Syntheseroute basierend auf der Reaktion von [AuF_3(SIMes)] mit den entsprechenden perfluorierten Ketonen entwickelt. In den meisten Fällen wurde eine selektive Substitution unter Erhalt eines Produkts des Typs *trans*-[AuF_2X(SIMes)] beobachtet. Jedoch wurde für die Trifluormethyl-Gruppe die komplette Serie von [$Au(CF_3)_xF_{3-x}$(SIMes)] (x = 1–3) Komplexen durch die Veränderung des Lösungsmittels und der Stöchiometrie der Reaktion erhalten. Im Fall des Cyanids und Azids wurde eine selektive Substitution von einem oder allen Fluoriden erhalten, abhängig von der verwendeten Menge an Trimethylsilyl-Reagenz. Für alle erhaltenen Komplexe wurde eine Korrelation zwischen der berechneten SIMes-Affinität und der chemischen Verschiebung des Carben-Kohlenstoffatoms in den ^{13}C-NMR-Spektren gefunden, welche zu einer Einordnung der eingeführten Liganden in Bezug auf ihren *trans*-Einfluss und einer einstellbaren Lewis-Azidität des Goldzentrums führte.

Im zweiten Teil dieser Arbeit wurde eine verbesserte Syntheseroute für das einzig bekannte Gold-Pentafluoroorthotellurat (Teflat), [$Au(OTeF_5)_3]_2$, entwickelt. Es wurde quantitativ durch die Reaktion von handelsüblichem $AuCl_3$ mit reinem $ClOTeF_5$ bei Raumtemperatur erhalten. Basierend auf experimentellen und rechnerischen Methoden wurde gezeigt, dass das dimere $Au(OTeF_5)_3$ eine auffallend erhöhte Lewis-Azidität im Vergleich zu seinem fluorierten Analogon AuF_3 aufweist. Dementsprechend wurde es als Lewis-Supersäure eingestuft in der ersten ausgiebigen Studie zur Lewis-Azidität eines Übergangsmetallteflat-Komplexes. Darüber hinaus wurden die ersten Goldteflat-Komplexe, welche die monomere $Au(OTeF_5)_3$-Einheit enthalten, in Form von Acetonitril- und Triphenylphosphanoxid-Addukten erhalten. Das bisher unbekannte $[Au(OTeF_5)_4]^-$-Anion wurde in quantitativer Ausbeute mit Alkalimetall- und *N*-Alkylammonium-

Kationen unter Verwendung der entsprechenden $[AuCl_4]^-$-Salze und $ClOTeF_5$ erfolgreich dargestellt.

“To believe in God, all you need is faith.
To believe in science, you need to see the truth. You need to speak the truth.”

- Alan Shore

1 Introduction

1.1 Gold

Gold is usually found in its elemental form in nature and possesses unique properties. Compared to other metals, it has a high density (19.32 $g \cdot cm^{-3}$), low melting point (1064.4 °C) and the highest ductility.[1] Due to these properties, gold was the first metal to be extracted by mankind with the invention of gold metallurgy over 6000 years ago.[2] Gold is known to be the most noble of all metals, as it possesses the highest electronegativity (2.4 on the Pauling scale),[3] the highest redox potential (1.69 V),[1] the highest electron affinity (−2.30863(3) eV) and, after mercury and zinc, the third highest ionization energy (9.2255 eV).[4] This robustness, combined with its yellow appearance, led to the use of gold in jewelry, currency and clothing.[1]

Most of the aforementioned properties of gold are due to relativistic effects, which have been extensively investigated.[5,6–10] In a nonrelativistic approximation, the average radial velocity of the 1s electrons equals the atomic number. Gold has the atomic number 79 and the velocity of its 1s electrons is roughly more than half the speed of light, which results in an increase in their mass according to the special theory of relativity. This leads to a contraction of the 1s orbital, as the radius of an orbital is inversely proportional to its mass. This effect applies to all orbitals that have a significant radial probability in proximity to the nucleus, i.e. all s orbitals and, to a smaller extent, all p orbitals. The smaller radius leads to a stronger electrostatic attraction between the respective orbitals and the nucleus. Hence, this so-called ‘direct relativistic effect’ results in an energetic lowering of the s and p orbitals. Due to this strong shielding, the more diffuse d and f orbitals experience an ‘indirect relativistic effect’, i.e. an energetic destabilization. It was shown that the contraction of the 6s orbital reaches a local maximum for gold due to its filled 5d shell and the lanthanide contraction[6] caused by the filled 4f shell.

Elemental gold has an electron configuration of $[Xe]4f^{14}5d^{10}6s^{1}$. Hence, the relative energetic stabilization of the 6s orbital (direct relativistic effect) explains the high ionization energy of gold and the relative instability of Au(I) complexes compared to those of Ag(I). The energetic destabilization of the 5d orbitals (indirect relativistic effect) results in surprisingly stable Au(III) complexes in contrast to those of Ag(III),

where AgF_3 is one of the strongest oxidizing reagents known.[11] The comparably smaller energy difference between the 5d and 6s orbitals leads to the absorption of blue light and gold appears in the complementary color yellow. For most metals, this energy difference lies in the ultraviolet region.[1]

Relativistic effects are also one reason for the phenomenon of 'aurophilicity', i.e. the tendency of gold to form Au–Au bonds, especially in Au(I) complexes. It was shown to be a closed-shell interaction with the Au–Au interaction energy being in a similar range to hydrogen bonding.[12,13] Recently, also examples of aurophilic interactions in Au(III) complexes were observed and investigated.[13,14]

Due to its high ionization energy, gold was historically considered chemically inert. About 200 years ago, it was discovered that gold can be dissolved in aqua regia giving $H[AuCl_4]$.[15] Its sodium salt has been used as a drug against syphilis in the 19th century.[16] In aqueous cyanide solutions, gold is oxidized to $[Au(CN)_2]^-$, which was applied in gold coating baths.[17] It was not until the end of the last century that the potential of gold chemistry started to be explored, leading to the extensive use of organo gold compounds in medicine, nanotechnology and catalysis.[18,19,20] Especially in catalysis, gold complexes have gained increasing attention due to their distinct properties, which are also connected to relativistic effects.[21]

Apart from the oxidation state 0, +I and +III are the most stable oxidation states of gold in its compounds. Au^+ has an electron configuration of $[Xe]4f^{14}5d^{10}$, and because of the filled d orbitals, it prefers a linear coordination environment. Au^{3+} possesses an electron configuration of $[Xe]4f^{14}5d^8$, which results in an almost exclusive preference for a square-planar coordination geometry.[1] Due to its high electronegativity and electron affinity, gold can even reach the oxidation state of −I, e.g. in CsAu.[22] In a few cases, Au(II) compounds can be stabilized, mostly in the form of dimers, which contain Au–Au bonds.[19] However, they are important intermediates in a variety of reactions and a few monomeric Au(II) compounds are known.[23] A unique example is the $[AuXe_4]^{2+}$ dication, which was the first isolated compound with metal-xenon bonds.[24] The only known gold compound in oxidation state +IV is the $[AuO]^{2+}$ dication, which was detected by mass spectrometry.[25] The highest oxidation state known for gold is +V, which is also only accessible due to the relative destabilization of the 5d orbitals.[10] The two Au(V) compounds known thus far have been stabilized by fluorides in the form of AuF_5[26–28] and the more stable $[AuF_6]^-$ anion.[26–36] They will be described in more detail in Section 1.3.

1.2 Fluorine and Fluorinated Ligands

Fluorine is an element with an unparalleled set of properties, but for markedly different reasons than gold. Fluorine is the lightest of the halogens, has an electron configuration of $1s^2 2s^2 2p^5$ and only needs one electron to reach noble gas configuration. This particular place in the periodic table explains why it is the element with the highest electronegativity (4.0 on the Pauling scale),[3] the second highest electron affinity (−3.4011895(25) eV) after chlorine, and the third highest ionization energy (17.4228 eV) after helium and neon.[4] Helium and neon are also the only elements for which no compounds with fluorine are known. Due to these properties, elemental fluorine, a diatomic gas at ambient conditions, is considered the most reactive of all elements.[1]

The earth crust contains 0.027 w% fluorine, making it the 13th most abundant element in nature.[37] However, very few natural products containing fluorine atoms are known[38] and metabolic processes that contain fluorinated molecules are even less common.[39] Due to the aforementioned oxidative properties, it is almost exclusively found in its reduced form in minerals like fluorspar (CaF_2) or fluorapatite ($Ca_5(PO_4)_3F$).[1] An exception is the so-called ‘stinkspar’, which is a variety of CaF_2 that was shown to incorporate small amounts of elemental fluorine.[40] The first synthesis of elemental fluorine was performed by *Moissan* in 1886 by the electrolysis of a solution of KF in anhydrous HF (*a*HF).[41] The industrial preparation of elemental fluorine is still based on this approach, but a KF·2HF melt is used for the electrolysis.[37] A chemical synthesis of fluorine is difficult due to its high redox potential (3.05 eV)[1] and was achieved by *Christe* only in 1986. The route involved the reaction of $K_2[MnF_6]$ with SbF_5 to yield MnF_4, which was proposed to thermally decompose to MnF_3 under liberation of fluorine.[42] However, it was very recently shown that an Mn(II) species is formed and an excess of SbF_5 is crucial for the reduction to occur.[43] When working with elemental fluorine, special safety precautions have to be taken, as it reacts violently with water and organic substances. Even though dry fluorine does not etch glassware, opposed to HF, reactions are usually conducted in containers made of stainless steel or perfluorinated polymers like polytetrafluoroethylene (PTFE) or polyfluoroalkoxy alkanes (PFA).[37]

The strong reactivity of elemental fluorine can also be explained by consideration of the bond dissociation energies (BDE). With a BDE of 158.670 ± 0.096 kJ·mol^{-1}, the F–F bond is one of the weakest covalent bonds, while many other E–F (E = element) bonds are remarkably strong (see also Section 1.4 and Table 1).[4] An energy decomposition analysis showed that elemental fluorine experiences a strong Pauli repulsion, resulting in an unexpectedly long F–F bond and a weaker contribution of the electrostatic energy term.[44] *Shaik* and coworkers showed that the bond in elemental fluorine is not a classical covalent bond but an example of a so-called 'charge-shift bond' with a characteristic resonance energy stabilization by a covalent-ionic mixing.[45]

Due to its strong electron-withdrawing nature, the fluoride anion is able to stabilize many elements in their highest oxidation states, e.g. $[NF_4]^+$, OF_2, $[ClF_6]^+$, NiF_4, KrF_2, AgF_3, PtF_6, and AuF_5.[46] This renders it useful in organometallic and coordination chemistry as a ligand that yields a variety of transition metal (TM) complexes in medium to high oxidation states, often stabilized by neutral donor ligands.[47–49] A detailed description of fluorido organo gold complexes can be found in Section 1.4.

A more sterically demanding analogue of the fluoride anion is the pentafluoroorthotellurate (teflate, $OTeF_5$) group.[50] It was found to have a similar electronegativity as fluorine,[51–55] and hence, a variety of reactive compounds and elements in high oxidation states have been stabilized with the $OTeF_5$ group, e.g. $As(OTeF_5)_5$,[56] $U(OTeF_5)_6$,[57] $Xe(OTeF_5)_x$ (x = 2,[58] 4,[59] 6[60]), and $Kr(OTeF_5)_2$.[61] In addition, the teflate group is less prone to be a bridging ligand which often leads to monomeric compounds in comparison to the corresponding dimeric or polymeric fluoride species.[53] However, in cases like $[Au(OTeF_5)_3]_2$[62] and $[NMe_4]_2[Hg_2(OTeF_5)_6]$,[63] the teflate ligand can also bridge two metal centers.

A large variety of main group teflate species is known. They are typically prepared from the corresponding chlorides or fluorides using $HOTeF_5$[64] or $B(OTeF_5)_3$[65] as teflate-transfer reagents.[55] They have been thoroughly investigated and some of them were classified as Lewis superacids, usually exceeding the acidity of their fluoride analogues (see Section 1.6).[66] The addition of a teflate anion to such a species often yields weakly coordinating anions (WCA).[53–55] Examples are $[B(OTeF_5)_4]^-$[67] and $[Sb(OTeF_5)_6]^-$,[68] where the negative charge is delocalized over 20 or 30 fluorine atoms, respectively. The more bulky $[M(OTeF_5)_6]^-$ (M = As,

Nb, Sb, Bi) anions were found to be stable in the presence of strongly coordinating cations,[54,69] e.g. $[Xe(OTeF_5)]^+$,[70] $[Ag(S_8)_2]^+$,[71] and $[Ag_2(Se_6)(SO_2)_2]^{2+}$.[72] While most of the aforementioned compounds have been prepared in the last century, the recent synthesis of $[Al(OTeF_5)_4]^-$[73] has revitalized teflate chemistry, as it was the first WCA able to stabilize protonated white phosphorus in the condensed phase, forming $[P_4H][Al(OTeF_5)_4]$ as shown by NMR spectroscopy.[74] In contrast, although several transition metal (TM) teflate complexes are known, mainly with early TMs, the properties of this ligand in coordination chemistry have not been thoroughly investigated yet. This means that information on reactivity, magnetic properties or Lewis acidity of transition metal teflate complexes is scarce.[53–55,66] In fact, it was only recently that the teflate ligand has been claimed to be analogous to fluoride in ligand-field terms.[75]

Fluorine also plays a pivotal role in organic chemistry. It has been found that the substitution of a C–H by a C–F bond in an organic molecule drastically changes its properties. Compared to a C–H bond (338.4 ± 1.2 kJ·mol^{-1}), the C–F bond (513.8 ± 10.0 kJ·mol^{-1}) is much stronger[4] and shows an increased, inverted polarity.[76] This leads to a higher biological stability and lower activity of the compounds,[77] a changed lipophilicity, increased acidity and enhanced ability to form hydrogen bonds.[78] Thus, organofluorine compounds are of high importance as pharmaceuticals[77,79] and agrochemicals.[80] Between 2018 and 2022, almost 25 % of all newly approved pharmaceuticals in the United States contained at least one fluorine atom.[81]

The trifluoromethyl group is the simplest representative of a perfluorinated organic moiety and it is another example of the drastic changes that fluorination imparts on an organic molecule. It was shown that CF_3 has a group electronegativity comparable to chlorine[3,82] and is much more stable than a CH_3 group towards a nucleophilic attack due to the electron lone pairs of the fluorine atoms.[83] Hence, it is considered a distinct functional group instead of solely a fluorinated CH_3 group[84] and several reviews have been published about the introduction of CF_3 groups into organic molecules.[83–86] For this purpose, trifluoromethyl transition metal complexes can be used, as especially those of late TMs have shown the ability to lower the activation barriers for C–CF_3 reductive eliminations.[84,87] TM complexes with CF_3 ligands show a higher thermal stability compared to their non-fluorinated analogues. This increased stability is due to negative hyperconjugation[87,88] and

π-backbonding[87,89,90] from the filled d orbitals of middle to late TMs to the σ* orbitals of the trifluoromethyl group, resulting in a stabilization by the resonance structures shown in Scheme 1. These structures also explain the observed stronger M–C (compared to the non-fluorinated analogues) and weaker C–F (respective to organofluorine compounds) bonds in trifluoromethyl TM complexes, as well as their propensity to stabilize difluorocarbenes (see Section 1.5) by elimination of a fluoride anion.[87,89,91,92]

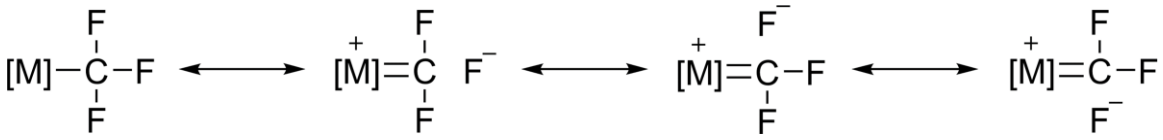

Scheme 1: Schematic illustration of the resonance structures caused by negative hyperconjugation and π-backbonding of a trifluoromethyl transition metal complex [M]–CF_3.[87,89]

In spite of its high group electronegativity, the CF_3 group has been claimed to be a stronger σ donor and to have a stronger *trans*-influence than the CH_3 group.[91,92,93] In addition, the CF_3 ligand has been shown to be a non-innocent ligand, as was controversially debated for the case of the $[Cu(CF_3)_4]^-$ anion.[94] It was shown to cause ligand field inversion and can therefore be described as a Cu^I complex.[95] A similar behavior was observed for the higher coinage metal homologues.[96]

A typical way to introduce the CF_3 group to low-valent transition metals is the oxidative addition by CF_3I.[87,97] In the past, transmetallation reactions of TM halides with group 12 trifluoromethyl complexes like $Cd(CF_3)_2$·DME (DME = 1,2-dimethoxyethane) were performed.[87,97] Due to its toxicity, $Cd(CF_3)_2$·DME was widely replaced by the *Ruppert-Prakash* reagent, Me_3SiCF_3,[87,98] which is commonly used in organic chemistry.[86,99] Me_3SiCF_3 is typically combined with a fluoride source and forms a five-coordinate Si(IV) anion in coordinating solvents,[100] as shown in Scheme 2, from which the CF_3 group is readily transferred. In addition to these nucleophilic CF_3 transfer reagents, also electrophilic trifluoromethylation agents exist, as for example (perfluoroalkyl)chalcogen salts like *Umemoto*'s reagent[101] or the hypervalent iodine(III) compounds described by the group of *Togni*.[102]

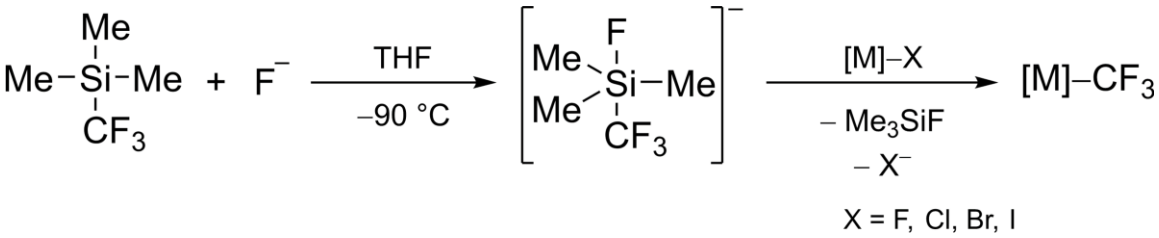

Scheme 2: General reaction scheme for a trifluoromethylation of a transition metal halide [M]–X with the *Ruppert-Prakash* reagent Me_3SiCF_3 in combination with an excess of a fluoride source. Prior to the transfer of the CF_3 group, a five-coordinate Si(IV) anion is formed as an intermediate at low temperatures.[100]

1.3 Binary Gold Fluorides

As shown in the previous sections, compounds containing fluorine or gold have unparalleled features compared to their respective homologues. This is especially true for species that have Au–F bonds, as they often show an exceptional reactivity.[103–105] In this section, the chemistry of binary gold fluorides and their corresponding anions will be summarized, while compounds with ancillary ligands, i.e. fluorido organo gold complexes, are described in Section 1.4.

The simplest representative of a binary gold fluoride, AuF with gold in an oxidation state of +I, was shown to be instable based on lattice energy calculations. In fact, it is neither stable with respect to the decomposition into the elements nor towards disproportionation to elemental Au and AuF_3.[106] One reasoning for its instability is the difference between the very hard base F^- and the soft acid Au^+ according to the concept of hard and soft acids and bases (HSAB) as defined by *Pearson*.[107] However, AuF was proposed to have been detected in the emission spectra of glow-discharge plasmas from gold films that were etched with O_2/CF_4 or O_2/SF_6 mixtures but the authors commented that the observed lines could be also originated from ionic $[AuF]^+$ or $[AuO]^+$.[108] High-level quantum-chemical calculations suggested the existence of AuF in the gas phase and its predicted spectral properties supported the experimental findings.[7–9] In 1994, *Schwarz* and coworkers unambiguously proved its existence by neutralization-reionization mass spectrometry and its minimal lifetime was determined to be 25 µs.[109] In addition, microwave spectroscopy of laser-ablated Au metal with SF_6 or CF_3I as fluorine precursors produced AuF in the gas phase with a lifetime of over 100 µs and an Au–F bond distance of 191.8(1) pm was determined.[110] AuF was also stabilized by noble gases, forming NgAuF (Ng = Ne,[111,112] Ar,[111–113] Kr,[114] Xe[115]), as evidenced by microwave and matrix isolation IR spectroscopy, underlining its high instability as a binary compound.

The corresponding anion $[AuF_2]^-$ was predicted to be the most stable of the $[AuX_2]^-$ anions (X = F, Cl, Br, I), which is in contrast to the relative stability of the diatomic AuX compounds.[9,116] Still, $[AuF_2]^-$ has only been detected in the gas phase by mass spectrometry as a fragmentation product of $[AuF_4]^-$[117] and by tandem mass spectrometry of $[Au(CF_3)F]^-$, being a decomposition product of $[Au(O_2CCF_3)_2]^-$[118] or *trans*-$[Au(CF_3)_2F_2]^-$.[119]

AuF_3, the most stable binary gold fluoride, was first described by *Moissan* as an orange solid arising from the reaction of Au with elemental fluorine at 500–600 °C as early as 1889. After attempts from *Lenher*[120] and *Ruff*,[121] *Sharpe* showed a modified synthetic approach using milder conditions by the reaction of elemental Au with BrF_3 at 50 °C.[122] Under these conditions the adduct $[AuF_3 \cdot BrF_3]$ was formed, which can also be described as the ionic compound $[BrF_2][AuF_4]$.[123] At 180 °C, BrF_3 is liberated to give pure AuF_3 as an orange solid that decomposes into the elements only above 500 °C. AuF_3 can also be prepared by fluorination of $AuCl_3$ at elevated temperatures[124–126] or by an improved version of *Moissan*'s original method[127,128] (see Scheme 3). Due to the rather labile Au–F bond (see Section 1.4), AuF_3 reacts violently with water under the formation of $Au(OH)_3$ and HF and also ignites organic solvents like benzene or alcohols at ambient temperature. Chlorinated solvents such as carbon tetrachloride are subject to halogen exchange with AuF_3.[122] A detailed study of the stability of AuF_3 in a variety of solvents at room temperature showed that it is reduced by acetonitrile and pentafluoropyridine, while SO_2 and SO_2ClF also undergo reactions. Only perfluorinated solvents like perfluorohexane or alkanes such as *n*-pentane are inert towards AuF_3, yet not capable of dissolving it.[117]

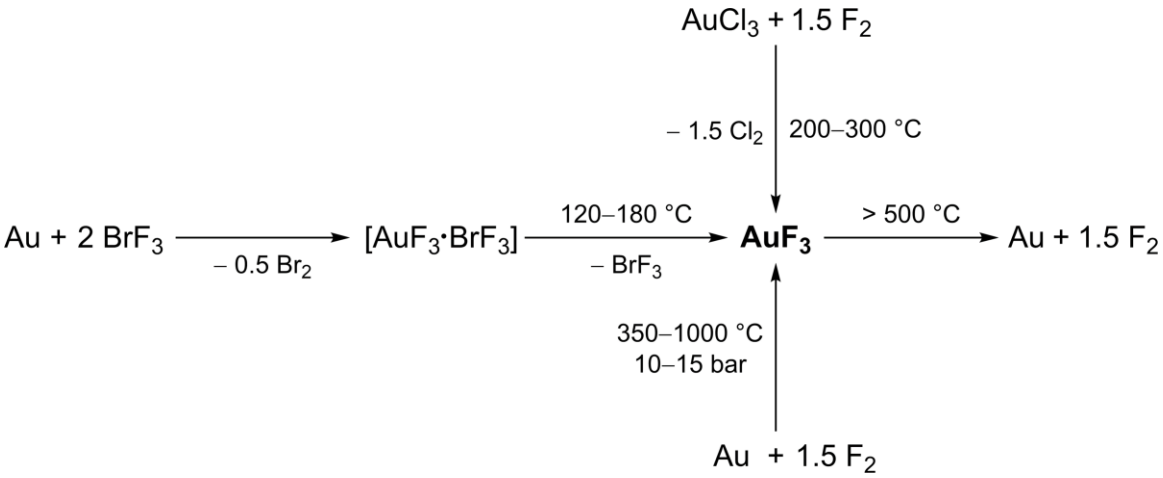

Scheme 3: Overview of the synthetic methods for the preparation of AuF_3 and its decomposition into the elements at temperatures above 500 °C.[122,124–128]

Initial powder X-ray diffraction analysis revealed that AuF_3 is not isostructural to MF_3 (M = Fe, Co, Ni, Ru, Rh, Pd, Ir, Pt) compounds of other middle to late transition metals, which often form mixed valent complexes of the type $M^{II}[M^{IV}F_6]$.[124] In fact,

the crystal structure of AuF_3 consists of square-planar $\{AuF_4\}$ units with two terminal and two bridging fluorine atoms in *cis* position that connect adjacent $\{AuF_4\}$ units leading to a helical chain (see Figure 1, left), similar to AgF_3.[127,129] The Au–F bond lengths are 187.6(3) pm and 199.8(2) pm for the terminal and bridging fluorine atoms, respectively. The gold atoms from one of these chains interact with two terminal fluorine atoms from adjacent chains with an Au–F distance of 276.1(3) pm, which is clearly below the sum of their van der Waals radii (360 pm),[130] resembling an elongated octahedral coordination at the gold centers (see Figure 1, right).[129] This structural motif is in contrast to other known binary gold(III) halides $AuCl_3$[131] and $AuBr_3$,[132] forming Au_2X_6 dimers in the solid state. The corresponding dimer Au_2F_6, along with the according to calculations T-shaped monomeric AuF_3,[10,133] has been detected by gas-phase electron diffraction[134] and matrix isolation IR spectroscopy.[111,112]

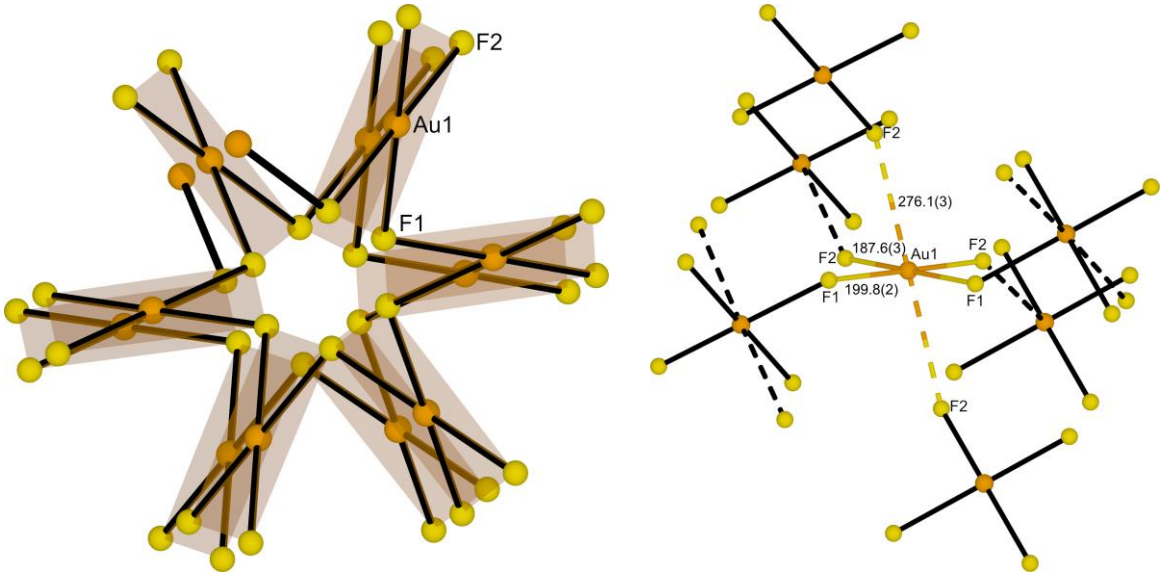

Figure 1: Excerpts of the crystal structure of AuF_3. F1 denotes bridging and F2 terminal fluorine atoms.[129] Left: Helical chain consisting of fluorine-bridged, square planar $\{AuF_4\}$ units, which are highlighted by planes. Right: Interaction of a part of one chain with terminal fluorine atoms from adjacent chains including Au–F bond lengths given in pm.

The first synthesis of the $[AuF_4]^-$ anion was achieved by *Sharpe*, by the reaction of the $[AuF_3{\cdot}BrF_3]$ adduct with $M[BrF_4]$ (M = Na, K, Ag). In this way, impure salts of the form $M[AuF_4]$ were obtained.[122] $Ag[AuF_4]$ is accessible directly from the metals in liquid BrF_3. *Peacock* improved the route for the preparation of pure $K[AuF_4]$ by the reaction of Au with KCl and BrF_3.[135] Alkali metal salts of the $[AuF_4]^-$ anion can

also be synthesized by the fluorination of the corresponding $[AuCl_4]^-$ salts, which are often used as starting materials for other gold compounds,[136] at 200–300 °C.[137] Several salts with divalent cations of the type $M[AuF_4]_2$ have been prepared by the reaction of AuF_3 with the corresponding MCl_2 (M = Ba, Hg) or MSO_4 (M = Mg, Ni, Zn, Cd) salt in diluted F_2 at around 300 °C.[138] They can also be synthesized by the solid state reaction of the corresponding metal fluoride MF_2 (M = Pd, Ag) and AuF_3 in sealed ampules at elevated temperatures.[138,139] Moreover, $[AuF_4]^-$ salts with cations containing lanthanides, actinides, and xenon were reported, namely $[M_2F][AuF_4]_5$ (M = Tb, Dy, Ho, Er),[125] $[MF][AuF_4]_2$ (M = Tm, Yb, Lu),[126] $[M_2F_7][AuF_4]$ (M = Th, U)[140] and $[XeF_5][AuF_4]$.[141] The fluorine-bridged anion $[Au_2F_7]^-$ was also stabilized in $Cs[Au_2F_7]$.[140,142] Fluorination of elemental gold in *a*HF yields the mixed-valent $Au[AuF_4]_2$, which is a rare case of gold in the oxidation state +II[143] (cf. Section 1.1).

Edwards and coworkers were the first to determine the structure of the $[AuF_4]^-$ anion by X-ray diffraction in the potassium salt $K[AuF_4]$. Therein, $[AuF_4]^-$ shows a square-planar coordination around the Au center with an Au–F bond length of 195(2) pm, which is in between those of the terminal and bridging fluorine atoms in AuF_3 (see Figure 1).[144]

The possibility of preparing $[AuF_4]^-$ salts starting from AuF_3 highlights the greater stability of the former, which is also underlined by a decrease in reactivity towards organic solvents of e.g. $Cs[AuF_4]$. Recently, the first $[AuF_4]^-$ salts with organic cations were prepared by the reaction of AuF_3 with $[NR_4]X$ (R = Me, Et; X = Cl, Br) in BrF_3.[117] The stability of the obtained compounds $[NR_4][AuF_4]$ decreases with increasing size of the cation and also explosions can occur when the amount of the salt and the concentration of BrF_3 are high enough. However, once prepared, the compounds can be handled and are well soluble in dry organic solvents. This way the first complexes of monomeric AuF_3, $[AuF_3(NCMe)]$ and $[AuF_3(py)]$, were obtained.[117]

The oxidation state +V is the highest known for gold and up to date it has only been stabilized by fluorides in the compounds AuF_5 and the corresponding anion $[AuF_6]^-$ (see Scheme 4).[103,104] The first salt of the $[AuF_6]^-$ anion was prepared by *Bartlett* and coworkers by the fluorination of AuF_3 in the presence of XeF_2. The latter is fluorinated to XeF_6 at 400 °C and the salt $[Xe_2F_{11}][AuF_6]$ is obtained. This compound can be converted to $Cs[AuF_6]$ by the reaction with CsF at 110 °C, with

the concomitant release of gaseous XeF_6.[29] $Cs[AuF_6]$,[32,34,35] as well as other salts of the type $M[AuF_6]$ (M = Li,[34,35] K,[32,34,35] Ag[34]) or $M[AuF_6]_2$ (M = Mg, Ca, Ni, Cu, Zn, Sr, Ag, Cd, Ba, Hg)[145] can be synthesized by the reaction of AuF_3 and the corresponding MF or MF_2 salt with elemental fluorine in *a*HF under UV light excitation. Salts of the $[AuF_6]^-$ anion with $[NO]^+$,[26,29,32] $[IF_5]^+$,[32] $[XeF_5]^+$[32] and $[Xe_2F_3]^+$[26] as well as the double salt $[AgF]_2[AgF_4][AuF_6]$[146] have also been reported. The dioxygenyl salt $[O_2][AuF_6]$ is the most extensively studied salt of this type and is usually prepared by the oxidation of AuF_3 or elemental gold using mixtures of O_2 and F_2 at high pressures and temperatures.[27,28,30–33,35] KrF_2 directly oxidizes elemental gold at ambient conditions in *a*HF, forming the compound $[KrF][AuF_6]$.[26]

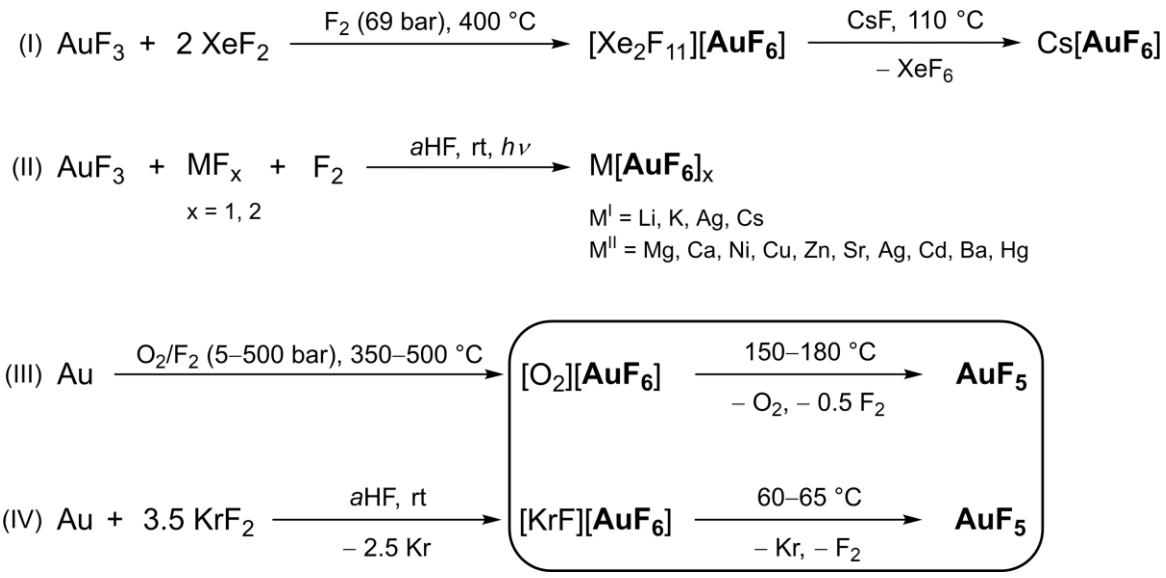

Scheme 4: Overview of the synthetic routes for the preparation of salts of the $[AuF_6]^-$ anion[26–35,145,146] and thermal decomposition of $[O_2][AuF_6]$ and $[KrF][AuF_6]$ leading to AuF_5 (framed).[26–28]

Both salts $[O_2][AuF_6]$ and $[KrF][AuF_6]$ decompose to give neutral AuF_5 at temperatures above 150 °C and 60 °C, respectively (see Scheme 4).[26–28] AuF_5 is the only pentafluoride that is a dimer in the solid state. The Au centers are bridged by two fluorine atoms, leading to both gold atoms in Au_2F_{10} having a distorted octahedral coordination environment.[28] Electron diffraction revealed that AuF_5 is not monomeric in the gas phase either, as an 82:18 mixture of dimers and trimers was detected.[147] AuF_5 is extremely reactive and even decomposes in *a*HF under reduction to AuF_3 at temperatures above 0 °C.[28] This is in contrast to salts of the $[AuF_6]^-$ anion, which can also be prepared in *a*HF (see Scheme 4).[36] Calculations

of the fluoride ion affinity (FIA; see Section 1.6) predict that AuF_5 is the strongest known Lewis acid in the condensed phase, explaining its instability as a monomer. The strong Lewis acidity is underlined by quantum-chemical calculations of a hypothetical $[AuSbF_{11}]^-$ anion, which is best described as $[AuF_6{\cdot}SbF_5]^-$, based on the calculated bond lengths.[28]

Regarding gold fluorides with gold in the oxidation states +II, +IV and +VI, only little is known. Neutral AuF_6 has not been prepared, but is predicted to be the strongest oxidizer of the known metal hexafluorides, following the trend among the 5d metal hexafluorides.[148,149] While PtF_6 is known to oxidize O_2[150] and Xe,[151] AuF_6, if prepared, might be able to oxidize even Kr.[152] Recent theoretical investigations proposed that AuF_6, like AuF_4 and AuF_2, is stable at pressures above 10 GPa.[153] AuF_2 has been the subject of further theoretical studies[154,155] and was detected in the IR spectra of laser-ablated Au with diluted F_2 in noble gas matrices.[111,112] Considering the corresponding fluoroaurates, the $[AuF_3]^-$ anion has only been mentioned in a quantum-chemical investigation of neutral and anionic coinage metal clusters,[155] as well as the $[AuF_7]^-$ anion, which is predicted to form weak F–F interactions between an $[AuF_6]^-$ unit and a fluorine atom.[149]

Neutral AuF_7 was claimed to have been prepared and to be stable at room temperature with decomposition observed at 100 °C.[156] However, high-level quantum-chemical calculations later showed that the decomposition of AuF_7 to AuF_5 and F_2 is strongly exothermic and does not have a high activation barrier.[157] In fact, the putative AuF_7 was found to be better described as a non-classical $[AuF_5{\cdot}F_2]$ complex, i.e. bearing a discrete $\{F_2\}$ unit. This compound consists of an $\{AuF_5\}$ unit in a close to square pyramidal geometry and a coordinated F_2 molecule in axial position, resulting in a distorted octahedral geometry at the gold center. This non-classical $[AuF_5{\cdot}F_2]$ complex was calculated to be more than 200 $kJ{\cdot}mol^{-1}$ lower in energy than the classical AuF_7, underlining that Au(V) is the highest known oxidation state of gold.[158]

1.4 Fluorido Organo Gold Complexes

As shown in Section 1.3, especially neutral binary gold fluorides are highly reactive, sensitive to moisture and hard to handle in organic solvents. In his review on gold fluorides in 2014, *Toste* concluded: *"The complexes AuF_3, AuF_5 and the anion $[AuF_6]^-$ are all powerful oxidants that fluorinate both organic and inorganic substrates in an uncontrolled manner and, as a result, they are of little use to the synthetic chemist."*[104] These properties, combined with the sophisticated experimental techniques needed to handle highly oxidizing and/or fluorinating compounds (see Section 1.2), explain why fluorido organo gold complexes, i.e. complexes containing both Au–C and Au–F bonds,[47] are much less investigated than their chloride analogues.[103]

The reactivity of Au–F bonds does not stem from an intrinsic instability, as AuF_3 was shown to have a high thermal stability under strictly anhydrous conditions (see Section 1.3).[122] In fact, the Au–F bond is the strongest of all Au–X (X = F, Cl, Br, I) bonds, but only by a small margin.[159] In contrast, especially main group elements like boron, carbon, or silicon, form their by-far strongest bonds to fluorine, as underlined by the BDE values of E–X (E = Au, B, C, Si) compounds given in Table 1.[159]

Table 1: Overview of experimentally determined bond dissociation energies at 25 °C for different diatomic compounds of the type E–X (E = Au, B, C, Si; X = F, Cl, Br, I). Values given in $kJ \cdot mol^{-1}$.[159]

E: \ X:	F	Cl	Br	I
Au	294.1	280 ± 13	213 ± 21	276
B	732	427	390.9 ± 0.5	361
C	513.8 ± 10.0	394.9 ± 13.4	318.0 ± 8.4	253.1 ± 35.6
Si	576.4 ± 17	416.7 ± 6.3	358.2 ± 8.4	243.1 ± 8.4

As a result, compounds containing Au–F bonds are prone to undergo reactions in the presence of many organic molecules with the driving force to form highly stable E–F bonds. In Scheme 5, this is schematically depicted for a halogen exchange reaction with halides of boron, carbon, or silicon.

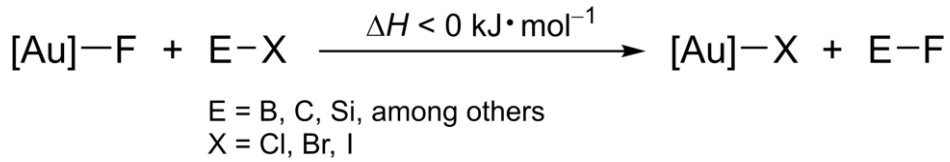

Scheme 5: Schematic reaction equation showing the reactivity of a fluorido gold complex [Au]–F towards compounds containing heavier halides, based on the data shown in Table 1.

For halido complexes of late transition metals, a relative destabilization of the filled metal d orbitals of appropriate symmetry occurs by the interaction with the lone pairs of the halide, which is an example of filled/filled orbital interactions.[160,161] As fluorine is the strongest π donor of the halogens[161] and its 2p valence orbitals have no radial nodes which leads to comparably shorter E–F bonds,[162] this repulsive interaction is strongest in the respective fluorido complexes, leading to a weakening of the M–F bond.[160] Hence, gold prefers to bind to main group donor atoms of the third row in the periodic table or below and was thus classified as a 'class b' metal by *Ahrland*, *Chatt* and *Davies*.[163]

However, fluorido organo gold species are known to play a decisive role as intermediates in many gold-catalyzed or -mediated reactions like C–C or C–F bond formation reactions and an improved understanding of their reactivity is a key step for the development of more efficient catalysts.[104,105,164,165] All known fluorido organo gold complexes have been synthesized in the last two decades, although the number of detected and/or isolated compounds of this kind has remained limited.[104,105,166]

The first species containing both an Au–C and an Au–F bond was prepared in 2004 by *Willner* and coworkers. They performed the reaction of the $[Au(CN)_4]^-$ anion with ClF in DCM and detected a mixture of species of the type $[Au(CF_3)_{4-x-y}Cl_xF_y]^-$ (x = 0–2, y = 0–4) by ^{13}C and ^{19}F NMR spectroscopy, but none of these products could be isolated.[167] The first isolation of a fluorido organo gold complex was accomplished by the group of *Sadighi* in 2005, when they prepared [AuF(SIPr)] (SIPr = 1,3-bis(2,6-diisopropylphenyl)-4,5-dihydroimidazol-2-ylidene) by the protonation of [Au(O^{t}Bu)(SIPr)] with HF, added in the easy-to-handle form of $NEt_3 \cdot 3HF$ (see Scheme 6, I).[168] It was later discovered that when the fluoride is introduced by using the aprotic fluoride source benzoyl fluoride, the yield increased from 48 % to 91 %.[169] This complex is one of the rare examples of a fluorido organo gold(I) complex and the stabilization of such species relies on the use of

an *N*-heterocyclic carbene (NHC). NHCs are strong σ donors and sterically demanding (see Section 1.5), thus effectively shielding the gold center against a nucleophilic attack. However, [AuF(SIPr)] is light-sensitive and shows substantial decomposition in a DCM solution after 1 day at room temperature.

Insertion of different alkynes into the Au–F bond in [AuF(SIPr)] was shown to be reversible and yielded *β*-(fluoro)vinyl gold(I) complexes. Although the possibility to isolate the product depended on the used alkyne, acidic workup resulted in the corresponding (*Z*)-fluoroalkene as the main stereoisomer (see Scheme 6, II).[170] On the other hand, the reaction of [AuF(SIPr)] with $[Ph_3C][BF_4]$ led to a fluoride abstraction that yielded the binuclear $[\{Au(SIPr)\}_2(\mu\text{-}F)]^+$ cation, which contains a bridging fluorido ligand (see Scheme 6, III). This highly reactive compound was shown to add to the allene 3-methyl-1,2-butadiene to yield a diaurated allylic fluoride. This allylic fluoride showed an asymmetric binding to the gold centers, i.e. one σ and one π bond, in a rapid equilibrium on the NMR time scale.[169]

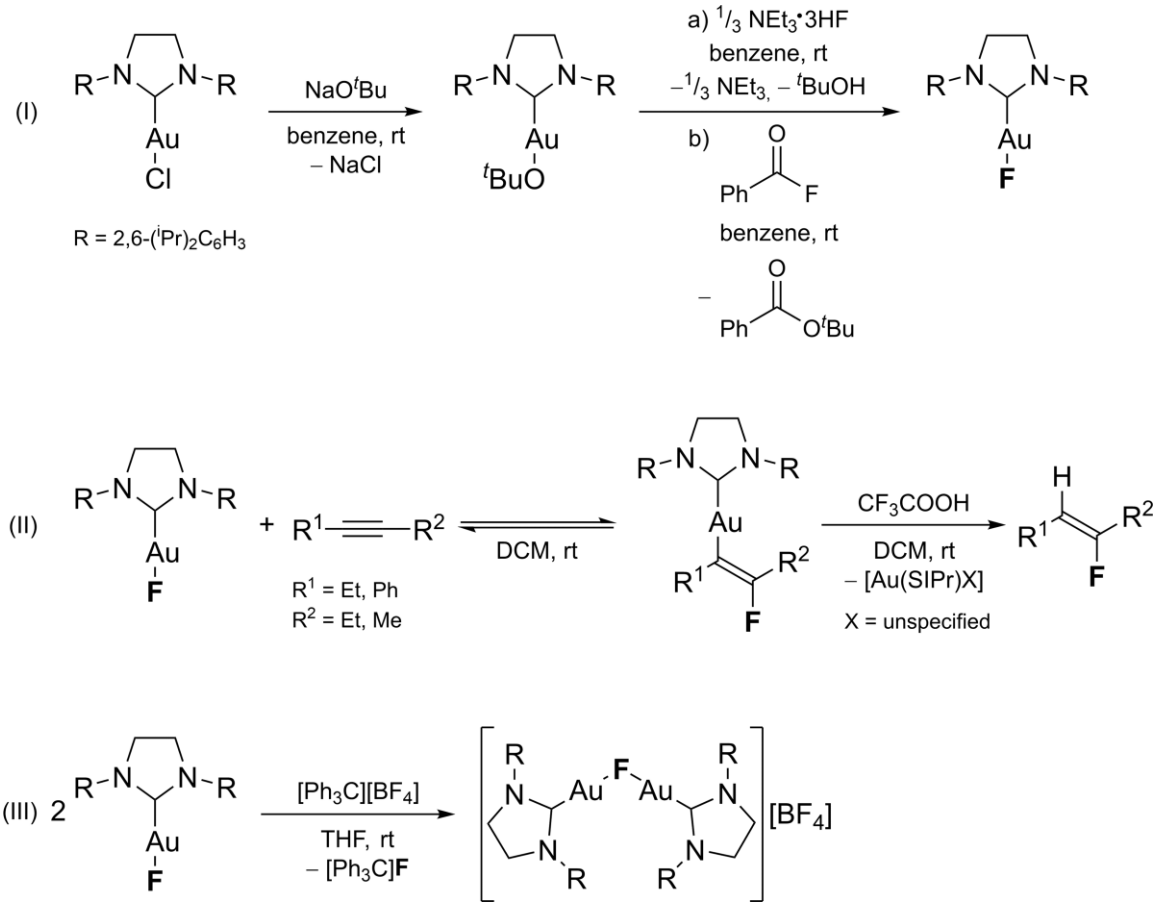

Scheme 6: (I) Preparation of the first isolated fluorido organo gold(I) complex [AuF(SIPr)] by using (a) $NEt_3 \cdot 3HF$[168] or (b) benzoyl fluoride.[169] (II) Reaction of [AuF(SIPr)] with alkynes to give the corresponding *β*-(fluorovinyl)gold(I) complexes, which yield (*Z*)-fluoroalkenes after acidic workup.[170] (III) Fluoride abstraction from [AuF(SIPr)] to yield a cationic, fluorine-bridged digold complex.[169]

The related complex with an unsaturated imidazolidine backbone, [AuF(IPr)] (IPr = 1,3-bis(2,6-diisopropylphenyl)imidazol-2-ylidene) was obtained as a product from the reductive elimination of difluorido alkyl gold(III) complexes (cf. Scheme 9, II)[171] and by the reaction of [Au(IPr)(OH)] with K[HF_2].[172] Similarly, [AuF(PR_3)] (R = Ph, Cy) was detected as the main product from the reductive elimination of 4-X-$C_6F_4CF_3$ (X = Me, F) from [Au(4-X-C_6H_4)(CF_3)F(PR_3)] complexes (cf. Scheme 9, III).[173]

Very recently, *Braun* and coworkers prepared the fluorido organo gold(I) compounds [AuF(IPr)] and [AuF(SIPr)] by an I/F exchange using AgF. In the same way, they synthesized related gold(I) fluorides which are stabilized by sterically demanding phosphane ligands (see Scheme 7).[174] Follow-up reactivity studies were centered around the phosphane-stabilized complex [AuF(SPhos)] (SPhos = dicyclohexyl(2',6'-dimethoxy[1,1'-biphenyl]-2-yl)phosphane) and will be summarized in the following paragraph.

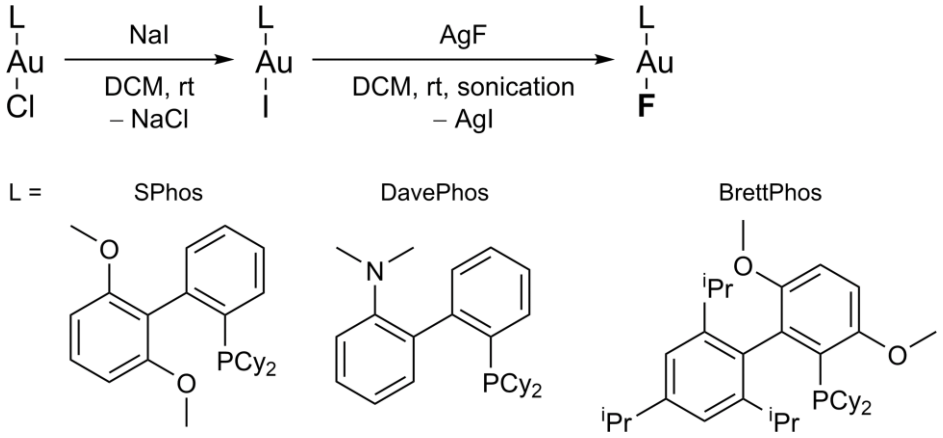

Scheme 7: Preparation of gold(I) fluorides stabilized by sterically demanding phosphane ligands.[174]

The fluorido ligand in [AuF(SPhos)] can be substituted by fluorinated alkyl groups or alkynes (see Scheme 8, top).[174] [AuF(SPhos)] showed a similar reactivity to [AuF(SIPr)] for the hydrofluorination of alkynes resulting in *β*-(fluoro)vinyl gold species that reacted with acids to the corresponding (*Z*)-fluoroalkenes. The reaction with an ynone yielded the fluoroenone (see Scheme 8, left). When [AuF(SPhos)] was reacted with a dialkyne, however, a mixture of different *trans*- and *cis*-hydrofluorinated alkenes was obtained. Terminal alkynes either gave the alkynyl gold(I) complex or the fluorinated olefin, depending on the stoichiometry. Based on the results, [AuF(SPhos)] was tested as a catalyst for the catalytic

hydrofluorination of 1-phenyl-1-propyne with $NEt_3 \cdot 3HF$ and showed comparable results to other typical gold(I) catalysts.[175] In a subsequent study, [AuF(SPhos)] was reacted with the electrophilic fluorination agent *N*-fluorobenzenesulfonimide to give the *N*-fluoroamido derivative [Au{N(F)SO_2Ph}(SPhos)], which showed an unprecedented insertion into the N–F bond when CO was added. However, with alkyl or vinyl iodides or alkyl bromides, the Au–N bond was cleaved, and the fluoroamido group was transferred to the organic moiety, yielding *N*-fluoroamine derivatives (see Scheme 8, right).[176] [AuF(SPhos)], as well as the NHC-stabilized complexes [AuF(SIPr)] and [AuF(IPr)], have shown hydrogen bonding when reacted with the easy-to-handle HF source poly[4-vinylpyridinium poly(hydrogen fluoride)] (PVPHF). All products contained an asymmetrical bifluorido ligand, as revealed by low-temperature NMR spectroscopy and quantum-chemical calculations. In addition, [AuF(SPhos)] showed halogen bonding towards C_6F_5I, forming the complex [Au(F·IC_6F_5)(SPhos)] (see Scheme 8, bottom).[177]

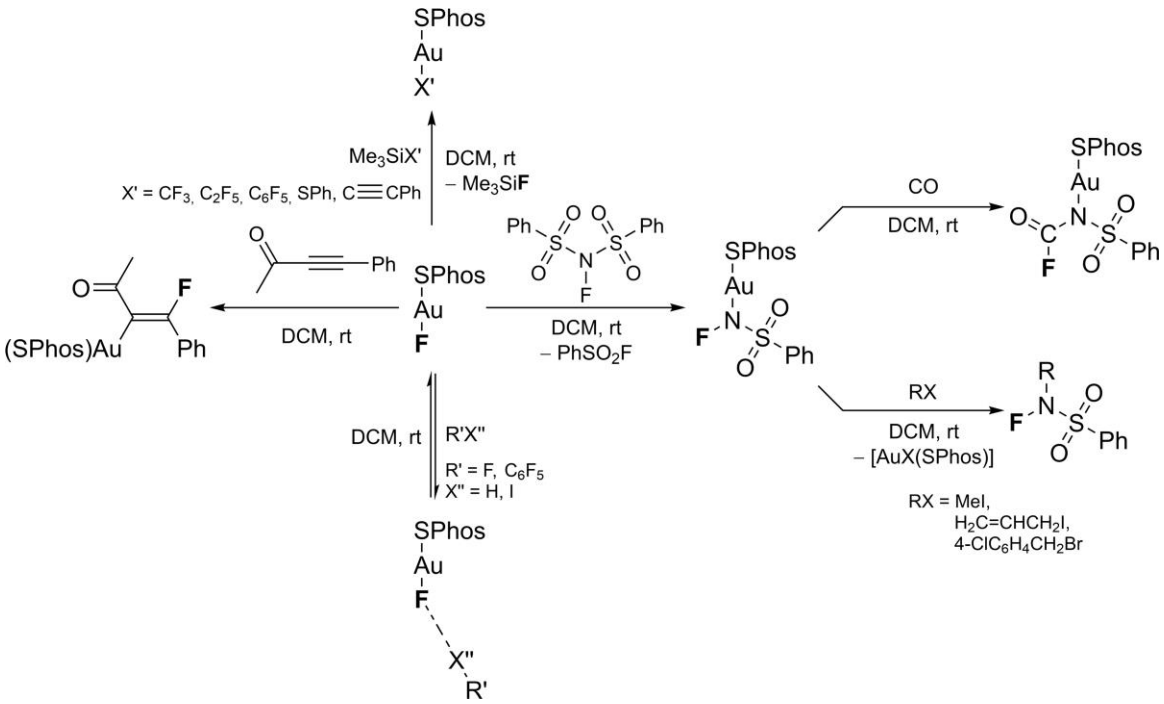

Scheme 8: Reactivity of [AuF(SPhos)], including substitution of the fluorido ligand by using trimethylsilyl derivatives (top),[174] insertion of an ynone (left)[175] and a sulfonimide (and its reactivity; right)[176] into the Au–F bond, and examples of hydrogen as well as halogen bonding (bottom).[177]

Apart from these few examples described above, the only other neutral gold(I) species containing an Au–F bond is [Au(IPr^{Cl})(FBF_3)] (IPr^{Cl} = 1,3-bis(2,6-diisopropylphenyl)-4,5-dichloroimidazol-2-ylidene), in which the usually weakly

coordinating anion $[BF_4]^-$ is coordinated to the gold center in the absence of a solvent. By the addition of a substrate or solvent, the compound $[Au(IPr^{Cl})(L)][BF_4]$ (L = substrate, solvent) with an outer-sphere coordination of the $[BF_4]^-$ anion is formed.[178] In addition, the $[Au(CF_3)F]^-$ anion was detected by tandem mass spectrometry.[118,179]

The only literature-known gold(II) complex with an Au–F bond that was isolated is the dimeric $[Au_2F_2(2,6\text{-dimethylformyl})_2]$ complex, which contains an Au–Au bond and was prepared by the reaction of the corresponding nitrato compound with KF.[180] Quantum-chemical investigations of the mechanism for the gold-catalyzed oxidative heteroarylation of alkenes with arylboronic acids proposed a transition state that also contains an Au(II)–Au(II) bond, which undergoes a bimetallic reductive elimination.[181] However, experimental evidence for such a species is missing to date.

Similar to the binary gold fluorides, fluorido organo gold complexes with gold in the oxidation state +III are by far the most extensively studied group. The redox pair Au^I/Au^{III} has been investigated as a catalytic system for many functionalization reactions.[20,164,166,182–187] In combination with fluorinating reagents, products resulting from either C–F bond formation[104,105,188] or oxidative homo- or cross-coupling are obtained.[104,105,165,185,186,189] For an oxidative addition at the gold center to occur, the rather high oxidation potential compared to the widely used Pd^0/Pd^{II} system (1.41 V vs. 0.92 V)[190] must be overcome, requiring a sacrificial oxidant.[164,165,182,184,187] The most commonly used sacrificial oxidant is 1-chloromethyl-4-fluoro-1,4-diazoniabicyclo[2.2.2]octane bis(tetrafluoroborate), also known as Selectfluor®, which is an efficient electrophilic fluorination agent.[191] In such reactions[192] a gold(I) catalyst [AuLX] (L = neutral donor ligand, e.g. NHC or phosphane; X = anionic labile ligand, i.e. halide) is oxidized with the electrophilic Selectfluor®, which is proposed to transfer a formal 'F^+' to the gold center, yielding $[AuFLX]^+$. This transient species has a vacant fourth coordination site, where the reactant can coordinate to give the desired coupling product after reductive elimination. However, none of these proposed fluorido organo gold(III) species has been detected as of now.

The first neutral fluorido organo gold(III) complexes were prepared by the group of *Toste* by oxidation of [Au(NHC)R] (NHC = IPr, SIPr, R = Me, ^{t}Bu) with XeF_2, which yielded the corresponding *cis*-$[AuF_2(NHC)R]$ compounds. In solution, they are in

an equilibrium with a dimeric $[Au_2(\mu\text{-}F)_2(NHC)_2R_2]^{2+}$ dication with two bridging fluorido ligands, as detected by NMR spectroscopy (see Scheme 9, I). The equilibrium can be shifted depending on the NHC and R groups. However, even for the case of *cis*-$[AuF_2(IPr)Me]$, where the NMR spectrum only showed the monomeric species, crystallization attempts yielded the dimeric compound. The complex *cis*-$[AuF_2(IPr)Me]$ was used stoichiometrically for C–C coupling reactions with a number of arylboronic acids that had varying electronic and steric properties which gave insight into the mechanism of gold-catalyzed C–C couplings.[193] In a subsequent study, several [Au(IPr)R] (R = (cyclo)alkyl) complexes were oxidized with XeF_2 and yielded *cis*-$[AuF_2(IPr)R]$, from which a subsequent reductive elimination to form C–F bonds could take place (see Scheme 9, II). If R contained *β*-H atoms, *β*-hydride elimination would compete with the C–F reductive elimination.[171]

Complexes of the type $[Au(4\text{-}X\text{-}C_6H_4)(CF_3)F(PR_3)]$ (X = Me, F; R = Ph, Cy) were prepared via I/F exchange using AgF.[173] The investigation of the reductive elimination of these complexes showed that only the C–C bond-formation products are obtained, while no C–F bond formation was detected (see Scheme 9, III). In contrast, if the iodido complex is used instead of the fluorido complex, the reactivity is the direct opposite, leading to the C–I coupling product, while the bromido and chlorido complexes showed a mixture of both elimination products.[173] For the iodido complex, it was later shown that the C–C bond-formation product can be obtained when a silver salt is added.[194] A subsequent quantum-chemical study revealed that independent of the halide, the C–C elimination product should be favored. However, for the heavier halides, an autocatalytic mechanism with an intermediate binuclear Au^{I}–Au^{III} species needs to be taken into account, which yields the corresponding halogenated aryl compounds instead.[195]

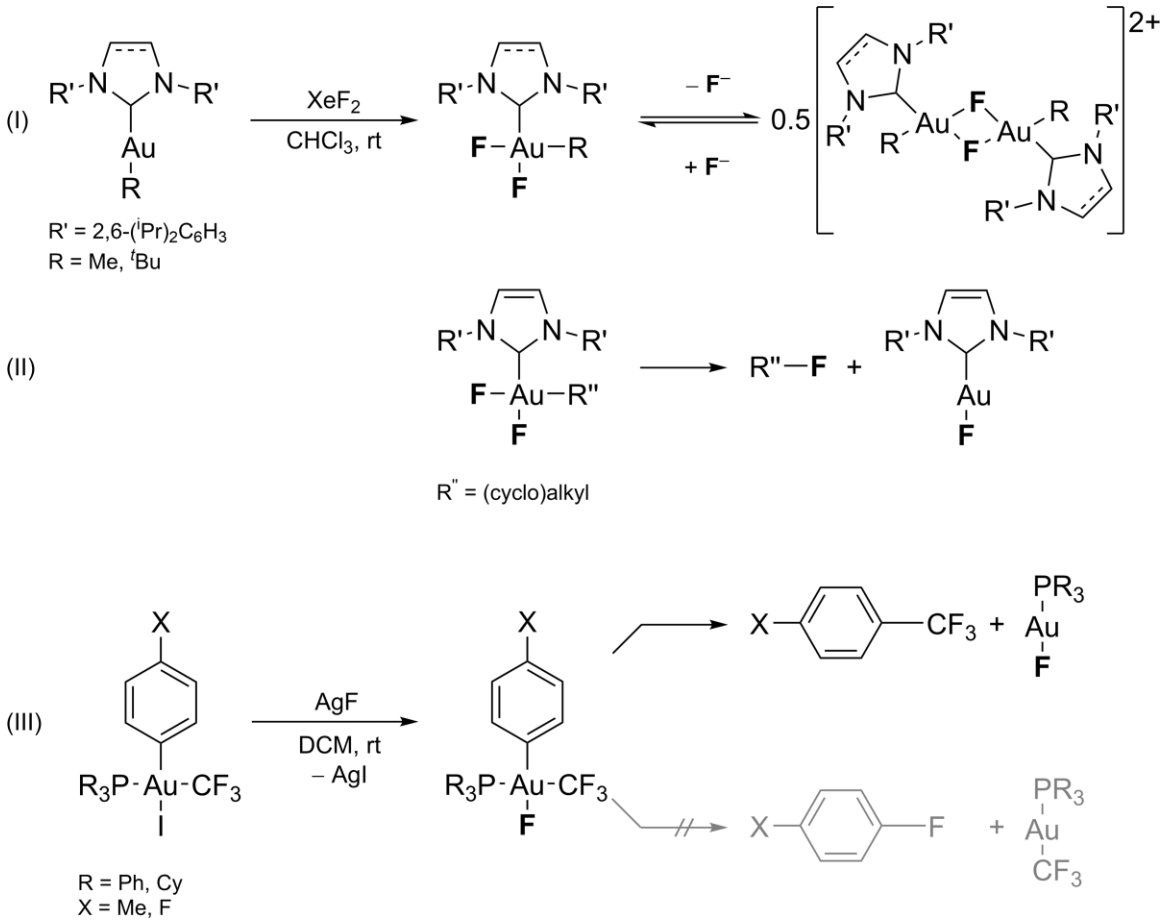

Scheme 9: (I) Preparation of a *cis*-difluorido organo gold(III) complex by the oxidative addition of XeF_2 to an organo gold(I) complex.[193] (II) Reductive elimination from a *cis*-difluorido organo gold(III) complex under C–F bond formation.[171] (III) Preparation of fluorido organo gold(III) complexes by I/F exchange using AgF and their reductive elimination that selectively yields C–C instead of C–F bonds.[173]

The group of *Nevado* has prepared a variety of mono- and difluorido organo gold(III) complexes with several (N^C), (N^C^C) or (N^P) pincer ligands by halogen exchange of halido organo gold(III) complexes with AgF, as shown in Scheme 10. Complexes with different [AuF(N^C^C)] scaffolds were found to be luminescent in investigations of their photophysical properties. Furthermore, the fluorido ligand was exchanged by differently substituted terminal alkynes (Scheme 10, I).[196] Using a bidentate (N^C) pincer ligand, they stabilized a *cis*-difluorido organo gold(III) complex and investigated its reactivity towards arylboronic acids. With electron-poor aryl substituents, the corresponding *cis*-diaryl gold(III) complex was obtained by transmetallation. However, when electron-rich aryl groups are used, the C–C coupling product was formed selectively and no diaryl gold(III) complex was observed (see Scheme 10, II).[197] The reactivity of monofluorido [AuF(N^C)R] (R = aryl or alkyl) complexes containing the same pincer ligand towards arylboronic

acids was also studied. Depending on the substrate, two different reactivities were observed. One possibility was an intermolecular reductive elimination, in which a bond between the R group and the aryl group of the arylboronic acid is formed, and concomitantly, the fluorido ligand is abstracted by the boronic acid. The other possibility was an intramolecular reaction of the transmetallation product, where a bond is formed between the R group and the carbon donor atom of the pincer ligand.[197] It was shown that the fluorido ligand in cationic gold(III) fluorides of the type $[AuArF(N^P)]^+$ (Ar = substituted aryl group) can be exchanged by cyanido or several alkynyl ligands. The formed products can undergo subsequent reductive elimination to yield C(sp^2)–C(sp) bonds (Scheme 10, III).[198]

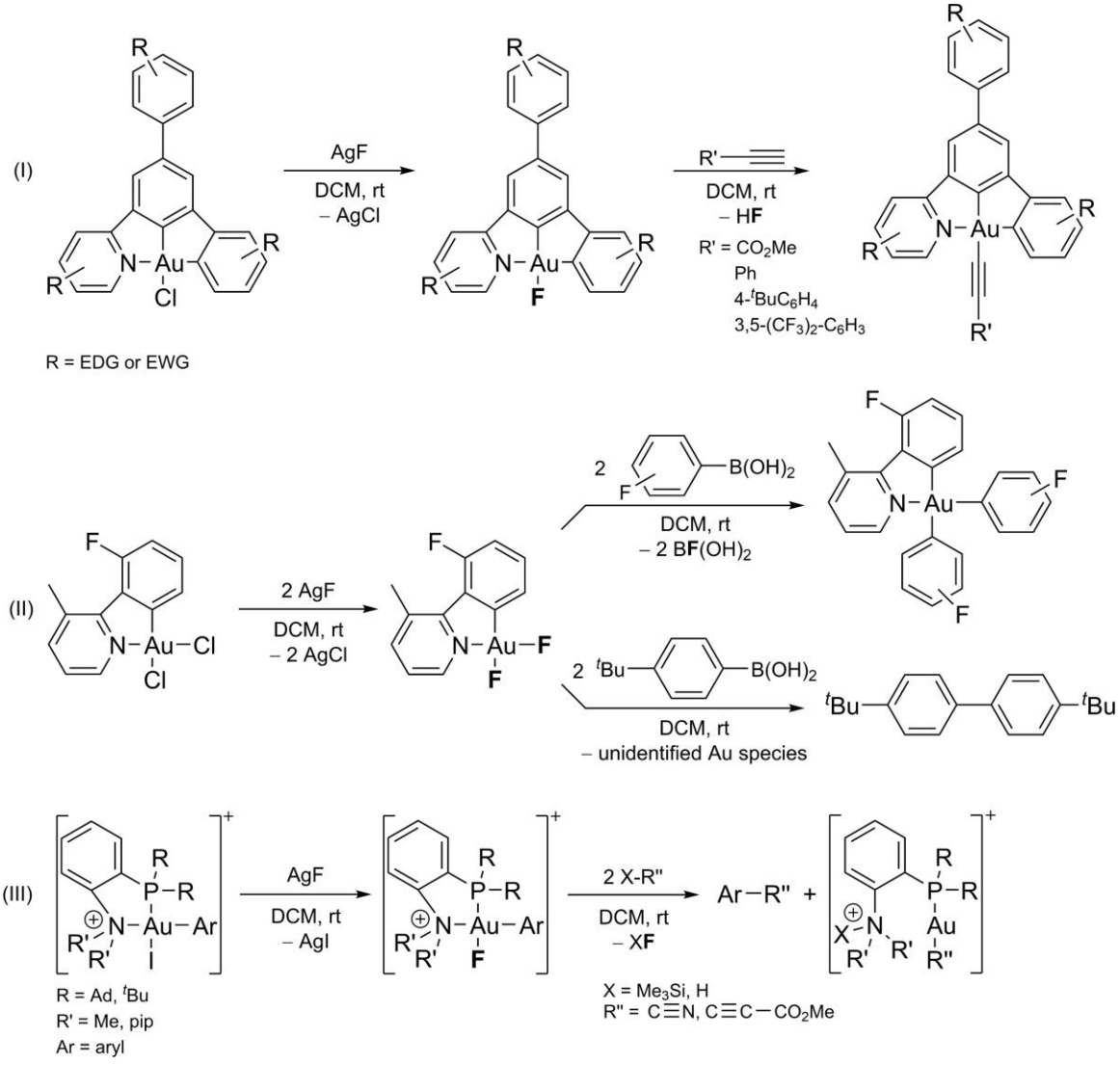

Scheme 10: (I) Preparation of fluorido organo gold(III) complexes stabilized by pincer ligands and their reactivity yielding alkynyl gold(III) complexes under elimination of HF.[196] (II) Preparation of aryl-substituted organo gold(III) complexes by transmetallation (upper route)[197] or C–C coupling products by reductive elimination (lower route).[197] (III) Preparation of C–C coupling products by reductive elimination from cationic gold(III) fluorides (the counterion is $[BF_4]^-$).[198]

Recently, the first fluorido organo gold(III) complex prepared by the oxidation of an organo gold(I) species with Selectfluor® was isolated. The complex was stabilized by a bis(mesoionic carbene)carbazolide (C^N^C) pincer ligand, yielding the $[Au(C^N^C)F]^+$ cation. The complex was studied for its photophysical properties and compared to the organo gold(I) complex [Au(C^N^C)], which shows an unusual T-shaped coordination of the gold center by the pincer ligand.[199]

Apart from these neutral and cationic species, *Menjón* and coworkers also succeeded in the preparation of fluorido organo aurate(III) complexes, starting from the $[Au(CF_3)_2]^-$ anion. They either oxidized it with CF_3I, yielding $[Au(CF_3)_3I]^-$, which can be fluorinated by XeF_2 or AgF to result in $[Au(CF_3)_3F]^-$ (see Scheme 11, top)[179] or oxidized and fluorinated in one step with XeF_2. Surprisingly, they did not observe the *cis*-difluorido complex in the latter case, but selectively prepared the *trans*-$[Au(CF_3)_2F_2]^-$ anion.[119] The observed products were studied by tandem mass spectrometry. For *trans*-$[Au(CF_3)_2F_2]^-$, also substitution of the fluorido ligands was achieved in the bulk, forming anions of the type *trans*-$[Au(CF_3)_2X_2]^-$ (X = Cl, Br, I, CN) by addition of KX in acetone (see Scheme 11, bottom).[119]

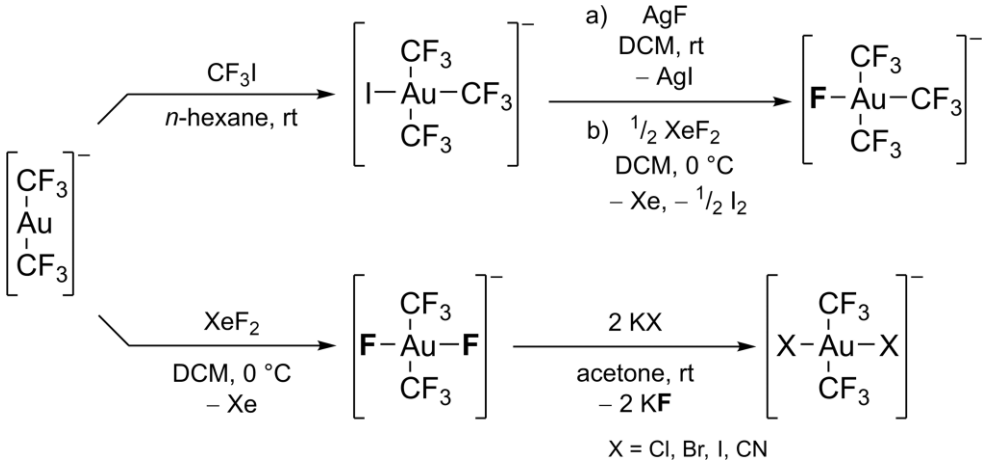

Scheme 11: Preparation of fluorido organo aurates(III) either by I/F exchange from the corresponding iodido organo aurate(III) (top)[179] or by oxidation of the organo aurate(I) with XeF_2 (bottom).[119] Note that the latter yields a *trans*-difluorido complex opposed to the *cis*-difluorido complexes shown in Scheme 9 and Scheme 10. The fluorido ligands in *trans*-$[Au(CF_3)_2F_2]^-$ can be substituted by the heavier halido or cyanido ligands. In all cases, the counterion is $[PPh_4]^+$.

Dutton and coworkers have also reported cationic gold(III) difluorides with a *trans*-arrangement, which they have prepared by oxidative addition with XeF_2. Therein, the gold(III) difluorides are stabilized by *N*-donor ligands like pyridyl or imidazole ligands.[200] The fluorido ligands can be substituted in metathesis reactions with

iodine(III) complexes[201] or by using Me_3SiX or HX (X = pyridyl, alkynyl, cyanide, acetate) reagents.[202]

The group of *Riedel* reported on the use of AuF_3 as the starting material together with different N- or C-donor ligands, in contrast to the fluorination of organo gold complexes described above. As described in Section 1.3, AuF_3 is stable in the solid state, but is either insoluble or decomposes rapidly in organic solvents at room temperature. However, it can be handled in some organic solvents at lower temperatures. In this way, *Riedel* and coworkers were able to stabilize [AuF_3(NCMe)] at temperatures below −25 °C and showed NMR spectroscopic evidence for [AuF_3(py)] (py = pyridine). Similar to *cis*-[AuF_2(IPr)Me] (see Scheme 9, top), [AuF_3(py)] undergoes dimerization under fluoride abstraction to form $[Au_2F_4(py)_2]^{2+}$.[117] In a subsequent study, they isolated the first trifluorido organo gold(III) complex using the NHC SIMes (1,3-bis(2,4,6-trimethylphenyl)-4,5-dihydroimidazol-2-ylidene) for the stabilization of the AuF_3 unit (see Scheme 12).[203] [AuF_3(SIMes)] is well soluble and stable in many organic solvents and contains the strongly Lewis acidic AuF_3 in a monomeric form. In the structure of [AuF_3(SIMes)] in the solid state, the square-planar coordinated gold center shows two different Au–F bond lengths. Therein, the Au–F bond in *trans* position to the SIMes ligand is about 5 pm longer than those in *cis* position. This can be explained by the stronger *trans*-influence of the strong σ donor SIMes compared to the fluorido ligands.[203] This finding was exploited in a subsequent study, where the *trans*-fluorido ligand was selectively substituted by a chloride or teflate group by using the corresponding trimethylsilyl compounds, yielding *trans*-[AuF_2X(SIMes)] (X = Cl, $OTeF_5$), as shown in Scheme 12. Note that no external fluoride source, which is usually added when using trimethylsilyl compounds, was added for the introduction of the Cl and $OTeF_5$ group. The Lewis acidity of the {AuF_2X} moiety in these complexes was compared by the measurement of the chemical shift of the carbene carbon atom in the ^{13}C NMR spectra, revealing that the {$AuF_2(OTeF_5)$} moiety is even more Lewis acidic than the {AuF_3} moiety.[204] The *trans*-[AuF_2X(SIMes)] complexes are the first examples of products obtained by a substitution reaction of fluorido ligands at a gold center in which not all of them were substituted.

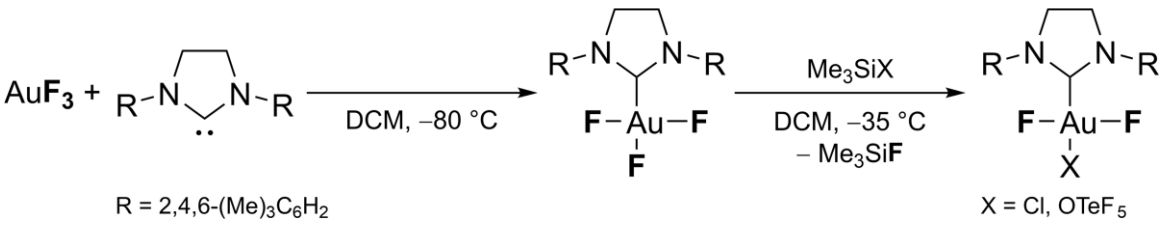

Scheme 12: Preparation of the first trifluorido organo gold complex $[AuF_3(SIMes)]$[203] and the selective substitution of the *trans*-fluorido ligand by chloride or teflate.[204]

1.5 *N*-Heterocyclic Carbenes

Carbenes are classified as compounds that contain a divalent, neutral carbon atom with two non-bonded electrons, resulting in an electron sextet at the carbene carbon atom.[205] The parent compound CH_2, also known as methylene, was first attempted to be prepared by the dehydration of methanol almost 200 years ago.[206] Due to their electron deficiency, most free carbenes are highly unstable, having lifetimes of less than 1 s.[205] The two non-bonded electrons can either be paired, leading to a singlet carbene and a bent coordination due to an sp^2 hybridization, or unpaired, resulting in a triplet carbene with an sp hybridization and a linear geometry.[207] CH_2 was shown to have a triplet ground state, whereas the fluorinated analogue CF_2 is a singlet carbene.[208] CF_2 is an important intermediate in the preparation of polytetrafluoroethylene (PTFE). It is prepared by the thermal dehydrohalogenation of $CHClF_2$ and quickly dimerizes to C_2F_4,[209] which can be polymerized to PTFE.[208]

The dichlorocarbene CCl_2 was shown to have an increased stability and was successfully introduced into organic molecules in 1954.[210] The first mention of a carbene complex in organometallic chemistry was $[W(CO)_5(COCH_3)(CH_3)]$, where the $COCH_3$ ligand was described as a methoxymethylcarbene.[211] In 1968, the groups of *Schönherr*[212] and *Öfele*[213] independently reported on the stabilization of carbene complexes of mercury and chromium, respectively. In both cases, *N*-heterocyclic carbenes (NHC) were used. Classical NHCs consist of a five-membered ring with two nitrogen atoms adjacent to the carbene carbon atom, which stabilize the singlet carbene by π-donation into the empty p orbital.[214] This stabilization, combined with sterically demanding substituents on the nitrogen atoms, can lead to isolable carbenes. The first solid state structure of a carbene was determined by the group of *Arduengo* in 1991, using the adamantyl substituted carbene IAd (1,3-di(1-adamantyl)imidazol-2-ylidene) (see Figure 2, left).[215] This breakthrough led to the development of other NHCs[214] with e.g. 2,4,6-(trimethyl)phenyl (see Figure 2, middle)[216,217] and 2,6-(diisopropyl)phenyl (see Figure 2, right)[217] groups, but also to a variety of NHC-related subclasses,[218] like cyclic (alkyl)(amino)carbenes (CAAC)[219] and mesoionic carbenes (MIC).[220]

Despite the recent development of new subclasses, classical NHCs are still widely used due to their versatility. Several parameters can be changed in the design of

an NHC, i.e. the substituents on the nitrogen atoms (see Figure 2), the size of the ring, and the backbone, which can be saturated, unsaturated, or even substituted.[214] In combination with the nucleophilic character of the carbene carbon atom resulting in a strong σ donor ability, it is possible to design tailor-made NHCs for various applications.[221]

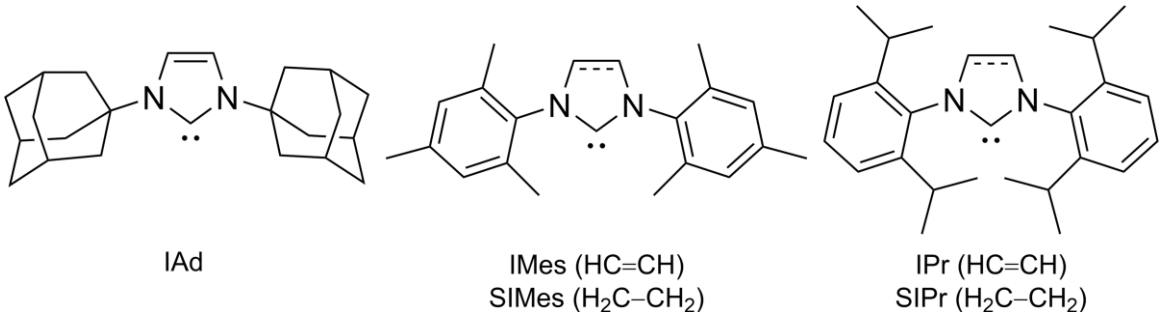

Figure 2: Overview of selected *N*-heterocyclic carbenes (NHCs). Left: First isolated, adamantyl-substituted NHC IAd;[215] middle: 2,4,6-(trimethyl)phenyl substituted NHCs IMes and SIMes;[216,217] right: 2,6-(diisopropyl)phenyl substituted NHCs IPr and SIPr.[217]

NHCs have found application as organocatalysts for a variety of reactions such as 1,2-additions or condensation reactions.[222] In organometallic chemistry, they were shown to be useful for the stabilization of late transition metals[223] and 3d metal complexes in high oxidation states.[48,49,224] Late TM carbene complexes are also established as catalysts for several organic reactions,[225] especially for the Ru-catalyzed olefin metathesis and Pd-catalyzed cross-coupling reactions.[214]

NHC complexes with Ag(I) and Au(I) are used for medicinal applications as antibacterial or anticancer drugs.[226] Especially Au(I)-NHC complexes have shown to be selectively toxic against cancer cells[227] or to be inhibitors with antitumor features.[228] Recently, they have been shown to be rather effective inhibitors of the SARS-CoV-2 (severe acute respiratory syndrome coronaviruses) spike protein.[229]

The chemical shift of the carbene carbon atom in the ^{13}C NMR spectra of NHCs was found to be sensitive to the donor strength of the ligand *trans* to it, resulting in the definition of a ligand electronic parameter.[230] The correlation between the carbene chemical shift and the *trans*-influence was also subject of theoretical investigations, highlighting the influence of spin-orbit coupling.[231] For a series of gold NHC complexes, the $^{13}C_{carbene}$ chemical shift was recently correlated with a calculated SIMes affinity in order to estimate the Lewis acidity of the coordinated fragment.[204]

1.6 Lewis Superacids

In 1887, *Arrhenius* discovered that molecules can dissociate in water under the formation of ions. He defined acids as molecules that dissociate giving protons, while bases yield hydroxide anions.[232] *Brønsted*[233] and *Lowry*,[234] independently, generalized this concept, stating that acids act as proton donors, while bases are proton acceptors, regardless of the solvent. The general relation between an acid HA and a base B to yield the conjugate base A^- and the conjugate acid HB^+ is shown in Equation (1).

$$HA + B \rightleftharpoons A^- + HB^+ \quad (1)$$

Lewis extended the concept of acids and bases, to define acids as electron pair acceptors and bases as electron pair donors.[235] A Lewis acid LA and a Lewis base LB can undergo a reaction forming the Lewis acid-base pair LA–LB, as shown in Equation (2). Since the Lewis base is formally donating both electrons to the bond, this bond can be interpreted as a dative bond.

$$LA + LB \rightleftharpoons LA{-}LB \quad (2)$$

Lewis acids have been extensively studied for their properties and reactivity, which led to various applications in organic synthesis, e.g. as catalysts for a vast number of functionalization reactions.[236] Probably the most remarkable reaction is the *Friedel-Crafts* alkylation,[237] while other examples comprise electrophilic additions to C=C[238] or C≡C bonds,[239] the degradation of perfluoropolyethers[240] and the hydroboration of olefins.[241]

In the case of Brønsted acids the degree of dissociation, i.e. the number of protons or protonated base molecules that exist when dissolved in a given solvent, can be measured by the Hammett acidity function H_0,[242] or the unified acidity scale using the absolute pH value $pH_{abs.}$[243] In contrast, no universal scale exists to assess Lewis acidity, yet the strength of a Lewis acid generally correlates with the tendency to form a Lewis acid-base pair. In fact, the *International Union of Pure and Applied Chemistry* (IUPAC) defined Lewis acidity as the thermodynamic propensity to form an adduct with a Lewis base, as described in Equation (2).[244] A suitable measurement for the determination of Lewis acidity is the equilibrium constant of the bond formation with a reference Lewis base. However, the choice

of the Lewis base is not straightforward due to the diverse nature of Lewis acids and their properties.[66] For example, depending on the hard or soft character of the Lewis acid, a stronger bond with a hard or soft base will be formed, according to the HSAB principle (see Section 1.3).[107] More precisely, the interaction of a hard acid and a hard base has a strong electrostatic character, while the soft-soft interaction is mainly of covalent nature.[245] Hence, the ordering of the strength of a set of Lewis acids will differ depending on the reference Lewis base. *Greb* categorized the known scaling methods for Lewis acidity into three different groups: intrinsic, effective, and global.[66,246]

Intrinsic Lewis acidity focuses on the properties of the free Lewis acid and is determined by non-invasive spectroscopy or quantum-chemical calculations. Examples are the LUMO energy[247] or the global electrophilicity index.[248] While the independence of a reference system is supposedly ideal for a general classification of Lewis acidity, the neglection of the interaction with a Lewis base is problematic. It has been shown that only a correlation between compounds with comparable structures is reasonable.[249]

Effective Lewis acidity investigates the change of a distinct spectroscopic property of a reference Lewis base when it forms an adduct with the Lewis acid. Most of the established experimental Lewis acidity scales are based on effective Lewis acidity. The blue-shift of the C≡N stretching vibration in a Lewis acid-acetonitrile adduct,[250] the change in *g* value in EPR spectra of Lewis acid-superoxides,[251] and the red-shift in the maximum of the fluorescence spectra of suitable Lewis bases[252] are just a few examples. However, the most frequently used method is the *Gutmann-Beckett* method, which measures the change in the ^{31}P NMR chemical shift of the triethylphosphane oxide upon adduct formation with the corresponding Lewis acid.[253] The advantages of this method are its very simple execution and the broad variety of substances that can be investigated. However, since Et_3PO is a rather hard base, soft acids tend to be underestimated. Soft acids can be better compared using Et_3PE (E = S, Se)[254] or the *Childs* method, which measures the change of the chemical shift in the ^{1}H NMR spectrum of *trans*-crotonaldehyde.[255] It was observed that many of these methods give qualitative orderings, but do not yield quantitative correlation with e.g. calorimetry[255] or cyclic voltammetry.[256]

Global Lewis acidity is derived from the aforementioned IUPAC definition of Lewis acidity. It analyzes the thermodynamic properties, i.e. changes in enthalpy (ΔH) or

Gibbs energy (Δ*G*), of the adduct formation with a given Lewis base. The best-known example is the fluoride ion affinity (FIA), in which the reaction energy of the respective Lewis acid with a fluoride ion is determined from spectroscopic data[257] or quantum-chemical calculations.[247,258] For the latter, isodesmic calculations are performed using either the COF_2[259] or Me_3SiF[247] anchor system, which have well-known FIA values obtained experimentally or by high-level quantum-chemical calculations, respectively. In this way, the difficult description of a 'naked' fluoride ion is circumvented. The advantage of this method is the general possibility to calculate the FIA of any Lewis acid, yet it also has some drawbacks. The fluoride ion is a very hard base, leading to an underestimation of rather soft acids, for which the hydride ion affinity was demonstrated to be more useful.[247] Furthermore, it was recently pointed out that the results are strongly dependent on the used method, and that the inclusion of solvent effects can have a distinct influence on the FIA value.[258]

All in all, there are a variety of methods to determine and scale Lewis acidity, but a quantitative measure is yet to be found. Even a qualitative ordering is difficult, since two methods might give contradicting results, especially when they focus on different aspects of Lewis acidity.[66] However, with the field of strong Lewis acids constantly growing, several somewhat arbitrary definitions of the border for Lewis superacidity have been proposed. *Olah* defined superacids as those that are stronger than anhydrous $AlCl_3$, the catalyst for the aforementioned *Friedel-Crafts* alkylation.[260] A more recent and widely used definition was given by *Krossing*, stating that Lewis superacids are those species with a higher FIA than monomeric SbF_5 in the gas phase.[261] Since SbF_5 is toxic, corrosive and reacts with moisture to form HF,[262] similar to other highly Lewis acidic binary fluorides like BF_3[263] or AuF_5,[28] its applicability in organic chemistry is limited. In the last decades, a variety of Lewis superacids have been prepared with C-, N-, or O-donor ligands, i.e. $B(4\text{-}CF_3\text{-}C_6F_4)_3$,[264] $Al[N(C_6F_5)_2]_3$,[265] and $Al(OTeF_5)_3$[266] (see Figure 3) which are easier to handle and less harmful.[66] The latter, as well as AuF_5, cannot be isolated in monomeric form, but is stabilized by donor ligands or forms dimers.[28,266]

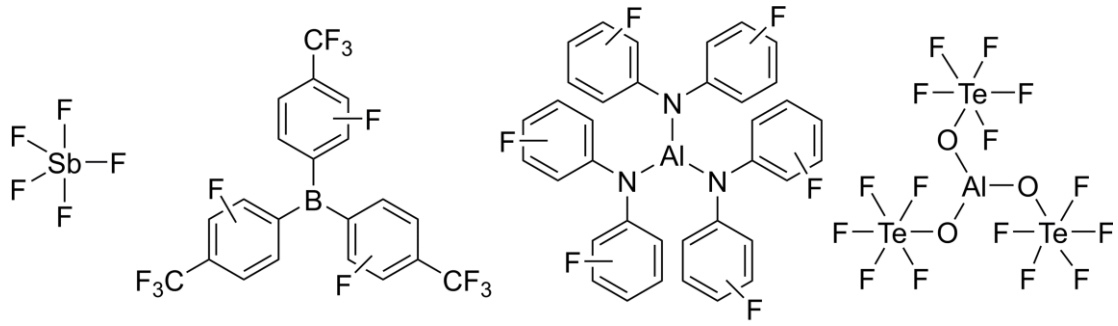

FIA	493	499	555	591

Figure 3: Selected examples of Lewis superacids and their FIA values in kJ·mol^{-1}, calculated at the RI-BP86/def-SV(P) level of theory.[247,264–266]

2 Objectives

Fluorido organo gold complexes play a distinct role in gold-mediated and -catalyzed reactions. A variety of mono- or difluorido organo gold complexes was prepared, typically by oxidative addition of organo gold complexes or halogen exchange reactions from chlorido organo gold complexes.[104,105] The first trifluorido organo gold complex, [AuF_3(SIMes)], was recently obtained by a different approach, namely by stabilization of the monomeric form of the binary gold fluoride AuF_3 by direct coordination of the *N*-heterocyclic carbene SIMes.[203] [AuF_3(SIMes)] is stable in organic solvents and has shown a selective substitution of the fluorido ligand in *trans* position to SIMes by Cl and the $OTeF_5$ group.[204]

The aim of this thesis was to perform an in-depth investigation of the introduction of organic molecules into [AuF_3(SIMes)]. By exploitation of the lability of the fluorido ligand in *trans* position to SIMes, a variety of C-, N-, and O-donor ligands with different electronic properties should be introduced. The effects of the substitution on the Lewis acidity of the gold center should be studied spectroscopically and by quantum-chemical calculations.

The pentafluoroorthotellurate (teflate) group is considered to be a sterically demanding analogue of the fluoride in terms of electron-withdrawing properties.[51,52] Hence, it can be used to stabilize elements in high oxidation states.[55] While teflate compounds with main group elements have been extensively studied, the properties of transition metal teflate complexes are much less explored. The only known gold teflate, $Au(OTeF_5)_3$, was synthesized by a sophisticated procedure starting from AuF_3, which is a polymer in the solid state, and $B(OTeF_5)_3$.[62] $Au(OTeF_5)_3$ was characterized by X-ray diffraction, revealing a dimeric structure, but no further studies of this compound were performed.

Therefore, the second aim of this work was to develop an improved synthetic procedure for $Au(OTeF_5)_3$ and to study its reactivity and Lewis acidity. This way, more information on the analogy between fluoride and teflate in transition metal chemistry should be obtained. Furthermore, the so-far unknown $[Au(OTeF_5)_4]^-$ anion should be synthesized in order to widen the scope of gold teflate complexes.

3 Publications

3.1 Trifluoromethylation of [AuF$_3$(SIMes)]: Preparation and Characterization of [Au(CF$_3$)$_x$F$_{3-x}$(SIMes)] (x = 1–3) Complexes

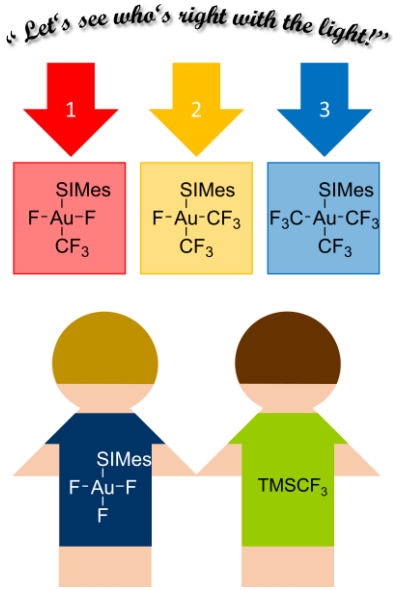

Marlon Winter, Niklas Limberg, Mathias A. Ellwanger, Alberto Pérez-Bitrián, Karsten Sonnenberg, Simon Steinhauer, and Sebastian Riedel.

Chem. Eur. J. **2020**, *26*, 16089.

https://doi.org/10.1002/chem.202002940

Author contributions

Marlon Winter designed the project, performed the majority of the experiments, as well as quantum-chemical calculations, and wrote the manuscript. Niklas Limberg performed some of the experiments during his Bachelor's thesis and research internship under the supervision of Marlon Winter. Mathias A. Ellwanger gave scientific advice, helped with the quantum-chemical calculations and revised the manuscript. Alberto Pérez-Bitrián gave scientific advice, offered starting material for the [Au(CF$_3$)$_3$(NCMe)] reagent and revised the manuscript. Karsten Sonnenberg and Simon Steinhauer measured and refined the crystal structures. Sebastian Riedel supervised the project and revised the manuscript.

Chemistry–A European Journal | Full Paper
doi.org/10.1002/chem.202002940

Organometallic Chemistry | *Hot Paper*

Trifluoromethylation of $[AuF_3(SIMes)]$: Preparation and Characterization of $[Au(CF_3)_xF_{3-x}(SIMes)]$ ($x = 1–3$) Complexes

Marlon Winter,[a] Niklas Limberg,[a] Mathias A. Ellwanger,[a] Alberto Pérez-Bitrián,[a, b] Karsten Sonnenberg,[a] Simon Steinhauer,[a] and Sebastian Riedel*[a]

Abstract: Trifluoromethylation of $[AuF_3(SIMes)]$ with the Ruppert–Prakash reagent $TMSCF_3$ in the presence of CsF yields the product series $[Au(CF_3)_xF_{3-x}(SIMes)]$ ($x = 1–3$). The degree of trifluoromethylation is solvent dependent and the ratio of the species can be controlled by varying the stoichiometry of the reaction, as evidenced from the ^{19}F NMR spectra of the corresponding reaction mixtures. The molecular structures in the solid state of *trans*-$[Au(CF_3)F_2(SIMes)]$ and $[Au(CF_3)_3(SIMes)]$ are presented, together with a selective route for the synthesis of the latter complex. Correlation of the calculated SIMes affinity with the carbene carbon chemical shift in the ^{13}C NMR spectrum reveals that *trans*-$[Au(CF_3)F_2(SIMes)]$ and $[Au(CF_3)_3(SIMes)]$ nicely follow the trend in Lewis acidities of related organo gold(III) complexes. Furthermore, a new correlation between the $Au–C_{carbene}$ bond length of the molecular structure in the solid state and the chemical shift of the carbene carbon in the ^{13}C NMR spectrum is presented.

Introduction

Fluorido organo gold complexes are highly reactive species which take part in a large variety of gold-catalyzed or -mediated reactions.[1,2] Their reactivity derives from the relatively low Au–F bond dissociation energy compared to many other known E–F (E = element) bonds.[3] Due to the lack of synthetic routes, their study and application in catalysis was scarce until recent years,[1,2] when it was shown that the corresponding fluorido organo gold species can be synthesized in situ. Typical synthetic routes are the oxidation of organo gold(I) complexes with XeF_2[4] or Selectfluor®,[5] but fluorination of organo gold(I) complexes with $Et_3N{\cdot}3\,HF$[6] has also been used. Despite their utility in organometallic reactions, the high reactivity of fluorido gold complexes limits their isolation and characterization.[2,7] However, isolation of some derivatives has been reported, either from more accessible halido gold complexes through X/F exchange reactions (X = Cl, Br, I)[8,9,10] or by oxidation with XeF_2.[11,12]

N-Heterocyclic carbene (NHC) ligands have attracted increasing attention for the stabilization of highly reactive compounds, for example, complexes that contain transition metals in high oxidation states, due to their steric demand and strong σ-donating properties.[13] Recently, our group reported on the stabilization of AuF_3 using the SIMes (1,3-bis(2,4,6-trimethylphenyl)-4,5-dihydroimidazol-2-ylidene) ligand.[14] The resulting complex $[AuF_3(SIMes)]$ contains the highly Lewis acidic AuF_3 unit in monomeric form and is stable in common organic solvents such as dichloromethane. This is contrary to AuF_3, which is a fluorine-bridged polymer in the solid state and reacts unselectively and sometimes violently with most organic solvents.[15]

The small size and high electronegativity of fluorine leads to significantly changed properties of a compound when fluorine atoms are introduced.[16–18] The increased lipophilicity and stability of fluorinated organic compounds compared to non-fluorinated ones make them useful in a wide range of applications in pharmaceutical[19] and agrochemical[20] industries. The smallest perfluorinated organic moiety is the trifluoromethyl group, which exhibits an increased electron withdrawing property based on its high group electronegativity, which is similar to that of chlorine.[21] However, the selective introduction of CF_3 groups into organic molecules is still challenging.[17,18]

An interesting synthetic approach is the metal-mediated C–CF_3 bond formation, a field where gold complexes have played an increasing role since the last decade.[9,24–27] Since the preparation of the first trifluoromethyl gold complex, $[Au(CF_3)Me_2(PMe_3)]$ in 1973,[28] a limited number of such complexes with gold in oxidation states +I, +II and +III have been synthesized.[29] Several synthetic strategies have been es-

[a] M. Winter, N. Limberg, Dr. M. A. Ellwanger, Dr. A. Pérez-Bitrián, Dr. K. Sonnenberg, Dr. S. Steinhauer, Prof. Dr. S. Riedel
Fachbereich Biologie, Chemie, Pharmazie
Institut für Chemie und Biochemie—Anorganische Chemie
Fabeckstr. 34/36, 14195 Berlin (Germany)
E-mail: s.riedel@fu-berlin.de

[b] Dr. A. Pérez-Bitrián
On leave from: Instituto de Síntesis Química y Catálisis Homogénea (iSQCH)
CSIC-Universidad de Zaragoza
C/ Pedro Cerbuna 12, 50009 Zaragoza (Spain)

Supporting information and the ORCID identification number(s) for the author(s) of this article can be found under: https://doi.org/10.1002/chem.202002940.

Chemistry–A European Journal | Full Paper doi.org/10.1002/chem.202002940 | Chemistry Europe European Chemical Societies Publishing

tablished for their preparation (see Scheme 1). They include the oxidative addition of CF_3I to organo gold(I) complexes,[10,22,24,28–31] and transmetallation reactions of halido organo gold compounds with $Cd(CF_3)_2$·DME (DME = 1,2-dimethoxyethane)[22,31,32] or of halido or alkoxido organo gold complexes with the Ruppert–Prakash reagent trimethyl(trifluoromethyl)silane ($TMSCF_3$) in the presence of a nucleophilic fluoride source when required.[23,26,33–36] Reactions of $[Au(CN)_4]^-$ with ClF in CH_2Cl_2[37] and $[Au(CN)_2]^-$ with $[ClF_4]^-$ in $CHFCl_2$[38] were not selective and yielded several products that could not be isolated. Reactions of gold vapors with $^{\bullet}CF_3$ radicals[39] or CF_3X (X = Br, I)[40] were also reported, but are of little synthetic use. The increasing interest in trifluoromethyl gold complexes led to studies on their usage in gold-mediated C–E (E = C, N, Hal.) bond formations and on further functionalizations of these complexes over the last decade.[9,10,12,24–27,29,33–36,41,42] Despite the variety of known trifluoromethyl gold complexes, only four complexes containing trifluoromethyl and fluorido ligands at the same gold center have been isolated, namely $[Au(CF_3)(4\text{-}CH_3\text{–}C_6H_4)F(PPh_3)]$,[9] $[Au(CF_3)(4\text{-}F\text{–}C_6H_4)F(PCy_3)]$,[9] $[PPh_4][Au(CF_3)_3F]$[10] and $[PPh_4][trans\text{-}Au(CF_3)_2F_2]$[12] (see Scheme 2). In addition, the series of $[Au(CF_3)_xF_{4-x}]^-$ anions (x = 1–3) and other chlorido fluorido trifluoromethyl gold anions,[37] as well as the $[cis\text{-}Au(CF_3)(CN)F_2]^-$ anion[38] were detected by ^{19}F NMR spectroscopy. Those complexes can be of interest for further studies on gold-mediated or -catalyzed coupling reactions.

Herein, we report on the synthesis and characterization of the hitherto unknown series $[Au(CF_3)_xF_{3-x}(SIMes)]$ (x = 1–3) by the trifluoromethylation of $[AuF_3(SIMes)]$. $[Au(CF_3)_3(SIMes)]$ was isolated and the molecular structures in the solid state of *trans*-$[Au(CF_3)F_2(SIMes)]$ and $[Au(CF_3)_3(SIMes)]$ will be discussed. These complexes represent the first fluorido trifluoromethyl gold complexes which are prepared by the trifluoromethylation of fluorido gold complexes and not vice versa (cf. Scheme 2).

Sanner et al., 1989

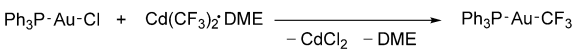

Usui et al., 2000

Winston et al., 2014

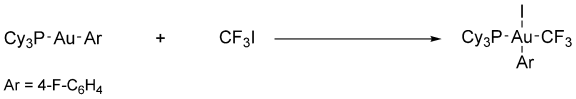

Scheme 1. Overview of the different literature-known pathways for the preparation of trifluoromethyl gold complexes.[22–24]

Winston et al., 2015

Peréz-Bitrián et al., 2017

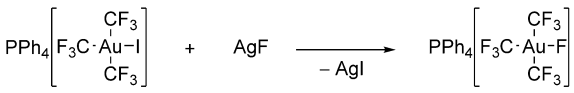

Peréz-Bitrián et al., 2018

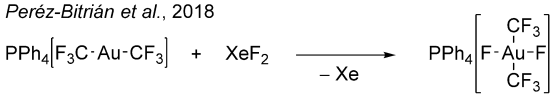

Scheme 2. Overview of the preparation of the four literature-known, isolated fluorido trifluoromethyl gold complexes.[9,10,12]

Results and Discussion

The molecular structure of $[AuF_3(SIMes)]$ in the solid state reveals that the Au–F bond with the fluorido ligand in *trans* position to the SIMes ligand is about 5 pm longer than those to the *cis*-fluorido ligands.[14] In accordance with this finding, a selective substitution of the *trans*-fluorido ligand by a chlorido or a pentafluoridoorthotellurato ($OTeF_5$) ligand was recently reported by us.[43] Hence, the trifluoromethylation of $[AuF_3(SIMes)]$ is expected to yield *trans*-$[Au(CF_3)F_2(SIMes)]$ (**1**). Indeed, when $TMSCF_3$ is condensed into a DCM solution of $[AuF_3(SIMes)]$ at −80 °C in the presence of the nucleophilic fluoride source CsF, compound **1** is formed. ^{19}F NMR spectroscopy investigations show that first only compound **1** is formed, but during the consumption of $[AuF_3(SIMes)]$, a second substitution reaction of a fluorido ligand by a trifluoromethyl group is observed, forming *cis*-$[Au(CF_3)_2F(SIMes)]$ (**2**) in solution (cf. Scheme 3). After a few hours, no $[AuF_3(SIMes)]$ is left and the ratio of the products stays constant for several days, even though unreacted $TMSCF_3$ is left in the reaction mixture (see Supporting Information, Figures S9–S15). Therefore, the reaction proceeds rather fast and the reaction time does not have a relevant influence on the product ratio. Instead, the stoichiometry of the reactants has a decisive impact on the ratio between **1** and **2**. As expected, the formation of *trans*-$[Au(CF_3)F_2(SIMes)]$ (**1**) is favored by ≈0.5 equivalents of $TMSCF_3$, while an excess of $TMSCF_3$ increases the amount of *cis*-$[Au(CF_3)_2F(SIMes)]$ (**2**), as shown in Table 1. HCF_3 and *trans*-$[AuClF_2(SIMes)]$ are formed as by-products, the presence of the former being probably due to side reactions of the highly basic transient CF_3^- anion with any proton sources, for example, from the solvent,[44,45,46] while the latter is formed by a chlorine/fluorine exchange reaction between $[AuF_3(SIMes)]$ and DCM, possibly promoted by the fluoride anions of CsF.[14] The amount of by-products depends on the stoichiometry. The more $TMSCF_3$ is used, the more HCF_3 is formed, while less

Chemistry–A European Journal | Full Paper doi.org/10.1002/chem.202002940 | Chemistry Europe European Chemical Societies Publishing

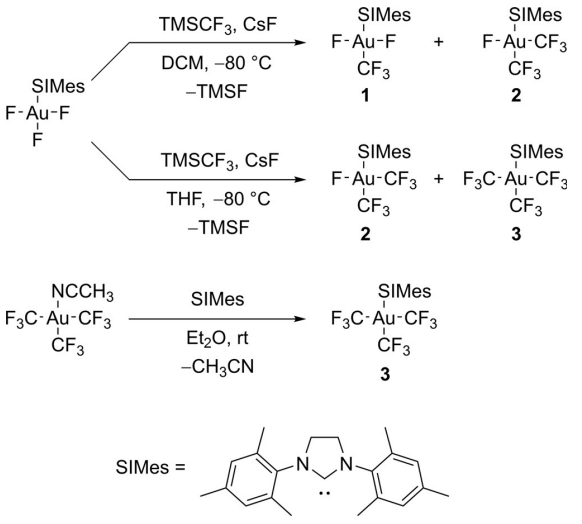

Scheme 3. Reaction scheme for the preparation of the target compounds *trans*-[Au(CF_3)F_2(SIMes)] (**1**), *cis*-[Au(CF_3)$_2$F(SIMes)] (**2**) and [Au(CF_3)$_3$(SIMes)] (**3**). They can be prepared by trifluoromethylation of [AuF_3(SIMes)] in DCM (top) and THF (middle), and compound **3** can also be prepared by ligand substitution of [Au(CF_3)$_3$($NCCH_3$)] (bottom). In case of the trifluoromethylation, the outcome of the reaction depends on the solvent. In either case, the product ratio can be controlled by the stoichiometry of the reactants, see Table 1 and Table 2 for DCM and THF, respectively.

Table 1. Product ratio dependence of the stoichiometric factors in the reaction between [AuF_3(SIMes)] and $TMSCF_3$ in DCM determined by the integral ratios of the signals in the ^{19}F NMR spectra (see Supporting Information, Figures S9–S15). Note that the amount of $TMSCF_3$ can slightly deviate from the values listed in the table, due to the inherent uncertainty of the used manometer for determining the pressure of $TMSCF_3$.

eq. ([AuF_3(SIMes)])	eq. ($TMSCF_3$)	*trans*-[Au(CF_3) : *cis*-[Au(CF_3)$_2$ F_2(SIMes)] (**1**) : F(SIMes)] (**2**)
1	0.5	7 : 1
1	1	2 : 1
1	5	1 : 1

[AuClF_2(SIMes)] is present (see Supporting Information, Figures S10, S13 and S15). Compounds **1** and **2** partially decompose in solution at room temperature within a few days, leading to the formation of elemental gold. However, the ^{19}F NMR spectra still show signals of the products after several weeks.

If the trifluoromethylation of [AuF_3(SIMes)] is performed in THF, compound **1** is not observed in the ^{19}F NMR spectrum of the reaction mixture. Instead, compound **2** and the three times substituted complex [Au(CF_3)$_3$(SIMes)] (**3**) are formed (cf. Scheme 3). The reason for the formation of higher substituted products in THF is most likely the better solubility of CsF in THF compared to DCM. This leads to an enhanced activation of the $TMSCF_3$ forming a pentacoordinated silicon(IV) anion, which acts as a highly potent CF_3 transfer reagent, as shown by Naumann et al.[46] In contrast to the reaction in DCM, no $TMSCF_3$ is left in the reaction mixture after a few hours (see Supporting Information, Figures S16 and S17). The stoichiometry of the reactants has a significant influence on the product ratio. When [AuF_3(SIMes)] and $TMSCF_3$ are used in roughly a 1:1 ratio, compounds **2** and **3** are formed in almost equal amounts. If only about half an equivalent of $TMSCF_3$ is used, five times more **2** than **3** is formed (cf. Table 2). The transfer of two or three CF_3 groups, even though not more than one equivalent of $TMSCF_3$ is used, can most likely be explained by the lower solubility of [AuF_3(SIMes)] in THF. Furthermore, the formation of HCF_3 and the [Au(CF_3)$_4$]$^-$ anion as by-products is observed, which increases with the amounts of $TMSCF_3$ (see Supporting Information, Figures S16 and S17). The existence of the former is probably due to a reaction of the highly basic CF_3^- anion, which is abstracted from the pentacoordinated silicon(IV) anion, with proton sources in the reaction mixture,[44,46] while the latter is possibly formed by the trifluoromethylation of traces of the [AuF_4]$^-$ anion.

[Au(CF_3)$_3$(SIMes)] can be isolated via a different route, starting from the literature-known complex [Au(CF_3)$_3$($NCCH_3$)][42] by substitution of the acetonitrile ligand with SIMes. A room temperature solution of **3** in DCM or THF is stable for several weeks. In pure form, compound **3** can be stored under an argon atmosphere at room temperature for months and it is stable under air for several days without decomposition. The synthetic routes for the preparation of the target compounds *trans*-[Au(CF_3)F_2(SIMes)] (**1**), *cis*-[Au(CF_3)$_2$F(SIMes)] (**2**) and [Au(CF_3)$_3$(SIMes)] (**3**) are summarized in Scheme 3 and an overview on the chemical shifts in the ^{19}F NMR spectra, which will be discussed below, is given in Table 3.

Table 2. Product ratio dependence of the stoichiometric factors in the reaction between [AuF_3(SIMes)] and $TMSCF_3$ in THF determined by the integral ratios of the signals in the ^{19}F NMR spectra (see Supporting Information, Figures S16 and S17). Note that the amount of $TMSCF_3$ can slightly deviate from the values listed in the table, due to the inherent uncertainty of the used manometer for determining the pressure of $TMSCF_3$.

eq. ([AuF_3(SIMes)])	eq. ($TMSCF_3$)	*cis*-[Au(CF_3)$_2$: [Au(CF_3)$_3$ F(SIMes)] (**2**) : (SIMes)] (**3**)
1	0.5	5 : 1
1	1	1 : 1

Table 3. ^{19}F NMR spectroscopic data of the target compounds *trans*-[Au(CF_3)F_2(SIMes) (**1**), *cis*-[Au(CF_3)$_2$F(SIMes)] (**2**) and [Au(CF_3)$_3$(SIMes)] (**3**). The subscripts c and t stand for CF_3 groups in *cis* or *trans* position to the SIMes ligand, respectively.[a]

Compound	$\delta(CF_{3,c})$	$\delta(CF_{3,t})$	δ(F)	$^3J(^{19}F,^{19}F)$, *cis*	$^3J(^{19}F,^{19}F)$, *trans*	$^4J(^{19}F,^{19}F)$
trans-[Au(CF_3)F_2(SIMes)] (**1**)		−46.5	−329.7	18		
cis-[Au(CF_3)$_2$F(SIMes)] (**2**)	−23.9	−41.2	−254.0	14	57	7
[Au(CF_3)$_3$(SIMes)] (**3**)	−31.5	−34.3				7

[a] Chemical shifts are given in ppm and coupling constants in Hz.

Chemistry–A European Journal | Full Paper doi.org/10.1002/chem.202002940 | Chemistry Europe European Chemical Societies Publishing

The ^{19}F NMR spectrum of *trans*-[$Au(CF_3)F_2$(SIMes)] (**1**) shows a triplet at −46.5 ppm and a quartet at −329.7 ppm with a $^3J(^{19}F,^{19}F)$ coupling constant of 18 Hz, which correspond to the trifluoromethyl and the two fluorido ligands, respectively (see Figure 1). The former resonance is in the upfield range of chemical shifts of the corresponding trifluoromethyl groups in literature-known fluorido trifluoromethyl gold(III) complexes[9,10,12,37] and almost identical to the one in the [*trans*-$Au(CF_3)_2F_2]^-$ anion ($\delta = -46.2$ ppm).[12] The latter is 4 ppm −19 ppm upfield shifted compared to the *cis*-fluorido ligands in the literature-known *trans*-[AuF_2X(SIMes)] (X = Cl, F, $OTeF_5$) complexes.[14,43] An interesting feature of metal complexes with NHC ligands is the chemical shift of the carbene carbon atom in the ^{13}C NMR spectra, which was proven to be a measure of the Lewis acidity of the metal center.[14,43,47] In the $^1H,^{13}C$ HMBC NMR spectrum of **1**, the resonance of the carbene carbon atom was detected at 192.3 ppm, which is 26 ppm −45 ppm downfield shifted compared to the literature-known *trans*-[AuF_2X(SIMes)] (X = Cl, F, $OTeF_5$)[14,43] complexes (cf. Table 4) due to the weaker Lewis acidity of the gold center in compound **1**. This is in good agreement with the corresponding Au–$C_{carbene}$ bond lengths in the solid state and the calculated dissociation energy of the Au–$C_{carbene}$ bond, as discussed in detail below.

Single crystals of compound **1** suitable for X-ray diffraction were obtained by slow vapor diffusion of *n*-pentane at 5 °C into a DCM solution of the reaction between [AuF_3(SIMes)] and $TMSCF_3$. Compound **1** crystallizes in the orthorhombic space group *Pnma* with a square planar coordination around the gold center (see Figure 2). The Au–F bond lengths (193.2(5) pm, 193.2(10) pm) are comparable to the corresponding Au–F bond lengths in the starting compound [AuF_3(SIMes)] (191.6(1) pm, 192.1(1) pm).[14] The Au–CF_3 bond length (203.6(10) pm) is similar to those in the literature-known anion *trans*-[$Au(CF_3)_2F_2]^-$ (205.5(5) pm, 205.3(5) pm)[12] and of the corresponding Au–CF_3 bond in the neutral isocyanide complex [$Au(CF_3)_3(CNC(CH_3)_3)$] (205.8(5) pm).[42] The Au–$C_{carbene}$ bond length (203.5(9) pm) is slightly elongated compared to *trans*-[$AuClF_2$(SIMes)] (200.8(3) pm),[43] [AuF_3(SIMes)] (197.3(1) pm)[14] and *trans*-[$AuF_2(OTeF_5)$(SIMes)] (196.9(5) pm).[43] This trend can be explained by the strong *trans*-influence of the CF_3 group, which is discussed in detail below (cf. Table 4 and Figure 7).

The ^{19}F NMR spectrum of *cis*-[$Au(CF_3)_2F$(SIMes)] (**2**) (see Figure 3) consists of two doublets of quartets at −23.9 ppm and −41.2 ppm, where the latter appears to be a sextet due to the coupling constants of 7 Hz and 14 Hz, and a quartet of quartets at −254.0 ppm in an integral ratio of 3:3:1. The latter resonance belongs to the remaining fluorido ligand, while the two other signals are due to the two chemically inequivalent

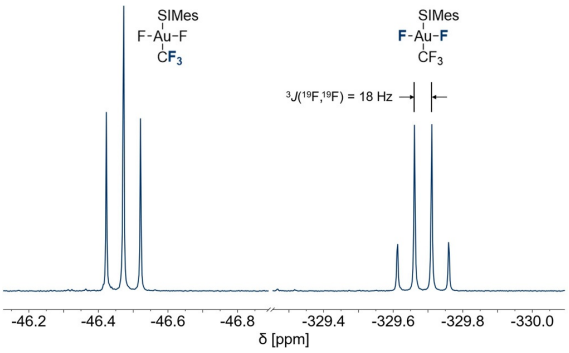

Figure 1. ^{19}F NMR spectrum (377 MHz, CD_2Cl_2, 20 °C) of *trans*-[$Au(CF_3)_2F_2$(SIMes)] (**1**).

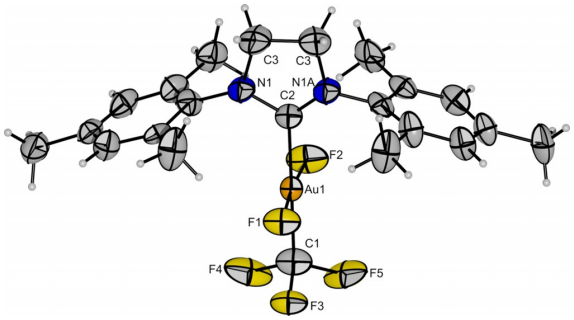

Figure 2. Molecular structure of *trans*-[$Au(CF_3)_2F_2$(SIMes)] in the solid state. Disorders of the SIMes ligand and the CF_3 group are omitted for clarity (cf. Supporting Information, Figure S1). Thermal ellipsoids are set at 50% probability. Bond lengths [pm] to the central gold atom: 193.2(5) (F1–Au1), 193.2(10) (F2–Au1), 203.6(10) (C1–Au1), 203.5(9) (C2–Au1).

Table 4. Comparison of the calculated SIMes affinities ($-\Delta_r G_{diss}$), gold carbon distances in the molecular structures in the solid state (r(Au–$C_{carbene}$)) and chemical shifts of the carbene carbon atoms in the ^{13}C NMR spectra ($\delta(^{13}C_{carbene})$ of *trans*-[$Au(CF_3)_2F_2$(SIMes)] (**1**) and similar, literature-known compounds.

Compound	$-\Delta_r G_{diss}$ [kJ mol^{-1}]	r(Au–$C_{carbene}$) [pm]	$\delta(^{13}C_{carbene})$ [ppm]
trans-[$Au(CF_3)_2F_2$(SIMes)] (**1**)	251	203.5(9)	192
trans-[$AuClF_2$(SIMes)]	342	200.8(3)	166
[AuF_3(SIMes)]	405	197.3(1)	152
trans-[$AuF_2(OTeF_5)$(SIMes)]	432	196.9(5)	149

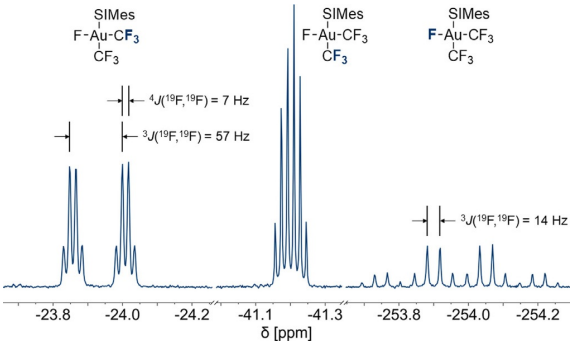

Figure 3. ^{19}F NMR spectrum (377 MHz, CD_2Cl_2, 20 °C) of *cis*-[$Au(CF_3)_2F$(SIMes)] (**2**).

Chemistry–A European Journal | Full Paper doi.org/10.1002/chem.202002940 | Chemistry Europe European Chemical Societies Publishing

CF_3 groups. The chemical shifts are all similar to the literature-known $[Au(CF_3)_3F]^-$ anion.[10] The $^3J(^{19}F,^{19}F)$ coupling constants between the fluorine nuclei of the trifluoromethyl groups and the fluorido ligand are 57 Hz and 14 Hz for the signals at −23.9 ppm and −41.2 ppm, respectively. It is known that *trans* coupling constants are usually larger than *cis* coupling constants,[37] for example, in the $[Au(CF_3)_3F]^-$ anion, the coupling constants are 55.8 Hz (*trans*) and 12.3 Hz (*cis*).[10] Furthermore, the coupling constant of 14 Hz is in good agreement with the $^3J(^{19}F,^{19}F)$ *cis* coupling in **1** (18 Hz) and the literature-known *trans*-$[Au(CF_3)_2F_2]^-$ anion (16.5 Hz).[12] Therefore, the signals at −23.9 ppm and −41.2 ppm can be assigned to the CF_3 groups *cis* and *trans* to the carbene ligand, respectively (cf. Figure 3 and Table 3).

Figure 4 shows the ^{19}F NMR spectrum of $[Au(CF_3)_3(SIMes)]$ (**3**), which consists of a quartet at −31.5 ppm and a septet at −34.3 ppm with an integral ratio of 2:1. The quartet belongs to the two *trans*-positioned CF_3 groups and the septet to the CF_3 group in *trans*-position to the SIMes ligand. The coupling constant of 7 Hz is identical to the $^4J(^{19}F,^{19}F)$ coupling constant of the two CF_3 groups in compound **2** and fits nicely within the range of neutral complexes containing the $Au(CF_3)_3$ fragment prepared by Menjón et al. (6.0–7.5 Hz).[42] Compared to the acetonitrile complex $[Au(CF_3)_3(NCCH_3)]$, which was used as a starting material for the selective synthesis of compound **3**, the relative position of the two resonances are interchanged.[42] In the $^1H,^{13}C$ HMBC NMR spectrum, the resonance of the carbene carbon atom in compound **3** is observed at 191.4 ppm, which is only 1 ppm upfield shifted compared to compound **1**, and thus points towards a similar Lewis acidity (cf. discussion below).

In order to obtain single crystals of compound **3** suitable for X-ray diffraction, a pure sample of **3** prepared by the reaction between $[Au(CF_3)_3(NCCH_3)]$ and SIMes was dissolved in dichloromethane, chloroform, acetone or tetrahydrofuran, and each of the solutions was layered by *n*-hexane at 5 °C. From all four solvents, compound **3** crystallizes in the monoclinic space group $P2_1/c$ with a square planar coordination around the gold center and contains half a co-crystallized, disordered solvent molecule. Since the four structures are homeotypic (see Supporting Information, Figures S3–S6), the following discussion is based on the structural data of $[Au(CF_3)_3(SIMes)]\cdot 0.5\ CH_2Cl_2$ (Figure 5). The Au–CF_3 bond lengths to the two CF_3 groups in *cis* position to the SIMes ligand (208.3(3) pm, 208.6(3) pm) are in the typical range for neutral $[Au(CF_3)_3L]$ complexes (207.4(9)–209.8(2) pm)[42] and similar to those in $[NBu_4][Au(CF_3)_4]$ (207.5(6) pm, 208.5(7) pm).[34] The Au–CF_3 bond length of the CF_3 group *trans* to the SIMes ligand (207.8(3) pm) is comparable to the other two Au–CF_3 bonds and in the upper range of neutral $[Au(CF_3)_3L]$ complexes (200.1(3)–209.0(3) pm).[42] The Au–C bond to the SIMes ligand (208.1(2) pm) is slightly longer than in compound **1** (203.5(9) pm; cf. Figure 2) and 3–11 pm longer than in other literature-known $[AuX_3(SIMes)]$ complexes (X = F, Cl, Br).[14,48] The elongation of this Au–C bond is due to the strong *trans*-influence of the CF_3 group compared to the halides,[49–51] which also explains why the Au–CF_3 bond lengths of the two *trans*-standing CF_3 groups are usually longer than that of the CF_3 group *trans* to the donor ligand in similar complexes.[42]

Recently, our group reported on the calculation and experimental access to the "SIMes affinity" of gold(III) moieties. Therein, the Gibbs free energy $\Delta_r G_{diss}$ of the dissociation of the SIMes ligand from $[AuF_2X(SIMes)]$ and $[AuX_3(SIMes)]$ complexes (X = Cl, F, $OTeF_5$) forming SIMes and the corresponding $[AuF_2X]$ or $[AuX_3]$ fragment on the RI-B3LYP-D3/def2-TZVPP level of theory at 0 °C were calculated.[43] This SIMes affinity can be correlated with the chemical shift of the carbene carbon atom in the ^{13}C NMR spectrum. We found a nearly linear relationship between an increase of the SIMes affinity and an upfield shift in the ^{13}C NMR spectrum.[43] We have now determined the SIMes affinities of *trans*-$[Au(CF_3)F_2(SIMes)]$ (**1**) and $[Au(CF_3)_3(SIMes)]$ (**3**) to be 251 kJ mol^{-1} and 240 kJ mol^{-1}, respectively. The corresponding complexes with Cl, F and/or $OTeF_5$ ligands exhibit significantly higher SIMes affinities, ranging from 300 kJ mol^{-1} to 430 kJ mol^{-1}. This trend is in accordance with the chemical shifts of the carbene carbon atom in the ^{13}C NMR spectra, as depicted in Figure 6. Theoretical studies show that a downfield shift of the carbene carbon atom in gold complexes results from a deshielding of the carbene

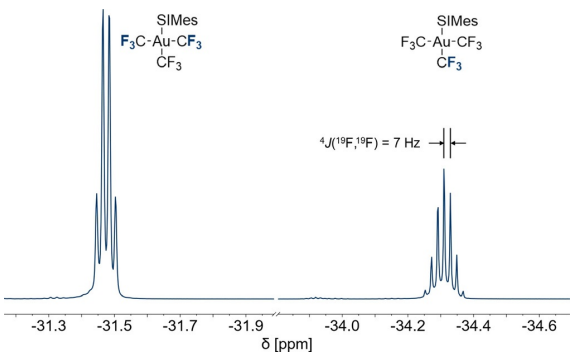

Figure 4. ^{19}F NMR spectrum (377 MHz, CD_2Cl_2, 21 °C) of $[Au(CF_3)_3(SIMes)]$ (**3**).

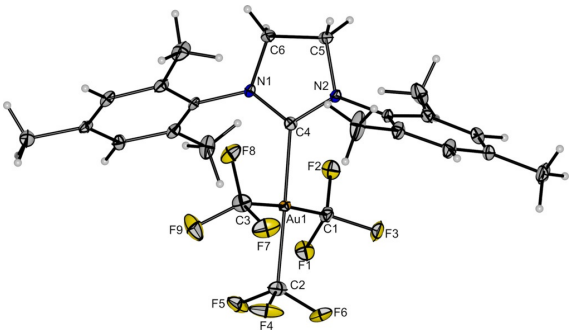

Figure 5. Molecular structure of $[Au(CF_3)_3(SIMes)]\cdot 0.5\ CH_2Cl_2$ in the solid state. The disordered CH_2Cl_2 molecule is omitted for clarity. Thermal ellipsoids are set at 50% probability. Bond lengths [pm] to the central gold atom: 208.6(3) (C1–Au1), 207.8(3) (C2–Au1), 208.3(3) (C3–Au1), 208.1(2) (C4–Au1).

Chemistry–A European Journal
Full Paper
doi.org/10.1002/chem.202002940
Chemistry Europe
European Chemical Societies Publishing

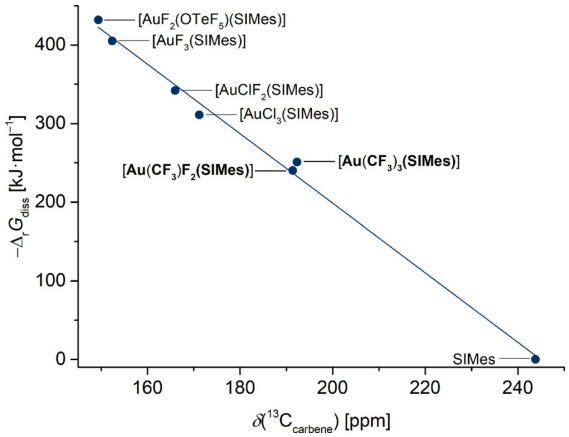

Figure 6. Correlation between the calculated SIMes affinity ($-\Delta_r G_{diss}$) with the chemical shifts of the carbene carbon atoms in the ^{13}C NMR spectra ($\delta(^{13}C_{carbene})$) of *trans*-[$Au(CF_3)F_2$(SIMes)] (**1**), [$Au(CF_3)_3$(SIMes)] (**3**) (both highlighted in bold) and similar, literature-known compounds.[43] The ^{13}C chemical shift of uncoordinated SIMes, which has by definition a SIMes affinity of 0 kJ mol^{-1}, is also included.[55]

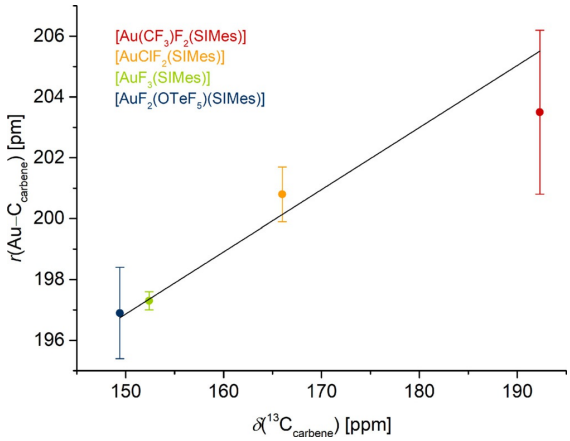

Figure 7. Correlation between the gold carbon distances (r(Au–$C_{carbene}$)) in the molecular structures in the solid state with the chemical shifts of the carbene carbon atoms in the ^{13}C NMR spectra ($\delta(^{13}C_{carbene})$) of *trans*-[$Au(CF_3)F_2$(SIMes)] (**1**) (red) and similar, literature-known compounds. The error bars of the *y*-axis equal three times the estimated standard deviation (the error in the last digit written in brackets in Table 4).

carbon atom by ligands with a strong *trans*-influence.[52] Our results are in good agreement with the literature, where the trifluoromethyl group was determined to have a *trans*-influence in the order of the methyl group, which is one of the strongest *trans*-influencing ligands, and a much stronger *trans*-influence than the halides.[49–51,53] A recent study on hydrido gold(III) complexes showed that also the *cis*-influence can change the chemical shift.[54] However, this is not the case in our trifluoromethyl gold complexes, since compounds **1** and **3** have similar SIMes affinities and $^{13}C_{carbene}$ chemical shifts.

Regarding the series of [AuF_2X(SIMes)] complexes (X = CF_3, Cl, F, $OTeF_5$), the theoretically determined SIMes affinity is a good measure for the strength of the Au–$C_{carbene}$ bond, which is inversely proportional to the experimentally determined Au–$C_{carbene}$ bond length in the molecular structures in the solid state. Table 4 lists the SIMes affinities, gold carbon distances and ^{13}C chemical shifts of the carbene carbon atom in these complexes. Figure 7 shows the nearly linear relationship between the Au–$C_{carbene}$ bond length and the chemical shift of the carbene carbon atom, which underlines the use of the calculated Gibbs free energies as a measure of the strength of the Au–$C_{carbene}$ bond. The *trans*-influence rises in the order $OTeF_5 < F < Cl \ll CF_3$. In summary, the higher *trans*-influence of the CF_3 ligand in **1** leads to a lower Lewis acidity of the gold(III) center, resulting in a longer Au–$C_{carbene}$ bond length and a deshielding of the carbene carbon atom.

Conclusions

In summary, the trifluoromethylation of [AuF_3(SIMes)] with $TMSCF_3$ to result in unprecedented products of the series [$Au(CF_3)_xF_{3-x}$(SIMes)] (x = 1–3) in different solvents has been described, being the first synthetic route for those kind of complexes starting from fluorido gold complexes. When the reaction is performed in DCM, *trans*-[$Au(CF_3)F_2$(SIMes)] (**1**) and *cis*-[$Au(CF_3)_2F$(SIMes)] (**2**) are formed, while the reaction in THF yields a mixture of *cis*-[$Au(CF_3)_2F$(SIMes)] (**2**) and [$Au(CF_3)_3$(SIMes)] (**3**). In both cases, the product ratio does not change significantly with longer reaction times, but it can be controlled by the stoichiometry of the reaction, as evidenced by the ^{19}F NMR spectra. More $TMSCF_3$ leads to a larger amount of the higher-substituted product. Furthermore, for the selective preparation of compound **3**, an alternative synthetic route starting from [$Au(CF_3)_3(NCCH_3)$] is described. The ^{13}C NMR shifts of the carbene carbon atoms in compounds **1** and **3** can be correlated with the calculated dissociation energies of the Au–$C_{carbene}$ bond, revealing a significantly lower Lewis acidity compared to literature-known [AuF_2X(SIMes)] or [AuX_3(SIMes)] complexes (X = Cl, F, $OTeF_5$). These dissociation energies are in accordance with the trend in the Au–$C_{carbene}$ bond lengths in the [AuF_2X(SIMes)] series. This article offers a new synthetic route to the rare group of fluorido trifluoromethyl gold(III) complexes which could find interesting properties for gold-mediated coupling reactions.

Experimental Section

CAUTION! Strong Oxidizers! All reactions should be performed under strictly anhydrous conditions. The combination of AuF_3 with organic materials can lead to violent reactions. On contact with only small amounts of moisture, all used fluoride-containing compounds decompose under the formation of HF. Therefore, appropriate treatment procedures should be available in case of a contamination with HF-containing solutions.

Materials, chemicals and procedures: All experiments were performed under rigorous exclusion of air and moisture using standard Schlenk techniques. All solids were handled in an MBRAUN UNIlab plus glovebox with an argon atmosphere (O_2 < 0.5 ppm,

Chemistry–A European Journal | Full Paper doi.org/10.1002/chem.202002940 | Chemistry Europe European Chemical Societies Publishing

$H_2O < 0.5$ ppm). Solvents were dried using freshly ground CaH_2 in case of CH_2Cl_2, $CHCl_3$, CD_2Cl_2 and *ortho*-difluorobenzene, SICAPENT® in case of CH_3CN, potassium in case of Et_2O and sodium in case of THF, *n*-pentane and *n*-hexane. Acetone was distilled prior to use. All solvents were stored over 4 Å molecular sieves, except for CH_3CN, which was stored over 3 Å molecular sieves. AuF_3,[56] 1,3-bis(2,4,6-trimethylphenyl)-4,5-dihydroimidazol-2-ylidene (SIMes)[57] and $[Au(CF_3)_3(NCCH_3)]$[42] were prepared using literature-known methods. Raman spectra were recorded at room temperature using a Bruker MultiRAM FT-Raman spectrometer with a 1064 nm wavelength ND:YAG laser. The spectra were measured directly inside the reaction flask with a laser power of 30 mW and 64 scans with a resolution of 2 cm^{-1}. IR spectra were measured at room temperature inside a glovebox under argon atmosphere using a Bruker ALPHA FTIR spectrometer with a diamond ATR attachment with 32 scans and a resolution of 4 cm^{-1}. Raman and IR spectra were processed using OPUS 7.5 and Origin 9.1[58] was used for their graphical representation. NMR spectra were recorded using a JEOL 400 MHz ECZ or ECS spectrometer and all chemical shifts are referenced as defined in the IUPAC recommendations of 2001.[59] MestReNova 14.0 was used to process the spectra and for their graphical representation. X-ray diffraction measurements were performed on a Bruker D8 Venture with MoK_α ($\lambda =$ 0.71073 nm) radiation at 100 K. Single crystals were picked in perfluoroether oil at 0 °C under nitrogen atmosphere and mounted on a 0.15 mm Mitegen micromount. They were solved using the ShelXT[60] structure solution program with intrinsic phasing and were refined with the refinement package ShelXL[61] using least squares minimizations by using the program OLEX2.[62] Diamond 3 and POV-Ray 3.7 were used for their graphical representation. Quantum chemical calculations were performed using the functional B3LYP[63] with RI[64] and Grimme-D3[65] and the basis set def2-TZVPP[66] as incorporated in TURBOMOLE.[67]

Preparation of $[AuF_3(SIMes)]$: The synthesis of $[AuF_3(SIMes)]$ was based on a literature-known procedure[43] with slight deviations and upscaling of the synthesis. In a typical experiment, AuF_3 (400 mg, 1.58 mmol, 1 equiv.) and SIMes (483 mg, 1.58 mmol, 1 equiv.) were dissolved in dichloromethane (20 mL) and stirred for 30 minutes at −80 °C. *Ortho*-difluorobenzene (20 mL) was added and the mixture was stirred for 30 minutes at −80 °C. Volatiles were removed under reduced pressure at −40 °C until a dark grey precipitate was formed. The resulting yellowish solution was filtered off. *ortho*-Difluorobenzene (20 mL) was added to the solid residue, the mixture was stirred for 30 minutes at −40 °C and the solution was filtered off. This washing process was repeated until the filtrated solution was colorless (usually, three times were sufficient). Dichloromethane (20 mL) was added and the mixture was stirred for 30 minutes at −80 °C, yielding a dark solution. The mixture was filtered through a hydrophobic PTFE filter (0.2 µm). *ortho*-Difluorobenzene (20 mL) was added to the colorless solution, the mixture was stirred for 30 minutes at −80 °C and volatiles were removed at −40 °C until a colorless precipitate was formed. The colorless solution was filtered off and residual solvent was removed under reduced pressure. The product (206 mg, 0.368 mmol, 23 %) was obtained as a colorless powder. ^{1}H NMR (400 MHz, CD_2Cl_2, 21 °C): $\delta = 7.05$ (s, 4 H, *meta*-CH), 4.28 (s, 4 H, NCH_2CH_2N), 2.34 (s, 6 H, *para*-CH_3), 2.33 (s, 12 H, *ortho*-CH_3) ppm. ^{19}F NMR (377 MHz, CD_2Cl_2, 21 °C): $\delta = -216.9$ (t, 1F, *trans*-F, $^2J(^{19}F,^{19}F) = 49$ Hz), −315.7 (d, 2F, *cis*-F) ppm.

Trifluoromethylation of $[AuF_3(SIMes)]$ in dichloromethane: In a typical experiment, $[AuF_3(SIMes)]$ (10 mg, 17.8 µmol, 1 equiv.) and CsF (2.7 mg, 17.8 µmol, 1 equiv.) were dissolved in dichloromethane (1 mL) and at −196 °C, trimethyl(trifluoromethyl)silane (2.5 mg, 17.5 µmol, 1 equiv.) was condensed onto this mixture. The mixture was allowed to warm up to −80 °C, the resulting solution was stirred for 1 hour, warmed to room temperature and left stirring overnight. Main reaction products identified by ^{19}F NMR spectroscopy are *trans*-$[Au(CF_3)F_2(SIMes)]$ (**1**) and *cis*-$[Au(CF_3)_2F(SIMes)]$ (**2**), HCF_3 and *trans*-$[AuClF_2(SIMes)]$ are formed as by-products (see Figures S9–S15). Single crystals of **1** suitable for X-ray diffraction were obtained by slow vapor diffusion of *n*-pentane into a dichloromethane solution at 5 °C.

trans-$[Au(CF_3)F_2(SIMes)]$ (**1**): ^{1}H NMR (400 MHz, CD_2Cl_2, 20 °C): $\delta =$ 7.04 (s, 4 H, *meta*-CH), 4.12 (s, 4 H, NCH_2CH_2N), 2.33 (s, 18 H, *ortho*-CH_3 + *para*-CH_3) ppm. ^{13}C NMR (101 MHz, CD_2Cl_2, 20 °C): $\delta = 192.3$ (s, NCN carbene), 139.7 (s, C_{Ar}), 136.3 (s, C_{Ar}), 132.5 (s, C_{Ar}), 129.6 (s, C_{Ar}), 51.4 (s, NCH_2CH_2N), 20.6 (s, CH_3), 16.8 (s, CH_3) ppm. ^{19}F NMR (377 MHz, CD_2Cl_2, 20 °C): $\delta = -46.5$ (t, 3F, *trans*-CF_3, $^3J(^{19}F,^{19}F) =$ 18 Hz), −329.7 (q, 2F, *cis*-F) ppm.

cis-$[Au(CF_3)_2F(SIMes)]$ (**2**): ^{19}F NMR (377 MHz, CD_2Cl_2, 20 °C): $\delta =$ −23.9 (dq, 3F, *cis*-CF_3, $^3J(^{19}F,^{19}F) = 57$ Hz, $^4J(^{19}F,^{19}F) = 7$ Hz), −41.2 (dq, 3F, *trans*-CF_3, $^3J(^{19}F,^{19}F) = 14$ Hz), −254.0 (qq, 1F, *cis*-F) ppm.

Trifluoromethylation of $[AuF_3(SIMes)]$ in tetrahydrofuran: In a typical experiment, CsF (2.7 mg, 17.8 µmol, 1 equiv.) was dissolved in tetrahydrofuran (1 mL) and at −196 °C, trimethyl(trifluoromethyl)silane (2.5 mg, 17.5 µmol, 1 equiv.) was added. The mixture was allowed to warm up to −80 °C and the resulting solution was stirred for 30 minutes. Thereafter, a solution of $[AuF_3(SIMes)]$ (10 mg, 17.8 µmol, 1 equiv.) in tetrahydrofuran (1 mL) was added and the resulting mixture was stirred for 1 hour at −80 °C, warmed to room temperature and left stirring overnight. Main reaction products identified by ^{19}F NMR spectroscopy are *cis*-$[Au(CF_3)_2F(SIMes)]$ (**2**) and $[Au(CF_3)_3(SIMes)]$ (**3**), HCF_3 and $[Au(CF_3)_4]^-$ are formed as by-products (Supporting Information, Figures S16 and S17).

cis-$[Au(CF_3)_2F(SIMes)]$ (**2**): ^{19}F NMR (377 MHz, ext. $(CD_3)_2CO$, 20 °C): $\delta = -24.1$ (dq, 3F, *cis*-CF_3, $^3J(^{19}F,^{19}F) = 57$ Hz, $^4J(^{19}F,^{19}F) = 7$ Hz), −41.2 (dq, 3F, *trans*-CF_3, $^3J(^{19}F,^{19}F) = 14$ Hz), −253.6 (qq, 1F, *cis*-F) ppm. $[Au(CF_3)_3(SIMes)]$ (**3**): ^{19}F NMR (377 MHz, ext. $(CD_3)_2CO$, 20 °C): $\delta =$ −31.3 (q, 6F, *cis*-CF_3, $^4J(^{19}F,^{19}F) = 7$ Hz), −34.1 (sep, 3F, *trans*-CF_3) ppm.

Selective preparation of $[Au(CF_3)_3(SIMes)]$ (3): $[Au(CF_3)_3(NCMe)]$ (45 mg, 0.101 mmol, 1 equiv.) and SIMes (31 mg, 0.101 mmol, 1 equiv.) were dissolved in diethyl ether (1 mL) and stirred for 30 minutes at room temperature. The resulting suspension was filtered off, the colorless residue was washed with *n*-hexane (2 mL) and residual solvent was removed under reduced pressure. The product was obtained as a colorless powder. Single crystals suitable for X-ray diffraction were obtained from solutions of **3** in acetone, chloroform, dichloromethane or tetrahydrofuran, by layering them with *n*-hexane. ^{1}H NMR (400 MHz, CD_2Cl_2, 21 °C): $\delta = 6.99$ (s, 4 H, *meta*-CH), 4.13 (s, 4 H, NCH_2CH_2N), 2.33 (s, 12 H, *ortho*-CH_3), 2.30 (s, 6 H, *para*-CH_3) ppm. ^{13}C NMR (101 MHz, CD_2Cl_2, 21 °C): $\delta = 191.4$ (s, NCN carbene), 139.2 (s, C_{Ar}), 135.4 (s, C_{Ar}), 132.4 (s, C_{Ar}), 129.6 (s, C_{Ar}), 52.6 (s, NCH_2CH_2H), 20.4 (s, CH_3), 17.5 (s, CH_3) ppm. ^{19}F NMR (377 MHz, CD_2Cl_2, 21 °C): $\delta = -31.5$ (q, 6F, *cis*-CF_3, $^4J(^{19}F,^{19}F) = 7$ Hz), −34.3 (sep, 3F, *trans*-CF_3) ppm. IR (ATR, 25 °C, 4 cm^{-1}): $\tilde{\nu} = 3007$ (w), 2960 (w), 2925 (w), 2869 (w), 1609 (m), 1495 (s), 1447 (m), 1380 (m), 1316 (w), 1272 (s), 1221 (w), 1159 (s, $\nu_{as}(CF_3)$), 1109 (s, $\nu_{as}(CF_3)$), 1069 (vs., $\nu_{as}(CF_3)_{trans}$), 1018 (s, $\nu_{as}(CF_3)_{cis}$), 949 (m), 916 (m), 886 (m), 862 (m), 740 (m), 631 (m), 579 (m), 565 (w), 532 (w), 502 (w), 434 (w) cm^{-1}. FT-Raman (25 °C, 30 mW, 2 cm^{-1}): $\tilde{\nu} = 3004$ (m), 2927 (m), 2741 (w), 1823 (w), 1610 (m), 1494 (m), 1454 (m), 1387 (m), 1316 (m), 1225 (w), 1158 (w), 1089 (w), 1020 (w), 951 (w), 723 (m, $\nu_s(CF_3)$), 581 (m), 566 (m), 517 (w), 475 (w), 340 (w), 260 (m, ν(AuC)), 233 (m, ν(AuC)), 86 (s) cm^{-1}.

Chemistry–A European Journal | Full Paper doi.org/10.1002/chem.202002940 | Chemistry Europe European Chemical Societies Publishing

Crystallographic data: Deposition numbers 2001090, 2000997, 2000994, 2000995, and 2000996 (**1**, **3a**, **3b**, **3c**, and **3d**) contain the supplementary crystallographic data for this paper. These data are provided free of charge by the joint Cambridge Crystallographic Data Centre and Fachinformationszentrum Karlsruhe Access Structures service.

Acknowledgements

The authors would like to thank the HPC Service of ZEDAT, Freie Universität Berlin, for computing time. M.W. thanks the Dahlem Research School for financial support, Dr. Babil Menjón and Dr. Julia Bader for help revising the manuscript and Dr. Günther Thiele for help solving the solid state structures. A.P.B. thanks the Spanish Ministerio de Ciencia, Innovación *y* Universidades for financial support (FPU15/03940 and EST18/00114), as well as Campus Iberus for the management of an Erasmus+ scholarship in international mobility activities for PhD students, financed by the European Commission through the Erasmus+ program. Funded by the Deutsche Forschungsgemeinschaft (DFG, German Research Foundation)–Project-ID 387284271-SFB 1349". Open access funding enabled and organized by Projekt DEAL.

Conflict of interest

The authors declare no conflict of interest.

Keywords: fluorides · *N*-heterocyclic carbenes · organo gold chemistry · solvent effects · trifluoromethyl ligand

[1] J. Miró, C. del Pozo, *Chem. Rev.* **2016**, *116*, 11924.
[2] W. J. Wolf, F. D. Toste, *Patai's chemistry of functional groups*, Eds.: Z. Rappoport, J. F. Liebman, I. Marek, Wiley, Chichester, **2014**, pp. 391 – 408.
[3] *CRC Handbook of Chemistry and Physics* (Ed.: D. R. Lide), Taylor & Francis, Boca Raton, FL., **2006**.
[4] N. P. Mankad, F. D. Toste, *Chem. Sci.* **2012**, *3*, 72.
[5] a) G. Zhang, Y. Peng, L. Cui, L. Zhang, *Angew. Chem. Int. Ed.* **2009**, *48*, 3112; *Angew. Chem.* **2009**, *121*, 3158; b) Y. Peng, L. Cui, G. Zhang, L. Zhang, *J. Am. Chem. Soc.* **2009**, *131*, 5062; c) G. Zhang, L. Cui, Y. Wang, L. Zhang, *J. Am. Chem. Soc.* **2010**, *132*, 1474; d) W. E. Brenzovich, Jr., D. Benitez, A. D. Lackner, H. P. Shunatona, E. Tkatchouk, W. A. Goddard III, F. D. Toste, *Angew. Chem. Int. Ed.* **2010**, *49*, 5519 – 5522; *Angew. Chem.* **2010**, *122*, 5651 – 5654; e) A. D. Melhado, W. E. Brenzovich Jr., A. D. Lackner, F. D. Toste, *J. Am. Chem. Soc.* **2010**, *132*, 8885; f) L. T. Ball, M. Green, G. C. Lloyd-Jones, C. A. Russell, *Org. Lett.* **2010**, *12*, 4724; g) W. E. Brenzovich Jr., J.-F. Brazeau, F. D. Toste, *Org. Lett.* **2010**, *12*, 4728.
[6] J. A. Akana, K. X. Bhattacharyya, P. Müller, J. P. Sadighi, *J. Am. Chem. Soc.* **2007**, *129*, 7736.
[7] F. Mohr, *Gold Bull.* **2004**, *37*, 164.
[8] a) D. S. Laitar, P. Müller, T. G. Gray, J. P. Sadighi, *Organometallics* **2005**, *24*, 4503; b) R. Kumar, A. Linden, C. Nevado, *Angew. Chem. Int. Ed.* **2015**, *54*, 14287; *Angew. Chem.* **2015**, *127*, 14495; c) R. Kumar, A. Linden, C. Nevado, *J. Am. Chem. Soc.* **2016**, *138*, 13790.
[9] M. S. Winston, W. J. Wolf, F. D. Toste, *J. Am. Chem. Soc.* **2015**, *137*, 7921.
[10] A. Pérez-Bitrián, S. Martínez-Salvador, M. Baya, J. M. Casas, A. Martín, B. Menjón, J. Orduna, *Chem. Eur. J.* **2017**, *23*, 6919.
[11] a) N. P. Mankad, F. D. Toste, *J. Am. Chem. Soc.* **2010**, *132*, 12859; b) M. Albayer, R. Corbo, J. L. Dutton, *Chem. Commun.* **2018**, *54*, 6832.
[12] A. Pérez-Bitrián, M. Baya, J. M. Casas, A. Martín, B. Menjón, J. Orduna, *Angew. Chem. Int. Ed.* **2018**, *57*, 6517; *Angew. Chem.* **2018**, *130*, 6627.
[13] a) J. Cheng, L. Wang, P. Wang, L. Deng, *Chem. Rev.* **2018**, *118*, 9930; b) W. Levason, F. M. Monzittu, G. Reid, *Coord. Chem. Rev.* **2019**, *391*, 90.
[14] M. A. Ellwanger, S. Steinhauer, P. Golz, T. Braun, S. Riedel, *Angew. Chem. Int. Ed.* **2018**, *57*, 7210; *Angew. Chem.* **2018**, *130*, 7328.
[15] F. W. B. Einstein, P. R. Rao, J. Trotter, N. Bartlett, *J. Chem. Soc. A* **1967**, 478.
[16] M. Shimizu, T. Hiyama, *Angew. Chem. Int. Ed.* **2004**, *43*, 214; *Angew. Chem.* **2004**, *117*, 218.
[17] T. Furuya, A. S. Kamlet, T. Ritter, *Nature* **2011**, *473*, 470.
[18] T. Liang, C. N. Neumann, T. Ritter, *Angew. Chem. Int. Ed.* **2013**, *52*, 8214; *Angew. Chem.* **2013**, *125*, 8372.
[19] a) S. Purser, P. R. Moore, S. Swallow, V. Gouverneur, *Chem. Soc. Rev.* **2008**, *37*, 320; b) J. Wang, M. Sánchez-Roselló, J. L. Aceña, C. del Pozo, A. E. Sorochinsky, S. Fustero, V. A. Soloshonok, H. Liu, *Chem. Rev.* **2014**, *114*, 2432; c) H.-J. Böhm, D. Banner, S. Bendels, M. Kansy, B. Kuhn, K. Müller, U. Obst-Sander, M. Stahl, *ChemBioChem* **2004**, *5*, 637; d) K. Müller, C. Faeh, F. Diederich, *Science* **2007**, *317*, 1881; e) E. P. Gillis, K. J. Eastman, M. D. Hill, D. J. Donnelly, N. A. Meanwell, *J. Med. Chem.* **2015**, *58*, 8315; f) H. Mei, J. Han, S. Fustero, M. Medio-Simon, D. M. Sedgwick, C. Santi, R. Ruzziconi, V. A. Soloshonok, *Chem. Eur. J.* **2019**, *25*, 11797.
[20] a) T. Fujiwara, D. O'Hagan, *J. Fluorine Chem.* **2014**, *167*, 16; b) P. Jeschke, *ChemBioChem* **2004**, *5*, 570.
[21] a) J. E. Huheey, E. A. Keiter, R. L. Keiter, R. Steudel, *Anorganische Chemie. Prinzipien von Struktur und Reaktivität*, de Gruyter, Berlin, **2012**; b) J. E. True, T. D. Thomas, R. W. Winter, G. L. Gard, *Inorg. Chem.* **2003**, *42*, 4437.
[22] R. D. Sanner, J. H. Satcher, M. W. Droege, *Organometallics* **1989**, *8*, 1498.
[23] Y. Usui, J. Noma, M. Hirano, S. Komiya, *Inorg. Chim. Acta* **2000**, *309*, 151.
[24] M. S. Winston, W. J. Wolf, F. D. Toste, *J. Am. Chem. Soc.* **2014**, *136*, 7777.
[25] M. D. Levin, T. Q. Chen, M. E. Neubig, C. M. Hong, C. A. Theulier, I. J. Kobylianskii, M. Janabi, J. P. O'Neil, F. D. Toste, *Science* **2017**, *356*, 1272.
[26] S. Liu, K. Kang, S. Liu, D. Wang, P. Wei, Y. Lan, Q. Shen, *Organometallics* **2018**, *37*, 3901.
[27] S. Kim, F. D. Toste, *J. Am. Chem. Soc.* **2019**, *141*, 4308.
[28] A. Johnson, R. J. Puddephatt, *Inorg. Nucl. Chem. Lett.* **1973**, *9*, 1175.
[29] J. Gil-Rubio, J. Vicente, *Dalton Trans.* **2015**, *44*, 19432.
[30] A. Johnson, R. J. Puddephatt, *J. Chem. Soc. Dalton Trans.* **1976**, 1360.
[31] H. K. Nair, J. A. Morrison, *J. Organomet. Chem.* **1989**, *376*, 149.
[32] a) H. H. Murray, J. P. Fackler, L. C. Porter, D. A. Briggs, M. A. Guerra, R. J. Lagow, *Inorg. Chem.* **1987**, *26*, 357; b) N. H. Dryden, J. G. Shapter, L. L. Coatsworth, P. R. Norton, R. J. Puddephatt, *Chem. Mater.* **1992**, *4*, 979; c) A. Gräfe, T. Kruck, *J. Organomet. Chem.* **1996**, *506*, 31.
[33] D. Zopes, S. Kremer, H. Scherer, L. Belkoura, I. Pantenburg, W. Tyrra, S. Mathur, *Eur. J. Inorg. Chem.* **2011**, 273.
[34] S. Martínez-Salvador, L. R. Falvello, A. Martin, B. Menjon, *Chem. Eur. J.* **2013**, *19*, 14540.
[35] M. Blaya, D. Bautista, J. Gil-Rubio, J. Vicente, *Organometallics* **2014**, *33*, 6358.
[36] A. G. Tskhovrebov, J. B. Lingnau, A. Fürstner, *Angew. Chem. Int. Ed.* **2019**, *58*, 8834; *Angew. Chem.* **2019**, *131*, 8926.
[37] E. Bernhardt, M. Finze, H. Willner, *J. Fluorine Chem.* **2004**, *125*, 967.
[38] P. Pröhm, J. R. Schmid, K. Sonnenberg, S. Steinhauer, C. J. Schattenberg, R. Müller, M. Kaupp, P. Voßnacker, S. Riedel, *Angew. Chem. Int. Ed.* **2020**, *59*, 16002; *Angew. Chem.* **2020**, *132*, 16136.
[39] M. A. Guerra, T. R. Bierschenk, R. J. Lagow, *J. Organomet. Chem.* **1986**, *307*, C58 – C62.
[40] J. L. Margrave, K. H. Whitmire, R. H. Hauge, N. T. Norem, *Inorg. Chem.* **1990**, *29*, 3252.
[41] a) S. Martínez-Salvador, J. Fornies, A. Martin, B. Menjon, *Angew. Chem. Int. Ed.* **2011**, *50*, 6571; *Angew. Chem.* **2011**, *123*, 6701; b) D. Zopes, C. Hegemann, W. Tyrra, S. Mathur, *Chem. Commun.* **2012**, *48*, 8805; c) S. Martínez-Salvador, L. R. Falvello, A. Martín, B. Menjón, *Chem. Sci.* **2015**, *6*, 5506; d) M. Baya, A. Pérez-Bitrián, S. Martínez-Salvador, J. M. Casas, B. Menjón, J. Orduna, *Chem. Eur. J.* **2017**, *23*, 1512; e) M. Baya, A. Pérez-Bitrián, S. Martínez-Salvador, A. Martín, J. M. Casas, B. Menjón, J. Orduna, *Chem. Eur. J.* **2018**, *24*, 1514; f) J. A. Schlüter, J. M. Williams, U. Geiser, J. D. Dudek, S. A. Sirchio, M. E. Kelly, J. S. Gregar, W. H. Kwok, J. A. Fendrich, J. E. Schirber, W. R. Bayless, D. Naumann, T. Roy, *J. Chem. Soc. Chem. Commun.* **1995**, 1311.
[42] A. Pérez-Bitrián, M. Baya, J. M. Casas, L. R. Falvello, A. Martín, B. Menjón, *Chem. Eur. J.* **2017**, *23*, 14918.

Chemistry–A European Journal | Full Paper doi.org/10.1002/chem.202002940

Chemistry Europe
European Chemical Societies Publishing

[43] M. A. Ellwanger, C. von Randow, S. Steinhauer, Y. Zhou, A. Wiesner, H. Beckers, T. Braun, S. Riedel, *Chem. Commun.* **2018**, *54*, 9301.
[44] G. K. Surya Prakash, A. K. Yudin, *Chem. Rev.* **1997**, *97*, 757.
[45] a) D. J. Adams, J. H. Clark, L. B. Hansen, V. C. Sanders, S. J. Tavener, *J. Fluorine Chem.* **1998**, *92*, 123; b) J.-B. Behr, D. Chavaria, R. Plantier-Royon, *J. Org. Chem.* **2013**, *78*, 11477.
[46] N. Maggiarosa, W. Tyrra, D. Naumann, N. V. Kirij, Y. L. Yagupolskii, *Angew. Chem. Int. Ed.* **1999**, *38*, 2252; *Angew. Chem.* **1999**, *111*, 2392.
[47] a) W. A. Herrmann, O. Runte, G. Artus, *J. Organomet. Chem.* **1995**, *501*, C1–C4; b) M. V. Baker, P. J. Barnard, S. K. Brayshaw, J. L. Hickey, B. W. Skelton, A. H. White, *Dalton Trans.* **2005**, 37.
[48] a) S. Gaillard, A. M. Z. Slawin, A. T. Bonura, E. D. Stevens, S. P. Nolan, *Organometallics* **2010**, *29*, 394; b) P. de Frémont, R. Singh, E. D. Stevens, J. L. Petersen, S. P. Nolan, *Organometallics* **2007**, *26*, 1376.
[49] T. G. Appleton, M. H. Chisholm, H. C. Clark, L. E. Manzer, *Inorg. Chem.* **1972**, *11*, 1786.
[50] V. V. Grushin, W. J. Marshall, *J. Am. Chem. Soc.* **2006**, *128*, 4632.
[51] P. Sgarbossa, A. Scarso, G. Strukul, R. A. Michelin, *Organometallics* **2012**, *31*, 1257.
[52] a) J. Vícha, C. Foroutan-Nejad, T. Pawlak, M. L. Munzarová, M. Straka, R. Marek, *J. Chem. Theory Comput.* **2015**, *11*, 1509; b) A. H. Greif, P. Hrobárik, M. Kaupp, *Chem. Eur. J.* **2017**, *23*, 9790.
[53] a) M. A. Bennett, H.-K. Chee, G. B. Robertson, *Inorg. Chem.* **1979**, *18*, 1061; b) M. A. Bennett, H.-K. Chee, J. C. Jeffery, G. B. Robertson, *Inorg. Chem.* **1979**, *18*, 1071; c) A. G. Algarra, V. V. Grushin, S. A. Macgregor, *Organometallics* **2012**, *31*, 1467.
[54] L. Rocchigiani, J. Fernandez-Cestau, I. Chambrier, P. Hrobárik, M. Bochmann, *J. Am. Chem. Soc.* **2018**, *140*, 8287.
[55] A. J. Arduengo III, R. Krafczyk, R. Schmutzler, H. A. Craig, J. R. Goerlich, W. J. Marshall, M. Unverzagt, *Tetrahedron* **1999**, *55*, 14523.
[56] A. G. Sharpe, *J. Chem. Soc.* **1949**, 2901.
[57] a) M. Iglesias, D. J. Beetstra, J. C. Knight, L.-L. Ooi, A. Stasch, S. Coles, L. Male, M. B. Hursthouse, K. J. Cavell, A. Dervisi, I. A. Fallis, *Organometallics* **2008**, *27*, 3279; b) E. L. Kolychev, I. A. Portnyagin, V. V. Shuntikov, V. N. Khrustalev, M. S. Nechaev, *J. Organomet. Chem.* **2009**, *694*, 2454.
[58] OriginLab Corporation, *OriginPro*, *Version 9.1*, Northampton, MA, USA.
[59] R. K. Harris, E. D. Becker, S. M. Cabral de Menezes, R. Goodfellow, P. Granger, *Pure Appl. Chem.* **2001**, *73*, 1795.
[60] G. M. Sheldrick, *Acta Crystallogr. Sect. A* **2015**, *71*, 3.
[61] G. M. Sheldrick, *Acta Crystallogr. Sect. C* **2015**, *71*, 3.
[62] O. V. Dolomanov, L. J. Bourhis, R. J. Gildea, J. A. K. Howard, H. Puschmann, *J. Appl. Crystallogr.* **2009**, *42*, 339.
[63] A. D. Becke, *J. Chem. Phys.* **1993**, *98*, 5648.
[64] M. Sierka, A. Hogekamp, R. Ahlrichs, *J. Chem. Phys.* **2003**, *118*, 9136.
[65] S. Grimme, J. Antony, S. Ehrlich, H. Krieg, *J. Chem. Phys.* **2010**, *132*, 154104.
[66] a) F. Weigend, R. Ahlrichs, *Phys. Chem. Chem. Phys.* **2005**, *7*, 3297; b) F. Weigend, M. Häser, H. Patzelt, R. Ahlrichs, *Chem. Phys. Lett.* **1998**, *294*, 143.
[67] TURBOMOLE GmbH, *TURBOMOLE V7.0.1*, **2015**.

Manuscript received: June 18, 2020
Accepted manuscript online: July 15, 2020
Version of record online: October 27, 2020

3.2 Reactivity of [AuF_3(SIMes)]: Pathway to Unprecedented Structural Motifs

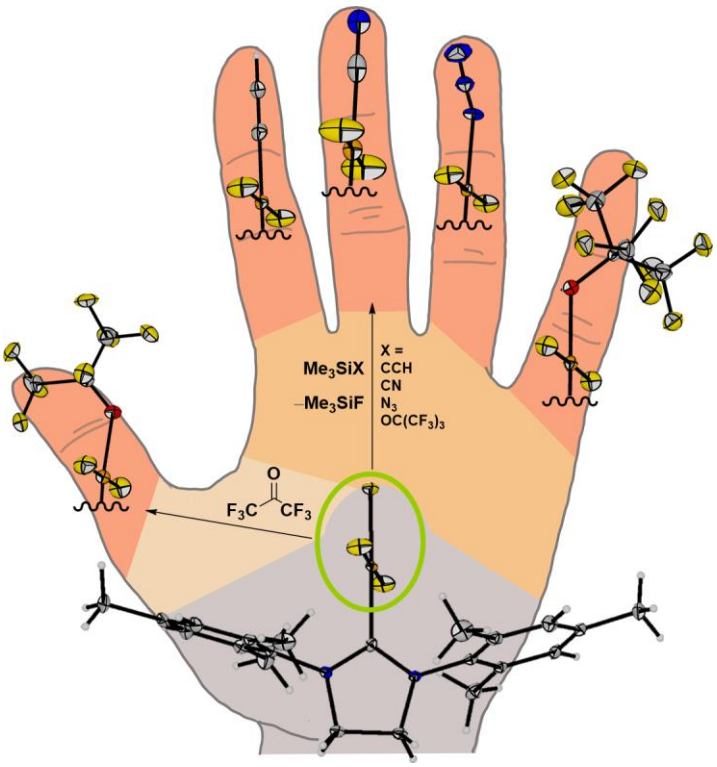

Marlon Winter, Mathias A. Ellwanger, Niklas Limberg, Alberto Pérez-Bitrián, Patrick Voßnacker, Simon Steinhauer, and Sebastian Riedel.

Chem. Eur. J. **2023**, e202301684.

https://doi.org/10.1002/chem.202301684

Author contributions

Marlon Winter designed the project, performed the majority of the experiments, as well as quantum-chemical calculations, and wrote the manuscript. Mathias A. Ellwanger helped designing the project, performed some of the experiments and revised the manuscript. Niklas Limberg performed some of the experiments during his research internship under the supervision of Marlon Winter. Alberto Pérez-Bitrián and Simon Steinhauer gave scientific advice and revised the manuscript. Patrick Voßnacker and Simon Steinhauer measured and refined the crystal structures. Sebastian Riedel supervised the project and revised the manuscript.

Check for updates

Chemistry–A European Journal

Research Article
doi.org/10.1002/chem.202301684

Chemistry Europe
European Chemical Societies Publishing

www.chemeurj.org

Reactivity of $[AuF_3(SIMes)]$: Pathway to Unprecedented Structural Motifs

Marlon Winter,[a] Mathias A. Ellwanger,[a, b] Niklas Limberg,[a] Alberto Pérez-Bitrián,[a] Patrick Voßnacker,[a] Simon Steinhauer,[a] and Sebastian Riedel*[a]

We report on a comprehensive reactivity study starting from $[AuF_3(SIMes)]$ to synthesize different motifs of monomeric gold(III) fluorides. A plethora of different ligands has been introduced in a mono-substitution yielding *trans*-$[AuF_2X(SIMes)]$ including alkynido, cyanido, azido, and a set of perfluoroalkoxido complexes. The latter were better accomplished via use of perfluorinated carbonyl-bearing molecules, which is unprecedented in gold chemistry. In case of the cyanide and azide, triple substitution gave rise to the corresponding $[AuX_3(SIMes)]$ complexes. Comparison of the chemical shift of the carbene carbon atom in the $^{13}C\{^1H\}$ NMR spectrum, the calculated SIMes affinity and the Au–C bond length in the solid state with related literature-known complexes yields a classification of *trans*-influences for a variety of ligands attached to the gold center. Therein, the mixed fluorido perfluoroalkoxido complexes have a similar SIMes affinity to AuF_3 with a very low Gibbs energy of formation when using the perfluoro carbonyl route.

Introduction

The chemistry of fluorido organo gold complexes is only scarcely studied compared to that of the heavier halides.[1] This is due to the rather low Au–F bond energy with respect to that of other E–F bonds (E = B, C, Si, P, among others),[2] resulting in a high reactivity of compounds containing Au–F bonds. However, fluorido organo gold complexes are proposed to be important intermediates in gold-mediated and -catalyzed processes, and understanding their reactivity is of great interest in order to develop more efficient catalysts.[3]

The stabilization of such highly reactive species can be achieved upon coordination of strong σ-donors like *N*-heterocyclic carbenes (NHCs) to the gold center. This was shown by the group of *Sadighi* in 2005 with the synthesis of the first fluorido organo gold(I) complex [AuF(SIPr)] (SIPr = 1,3-bis(2,6-diisopropylphenyl)-4,5-dihydroimidazol-2-ylidene),[4] which was later used for the hydrofluorination of alkynes.[5] In the case of gold(III), a handful isolated fluorido organo gold(III) complexes are known. They are either prepared by X/F exchange (X = Cl, Br, I)[6,7,8–10] or by oxidation with XeF_2[11,12] or Selectfluor®.[13] In 2018, our group developed a synthetic route to the first and only fluorido organo gold(III) complex that contains three fluorido ligands, $[AuF_3(SIMes)]$ (SIMes = 1,3-bis(2,4,6-trimethylphenyl)-4,5-dihydroimidazol-2-ylidene).[14] In this complex, the highly Lewis acidic and reactive AuF_3 moiety is stabilized by the NHC SIMes, which makes it easy to handle in standard organic solvents like dichloromethane. Therefore, $[AuF_3(SIMes)]$ can be used for reactivity studies of monomeric AuF_3, which as neat material is polymeric in the solid state[15] and reacts violently with many organic materials.[1]

The solid state structure of $[AuF_3(SIMes)]$ reveals that the Au–F bond length of the fluorido ligand *trans* to the NHC is about 5 pm longer than those of the fluorido ligands in *cis* position.[14] Subsequent studies on the substitution of the fluorido ligand in *trans* position were performed by our group to selectively introduce a chloride,[16] pentafluoro-orthotellurate,[16] and trifluoromethyl[17] group via trimethylsilyl reagents (Scheme 1, left). Interestingly, in the reaction with Me_3SiCF_3, also a second and third substitution can be observed, with their ratios depending on the reaction conditions.[17]

The findings summarized on the left side of Scheme 1 show that the combination of $[AuF_3(SIMes)]$ and trimethylsilyl reagents is a promising route for the introduction of a variety of ligands with different donor atoms to the gold center using the formation of gaseous trimethylsilyl fluoride as a driving force. First, we thought of using Me_3SiCCH for the transfer of an ethynido group, similar to a recent work, in which $Me_3SiCCPh$ was used for the successful substitution of fluorido by alkynido ligands.[18] Gold(III) alkynyls in combination with chelating ligands have found application as luminescent materials.[19–27] Furthermore, alkynyl gold(I) complexes bearing NHC ligands have recently shown potential as anticancer drugs.[28] However, corresponding gold(III) complexes are not known, yet. Another interesting group in gold chemistry are pseudohalides like

[a] M. Winter, Dr. M. A. Ellwanger, N. Limberg, Dr. A. Pérez-Bitrián, P. Voßnacker, Dr. S. Steinhauer, Prof. Dr. S. Riedel
Fachbereich Biologie, Chemie, Pharmazie
Institut für Chemie und Biochemie – Anorganische Chemie
Freie Universität Berlin
Fabeckstr. 34/36, 14195 Berlin (Germany)
E-mail: s.riedel@fu-berlin.de

[b] Dr. M. A. Ellwanger
Inorganic Chemistry Laboratory
Department of Chemistry
University of Oxford
South Parks Road, OX1 3QR Oxford, (UK)

Supporting information for this article is available on the WWW under https://doi.org/10.1002/chem.202301684

Chemistry–A European Journal
Research Article
doi.org/10.1002/chem.202301684
Chemistry Europe
European Chemical Societies Publishing

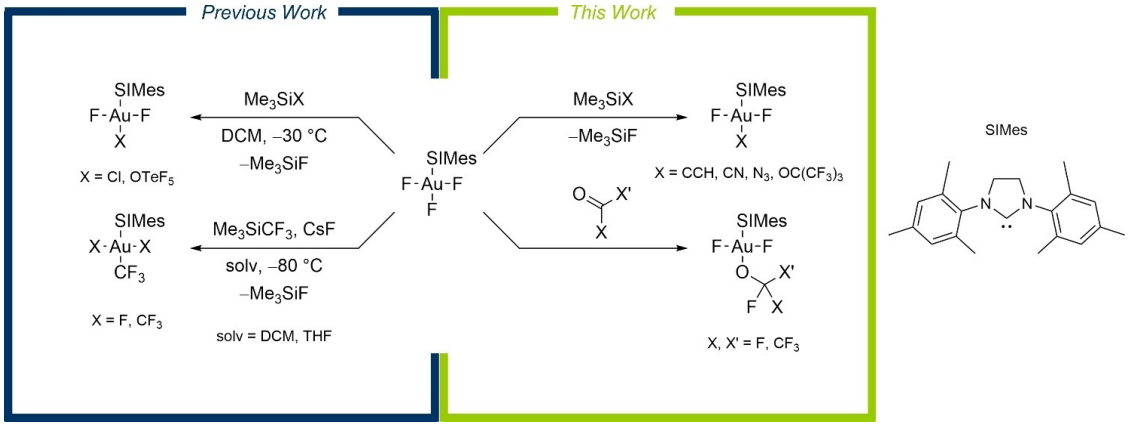

Scheme 1. Overview of the literature-known reactivity of [AuF_3(SIMes)] towards Me_3SiX (X = Cl,[16] $OTeF_5$,[16] CF_3[17]) reagents (left, blue) and the reactivity of [AuF_3(SIMes)] investigated in this work towards trimethylsilyl compounds and perfluorinated carbonyl-bearing molecules (right, green).

cyanide and azide. Cyanide gold chemistry is known for more than a decade.[29] In recent times, cyanido gold(III) complexes with fluorido ligands have been investigated[8,30] including analyses of reductive eliminations from such complexes as C–C bond formation reactions,[9,10] as well as substitution of fluorido by cyanido ligands using Me_3SiCN.[18] A few cyanido gold(I) complexes bearing NHC ligands are known[31,32] but surprisingly, to the best of our knowledge, no such gold(III) complexes are known so far. Azido gold complexes have attracted interest for cycloaddition reactions with alkynes in analogy to the classical copper-catalyzed click chemistry.[33,34] Selected examples of azido gold(I) complexes or compounds formed by their cycloaddition reactions have also been studied for their cytotoxic activity.[34,35] In contrast, for azido gold(III) complexes, only a handful species have been structurally characterized to date.[36–40]

In addition to these C- and N-based functional groups, we turned our attention to the introduction of perfluoroalkoxy groups. Their simplest representative, the trifluoromethoxy group, has distinct electronic[41] and structural[42] properties and metabolic stability. In fact, it has become an important functional group due to the drastic changes it induces in the lipophilicity of an organic compound.[43] In medicinal chemistry, molecules containing an OCF_3 group can be used as drugs for amyotrophic lateral sclerosis (ALS)[44] and work as a SARS-CoV-2 M^{pro} inhibitor.[45] The available methods for the introduction of OCF_3 groups into organic molecules have shown a significant increase in the last two decades, accounting for its importance.[46,47,48,49] However, there is still a lack of general methods and easy-to-handle reagents.[50] In this regard, a significant problem is the equilibrium of the trifluoromethoxide anion with carbonyl fluoride (COF_2) and a fluoride anion,[51–53] which potentially lead to the formation of the corresponding fluorinated molecules as side products, when using salts of the trifluoromethoxide anion.[54] Therefore, some synthetic pathways focus on the in situ preparation of the trifluoromethoxide anion by decomposition of larger molecules.[46,48] There is only one trifluoromethoxido gold complex known, i.e. [Au(OCF_3)(SIPr)], prepared by the reaction of [AuCl(SIPr)] with a solution of $AgOCF_3$ in MeCN.[49] Regarding the higher homologues, i.e. the pentafluoroethoxy and the heptafluoro-*iso*-propoxy groups, the literature-known procedures for their introduction are even scarcer[55] and no gold complexes are known. In contrast, analogous non-fluorinated alkoxido gold complexes are more thoroughly investigated[56] and have been used as a catalyst for Knöevenagel condensation reactions.[57] They can abstract hydrides from metal hydrides yielding gold metal complexes[58] or protons from several organic compounds,[59] as well as cleave C–S[60] and C–Si[61] bonds.

Herein, we present an extensive study of the reactivity of [AuF_3(SIMes)] based on NMR spectroscopy. This includes an expanded investigation of the reaction with trimethylsilyl reagents for the introduction of alkynido, cyanido and azido ligands (see Scheme 1, top right). For the preparation of the first perfluoroalkoxido gold(III) complexes, the route via trimethylsilyl compounds was not possible for the lighter perfluoroalkoxides due to their inherent instability and could only be used for the nonafluoro-*tert*-butoxy group. For the lighter homologues, we exploited the aforementioned equilibrium and directly reacted [AuF_3(SIMes)] with the corresponding perfluorinated carbonyl-bearing molecules (see Scheme 1, bottom right), a route that has also been used for the incorporation of perfluoroalkoxy moieties into phenols,[62] benzyl bromides[53] or metal centers.[51]

Results and Discussion

The ligands that were introduced in the reactivity study can be grouped into three main categories: i) electron donating ligands, i.e. alkynido; ii) pseudohalides, i.e. cyanido and azido; and iii) strongly electron withdrawing ligands, i.e. perfluoroalkoxido.

Chemistry–A European Journal | Research Article
doi.org/10.1002/chem.202301684
Chemistry Europe
European Chemical Societies Publishing

Introduction of electron-donating ligands

Addition of Me_3SiCCH to a solution of [AuF_3(SIMes)] in dichloromethane (DCM) at −80 °C leads to the desired ethynido complex *trans*-[Au(CCH)F_2(SIMes)] (**1**) (see Scheme 2, top). This compound shows a doublet at −340.8 ppm in the ^{19}F NMR spectrum with a coupling constant of $^4J(^{19}F,^1H) = 2.1$ Hz to the ethynyl proton, which gives the expected triplet in the ^{1}H NMR spectrum at 1.60 ppm (see Table 1). Additionally, the ^{19}F NMR spectrum shows another signal in the same region, a singlet at −340.2 ppm, which can be assigned to the corresponding trimethylsilyl-substituted alkynido complex *trans*-[Au(CCSiMe_3)F_2(SIMes)] (**2**). Compound **2** could be formed by elimination of HF, a reactivity that has been previously reported for related species.[6,10] In order to verify the formation of compound **2**, the reaction between [AuF_3(SIMes)] and $Me_3SiCCSiMe_3$ was investigated. Monitoring the reaction mixture by multinuclear NMR spectroscopy, the formation of **2** was confirmed (see Table 1 and Scheme 2, bottom). In the ^{13}C{^{1}H} NMR spectrum, **1** and **2** also have similar chemical shifts for the carbene carbon atom at 185.3 and 186.4 ppm, respectively, which is particularly sensitive to the nature of the Lewis acidic moiety bound to the Au atom (see below).[16,17,32,63]

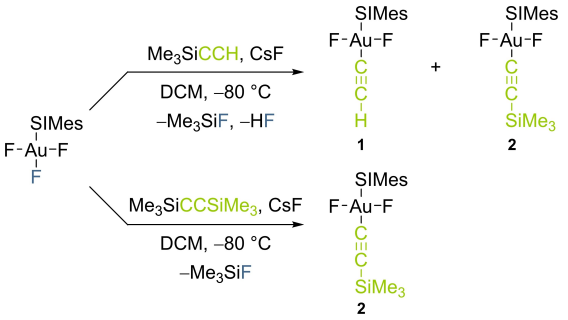

Scheme 2. Reaction of [AuF_3(SIMes)] with different alkynes. Note that the product ratio of the upper reaction depends on the amount of Me_3SiCCH and CsF (see Table S4 and Figure S13).

In order to investigate the conditions that lead to a favored formation of the desired product **1**, the ratio of the reactants and the addition of a fluoride source in the form of CsF was investigated (see Table S4). Without the presence of a fluoride source, *trans*-[Au(CCH)F_2(SIMes)] (**1**) is the main product and only traces of *trans*-[Au(CCSiMe_3)F_2(SIMes)] (**2**) are formed. However, addition of CsF strongly favors the formation of **2** (see Figure S13), as well as the general consumption of [AuF_3(SIMes)].

Single crystals of compound **1** suitable for X-ray diffraction were obtained by vapor diffusion of *n*-pentane onto a concentrated solution of the reaction mixture in DCM at 4 °C. Compound **1** crystallizes in the orthorhombic space group *Pnma* (see Figure 1) and was co-crystallized with about 6% of *trans*-[$AuClF_2$(SIMes)] (see Figure S1), which itself crystallizes in the same space group with similar lattice parameters.[16] The *trans*-[$AuClF_2$(SIMes)] is probably formed by Cl/F exchange of unreacted [AuF_3(SIMes)] with DCM, as observed previously when using this solvent.[14] The C≡C bond length of 119.2(8) pm is in the typical range of other gold(III) alkynyl complexes characterized in the solid state.[19–27,64] As expected, the Au–C bond length to the carbene carbon atom (Au–$C_{carbene}$) of 204.8(3) pm is slightly longer than in the literature-known *trans*-[AuF_2X(SIMes)] (X = F,[14] Cl,[16] $OTeF_5$,[16] CF_3[17]) complexes.

Table 1. Selected NMR spectroscopic data of the new compounds described in this article. Chemical shifts δ are given in ppm and coupling constants *J* in Hz.

Compound[a]	δ_F(Au*F*)[b]	δ_C(N*C*N)[c]	δ_H(Im-C*H*$_2$)[d]	Other NMR signals
[Au(CCH)F_2(SIMes)] (**1**)	−340.8 (d)	185.3	4.17	δ_H(CCH) = 1.60 (t), $^4J(^1H,^{19}F) = 2.1$
[Au(CCSiMe_3)F_2(SIMes)] (**2**)	−340.2	186.4	4.15	δ_H(CCSiMe_3) = 0.07 (s)
[Au(CN)F_2(SIMes)] (**3**)	−337.1	174.6	4.23	–
[Au(CN)$_3$(SIMes)] (**4**)	–	172.3	4.29	–
[$AuF_2(N_3)$(SIMes)] (**5**)	−311.1	172.5	4.26	–
[Au(N_3)$_3$(SIMes)] (**6**)	–	178.1	4.16	–
[AuF_2(OC(CF_3)$_3$)(SIMes)] (**7**)[e]	−311.9 (dec)	155.7	4.33	$\delta_F((CF_3)_3) = -74.2$ (t), $^5J(^{19}F,^{19}F) = 4.0$
[AuF_2(OCF_3)(SIMes)] (**8**)[e]	−314.1 (q)	152.7	4.35	$\delta_F(CF_3) = -40.2$ (t), $^4J(^{19}F,^{19}F) = 1.9$
[AuF_2(OC(CF_3)F_2)(SIMes)] (**9**)[f]	−314.8	153.6	4.35	$\delta_F(CF_2) = -63.1$ (s); $\delta_F(CF_3) = -86.1$ (s)
[AuF_2(OC(CF_3)$_2$F)(SIMes)] (**10**)[e]	−313.9 (dsept)	154.5	4.34	$\delta_F((CF_3)_2) = -82.0$ (dt), $^3J(^{19}F,^{19}F) = 3.2$, $^5J(^{19}F,^{19}F) = 1.7$; $\delta_F(CF) = -112.0$ (tsept), $^4J(^{19}F,^{19}F) = 2.4$[g]

[a] The prefix *trans*- was omitted for all *trans*-[AuF_2X(SIMes)] complexes for brevity. [b] δ_F(Au*F*) denotes the chemical shift in the ^{19}F NMR spectrum of the fluorido ligands bound to the gold center. The multiplicity is given in parenthesis in all cases which are not singlets. [c] δ_C(N*C*N) denotes the chemical shift in the ^{13}C{^{1}H} NMR spectrum of the carbene carbon atom. [d] δ_H(Im-C*H*$_2$) denotes the chemical shift in the ^{1}H NMR spectrum of the protons in the backbone of the imidazolidine ring of the NHC. [e] The couplings between the signals in the ^{19}F NMR spectrum were not always observed due to the high linewidth for the signals. Often, the coupling constants were only determinable at high resolution (0.1 Hz). [f] No coupling between the signals in the ^{19}F NMR spectrum was observed due to high linewidth for the signals. However, in the ^{19}F,^{19}F-COSY NMR spectrum, cross-peaks confirm the assignment to compound **9** (see Figure S41). [g] Coupling constant determined by simulation of the spectrum (see Figure S47).

Chemistry–A European Journal
Research Article
doi.org/10.1002/chem.202301684
Chemistry Europe
European Chemical Societies Publishing

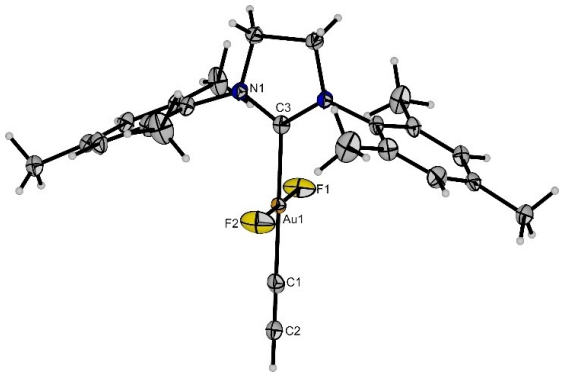

Figure 1. Molecular structure of *trans*-$[Au(CCH)F_2(SIMes)]$ (**1**) in the solid state. The co-crystallization of about 6% of *trans*-$[AuClF_2(SIMes)]$ is omitted for clarity (see Figure S1). Thermal ellipsoids are set at 50% probability. Selected bond lengths [pm]: 198.5(7) (C1–Au1), 204.8(3) (C3–Au1), 193.4(2) (F1–Au1), 193.6(2) (F2–Au1), 119.2(8) (C1–C2).

Introduction of pseudohalides

The introduction of the pseudohalides cyanide and azide to the gold center was performed by the reaction of $[AuF_3(SIMes)]$ with Me_3SiX (X = CN, N_3), as shown in Scheme 3. In both cases, the desired monosubstituted products, *trans*-$[Au(CN)F_2(SIMes)]$ (**3**) and *trans*-$[AuF_2(N_3)(SIMes)]$ (**5**), respectively, are formed. However, when more than one equivalent is used, the three times substituted complexes $[Au(CN)_3(SIMes)]$ (**4**) and $[Au(N_3)_3(SIMes)]$ (**6**) are obtained, respectively.

Interestingly, whereas in case of the cyanide the formation of compound **3** is complete within one day and it fully converts to **4** only after four weeks (see Figure S22), the reaction with the azide is much faster, compound **5** being formed after about one hour and the complete transformation to **6** being achieved within three days (see Figure S29). The only other known reaction of $[AuF_3(SIMes)]$ that led to manifold substitutions of fluorido ligands is the one with Me_3SiCF_3 (see Scheme 1, bottom left).[17] However, in the case of the reaction with Me_3SiCF_3, also the two times substituted product was observed by NMR spectroscopy, contrary to the reaction with Me_3SiX (X = CN, N_3) presented herein, in which none of the *cis*-$[AuFX_2(SIMes)]$ products are observed at any point.

All four compounds **3**–**6** were also analyzed by single-crystal X-ray diffraction. Suitable crystals were obtained in all cases by vapor diffusion of *n*-pentane onto a concentrated solution of the corresponding reaction mixture in DCM at 4 °C. The molecular structure of compound **3**, which crystallizes in the orthorhombic space group *Pnma*, is depicted in Figure 2. The Au–C bond lengths are in the typical range of literature-known cyanido gold(III) complexes.[8,9,12] The structure of compound **4** does not have enough quality to allow structural comparisons, yet it is useful to prove the connectivity and molecular shape of this three times substituted cyanido complex (see Figure S2).

The molecular structures of *trans*-$[AuF_2(N_3)(SIMes)]$ (**5**) and $[Au(N_3)_3(SIMes)]$ (**6**) are shown in Figure 3. Both compounds crystallize in the triclinic space group $P\bar{1}$. The former crystallizes with half a disordered DCM molecule (see Figure S3) and the latter with a unit cell consisting of two crystallographically independent molecules (see Figure S4). In compound **5**, the azido ligand is oriented parallel to the two fluorido ligands and shows a bent coordination with α(Au–N–N) = 116.9(2)°, which is in-between the average angles for the azido ligands in *cis* (114.2(3)°) and *trans* (119.1(3)°) position to the carbene in compound **6**. The Au–$C_{carbene}$ bond length of 200.9(2) pm in **5** is in the same range as the one in **6** (202.3(4) pm). The Au–N bond lengths in compound **6** do not deviate significantly between the azido ligands *cis* or *trans* to SIMes and lie between 203.1(4) and 204.6(4) pm, which is comparable to the one in **5** (203.5(2) pm), and in the typical range for literature-known gold(III) azido complexes.[36–40]

Introduction of electron-withdrawing ligands

In order to synthesize the first perfluoroalkoxido gold(III) complex, the reactivity of $[AuF_3(SIMes)]$ towards $Me_3SiOC(CF_3)_3$ was tested. By using this route, *trans*-$[AuF_2(OC(CF_3)_3)(SIMes)]$ (**7**) is generated (Scheme 4, top), as detected by ^{19}F NMR spectroscopy. The perfluoro-*tert*-butoxy group gives a triplet at −74.2 ppm, showing a coupling constant of $^5J(^{19}F,^{19}F) = 4.0$ Hz to the decet at −311.9 ppm which belongs to the fluorido ligands attached to the gold center (see Figure 4, left). In the $^{13}C\{^1H\}$ NMR spectrum, the carbene carbon atom of **7** has a

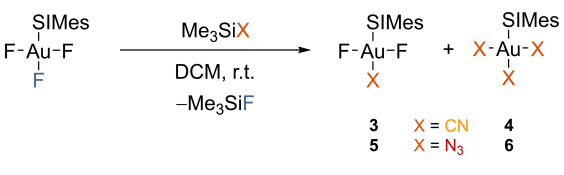

Scheme 3. Reaction of $[AuF_3(SIMes)]$ with Me_3SiX (X = CN, N_3). Note that the ratio of the products depends on the amount of trimethylsilyl reagent that is used. Addition of 1 equivalent of Me_3SiX leads to the monosubstituted products **3** and **5**, while an excess eventually yields the three times substituted complexes **4** and **6** (see Figure S23 and S30, respectively).

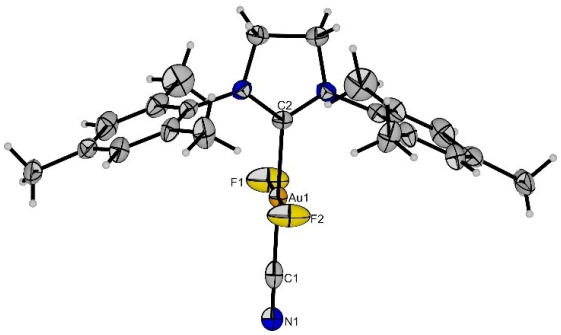

Figure 2. Molecular structure of *trans*-$[Au(CN)F_2(SIMes)]$ (**3**) in the solid state. Thermal ellipsoids are set at 50% probability. Selected bond lengths to the central gold atom [pm]: 202.2(12) (C1–Au1), 202.4(10) (C2–Au1), 191.7(7) (F1–Au1), 193.2(7) (F2–Au1).

Chemistry–A European Journal | Research Article
doi.org/10.1002/chem.202301684
Chemistry Europe
European Chemical Societies Publishing

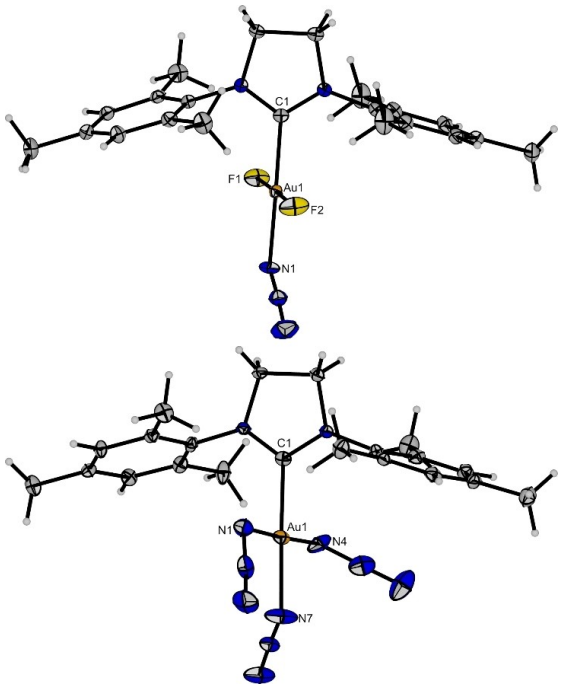

Figure 3. Top: Molecular structure of *trans*-[$AuF_2(N_3)$(SIMes)]·0.5 CH_2Cl_2 (**5**·0.5 CH_2Cl_2) in the solid state. The solvent molecule is omitted for clarity (see Figure S3). Thermal ellipsoids are set at 50% probability. Selected bond lengths to the central gold atom [pm]: 200.9(2) (C1–Au1), 193.4(2) (F1–Au1), 192.4(2) (F2–Au1), 203.5(2) (N1–Au1). Bottom: Molecular structure of [Au-$(N_3)_3$(SIMes)] (**6**) in the solid state. For clarity, only one of the two crystallographically independent molecules in the unit cell is shown (see Figure S4). Thermal ellipsoids are set at 50% probability. Selected bond lengths to the central gold atom [pm]: 202.3(4), *202.3(4)* (C1–Au1), 203.2(4), *203.1(4)* (N1–Au1), 203.1(4), *204.6(4)* (N4–Au1), 203.7(4), *204.3(3)* (N7–Au1). The values in italics denote the bond lengths for the second molecule, which is not shown here.

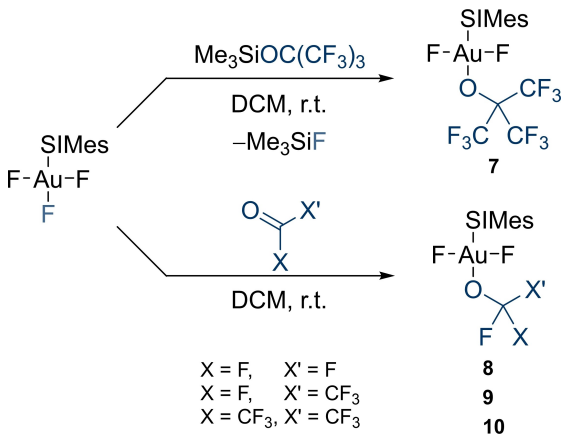

Scheme 4. Reaction of [AuF_3(SIMes)] with $Me_3SiOC(CF_3)_3$ (top) and different perfluorinated carbonyl-bearing molecules (bottom) for the formation of perfluoroalkoxido gold(III) complexes **7**–**10**.

chemical shift of 155.7 ppm, only 3 ppm high-field shifted compared to [AuF_3(SIMes)], indicating a comparable Lewis acidity (see below).

Crystals of *trans*-[$AuF_2(OC(CF_3)_3)$(SIMes)] (**7**) suitable for X-ray diffraction were obtained by slow vapor diffusion of *n*-pentane onto a concentrated solution of the reaction mixture in DCM at 4 °C. Compound **7** crystallizes in the monoclinic space group $P2_1/n$ with two disordered DCM molecules (see Figure S5), showing the typical square-planar coordination around the gold atom (see Figure 4). The Au–$C_{carbene}$ bond length of 198.4(6) pm is comparable to [AuF_3(SIMes)],[14] indicating the highly Lewis acidic character of the newly formed moiety of **7**.

Turning to the lighter homologues of perfluorinated alkoxides, the corresponding trimethylsilyl compounds are unknown. Inspired by examples of trifluoromethylation reactions using carbonyl fluoride and a fluoride salt,[51,53] we envisioned the investigation of the reactivity of [AuF_3(SIMes)] with carbonyl fluoride and other perfluorinated, carbonyl-bearing molecules, in order to obtain the corresponding alkoxido complexes (Scheme 4, bottom).

Addition of an excess of COF_2 onto a solution of [AuF_3(SIMes)] in DCM leads to the formation of the desired product *trans*-[$AuF_2(OCF_3)$(SIMes)] (**8**). Its ^{19}F NMR spectrum shows a triplet and a quartet at −40.2 ppm and −314.1 ppm, respectively, with a coupling constant $^4J(^{19}F,^{19}F) = 1.9$ Hz (see Figure 5). The chemical shift of the OCF_3 group is similar to that of the only literature-known trifluoromethoxido gold complex, which is an NHC-stabilized gold(I) complex.[49]

In analogy to the reaction with COF_2, addition of an excess of $CO(CF_3)F$ or $CO(CF_3)_2$ to a solution of [AuF_3(SIMes)] in DCM yields the compounds *trans*-[$AuF_2(OC(CF_3)F_2)$(SIMes)] (**9**) and *trans*-[$AuF_2(OC(CF_3)_2F)$(SIMes)] (**10**), respectively, as identified by multinuclear NMR spectroscopy (see Table 1). The ^{19}F NMR spectrum of compound **10** is depicted in Figure 6 and consists of a doublet of triplets at −82.0 ppm, a triplet of septets at −112.0 ppm and a doublet of septets at −313.8 ppm (see Table 1). Due to the high linewidth of the signals and small coupling constants of 1.7 Hz, 2.4 Hz and 3.2 Hz, the complex splitting patterns of the latter two cannot be directly seen in the ^{19}F NMR spectrum but were obtained via simulation (see Figure S47). Similarly, for compound **9**, no $^{19}F,^{19}F$ couplings can be resolved in the ^{19}F NMR spectrum. However, the signals that were assigned to compound **9** (−63.1 ppm, −86.1 ppm and −314.8 ppm, see Table 1) show a cross-peak in the $^{19}F,^{19}F$-COSY NMR spectrum (see Figure S41).

Crystals of compound **10** suitable for X-ray diffraction were obtained by vapor diffusion of *n*-pentane onto a solution of the reaction mixture in DCM. The molecular structure of *trans*-[$AuF_2(OC(CF_3)_2F)$(SIMes)] (**10**) in the solid state is shown in Figure 6. Compound **10** crystallizes in the triclinic space group $P\bar{1}$. The Au–$C_{carbene}$ and Au–O bond lengths of 197.8(2) pm and 201.3(2) pm, respectively, are comparable to the ones in compound **7** (198.4(6) pm and 202.7(4) pm, respectively, cf. Figure 4). Note, that the structure contains a co-crystallized solvent molecule and a disorder in the heptafluoro-iso-propyl group (see Figure S6).

Chemistry–A European Journal
Research Article
doi.org/10.1002/chem.202301684
Chemistry Europe
European Chemical Societies Publishing

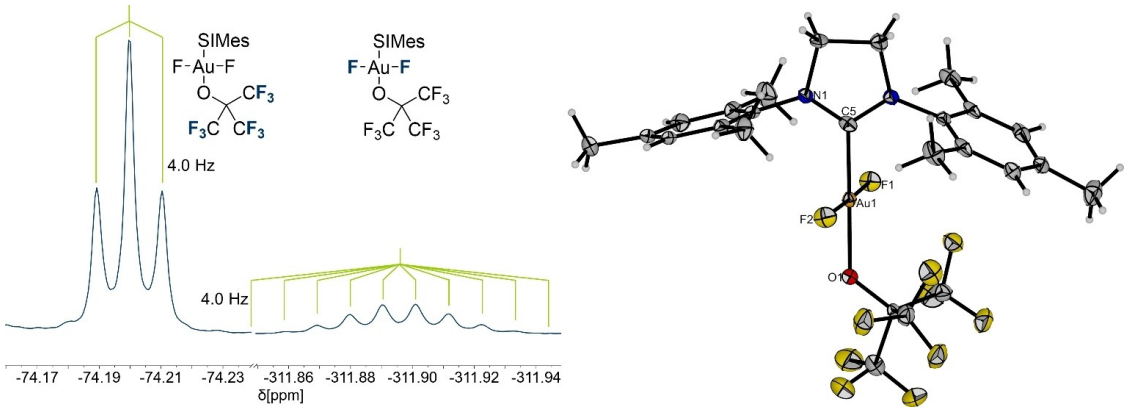

Figure 4. Left: ^{19}F NMR spectrum (377 MHz, DCM-d$_2$, 18 °C) of *trans*-[AuF$_2$(OC(CF$_3$)$_3$)(SIMes)] (**7**). Right: Molecular structure of *trans*-[AuF$_2$(OC(CF$_3$)$_3$)(SIMes)]·2 CH$_2$Cl$_2$ (**7**·2 CH$_2$Cl$_2$) in the solid state. The solvent molecules are omitted for clarity (see Figure S5). Thermal ellipsoids are set at 50% probability. Selected bond lengths to the central gold atom [pm]: 198.4(6) (C5–Au1), 192.5(3) (F1–Au1), 192.1(3) (F2–Au1), 202.7(4) (O1–Au1).

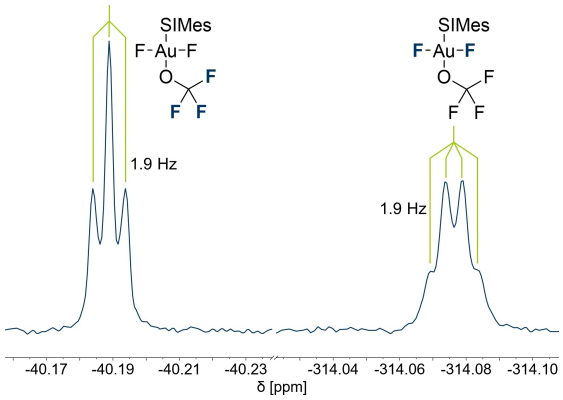

Figure 5. ^{19}F NMR spectrum (377 MHz, DCM-d$_2$, 18 °C) of *trans*-[AuF$_2$(OCF$_3$)(SIMes)] (**8**).

Comparing the four perfluoroalkoxido gold complexes **7**–**10**, it can be seen that the stability of the compound increases with the size of the perfluoroalkoxy group. While the trifluoromethoxido (**8**) and the pentafluoroethoxido (**9**) complexes decompose in solution within days (see Figure S36 and Figure S37 for **8**, as well as Figure S42 and Figure S43 for **9**) and have so far escaped crystallization, the heptafluoro-iso-propoxido (**10**) and nonafluoro-*tert*-butoxido (**7**) complexes are far more stable (see Figure S48 and Figure S49 for **10**), which also manifests in the successful crystallization of compounds **7** and **10**. This trend is also underlined by quantum-chemical calculations on the RI-B3LYP-D3/def2-TZVPP level of theory of the reaction energy of [AuF$_3$(SIMes)] and the corresponding perfluorinated carbonyl-bearing molecules to form compounds **8**–**10**. The Gibbs free energy $\Delta_r G$ for the formation of **8**, **9** and **10** at room temperature is 6 kJ·mol^{-1}, 1 kJ·mol^{-1} and −20 kJ·mol^{-1}, respectively, showing that the formation of the rather unstable compounds **8** and **9** is even slightly endergonic.

After the successful preparation of the perfluoroalkoxido gold complexes, we wanted to investigate the possibility of preparing the non-fluorinated analogues as well. As a test reaction, we tried to use acetone under the same conditions as for the reaction with hexafluoroacetone for the preparation of compound **10**. However, no reaction to the corresponding product *trans*-[AuF$_2$(OC(CH$_3$)$_2$F)(SIMes)] was observed, as the corresponding NMR spectra only showed the signals of the starting materials. Another reaction using benzophenone did not yield any new species, either. Therefore, the electrophilicity of the carbon atom in the used carbonyl-bearing molecule seems to play an important role. Furthermore, quantum-chemical calculations show that the Gibbs free energy $\Delta_r G$ at room temperature is 38 kJ·mol^{-1} for the reaction of [AuF$_3$(SIMes)] with acetone compared to −20 kJ·mol^{-1} for hexafluoroacetone.

SIMes affinity and Au–C bond lengths

As described above, the chemical shift of the carbene carbon atom $\delta(^{13}C_{carbene})$ is highly sensitive to the chemical environment of the SIMes and can be used as a measure of Lewis acidity of the corresponding gold(III) complex. It was shown by our group that this chemical shift correlates with the calculated "SIMes affinity" of those gold(III) moieties at the RI-B3LYP-D3/def2-TZVPP level of theory. The SIMes affinity was defined as the calculated Gibbs free energy $\Delta_r G_{diss}$ of the hypothetical dissociation of an [AuF$_2$X(SIMes)] or [AuX$_3$(SIMes)] complex into the free SIMes and the corresponding {AuF$_2$X} or {AuX$_3$} fragment, respectively. A nearly linear dependency can be found, i.e. the more upfield-shifted the chemical shift, the higher the SIMes affinity of the respective complex.[16,17] Figure 7 shows an updated version of this correlation including the new compounds **1**–**10**, together with related literature-known complexes.[14,16,17,65,66] All compounds **1**–**10** fit well within the whole set of complexes, underlining that this correlation is valid

Chemistry–A European Journal | Research Article
doi.org/10.1002/chem.202301684
Chemistry Europe
European Chemical Societies Publishing

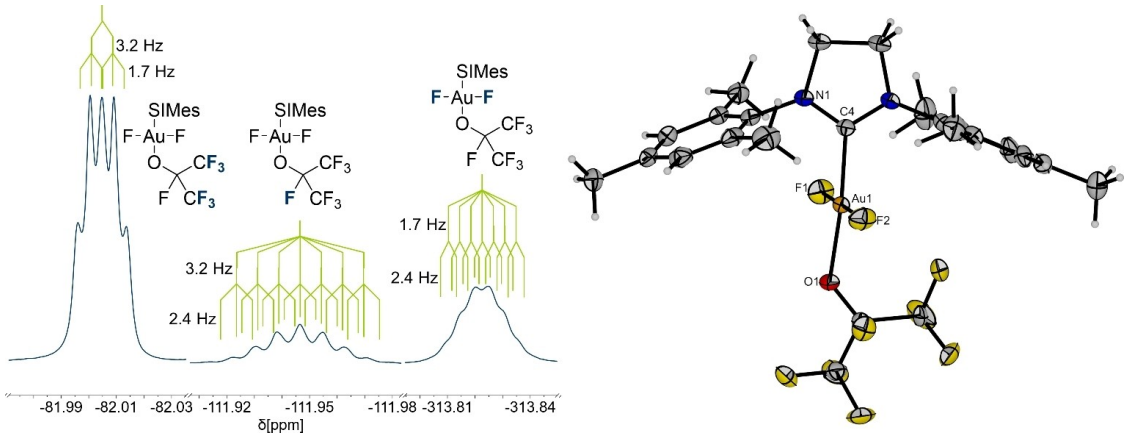

Figure 6. Left: ^{19}F NMR spectrum (377 MHz, DCM-d_2, 16 °C) of *trans*-[$AuF_2(OC(CF_3)_2F)(SIMes)$] (**10**). Right: Molecular structure of *trans*-[$AuF_2(OC(CF_3)_2F)(SIMes)$]·$CH_2Cl_2$ (**10**·CH_2Cl_2) in the solid state. The disorder in the heptafluoro-*iso*-propyl group and the solvent molecule are omitted for clarity (see Figure S6). Thermal ellipsoids are set at 50 % probability. Selected bond lengths to the central gold atom [pm]: 197.8(2) (C4–Au1), 192.3(2) (F1–Au1), 192.2(2) (F2–Au1), 201.3(2) (O1–Au1).

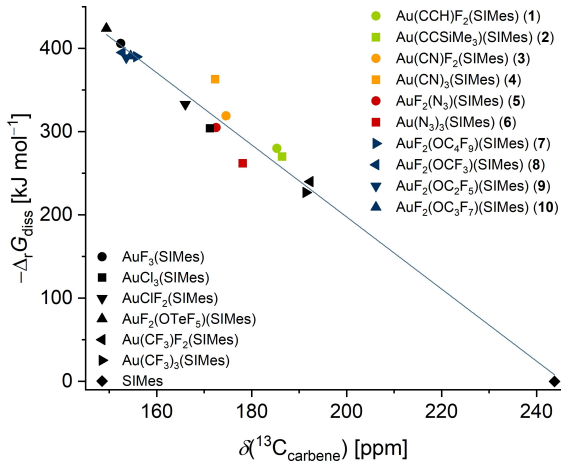

Figure 7. Correlation between the calculated SIMes affinity ($-\Delta_r G_{diss}$) and the chemical shift of the carbene carbon atom in the $^{13}C\{^1H\}$ NMR spectrum ($\delta(^{13}C_{carbene})$) of compounds **1**–**10** (green: alkynido complexes, orange: cyanido complexes, red: azido complexes, blue: perfluoroalkoxido complexes) and related, literature-known compounds (black).[14,16,17,65] The ^{13}C chemical shift of uncoordinated SIMes, which is plotted at a SIMes affinity of 0 kJ·mol^{-1}, is also included.[66]

for a plethora of ligands. Theoretical investigations connected a downfield shift of the carbene carbon atom with the deshielding from a ligand with a strong *trans*-influence.[67] Hence, the ligands can be classified by their *trans*-influence, following the order $OTeF_5 < F < OCF_3 \approx OC_2F_5 \approx OC_3F_7 \approx OC_4F_9 \ll Cl < CN \approx N_3 < CCH \approx CCSiMe_3 < CF_3$. In contrast to a study on gold hydrides, where also the *cis*-influence played a significant role,[68] the ligands in *cis* position do not have a pronounced influence on the deshielding as complexes of the type *trans*-[$AuF_2X(SIMes)$] and [$AuX_3(SIMes)$] with identical X have comparable chemical shifts and SIMes affinities.

Furthermore, this correlation can also be extended to the $Au–C_{carbene}$ bond lengths in the solid state. The more electron withdrawing the ligand in *trans* position to the carbene, the more Lewis acidic the gold(III) center and hence, the shorter, i.e. stronger the $Au–C_{carbene}$ bond.[32] This is well reflected in the overview of the $Au–C_{carbene}$ bond lengths of several different *trans*-[$AuF_2X(SIMes)$] and [$AuX_3(SIMes)$] complexes (Figure 8),[14,16,17,65] which follows the ordering of the *trans*-influence given above. Furthermore, for the complexes of the type *trans*-[$AuF_2X(SIMes)$] (X = CCH, CF_3, CN, N_3, OC_3F_7, OC_4F_9, Cl, F, $OTeF_5$), there is also a correlation between the chemical shift of the carbene carbon atom and the Au–C bond lengths (see Figure S50).

Conclusions

In conclusion, a detailed reactivity study of [$AuF_3(SIMes)$] was performed that gave rise to a variety of products of the type *trans*-[$AuF_2X(SIMes)$] that were characterized by NMR spectroscopy, structural and computational methods. By using trimethylsilyl compounds, alkynido, cyanido and azido ligands were introduced to the gold center, as well as a perfluoroalkoxido ligand. The pseudohalides cyanide and azide also yielded the corresponding [$AuX_3(SIMes)$] (X = CN, N_3) complexes when an excess of the Me_3SiX reagent was used. Furthermore, a second pathway, unprecedented in gold chemistry, is described for the introduction of the lighter perfluoroalkoxides consisting of the insertion of the corresponding perfluorinated carbonyl-bearing molecules into the Au–F bond *trans* to the SIMes ligand. Interestingly, the electrophilicity of the carbon atom was found to be crucial for the success of the reaction, as attempts to use the non-fluorinated analogues did not yield the desired products. Comparison of the perfluoroalkoxido gold complexes revealed that the stability of the complex decreases with

Chemistry–A European Journal
Research Article
doi.org/10.1002/chem.202301684
Chemistry Europe
European Chemical Societies Publishing

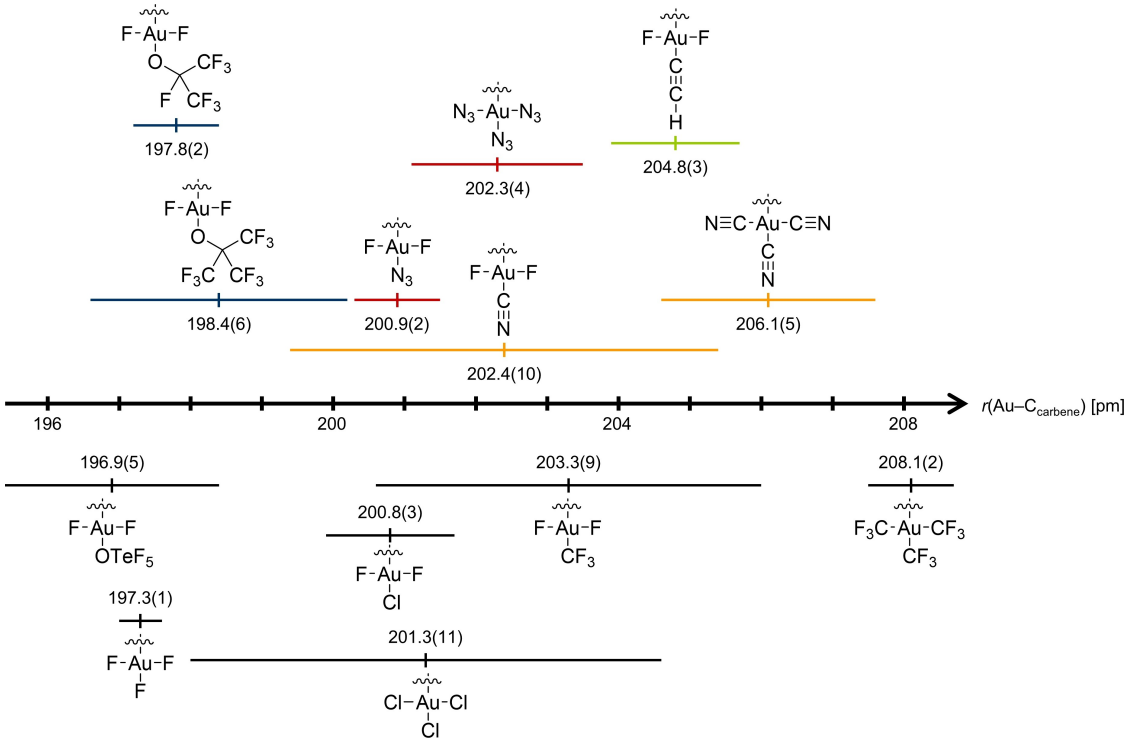

Figure 8. Overview of the Au–C bond lengths r(Au–$C_{carbene}$) of the complexes reported in this paper (top; green: alkynido complexes, orange: cyanido complexes, red: azido complexes, blue: perfluoroalkoxido complexes), and related, literature-known[14,16,17,65] complexes (bottom, black), including a range equal to three times the error in both directions. In the chemical formulae of the structures, the SIMes ligand is omitted for clarity.

smaller perfluorinated moieties bound to the central gold atom, as also supported by quantum-chemical calculations. The ^{13}C NMR chemical shift of the carbene carbon atoms in the prepared compounds was correlated with the calculated SIMes affinity, which, together with similar literature-known complexes, yielded an ordering of more than 10 ligands with respect to their *trans*-influence. The ^{13}C chemical shift was also shown to correlate with the Au–C bond lengths of *trans*-[AuF_2X(SIMes)] complexes. All complexes reported offer several attractive motifs for further reactions such as addition to multiple bonds, or transfer of thermodynamically labile perfluoroalkoxido groups, which could be investigated.

Experimental Section

CAUTION! Strong oxidizers!

All reactions should be conducted under rigorously anhydrous conditions. The presence of organic materials together with AuF_3 can lead to violent reactions. In contact with only small amounts of moisture, all used fluorine-containing substances decompose under the formation of HF. Hence, appropriate treatment procedures need to be available in case of a contamination with HF containing solutions.

Materials, chemicals and procedures: All experiments were performed under strict exclusion of moisture and air using standard Schlenk techniques. Solid compounds were handled inside an *MBRAUN UNIlab plus* glovebox with an argon atmosphere ($c(O_2) <$ 0.5 ppm, $c(H_2O) <$ 0.5 ppm). Solvents were dried using an *MBRAUN SPS-800* solvent system and stored over 4 Å molecular sieves. AuF_3,[69] 1,3-bis(2,4,6-trimethylphenyl)-4,5-dihydroimidazol-2-ylidene (SIMes),[70] and [AuF_3(SIMes)][17] were prepared using literature-known syntheses. NMR spectra were recorded with a *JEOL 400 MHz ECZ-R* or *ECS* spectrometer. All chemical shifts are referenced using the Ξ values given in the *IUPAC* recommendations of 2008 and the ^{2}H signal of the deuterated solvent as internal reference.[71] For external locking, acetone-d_6 was flame sealed in a glass capillary and the lock oscillator frequency was adjusted to give $\delta(^1H) =$ 7.26 ppm for a $CHCl_3$ sample locked on the capillary. For spin systems with high linewidths, coupling constants are reported as simulated in *gNMR*.[72] *MestReNova 14.2* was used for processing the spectra and for their graphical representation. X-ray diffraction measurements were performed on a *Bruker D8 Venture* diffractometer with MoK_α ($\lambda = 0.71073$ Å) radiation at 100 K. Single crystals were picked in perfluoroether oil at −40 °C under a nitrogen atmosphere and mounted on a 0.15 mm *Mitegen* micromount. They were solved using the *ShelXT*[73] structure solution program with intrinsic phasing and were refined with the refinement package *ShelXL*[74] using least squares minimizations by using the program *OLEX2*.[75] *Diamond 3* and *POV-Ray 3.7* were used for their graphical representation. Raman spectra of single crystals were recorded at −196 °C using a *Bruker RamanScope III* spectrometer with a resolution of 4 cm^{-1}. The samples were measured using a Teflon

Chemistry–A European Journal | Research Article doi.org/10.1002/chem.202301684 | Chemistry Europe European Chemical Societies Publishing

plate which is cooled by a copper block cooled with liquid nitrogen, producing a nitrogen atmosphere that kept the sample inert.[76] IR spectra were measured inside a glovebox under argon atmosphere at room temperature using a *Bruker ALPHA FTIR* spectrometer with a diamond ATR attachment with 32 scans and a resolution of 4 cm^{-1}. Raman and IR spectra were processed using *OPUS 7.5* and *Origin 2022*[77] was used for their graphical representation. Quantum chemical calculations were performed using the functional B3LYP[78] with RI[79] and Grimme-D3[80] corrections and the basis set def2-TZVPP[81] as incorporated in *TURBOMOLE V7.3*.[82] Reaction energies were calculated by subtraction of the energies of the starting materials from the ones of the products, which were obtained from the calculated SCF energy of geometry optimized minimum structures that were corrected for the enthalpy and entropy at standard temperature and pressure using the module *freeh* as incorporated in *TURBOMOLE V7.3* with a scaling factor of 0.9614.[82] All experiments were performed on a 10 mg scale for [AuF_3(SIMes)] and characterized from the reaction mixture.

Reaction between [AuF_3(SIMes)] and Me_3SiCCH: This reaction was performed with varying amounts of Me_3SiCCH and with or without the addition of CsF, see Table S4 for details. In the following, the reaction with CsF and an excess of Me_3SiCCH is described as an example for the procedure, which did not change except for the amounts of substances used. In a typical experiment, [AuF_3(SIMes)] (10 mg, 17.8 μmol, 1 equiv.) and CsF (3 mg, 19,7 μmol, 1.1 equiv.) were dissolved in CD_2Cl_2 (ca. 1 mL) and Me_3SiCCH (18 mg, 188 μmol, 10 equiv.) was condensed onto the frozen solution at −196 °C. The mixture was slowly thawed and the progress of the reaction was followed by NMR spectroscopy. The main reaction product identified by ^{19}F NMR spectroscopy was *trans*-[Au(CCH)F_2(SIMes)] (**1**). However, *trans*-[$AuClF_2$(SIMes)] and traces of *trans*-[Au($CCSiMe_3$)F_2(SIMes)] (**2**) were formed as side products (see Figure S9–Figure S12). Depending on the amount of Me_3SiCCH and the presence of CsF, the ratio of compound **1** and **2** can vary (cf. Table S4 and Figure S13).

trans-[Au(CCH)F_2(SIMes)] (**1**): **^{1}H NMR** (400 MHz, CD_2Cl_2, 21 °C) δ = 7.07 (s, 4H, *meta*-CH), 4.17 (s, 4H, NCH_2CH_2N), 2.36 (s, 6H, *para*-CH_3), 2.35 (s, 12H, *ortho*-CH_3), 1.60 (t, 1H, −CCH, $^4J(^1H,^{19}F)$ = 2.1 Hz) ppm. **$^{13}C\{^1H\}$ NMR** (101 MHz, CD_2Cl_2, 21 °C) δ = 185.3 (s, NCN carbene), 140.0 (s, C_{Ar}), 136.6 (s, C_{Ar}), 132.2 (s, C_{Ar}), 129.9 (s, C_{Ar}), 51.4 (s, NCH_2CH_2N), 20.9 (s, CH_3), 17.2 (s, CH_3) ppm. **^{19}F NMR** (377 MHz, CD_2Cl_2, 20 °C) δ = −340.8 (d, 2F, *cis*-F, $^4J(^{19}F,^1H)$ = 2.1 Hz) ppm. **IR** $\tilde{\nu}$ = 3305 (w, ν(C-H_{alkyne})), 2924 (w), 2022 (vw, ν(C≡C)), 1607 (w), 1523 (vs), 1459 (s), 1378 (m), 1323 (m), 1273 (vs), 1225 (m), 1185 (m), 1016 (w), 985 (vw), 949 (vw), 924 (vw), 852 (m), 739 (w), 652 (m), 620 (m), 584 (vs, $\nu_{as}(AuF_2)$), 452 (m) cm^{-1}. **FT-Raman** (50 mW, 1024 scans) $\tilde{\nu}$ = 2926 (m), 2031 (m, ν(C≡C)), 1607 (m), 1505 (m), 1384 (m), 1312 (m), 1018 (m), 579 (s, $\nu_{as}(AuF_2)$), 560 (s, $\nu_s(AuF_2)$), 457 (m), 78 (vs) cm^{-1}.

trans-[Au($CCSiMe_3$)F_2(SIMes)] (**2**): **^{1}H NMR** (400 MHz, CD_2Cl_2, 21 °C) δ = 7.07 (s, 4H, *meta*-CH), 4.15 (s, 4H, NCH_2CH_2N), 2.37 (s, 18H, *ortho*-CH_3 + *para*-CH_3), 0.07 (s, 9H, −$CCSiMe_3$) ppm. **$^{13}C\{^1H\}$ NMR** (101 MHz, CD_2Cl_2, 21 °C) δ = 186.4 (s, NCN carbene), 140.0 (s, C_{Ar}), 136.6 (s, C_{Ar}), 132.0 (s, C_{Ar}), 129.8 (s, C_{Ar}), 51.5 (s, NCH_2CH_2N), 20.6 (s, CH_3), 17.2 (s, CH_3) ppm. **^{19}F NMR** (377 MHz, CD_2Cl_2, 20 °C) δ = −340.2 (s, 2F, *cis*-F) ppm. **$^{29}Si\{^1H\}$-DEPT NMR** (80 MHz, CD_2Cl_2, 21 °C) δ = 7.4 (1Si, −$CCSiMe_3$) ppm.

Reaction between [AuF_3(SIMes)] and $Me_3SiCCSiMe_3$: In a typical experiment, [AuF_3(SIMes)] (10 mg, 17.8 μmol, 1 equiv.), CsF (3 mg, 19,7 μmol, 1.1 equiv.) and $Me_3SiCCSiMe_3$ (6 mg, 35.2 μmol, 2 equiv.) were weighed in and at −196 °C, CD_2Cl_2 (ca. 1 mL) was condensed onto the solids. The mixture was slowly thawed and the progress of the reaction was followed by NMR spectroscopy. The main reaction product identified by ^{19}F NMR spectroscopy was *trans*-[Au($CCSiMe_3$)F_2(SIMes)] (**2**), whereas *trans*-[$AuClF_2$(SIMes)] is formed as a side product (see Figure S14 and Figure S15).

Reaction between [AuF_3(SIMes)] and Me_3SiCN: In a typical experiment, [AuF_3(SIMes)] (10 mg, 17.8 μmol, 1 equiv.) was dissolved in CD_2Cl_2 (ca. 1 mL) and Me_3SiCN (2 mg, 20.1 μmol, 1.1 equiv.) was condensed onto the frozen solution at −196 °C. The mixture was slowly thawed and the progress of the reaction was followed by NMR spectroscopy. The main reaction product identified by ^{19}F NMR spectroscopy is *trans*-[Au(CN)F_2(SIMes)] (**3**) with some unreacted starting material after one day (see Figure S16–Figure S18). At −196 °C, more Me_3SiCN (5 mg, 54.1 μmol, 3 equiv.) was condensed onto the frozen solution. The progress of the reaction was followed by ^{19}F NMR spectroscopy and a full conversion of [AuF_3(SIMes)] found after one hour, yielding *trans*-[Au(CN)F_2(SIMes)] (**3**) and traces of [Au($CN)_3$(SIMes)] (**4**), together with an unknown side product. After four weeks, a full conversion of **3** to yield **4** is found (see Figure S19–Figure S21).

trans-[Au(CN)F_2(SIMes)] (**3**): **^{1}H NMR** (400 MHz, CD_2Cl_2, 16 °C) δ = 7.07 (s, 4H, *meta*-CH), 4.23 (s, 4H, NCH_2CH_2N), 2.37 (s, 6H, *para*-CH_3), 2.34 (s, 12H, *ortho*-CH_3) ppm. **$^{13}C\{^1H\}$ NMR** (101 MHz, CD_2Cl_2, 16 °C) δ = 174.6 (s, NCN carbene), 140.5 (s, C_{Ar}), 136.5 (s, C_{Ar}), 131.2 (s, C_{Ar}), 130.0 (s, C_{Ar}), 51.6 (s, NCH_2CH_2N), 21.0 (s, CH_3), 17.1 (s, CH_3) ppm. **^{19}F NMR** (377 MHz, CD_2Cl_2, 16 °C) δ = −337.1 (s, 2F, *cis*-F) ppm. **IR** $\tilde{\nu}$ = 2923 (m), 2161 (w, ν(N≡C)), 1631 (m), 1607 (m), 1533 (vs), 1480 (s), 1460 (s), 1380 (m), 1322 (m), 1276 (vs), 1221 (m), 1187 (m), 1014 (m), 983 (m), 951 (m), 852 (s), 737 (m), 710 (m), 635 (m), 599 (vs, $\nu_{as}(AuF_2)$), 570 (vs, $\nu_s(AuF_2)$), 445 (m), 419 (vs) cm^{-1}.

[Au($CN)_3$(SIMes)] (**4**): **^{1}H NMR** (400 MHz, CD_2Cl_2, 15 °C) δ = 7.05 (s, 4H, *meta*-CH), 4.29 (s, 4H, NCH_2CH_2N), 2.34 (s, 6H, *para*-CH_3), 2.31 (s, 12H, *ortho*-CH_3) ppm. **$^{13}C\{^1H\}$ NMR** (101 MHz, CD_2Cl_2, 15 °C) δ = 172.3 (s, NCN carbene), 141.1 (s, C_{Ar}), 135.3 (s, C_{Ar}), 130.8 (s, C_{Ar}), 129.6 (s, C_{Ar}), 52.6 (s, NCH_2CH_2N), 20.9 (s, CH_3), 17.7 (s, CH_3) ppm. **IR** $\tilde{\nu}$ = 2920 (w), 2186 (w, ν(N≡C))), 2149 (w, ν(N≡C)), 1607 (m), 1532 (s), 1501 (s), 1457 (s), 1381 (m), 1319 (m), 1275 (vs), 1220 (m), 1188 (m), 1014 (m), 949 (m), 850 (vs), 767 (m), 736 (m), 634 (m), 591 (m), 573 (s), 534 (m), 497 (m), 444 (s), 418 (s) cm^{-1}.

Reaction between [AuF_3(SIMes)] and Me_3SiN_3: In a typical experiment, [AuF_3(SIMes)] (10 mg, 17.8 μmol, 1 equiv.) was dissolved in CD_2Cl_2 (ca. 1 mL) and Me_3SiN_3 (2 mg, 17.4 μmol, 1 equiv.) was condensed onto the frozen solution at −196 °C. The mixture was slowly thawed and the progress of the reaction was followed by NMR spectroscopy. The reaction product identified by ^{19}F NMR spectroscopy is *trans*-[$AuF_2(N_3)$(SIMes)] (**5**) after one hour (see Figure S23–Figure S25). At −196 °C, more Me_3SiN_3 (6 mg, 52.1 μmol, 2.9 equiv.) was condensed onto the frozen solution. The progress of the reaction was followed by ^{19}F NMR spectroscopy and after three days, a full conversion of **5** to yield [$Au(N_3)_3$(SIMes)] (**6**) is found (see Figure S26–Figure S28).

trans-[$AuF_2(N_3)$(SIMes)] (**5**): **^{1}H NMR** (400 MHz, CD_2Cl_2, 16 °C) δ = 7.09 (s, 4H, *meta*-CH), 4.26 (s, 4H, NCH_2CH_2N), 2.37 (s, 6H, *para*-CH_3), 2.36 (s, 12H, *ortho*-CH_3) ppm. **$^{13}C\{^1H\}$ NMR** (101 MHz, CD_2Cl_2, 16 °C) δ = 172.5 (s, NCN carbene), 140.6 (s, C_{Ar}), 136.6 (s, C_{Ar}), 131.7 (s, C_{Ar}), 130.0 (s, C_{Ar}), 51.7 (s, NCH_2CH_2N), 21.0 (s, CH_3), 17.1 (s, CH_3) ppm. **^{19}F NMR** (377 MHz, CD_2Cl_2, 16 °C) δ = −311.1 (s, 2F, *cis*-F) ppm. **IR** $\tilde{\nu}$ = 2923 (m), 2048 (vs, $\nu(N_3)$), 1608 (m), 1534 (vs), 1481 (s), 1463 (s), 1380 (m), 1321 (m), 1277 (vs), 1230 (m), 1191 (m), 1017 (m), 986 (m), 952 (m), 851 (m), 712 (m), 644 (m), 632 (m), 604 (vs, $\nu_{as}(AuF_2)$), 564 (s, $\nu_s(AuF_2)$), 534 (vs), 419 (vs) cm^{-1}.

[$Au(N_3)_3$(SIMes)] (**6**): **^{1}H NMR** (400 MHz, CD_2Cl_2, 15 °C) δ = 7.06 (s, 4H, *meta*-CH), 4.16 (s, 4H, NCH_2CH_2N), 2.42 (s, 12H, *ortho*-CH_3), 2.35 (s, 6H, *para*-CH_3) ppm. **$^{13}C\{^1H\}$ NMR** (101 MHz, CD_2Cl_2, 15 °C) δ = 178.1 (s, NCN carbene), 140.3 (s, C_{Ar}), 136.2 (s, C_{Ar}), 132.0 (s, C_{Ar}), 130.0 (s, C_{Ar}), 51.9 (s, NCH_2CH_2N), 20.9 (s, CH_3), 17.4 (s, CH_3) ppm. **IR**

Chemistry–A European Journal | Research Article doi.org/10.1002/chem.202301684 | Chemistry Europe European Chemical Societies Publishing

$\tilde{\nu}$ = 2914 (m), 2039 (vs, $\nu(N_3)$), 2020 (vs, $\nu(N_3)$), 1607 (m), 1523 (s), 1499 (s), 1457 (s), 1376 (m), 1318 (m), 1272 (vs), 1239 (s), 1227 (s), 1183 (m), 1016 (m), 984 (m), 952 (m), 857 (s), 737 (m), 711 (m), 676 (m), 630 (s), 594 (m), 572 (s), 430 (vs), 413 (vs) cm^{-1}. **FT-Raman** (50 mW, 16384 scans) $\tilde{\nu}$ = 2311 (vw), 2239 (vw), 2075 (vw, $\nu(N_3)$), 1580 (vs), 1483 (vs), 1358 (vs), 1086 (vs), 72 (vs) cm^{-1}.

Reaction between [AuF_3(SIMes)] and $Me_3SiOC(CF_3)_3$: In a typical experiment, [AuF_3(SIMes)] (10 mg, 17.8 µmol, 1 equiv.) was dissolved in CD_2Cl_2 (ca. 1 mL) and $Me_3SiOC(CF_3)_3$ (25 mg, 81.1 µmol, 4.5 equiv.) was condensed onto the frozen solution at −196 °C. The mixture was slowly thawed and the progress of the reaction was followed by NMR spectroscopy. The main reaction product identified by ^{19}F NMR spectroscopy was *trans*-[$AuF_2(OC(CF_3)_3)$(SIMes)] (**7**), together with traces of an unknown side product (see Figure S30–Figure S32).

trans-[$AuF_2(OC(CF_3)_3)$(SIMes)] (**7**): **^1H NMR** (400 MHz, CD_2Cl_2, 18 °C) δ = 7.08 (s, 4H, *meta*-CH), 4.33 (s, 4H, NCH_2CH_2N), 2.36 (s, 18H, *ortho*-CH_3 + *para*-CH_3) ppm. **$^{13}C\{^1H\}$ NMR** (101 MHz, CD_2Cl_2, 18 °C) δ = 155.7 (s, NCN carbene), 140.6 (s, C_{Ar}), 136.4 (s, C_{Ar}), 131.2 (s, C_{Ar}), 129.8 (s, C_{Ar}), 51.2 (s, NCH_2CH_2N), 20.7 (s, CH_3), 17.1 (s, CH_3) ppm. **^{19}F NMR** (377 MHz, CD_2Cl_2, 18 °C) δ = −74.2 (t, 9F, −OC(*CF_3*)$_3$, $^5J(^{19}F,^{19}F)$ = 4.0 Hz), −311.9 (dec, 2F, *cis*-F) ppm. **IR** $\tilde{\nu}$ = 2926 (vw), 1701 (vw), 1609 (vw), 1542 (s), 1484 (m), 1380 (w), 1263 (vs, ν(C–C)), 1237 (vs, ν(C–C)), 1168 (vs, ν(C–O)), 1015 (vw), 966 (vs, $\delta_{ip}(CCF_3)$), 855 (m), 725 (s, $\delta_{oop}(CF_3)$), 651 (w), 602 (s, $\nu_{as}(AuF_2)$), 573 (m, ν_s (AuF_2)), 536 (w), 488 (vw), 422 (vw) cm^{-1}. **FT-Raman** (200 mW, 8192 scans) $\tilde{\nu}$ = 2927 (s), 2858 (s), 2083 (vw), 2027 (vw), 1506 (vw), 1313 (vw, ν(C–O)), 573 (s, $\nu_s(AuF_2)$), 537 (vw), 284 (vw), 253 (vw), 72 (vs) cm^{-1}.

Reaction between [AuF_3(SIMes)] and COF_2: In a typical experiment, [AuF_3(SIMes)] (10 mg, 17.8 µmol, 1 equiv.) was dissolved in CD_2Cl_2 (ca. 1 mL) and COF_2 (8 mg, 116 µmol, 6.5 equiv.) was condensed onto the frozen solution at −196 °C. The mixture was slowly thawed and the progress of the reaction was followed by NMR spectroscopy. The main reaction product identified by ^{19}F NMR spectroscopy was *trans*-[$AuF_2(OCF_3)$(SIMes)] (**8**) with traces of unknown side products (see Figure S33–Figure S35). Compound **8** decomposes within four days at room temperature to an unknown side product (see Figure S36 and Figure S37).

trans-[$AuF_2(OCF_3)$(SIMes)] (**8**): **^1H NMR** (400 MHz, CD_2Cl_2, 18 °C) δ = 7.09 (s, 4H, *meta*-CH), 4.35 (s, 4H, NCH_2CH_2N), 2.36 (s, 18H, *ortho*-CH_3 + *para*-CH_3) ppm. **$^{13}C\{^1H\}$ NMR** (101 MHz, CD_2Cl_2, 18 °C) δ = 152.7 (s, NCN carbene), 140.9 (s, C_{Ar}), 136.4 (s, C_{Ar}), 131.5 (s, C_{Ar}), 130.0 (s, C_{Ar}), 51.4 (s, NCH_2CH_2N), 20.9 (s, CH_3), 17.1 (s, CH_3) ppm. **^{19}F NMR** (377 MHz, CD_2Cl_2, 18 °C) δ = −40.2 (t, 3F, −OCF_3, $^4J(^{19}F,^{19}F)$ = 1.9 Hz), −314.1 (q, 2F, *cis*-F) ppm.

Reaction between [AuF_3(SIMes)] and $CO(CF_3)F$: In a typical experiment, [AuF_3(SIMes)] (10 mg, 17.8 µmol, 1 equiv.) was dissolved in CD_2Cl_2 (ca. 1 mL) and $CO(CF_3)F$ (13 mg, 116 µmol, 6.5 equiv.) was condensed onto the frozen solution at −196 °C. The mixture was slowly thawed and the progress of the reaction was followed by NMR spectroscopy. The main reaction product identified by ^{19}F NMR spectroscopy was *trans*-[$AuF_2(OC(CF_3)F_2)$(SIMes)] (**9**) with traces of an unknown side product (see Figure S38–Figure S41). Compound **9** decomposes within three days at room temperature to an unknown side product (see Figure S42 and Figure S43).

trans-[$AuF_2(OC(CF_3)F_2)$(SIMes)] (**9**): **^1H NMR** (400 MHz, CD_2Cl_2, 17 °C) δ = 7.10 (s, 4H, *meta*-CH), 4.35 (s, 4H, NCH_2CH_2N), 2.36 (s, 18H, *ortho*-CH_3 + *para*-CH_3) ppm. **$^{13}C\{^1H\}$ NMR** (101 MHz, CD_2Cl_2, 17 °C) δ = 153.6 (s, NCN carbene), 140.9 (s, C_{Ar}), 136.5 (s, C_{Ar}), 131.5 (s, C_{Ar}), 130.0 (s, C_{Ar}), 51.5 (s, NCH_2CH_2N), 21.0 (s, CH_3), 17.2 (s, CH_3) ppm. **^{19}F NMR** (377 MHz, CD_2Cl_2, 17 °C) δ = −63.1 (s, 2F, −OCF_2CF_3), −86.1 (s, 3F, −OCF_2CF_3), −314.8 (s, 2F, *cis*-F) ppm.

Reaction between [AuF_3(SIMes)] and $CO(CF_3)_2$: In a typical experiment, [AuF_3(SIMes)] (10 mg, 17.8 µmol, 1 equiv.) was dissolved in CD_2Cl_2 (ca. 1 mL) and $CO(CF_3)_2$ (19 mg, 116 µmol, 6.5 equiv.) was condensed onto the frozen solution at −196 °C. The mixture was slowly thawed and the progress of the reaction was followed by NMR spectroscopy. The main reaction product identified by ^{19}F NMR spectroscopy was *trans*-[$AuF_2(OC(CF_3)_2F)$(SIMes)] (**10**) with traces of an unknown side product (see Figure S44–Figure S47).

trans-[$AuF_2(OC(CF_3)_2F)$(SIMes)] (**10**): **^1H NMR** (400 MHz, CD_2Cl_2, 16 °C) δ = 7.09 (s, 4H, *meta*-CH), 4.34 (s, 4H, NCH_2CH_2N), 2.36 (s, 18H, *ortho*-CH_3 + *para*-CH_3) ppm. **$^{13}C\{^1H\}$ NMR** (101 MHz, CD_2Cl_2, 17 °C) δ = 154.5 (s, NCN carbene), 140.9 (s, C_{Ar}), 136.4 (s, C_{Ar}), 130.9 (s, C_{Ar}), 130.0 (s, C_{Ar}), 51.4 (s, NCH_2CH_2N), 20.7 (s, CH_3), 17.1 (s, CH_3) ppm. **^{19}F NMR** (377 MHz, CD_2Cl_2, 16 °C) δ = −82.0 (dt, 6F, −OCF(*CF_3*)$_2$, $^3J(^{19}F,^{19}F)$ = 3.2 Hz, $^5J(^{19}F,^{19}F)$ = 1.7 Hz), −112.0 (tsept, 1F, −*OCF*$(CF_3)_2$, $^4J(^{19}F,^{19}F)$ ≈ 2.4 Hz), −313.9 (dsept, 2F, *cis*-F) ppm. **FT-Raman** (100 mW, 4096 scans) $\tilde{\nu}$ = 2932 (m), 1609 (w), 1505 (w), 1465 (w), 1390 (w), 1314 (w, ν(C–O)), 1012 (vw), 776 (vw), 567 (m, $\nu_s(AuF_2)$), 422 (vw), 342 (w), 290 (w), 188 (w), 70 (vs) cm^{-1}.

Deposition Numbers 2262531 (for **1**), 2262543 (for **3**), 2262544 (for **4**·CH_2Cl_2), 2262532 (for **5**·0.5 CH_2Cl_2), 2262533 (for **6**), 2262545 (for **7**·2 CH_2Cl_2), 2262534 (for **10**·CH_2Cl_2) contain the supplementary crystallographic data for this paper. These data are provided free of charge by the joint Cambridge Crystallographic Data Centre and Fachinformationszentrum Karlsruhe Access Structures service.

Supporting Information

The authors have cited additional references within the Supporting Information.[14,16,17,83]

Acknowledgements

Funded by the ERC project HighPotOx (Grant agreement ID:818862). The authors would like to thank the HPC Service of ZEDAT, Freie Universität Berlin, for computing time and gratefully acknowledge the assistance of the Core Facility BioSupraMol supported by the DFG. M. W. thanks the Dahlem Research School for financial support, Dr. Günther Thiele for help solving the solid state structures and Elodie Lorentz for help designing the TOC graphic. A. P.-B. and M. A. E. thank the Alexander von Humboldt Foundation for a postdoctoral research fellowship. A. P.-B. also acknowledges the Department of Biology, Chemistry, Pharmacy of the Freie Universität Berlin for a Rising Star Junior Fellowship. Open Access funding enabled and organized by Projekt DEAL.

Conflict of Interests

The authors declare no conflict of interest.

Data Availability Statement

The data that support the findings of this study are available from the corresponding author upon reasonable request.

Chemistry–A European Journal | Research Article
doi.org/10.1002/chem.202301684
Chemistry Europe
European Chemical Societies Publishing

Keywords: gold(III) · gold fluorides · *N*-heterocyclic carbenes · organo gold chemistry · perfluoroalkoxides

[1] F. Mohr, *Gold Bull.* **2004**, *37*, 164.
[2] D. R. Lide, *CRC Handbook of Chemistry and Physics*, 87. Aufl., Taylor & Francis, Boca Raton, FL., **2006**.
[3] a) W. J. Wolf, F. D. Toste, in *Patai's chemistry of functional groups* (Hrsg.: Z. Rappoport, J. F. Liebman, I. Marek), Wiley, Chichester, **2014**, S. 391–408; b) J. Miró, C. del Pozo, *Chem. Rev.* **2016**, *116*, 11924.
[4] D. S. Laitar, P. Müller, T. G. Gray, J. P. Sadighi, *Organometallics* **2005**, *24*, 4503.
[5] J. A. Akana, K. X. Bhattacharyya, P. Müller, J. P. Sadighi, *J. Am. Chem. Soc.* **2007**, *129*, 7736.
[6] R. Kumar, A. Linden, C. Nevado, *Angew. Chem. Int. Ed.* **2015**, *54*, 14287; *Angew. Chem.* **2015**, *127*, 14495.
[7] a) M. S. Winston, W. J. Wolf, F. D. Toste, *J. Am. Chem. Soc.* **2015**, *137*, 7921; b) R. Kumar, A. Linden, C. Nevado, *J. Am. Chem. Soc.* **2016**, *138*, 13790.
[8] A. Pérez-Bitrián, S. Martínez-Salvador, M. Baya, J. M. Casas, A. Martín, B. Menjón, J. Orduna, *Chem. Eur. J.* **2017**, *23*, 6919.
[9] A. Genoux, J. A. González, E. Merino, C. Nevado, *Angew. Chem. Int. Ed.* **2020**, *59*, 17881; *Angew. Chem.* **2020**, *132*, 18037.
[10] A. Genoux, M. Biedrzycki, E. Merino, E. Rivera-Chao, A. Linden, C. Nevado, *Angew. Chem. Int. Ed.* **2021**, *60*, 4164; *Angew. Chem.* **2021**, *133*, 4210.
[11] a) N. P. Mankad, F. D. Toste, *J. Am. Chem. Soc.* **2010**, *132*, 12859; b) M. Albayer, R. Corbo, J. L. Dutton, *Chem. Commun.* **2018**, *54*, 6832.
[12] A. Pérez-Bitrián, M. Baya, J. M. Casas, A. Martín, B. Menjón, J. Orduna, *Angew. Chem. Int. Ed.* **2018**, *57*, 6517; *Angew. Chem.* **2018**, *130*, 3425.
[13] G. Kleinhans, A. K.-W. Chan, M.-Y. Leung, D. C. Liles, M. A. Fernandes, V. W.-W. Yam, I. Fernández, D. I. Bezuidenhout, *Chem. Eur. J.* **2020**, *26*, 6993.
[14] M. A. Ellwanger, S. Steinhauer, P. Golz, T. Braun, S. Riedel, *Angew. Chem. Int. Ed.* **2018**, *57*, 7210; *Angew. Chem.* **2018**, *130*, 7328–7332.
[15] F. W. B. Einstein, P. R. Rao, J. Trotter, N. Bartlett, *J. Chem. Soc. A* **1967**, 478.
[16] M. A. Ellwanger, C. von Randow, S. Steinhauer, Y. Zhou, A. Wiesner, H. Beckers, T. Braun, S. Riedel, *Chem. Commun.* **2018**, *54*, 9301.
[17] M. Winter, N. Limberg, M. A. Ellwanger, A. Pérez-Bitrián, K. Sonnenberg, S. Steinhauer, S. Riedel, *Chem. Eur. J.* **2020**, *26*, 16089.
[18] L. Sharp-Bucknall, L. Barwise, J. D. Bennetts, M. Albayer, J. L. Dutton, *Organometallics* **2020**, *39*, 3344.
[19] B. Y.-W. Wong, H.-L. Wong, Y.-C. Wong, M.-Y. Chan, V. W.-W. Yam, *Angew. Chem. Int. Ed.* **2017**, *56*, 302; *Angew. Chem.* **2017**, *129*, 308.
[20] V. W.-W. Yam, K. M.-C. Wong, L.-L. Hung, N. Zhu, *Angew. Chem. Int. Ed.* **2005**, *44*, 3107; *Angew. Chem.* **2005**, *117*, 3167.
[21] D. Zhou, W.-P. To, Y. Kwak, Y. Cho, G. Cheng, G. S. M. Tong, C.-M. Che, *Adv. Sci.* **2019**, *6*, 1802297.
[22] B. Y.-W. Wong, H.-L. Wong, Y.-C. Wong, V. K.-M. Au, M.-Y. Chan, V. W.-W. Yam, *Chem. Sci.* **2017**, *8*, 6936.
[23] J. A. Garg, O. Blacque, K. Venkatesan, *Inorg. Chem.* **2011**, *50*, 5430.
[24] V. K.-M. Au, W. H. Lam, W.-T. Wong, V. W.-W. Yam, *Inorg. Chem.* **2012**, *51*, 7537.
[25] V. K.-M. Au, D. P.-K. Tsang, K. M.-C. Wong, M.-Y. Chan, N. Zhu, V. W.-W. Yam, *Inorg. Chem.* **2013**, *52*, 12713.
[26] K. M.-C. Wong, L.-L. Hung, W. H. Lam, N. Zhu, V. W.-W. Yam, *J. Am. Chem. Soc.* **2007**, *129*, 4350.
[27] K. M.-C. Wong, X. Zhu, L.-L. Hung, N. Zhu, V. W.-W. Yam, H.-S. Kwok, *Chem. Commun.* **2005**, 2906.
[28] D. Curran, H. Müller-Bunz, S. I. Bär, R. Schobert, X. Zhu, M. Tacke, *Molecules* **2020**, *25*, 3474.
[29] a) P. Wilkinson, *Gold Bull.* **1986**, *19*, 75; b) I. R. Christie, B. P. Cameron, *Gold Bull.* **1994**, *27*, 12; c) T. A. Green, *Gold Bull.* **2007**, *40*, 105.
[30] E. Bernhardt, M. Finze, H. Willner, *J. Fluorine Chem.* **2004**, *125*, 967.
[31] a) H. G. Raubenheimer, L. Lindeque, S. Cronje, *J. Organomet. Chem.* **1996**, *511*, 177; b) S. Gaillard, A. M. Z. Slawin, S. P. Nolan, *Chem. Commun.* **2010**, *46*, 2742; c) M. A. Celik, C. Dash, V. A. K. Adiraju, A. Das, M. Yousufuddin, G. Frenking, H. V. R. Dias, *Inorg. Chem.* **2013**, *52*, 729; d) J. Ruiz, M. A. Mateo, *Organometallics* **2021**, *40*, 1515.
[32] M. V. Baker, P. J. Barnard, S. K. Brayshaw, J. L. Hickey, B. W. Skelton, A. H. White, *Dalton Trans.* **2005**, 37.
[33] a) D. V. Partyka, J. B. Updegraff, M. Zeller, A. D. Hunter, T. G. Gray, *Organometallics* **2007**, *26*, 183; b) T. J. Del Castillo, S. Sarkar, K. A. Abboud, A. S. Veige, *Dalton Trans.* **2011**, *40*, 8140; c) T. J. Robilotto, N. Deligonul, J. B. Updegraff, T. G. Gray, *Inorg. Chem.* **2013**, *52*, 9659; d) A. R. Powers, I. Ghiviriga, K. A. Abboud, A. S. Veige, *Dalton Trans.* **2015**, *44*, 14747.
[34] T. J. Robilotto, D. S. Alt, H. A. von Recum, T. G. Gray, *Dalton Trans.* **2011**, *40*, 8083.
[35] O. Dada, D. Curran, C. O'Beirne, H. Müller-Bunz, X. Zhu, M. Tacke, *J. Organomet. Chem.* **2017**, *840*, 30.
[36] T. Roth, H. Wadepohl, L. H. Gade, *Eur. J. Inorg. Chem.* **2016**, *2016*, 1184.
[37] E. Schuh, S. Werner, D. Otte, U. Monkowius, F. Mohr, *Organometallics* **2016**, *35*, 3448.
[38] K. Peng, A. Friedrich, U. Schatzschneider, *Chem. Commun.* **2019**, *55*, 8142.
[39] V. Levchenko, S. Øien-Ødegaard, D. Wragg, M. Tilset, *Acta Crystallogr. Sect. E* **2020**, *76*, 1725.
[40] A. Pérez-Bitrián, S. Alvarez, M. Baya, J. Echeverría, A. Martín, J. Orduna, B. Menjón, *Chem. Eur. J.* **2023**, *29*, e202203181.
[41] C. Hansch, A. Leo, R. W. Taft, *Chem. Rev.* **1991**, *91*, 165.
[42] B. Manteau, P. Genix, L. Brelot, J.-P. Vors, S. Pazenok, F. Giornal, C. Leuenberger, F. R. Leroux, *Eur. J. Org. Chem.* **2010**, *2010*, 6043.
[43] C. Hansch, A. Leo, S. H. Unger, K. H. Kim, D. Nikaitani, E. J. Lien, *J. Med. Chem.* **1973**, *16*, 1207.
[44] D. Moujalled, A. R. White, *CNS Drugs* **2016**, *30*, 227.
[45] J. Qiao, Y.-S. Li, R. Zeng, F.-L. Liu, R.-H. Luo, C. Huang, Y.-F. Wang, J. Zhang, B. Quan, C. Shen, X. Mao, X. Liu, W. Sun, W. Yang, X. Ni, K. Wang, L. Xu, Z.-L. Duan, Q.-C. Zou, H.-L. Zhang, W. Qu, Y.-H.-P. Long, M.-H. Li, R.-C. Yang, X. Liu, J. You, Y. Zhou, R. Yao, W.-P. Li, J.-M. Liu, P. Chen, Y. Liu, G.-F. Lin, X. Yang, J. Zou, L. Li, Y. Hu, G.-W. Lu, W.-M. Li, Y.-Q. Wei, Y.-T. Zheng, J. Lei, S. Yang, *Science* **2021**, *371*, 1374.
[46] A. A. Kolomeitsev, M. Vorobyev, H. Gillandt, *Tetrahedron Lett.* **2008**, *49*, 449.
[47] a) R. Koller, K. Stanek, D. Stolz, R. Aardoom, K. Niedermann, A. Togni, *Angew. Chem. Int. Ed. Engl.* **2009**, *48*, 4332; *Angew. Chem.* **2009**, *121*, 4396; b) J.-B. Liu, X.-H. Xu, F.-L. Qing, *Org. Lett.* **2015**, *17*, 5048; c) J.-B. Liu, C. Chen, L. Chu, Z.-H. Chen, X.-H. Xu, F.-L. Qing, *Angew. Chem. Int. Ed.* **2015**, *54*, 11839; *Angew. Chem.* **2015**, *127*, 12005; d) C. Chen, P. Chen, G. Liu, *J. Am. Chem. Soc.* **2015**, *137*, 15648; e) X. Qi, P. Chen, G. Liu, *Angew. Chem. Int. Ed.* **2017**, *56*, 9517; *Angew. Chem.* **2017**, *129*, 9645; f) C. Chen, P. M. Pflüger, P. Chen, G. Liu, *Angew. Chem. Int. Ed.* **2019**, *58*, 2392; *Angew. Chem.* **2019**, *131*, 2414; g) Y.-M. Yang, J.-F. Yao, W. Yan, Z. Luo, Z.-Y. Tang, *Org. Lett.* **2019**, *21*, 8003; h) J. J. Newton, B. J. Jelier, M. Meanwell, R. E. Martin, R. Britton, C. M. Friesen, *Org. Lett.* **2020**, *22*, 1785.
[48] O. Marrec, T. Billard, J.-P. Vors, S. Pazenok, B. R. Langlois, *J. Fluorine Chem.* **2010**, *131*, 200.
[49] C.-P. Zhang, D. A. Vicic, *Organometallics* **2012**, *31*, 7812.
[50] a) T. Besset, P. Jubault, X. Pannecoucke, T. Poisson, *Org. Chem. Front.* **2016**, *3*, 1004; b) A. Tlili, F. Toulgoat, T. Billard, *Angew. Chem. Int. Ed.* **2016**, *55*, 11726; *Angew. Chem.* **2016**, *128*, 11900.
[51] M. E. Redwood, C. J. Willis, *Can. J. Chem.* **1965**, *43*, 1893.
[52] W. B. Farnham, B. E. Smart, W. J. Middleton, J. C. Calabrese, D. A. Dixon, *J. Am. Chem. Soc.* **1985**, *107*, 4565.
[53] M. Nishida, A. Vij, R. L. Kirchmeier, J. M. Shreeve, *Inorg. Chem.* **1995**, *34*, 6085.
[54] G. L. Trainor, *J. Carbohydr. Chem.* **1985**, *4*, 545.
[55] a) A. A. Kolomeitsev, G. Bissky, J. Barten, N. Kalinovich, E. Lork, G.-V. Röschenthaler, *Inorg. Chem.* **2002**, *41*, 6118; b) T. M. Sokolenko, Y. A. Davydova, Y. L. Yagupolskii, *J. Fluorine Chem.* **2012**, *136*, 20; c) B. J. Jelier, J. L. Howell, C. D. Montgomery, D. B. Leznoff, C. M. Friesen, *Angew. Chem. Int. Ed.* **2015**, *54*, 2945; *Angew. Chem.* **2015**, *127*, 2988; d) M.-L. Fu, J.-B. Liu, X.-H. Xu, F.-L. Qing, *J. Org. Chem.* **2017**, *82*, 3702; e) J. W. Lee, D. N. Spiegowski, M.-Y. Ngai, *Chem. Sci.* **2017**, *8*, 6066; f) M. Zhou, C. Ni, Y. Zeng, J. Hu, *J. Am. Chem. Soc.* **2018**, *140*, 6801; g) C.-L. Tong, X.-H. Xu, F.-L. Qing, *Angew. Chem. Int. Ed.* **2021**, *60*, 22915; *Angew. Chem.* **2021**, *133*, 23097.
[56] M. A. Cinellu, G. Minghetti, *Gold Bull.* **2002**, *35*, 11.
[57] S. Komiya, T. Sone, Y. Usui, M. Hirano, A. Fukuoka, *Gold Bull.* **1996**, *29*, 131.
[58] a) B. R. Sutherland, K. Folting, W. E. Streib, D. M. Ho, J. C. Huffman, K. G. Caulton, *J. Am. Chem. Soc.* **1987**, *109*, 3489; b) Y. Usui, M. Hirano, A. Fukuoka, S. Komiya, *Chem. Lett.* **1997**, *26*, 981.
[59] S. Komiya, M. Iwata, T. Sone, A. Fukuoka, *J. Chem. Soc. Chem. Commun.* **1992**, 1109.
[60] Y. Usui, J. Noma, M. Hirano, S. Komiya, *J. Chem. Soc. Dalton Trans.* **1999**, 4397.
[61] Y. Usui, J. Noma, M. Hirano, S. Komiya, *Inorg. Chim. Acta* **2000**, *309*, 151.
[62] W. A. Sheppard, *J. Org. Chem.* **1964**, *29*, 1.

Chemistry–A European Journal
Research Article
doi.org/10.1002/chem.202301684
Chemistry Europe
European Chemical Societies Publishing

[63] W. A. Herrmann, O. Runte, G. Artus, *J. Organomet. Chem.* **1995**, *501*, C1–C4.
[64] a) D. Schneider, O. Schuster, H. Schmidbaur, *Organometallics* **2005**, *24*, 3547; b) O. Schuster, R.-Y. Liau, A. Schier, H. Schmidbaur, *Inorg. Chim. Acta* **2005**, *358*, 1429.
[65] S. Gaillard, A. M. Z. Slawin, A. T. Bonura, E. D. Stevens, S. P. Nolan, *Organometallics* **2010**, *29*, 394.
[66] A. J. Arduengo III, R. Krafczyk, R. Schmutzler, H. A. Craig, J. R. Goerlich, W. J. Marshall, M. Unverzagt, *Tetrahedron* **1999**, *55*, 14523.
[67] a) J. Vícha, C. Foroutan-Nejad, T. Pawlak, M. L. Munzarová, M. Straka, R. Marek, *J. Chem. Theory Comput.* **2015**, *11*, 1509; b) A. H. Greif, P. Hrobárik, M. Kaupp, *Chem. Eur. J.* **2017**, *23*, 9790.
[68] L. Rocchigiani, J. Fernandez-Cestau, I. Chambrier, P. Hrobárik, M. Bochmann, *J. Am. Chem. Soc.* **2018**, *140*, 8287.
[69] A. G. Sharpe, *J. Chem. Soc.* **1949**, 2901.
[70] a) M. Iglesias, D. J. Beetstra, J. C. Knight, L.-L. Ooi, A. Stasch, S. Coles, L. Male, M. B. Hursthouse, K. J. Cavell, A. Dervisi, I. A. Fallis, *Organometallics* **2008**, *27*, 3279; b) E. L. Kolychev, I. A. Portnyagin, V. V. Shuntikov, V. N. Khrustalev, M. S. Nechaev, *J. Organomet. Chem.* **2009**, *694*, 2454.
[71] R. K. Harris, E. D. Becker, S. M. Cabral de Menezes, P. Granger, R. E. Hoffman, K. W. Zilm, *Pure Appl. Chem.* **2008**, *80*, 59.
[72] Adept Scientific, *gNMR V 5.0*, **2005**.
[73] G. M. Sheldrick, *Acta Crystallogr. Sect. A* **2015**, *71*, 3.
[74] G. M. Sheldrick, *Acta Crystallogr. Sect. C* **2015**, *71*, 3.
[75] O. V. Dolomanov, L. J. Bourhis, R. J. Gildea, J. A. K. Howard, H. Puschmann, *J. Appl. Crystallogr.* **2009**, *42*, 339.
[76] P. Voßnacker, T. Keilhack, N. Schwarze, K. Sonnenberg, K. Seppelt, M. Malischewski, S. Riedel, *Eur. J. Inorg. Chem.* **2021**, *2021*, 1034.
[77] OriginLab Corporation, *OriginPro, Version 2022*, Northampton, MA, USA.
[78] A. D. Becke, *J. Chem. Phys.* **1993**, *98*, 5648.
[79] M. Sierka, A. Hogekamp, R. Ahlrichs, *J. Chem. Phys.* **2003**, *118*, 9136.
[80] S. Grimme, J. Antony, S. Ehrlich, H. Krieg, *J. Chem. Phys.* **2010**, *132*, 154104.
[81] a) F. Weigend, R. Ahlrichs, *Phys. Chem. Chem. Phys.* **2005**, *7*, 3297; b) F. Weigend, M. Häser, H. Patzelt, R. Ahlrichs, *Chem. Phys. Lett.* **1998**, *294*, 143.
[82] TURBOMOLE GmbH, *TURBOMOLE V7.3. a development of University of Karlsruhe and Forschungszentrum Karlsruhe*, **2018**.
[83] E. Schnell, E. G. Rochow, *J. Inorg. Nucl. Chem.* **1958**, *6*, 303.

Manuscript received: May 26, 2023
Accepted manuscript online: June 20, 2023
Version of record online: ■■, ■■

RESEARCH ARTICLE

Offering a hand in gold fluorine chemistry: The *trans*-F in $[AuF_3(SIMes)]$ can be substituted by several ligands with varying electronic properties, yielding complexes of the type *trans*-$[AuF_2X(SIMes)]$. They are introduced either by using trimethylsilyl compounds or, by using electron-deficient carbonyl-bearing molecules, the latter route being new in gold chemistry.

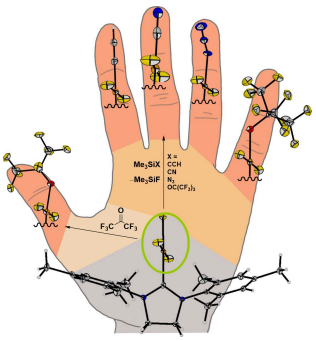

*M. Winter, Dr. M. A. Ellwanger, N. Limberg, Dr. A. Pérez-Bitrián, P. Voßnacker, Dr. S. Steinhauer, Prof. Dr. S. Riedel**

1 – 13

Reactivity of $[AuF_3(SIMes)]$: Pathway to Unprecedented Structural Motifs

3.3 Gold Teflates Revisited: From the Lewis Superacid $[Au(OTeF_5)_3]$ to the Anion $[Au(OTeF_5)_4]^-$

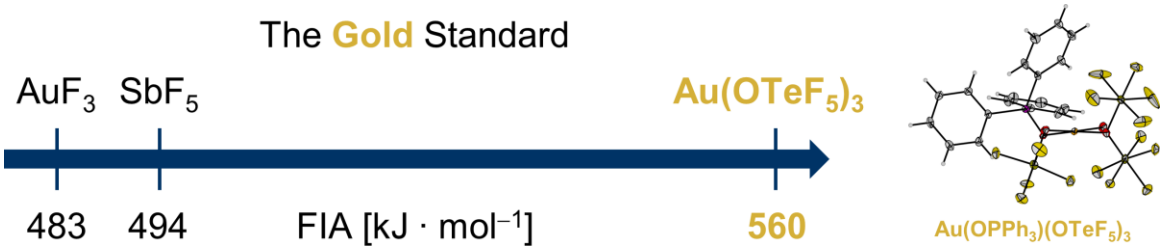

Marlon Winter, Natallia Peshkur, Mathias A. Ellwanger, Alberto Pérez-Bitrián, Patrick Voßnacker, Simon Steinhauer, and Sebastian Riedel.

Chem. Eur. J. **2023**, *29*, e202203634.

https://doi.org/10.1002/chem.202203634

Author contributions

Marlon Winter designed the project, performed the majority of the experiments, all quantum-chemical calculations, and wrote the manuscript. Natallia Peshkur performed some of the experiments during her Bachelor's thesis under the supervision of Marlon Winter. Mathias A. Ellwanger, Alberto Pérez-Bitrián and Simon Steinhauer gave scientific advice and revised the manuscript. Patrick Voßnacker measured and refined the crystal structures. Sebastian Riedel supervised the project and revised the manuscript.

Chemistry–A European Journal | Research Article
doi.org/10.1002/chem.202203634

Chemistry Europe
European Chemical Societies Publishing

www.chemeurj.org

Gold Teflates Revisited: From the Lewis Superacid $[Au(OTeF_5)_3]$ to the Anion $[Au(OTeF_5)_4]^-$

Marlon Winter,[a] Natallia Peshkur,[a] Mathias A. Ellwanger,[a, b] Alberto Pérez-Bitrián,[a] Patrick Voßnacker,[a] Simon Steinhauer,[a] and Sebastian Riedel*[a]

Abstract: A new synthetic access to the Lewis acid $[Au(OTeF_5)_3]$ and the preparation of the related, unprecedented anion $[Au(OTeF_5)_4]^-$ with inorganic or organic cations starting from commercially available and easy-to-handle gold chlorides are presented. In this first extensive study of the Lewis acidity of a transition-metal teflate complex by using different experimental and quantum chemical methods, $[Au(OTeF_5)_3]$ was classified as a Lewis superacid. The solid-state structure of the triphenylphosphine oxide adduct $[Au(OPPh_3)(OTeF_5)_3]$ was determined, representing the first structural characterization of an adduct of this highly reactive $[Au(OTeF_5)_3]$. Therein, the coordination environment around the gold center slightly deviates from the typical square planar geometry. The $[Au(OTeF_5)_4]^-$ anion shows a similar coordination motif.

Introduction

Since the definition by *Lewis* in 1923 that acids and bases are electron pair acceptors and donors, respectively,[1] the study of Lewis acids and their reactivity has led to various applications in organic synthesis, mainly as catalysts in different functionalization reactions.[2] Apart from the classical metal fluorides like SbF_5, which is the strongest conventional, binary Lewis acid, recent studies have focused on the preparation of strong Lewis acids containing bulkier O-, N- or C-donor ligands, mainly with main group elements, for example $[Al(OC(CF_3)_3)_3]$,[3] $[Al(N(C_6F_5)_2)_3]$[4] and $[B(p\text{-}CF_3\text{–}C_6F_4)_3]$.[5] In addition to their easier handling, some of these novel Lewis acids even exceed the fluoride ion affinity (FIA) of SbF_5 and can therefore be classified as Lewis superacids.[3,6]

In this regard, the pentafluoroorthotellurate (–$OTeF_5$, teflate) group has been known to combine strong electron-withdrawing properties and high charge capacity with an increased steric demand, therefore being able to stabilize elements in high oxidation states and reactive species,[7,8] for example $[As(OTeF_5)_5]$,[9,10] $Xe(OTeF_5)_2$,[11] or $[U(OTeF_5)_6]$.[12] Recently, $[Al(OTeF_5)_3]$ was prepared[13] and classified as a Lewis superacid[14] and the corresponding Brønsted acid was used to successfully protonate white phosphorus.[15] Furthermore, the first homoleptic nickel teflate complex $[Ni(OTeF_5)_4]^{2-}$ was prepared including a study of the properties of the teflate ligand in coordination chemistry.[16]

The gold teflate $[Au(OTeF_5)_3]$ was first prepared and characterized as a dimer (see below) by *Seppelt* and co-workers in 1985 but no further reactivity was investigated so far.[17] This compound can therefore be seen as the teflate analogue of AuF_3, which is a polymer in the solid state[18] and due to the relatively low Au–F bond energy compared to other E–F bonds (E=B, C, Si, P, among others),[19] it reacts violently with organic material.[20] Recent investigations show that the substitution of a fluorido ligand by a teflate in a gold(III) complex leads to an increase in Lewis acidity.[21] Therefore, we envisioned that $[Au(OTeF_5)_3]$ should combine a higher Lewis acidity with an increased stability due to the absence of reactive Au–F bonds.

Herein, we report on a new synthetic route to $[Au(OTeF_5)_3]$ and an extensive study of its Lewis acidity, which is, to our knowledge, the first experimental investigation of the Lewis acidity of a transition-metal teflate complex. Furthermore, we present the preparation of the hitherto unknown $[Au(OTeF_5)_4]^-$ anion with both inorganic and organic cations, which surprisingly has not been reported before, even though the complex anion can often be easier obtained than the corresponding Lewis acid.

[a] *M. Winter, N. Peshkur, Dr. M. A. Ellwanger, Dr. A. Pérez-Bitrián, P. Voßnacker, Dr. S. Steinhauer, Prof. Dr. S. Riedel*
Fachbereich Biologie, Chemie, Pharmazie
Institut für Chemie und Biochemie – Anorganische Chemie
Freie Universität Berlin
Fabeckstr. 34/36, 14195 Berlin (Germany)
E-mail: s.riedel@fu-berlin.de

[b] *Dr. M. A. Ellwanger*
Inorganic Chemistry Laboratory
Department of Chemistry
University of Oxford
South Parks Road, Oxford, OX1 3QR (UK)

Supporting information for this article is available on the WWW under https://doi.org/10.1002/chem.202203634

Chemistry–A European Journal
Research Article
doi.org/10.1002/chem.202203634
Chemistry Europe
European Chemical Societies Publishing

Results and Discussion

The Lewis Acid Tris(pentafluoroorthotellurato)gold(III)

We developed a new synthetic route for the preparation of $[Au(OTeF_5)_3]$, starting from the more easy-to-handle and available $AuCl_3$ and an excess of $ClOTeF_5$[22,23] as the teflate-transfer reagent, which has had only limited use for the introduction of teflate groups as of now[9,16,24] – in contrast to the literature-known procedure using AuF_3 and $[B(OTeF_5)_3]$.[17] Since $ClOTeF_5$ is a liquid at standard conditions, the reaction can be performed in neat $ClOTeF_5$ at room temperature (Scheme 1). The formation of chlorine during the reaction was confirmed by recording a UV/Vis spectrum of the gas phase (cf. Figure S24). We did not succeed in growing crystals suitable for single crystal X-ray diffraction by sublimation as it was shown in the literature.[17] However, the purity of the orange product was confirmed by powder X-ray diffraction (cf. Figure S3). Note, that $[Au(OTeF_5)_3]$ has a dimeric structure in the solid state with two bridging and four terminal $OTeF_5$ ligands, resulting in a near square planar coordination of the gold(III) centers (cf. Scheme 1 and Figure 1).

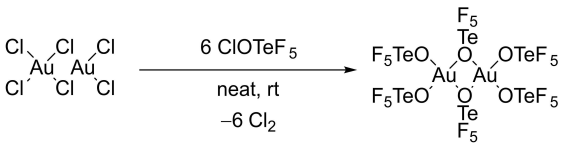

Scheme 1. Synthetic route to the dimeric Lewis acid $[Au_2(OTeF_5)_6]$ using Au_2Cl_6 and an excess of $ClOTeF_5$.

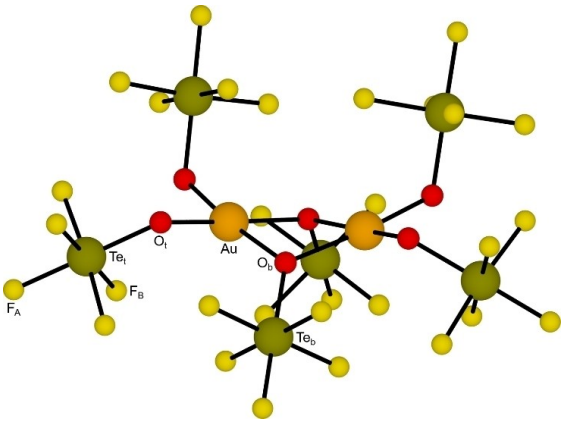

Figure 1. Optimized minimum structure of $[Au_2(OTeF_5)_6]$ on the RI-B3LYP-D3/def2-TZVPP level of theory. Average bond lengths [pm] with the range in brackets: 195.5(2) (Au–O_t), 208.7(6) (Au–O_b), 190.5(2) (O_t–Te), 194.6(8) (O_b–Te), 184.9(2) (Te_t–F_A), 184.0(1) (Te_b–F_A), 186(2) (Te_t–F_B), 185(1) (Te_b–F_B). Average bond angles [°] with the range in brackets: 92.0(7) (O_t–Au–O_t), 94.4(9) (O_t–Au–O_b, *cis*), 172.4(6) (O_t–Au–O_b, *trans*), 79.0(2) (O_b–Au–O_b), 97.5(3) (Au–O_b–Au), 122(3) (Au–O_t–Te_t), 125(3) (Au–O_b–Te_b), 178.2(7) (O_t–Te_t–F_A), 178.5(4) (O_b–Te_b–F_A), 91(4) (O_t–Te_t–F_B), 90(2) (O_b–Te_b–F_B), 89(2) (F_A–Te_t–F_B), 90.3(7) (F_A–Te_b–F_B), 89.8(9) (F_B–Te_t–F_B, *cis*), 177(2) (F_B–Te_t–F_B, *trans*), 90.0(1) (F_B–Te_b–F_B, *cis*), 179.0(2) (F_B–Te_t–F_B, *trans*). Note that the subscripts b and t denote O and Te atoms that are bridging and terminal, respectively, while A and B specify F atoms that are *trans* or *cis*, respectively, to the corresponding O atom of the –$OTeF_5$ group.

The Raman spectrum contains all bands reported in the literature,[17] but also additional minor bands at 754, 732, 725, 715, 652 and 637 cm^{-1}, which are in the typical region of Te–F stretching vibrations, and 326 cm^{-1}, which is in the region of Te–F deformation vibrations.[13] Both the experimental Raman and IR spectrum (the latter including the FIR region, cf. Figure S20) show a good agreement with the calculated spectra of the dimer at the RI-B3LYP-D3/def2-TZVPP level of theory (cf. Figure 1).

In order to investigate the Lewis acidity of $[Au(OTeF_5)_3]$ thoroughly, we performed the Gutmann-Beckett test,[25,26] recorded the frequency of the CN stretching vibration for the acetonitrile adduct,[27–29] and calculated the reaction enthalpies for the adduct formation of some Lewis bases including the fluoride ion affinity (FIA).[30,31]

In the Gutmann-Beckett method, the variation of the chemical shift of Et_3PO in the $^{31}P\{^1H\}$ NMR spectrum upon formation of an adduct with the Lewis acid of interest is investigated.[25,26] The stronger the shift $\Delta\delta(^{31}P)$ with regard to uncoordinated Et_3PO, the higher the acceptor number AN (AN = 2.21 ($\delta(^{31}P)-41$))[25] and thus, the higher the Lewis acidity. For $[Au(OPEt_3)(OTeF_5)_3]$, a chemical shift of $\delta(^{31}P) = 106.1$ ppm is observed in the $^{31}P\{^1H\}$ NMR spectrum (cf. Figure S6), which is shifted by $\Delta\delta(^{31}P) = 55.9$ ppm with respect to free Et_3PO ($\delta(^{31}P) = 50.2$ ppm) and corresponds to AN = 143.8. This AN is much higher than that of $[Au(CF_3)_3]$ (AN = 85.3).[32] Note that in the case of Et_3PO, the reaction needs to be done at −40 °C, since at room temperature further species are formed. Therefore, Ph_3PO was used as a similar but bulkier ligand, for which also Lewis acidity trends are known.[33,34] For $[Au(OPPh_3)(OTeF_5)_3]$, there is only one signal in the $^{31}P\{^1H\}$ NMR spectrum (cf. Figure S9) at room temperature at $\delta(^{31}P) = 66.5$ ppm, being shifted by $\Delta\delta(^{31}P) = 37.2$ ppm with respect to free Ph_3PO ($\delta(^{31}P) = 29.3$ ppm).[33] This shift is significantly larger than in $[Au(CF_3)_3]$ ($\Delta\delta(^{31}P) = 20.6$ ppm).[32]

Cooling a concentrated solution of $[Au(OPPh_3)(OTeF_5)_3]$ in DCM to −24 °C yielded single crystals suitable for X-ray diffraction. $[Au(OPPh_3)(OTeF_5)_3]$ crystallizes in the monoclinic space group $P2_1/n$ and is the first solid-state structure of an $[Au(OTeF_5)_3]$ adduct. Interestingly, the coordination around the gold(III) center is slightly distorted from the typical square planar geometry (cf Figure 2). While the angles α(O–Au–O) involving two oxygen atoms in *cis* position to each other are close to the expected 90° (88.8(2)°–91.3(2)°), α(O–Au–O) with *trans*-oriented oxygen atoms are lower than 180° (172.8(2)° and 173.0(2)°). Using the four-coordinate geometry index τ_4 ($\tau_4 = (360°-(\alpha+\beta))/141°$; α and β are the two largest angles) implemented by *Houser* et al.,[35] $\tau_4 = 0.10$ was determined, which is still close to the ideal square planar geometry ($\tau_4 = 0$). Due to the fact that the ligands are alternately oriented above and below the distorted square planar $\{AuO_4\}$ unit, the distance between the ligands is maximized, yielding a closest distance between two fluorine atoms of adjacent teflate groups of 301.4(6) pm. However, this structural motif is also a local minimum structure in quantum chemical calculations on the RI-

Chemistry–A European Journal | Research Article
doi.org/10.1002/chem.202203634
Chemistry Europe
European Chemical Societies Publishing

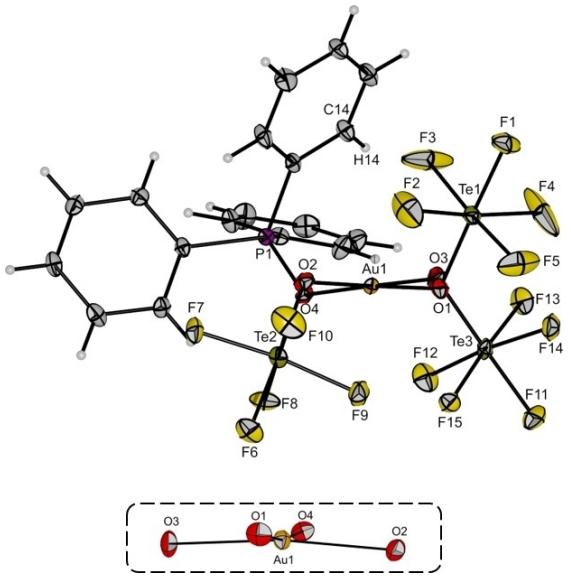

Figure 2. Molecular structure of $[Au(OPPh_3)(OTeF_5)_3]$ in the solid state (top) and excerpt of the $\{AuO_4\}$ unit highlighting the deviation from a square planar coordination (bottom). Thermal ellipsoids are set at 50% probability. Bond lengths [pm] and angles [°] involving the gold atom: 197.3(3) (Au1–O1), 197.7(3) (Au1–O2), 197.3(3) (Au1–O3), 197.3(3) (Au1–O4); 91.3(2) (O1–Au1–O2), 90.2(2) (O1–Au1–O3), 172.8(2) (O1–Au1–O4), 173.0(2) (O2–Au1–O3), 90.6(2) (O2–Au1–O4), 88.8(2) (O3–Au1–O4). The closest F–F distance of two adjacent $-OTeF_5$ groups is 301.4(6) pm (F4–F14).

B3LYP-D3/def2-TZVPP level (see Figure S26) and about 3 kJ mol^{-1} lower in energy than a structure similar to the $[I(OTeF_5)_4]^-$ anion[36] (see below), which is a transition state.

The Au–O bond lengths in $[Au(OPPh_3)(OTeF_5)_3]$ are between 197.3(3) pm and 197.7(3) pm. Compared to the Lewis acid itself, which is a dimer in the solid state, the bond lengths are significantly longer than those to the terminal oxygen atoms ($r(Au–O_{terminal}) = 178(4)$ pm and 182(3) pm) and significantly shorter than those to the bridging oxygen atoms ($r(Au–O_{bridging}) = 223(4)$ pm and 229(4) pm).[17] The only other known neutral, monomeric gold teflate species characterized by X-ray diffraction is $[AuF_2(OTeF_5)(SIMes)]$ with an Au–O bond length of 205.7(4) pm,[21] which is about 8 pm longer than in $[Au(OPPh_3)(OTeF_5)_3]$, due to the strong *trans*-influence of the *N*-heterocyclic carbene ligand. However, the *trans*-influence of the $-OPPh_3$ ligand seems to be similar to that of the $-OTeF_5$ group, since all Au–O bond lengths do not deviate significantly.

The acetonitrile adduct of $[Au(OTeF_5)_3]$ was prepared in order to investigate the blue shift in the stretching vibration ν(C≡N) compared to uncoordinated acetonitrile. A strong blue shift of ν(C≡N) in the IR spectrum is attributed to a strong Lewis acidity. Since for complexes with CH_3CN there is a Fermi resonance between ν(C≡N) and the combination mode (ν(C–C) + $\delta(CH_3)$), CD_3CN can be used for the adduct formation to circumvent this problem and get a more accurate value for the shift.[27–29] Therefore, the complex $[Au(CD_3CN)(OTeF_5)_3]$ was prepared by the addition of a stoichiometric amount of CD_3CN into a suspension of $[Au(OTeF_5)_3]$ in DCM. The IR spectrum of $[Au(CD_3CN)(OTeF_5)_3]$ (cf. Figure S21) shows a band at 2335 cm^{-1}, which is shifted by 73 cm^{-1} with respect to free CD_3CN (2262 cm^{-1}).[37] This shift is identical to the $SbF_5{\cdot}CD_3CN$ adduct.[27]

The ^{19}F NMR spectrum of a solution of $[Au(CD_3CN)(OTeF_5)_3]$ in CD_2Cl_2 consists of two AB_4X patterns, typical for $-OTeF_5$ groups, in a ratio of 2:1, as expected for the chemically inequivalent teflate ligands *cis* and *trans* to the CD_3CN ligand, highlighted in orange and red in Figure 3, respectively. The spectrum was successfully simulated so as to determine the parameters of interest (see Figure 3). Herein, the $-OTeF_5$ groups in *cis* position have a chemical shift of $\delta(F_{A,c}) = -44.5$ ppm and $\delta(F_{B,c}) = -49.1$ ppm with a coupling constant of $^2J(^{19}F_{A,c}, ^{19}F_{B,c}) =$ 181 Hz. For the teflate ligand in *trans* position to CD_3CN, the following values are obtained: $\delta(F_{A,t}) = -43.5$ ppm, $\delta(F_{B,t}) =$ -49.3 ppm and $^2J(^{19}F_{A,t}, ^{19}F_{B,t}) = 182$ Hz. All values are in the typical range for compounds containing covalently bound $-OTeF_5$ groups.

In the ^{125}Te NMR spectrum, the chemical shifts of the tellurium atoms can be found at 586 ppm and 587 ppm for the teflate ligands in *cis* and *trans* position to CD_3CN, respectively. However, the pattern is of higher order and cannot be properly simulated only considering the parameters obtained by the simulation of the AB_4X pattern in the ^{19}F NMR spectrum. Furthermore, a long-range coupling of the tellurium atom in *cis* position with the F_B fluorine atoms of the $-OTeF_5$ ligand in *trans* position and vice versa needs to be included (see Figure 4 and Figure S10). The values are $^5J(^{125}Te_c, ^{19}F_{B,t}) = 31$ Hz and $^5J(^{125}Te_t, ^{19}F_{B,c}) = 32$ Hz for the tellurium atoms in *cis* and *trans* position, respectively.

In order to further estimate and compare the Lewis acidity of $[Au(OTeF_5)_3]$, quantum chemical calculations of the FIA were done by performing isodesmic reactions with the trimethylsilyl fluoride anchor point on the RI-BP86/def-SV(P) level.[30,31]

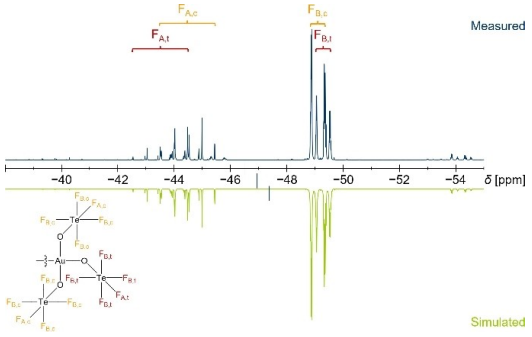

Figure 3. ^{19}F NMR spectrum (377 MHz, DCM-d_2, 20 °C) of $[Au(CD_3CN)(OTeF_5)_3]$ (top, blue) compared to the simulated spectrum (bottom, green). NMR spectroscopical parameters used in the simulation for the two $-OTeF_5$ ligands in *cis* position to CD_3CN: $\delta(F_{A,c}) = -44.5$ ppm, $\delta(F_{B,c}) = -49.1$ ppm, $^2J(^{19}F_{A,c}, ^{19}F_{B,c}) = 181$ Hz, $^1J(^{19}F_{A,c}, ^{125}Te_c) = 3535$ Hz, $^1J(^{19}F_{B,c}, ^{125}Te_c) = 3751$ Hz. NMR spectroscopical parameters used in the simulation for the $-OTeF_5$ ligand in *trans* position to CD_3CN: $\delta(F_{A,t}) = -43.5$ ppm, $\delta(F_{B,t}) = -49.3$ ppm, $^2J(^{19}F_{A,t}, ^{19}F_{B,t}) = 182$ Hz, $^1J(^{19}F_{A,t}, ^{125}Te_t) = 3501$ Hz, $^1J(^{19}F_{B,t}, ^{125}Te_t) = 3768$ Hz.

Chemistry–A European Journal
Research Article
doi.org/10.1002/chem.202203634
Chemistry Europe
European Chemical Societies Publishing

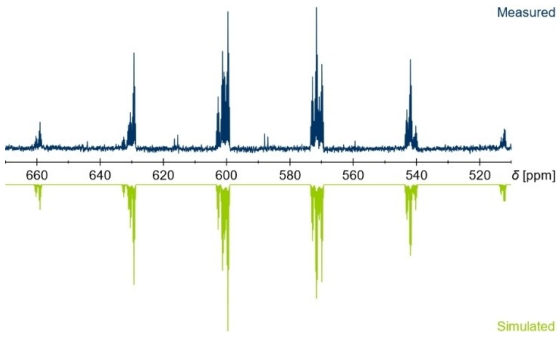

Figure 4. ^{125}Te NMR spectrum (126 MHz, DCM-d_2, 19 °C) of [Au-(CD_3CN)($OTeF_5$)$_3$] (top, blue) compared to the simulated spectrum (bottom, green). NMR spectroscopical parameters used in the simulation for the two –$OTeF_5$ ligands in *cis* position to CD_3CN: $\delta(Te_c) = 586$ ppm, $^1J(^{125}Te_c, ^{19}F_{A,c}) = 3535$ Hz, $^1J(^{125}Te_c, ^{19}F_{B,c}) = 3751$ Hz, $^5J(^{125}Te_c, ^{19}F_{B,t}) = 31$ Hz. NMR spectroscopical parameters used in the simulation for the –$OTeF_5$ ligand in *trans* position to CD_3CN: $\delta(Te_t) = 587$ ppm, $^1J(^{125}Te_t, ^{19}F_{A,t}) = 3501$ Hz, $^1J(^{125}Te_t, ^{19}F_{B,t}) = 3768$ Hz, $^5J(^{125}Te_t, ^{19}F_{B,c}) = 32$ Hz.

Furthermore, the pF^- value was determined ($pF^- =$ FIA[kcal mol^{-1}]/10).[38] The FIAs of the monomer and dimer are 557 ($pF^- = 13.30$) and 504 kJ mol^{-1} ($pF^- = 12.04$), respectively, both being higher than that of SbF_5 (495 kJ mol^{-1}; $pF^- =$ 11.82),[31] which is defined as the border for Lewis superacidity. Furthermore, the reactivity of the monomeric and dimeric Lewis acid towards different ligands L following Scheme 2 was calculated at the RI-BP86/def-SV(P) and RI-B3LYP-D3/def2-TZVPP levels, respectively. The results are summarized in Table 1. It can be seen that the adduct formation with CH_3CN, Et_3PO and Ph_3PO entails in all cases similar reaction energies within a range of about 20 kJ mol^{-1}. Furthermore, all reactions starting from [Au($OTeF_5$)$_3$] listed in Table 1 are about 150 kJ mol^{-1} more exothermic than the dimerization energy of [Au($OTeF_5$)$_3$], supporting the experimental finding that all of these adducts can be synthesized starting from the dimeric Lewis acid.

In order to confirm the classification of [Au($OTeF_5$)$_3$] as a Lewis superacid, its reaction with [PPh_4][SbF_6] in SO_2ClF was investigated with the aim of abstracting a fluoride ion from [SbF_6]$^-$. The ^{19}F NMR spectrum of the reaction mixture shows a similar pattern to the [Au($OTeF_5$)$_4$]$^-$ anion (see below) and $HOTeF_5$ as a side product, which is only plausible by the initial abstraction of a fluoride ion from [SbF_6]$^-$ and subsequent ligand scrambling. The formation of $HOTeF_5$ probably stems from the reaction of SbF_5 with the cation, yielding HF followed by reaction with the [Au($OTeF_5$)$_4$]$^-$ anion to form $HOTeF_5$. Similar findings have been recently published for the reaction of a solvent adduct of the corresponding aluminum-centered Lewis superacid [Al($OTeF_5$)$_3$(SO_2ClF)$_2$] with [PPh_4][SbF_6].[14] This result is an experimental evidence that [Au($OTeF_5$)$_3$] has a higher FIA than SbF_5 and hence, in addition to the other Lewis acidity measurements, can be classified as a Lewis superacid. This renders [Au($OTeF_5$)$_3$] just the second gold-centered Lewis superacid, after AuF_5. According to calculations of the FIA, AuF_3 is not considered a Lewis superacid, showing that the substitution of fluorides by teflates enhances the FIA and underlines the use of teflate groups for the stabilization of high oxidation states.[7]

Scheme 2. Schematic reaction equation for the calculated reaction energies between [Au($OTeF_5$)$_3$] and different ligands L summarized in Table 1.

Pentafluoroorthotelluratoaurate(III) Anions

In contrast to the Lewis acid, the corresponding homoleptic anion [Au($OTeF_5$)$_4$]$^-$ has not been reported. In order to synthesize it, we first attempted a reaction between [Cat][AuF_4] ([Cat]$^+$ = [NMe_4]$^+$, Cs^+) and $Me_3SiOTeF_5$, since the latter has proven useful in the substitution of fluorides by teflates.[21] However, no [Au($OTeF_5$)$_4$]$^-$ was formed, but [H($OTeF_5$)$_2$]$^-$ was detected as the main product.

Therefore, we changed our starting materials to the corresponding chloride salts [Cat][$AuCl_4$] (Cat$^+$ = Cs^+, [NMe_4]$^+$, [NEt_3Me]$^+$) and used $ClOTeF_5$ as the teflate-transfer reagent, in analogy to the preparation of [Au($OTeF_5$)$_3$] (see above). Preliminary experiments of the reaction between [NMe_4][$AuCl_4$] and $ClOTeF_5$ in DCM resulted in the formation of crystals suitable for X-ray diffraction by cooling down a concentrated solution of the reaction mixture to −16 °C. The crystals were determined to be [NMe_4][$AuCl_3$($OTeF_5$)], as shown in Figure 5. In this structure, the coordination around the gold(III) center is square planar ($\tau_4 = 0.05$). The Au–O bond length is 204.1(4) pm, and hence almost 7 pm longer than in [Au($OPPh_3$)($OTeF_5$)$_3$] (197.3(3) and 197.7(3) pm). This demonstrates the stronger *trans*-influence of the chlorido ligand compared to the teflate ligand, also supported by the fact that the Au–Cl bond *trans* to the oxygen atom is about 4 pm shorter than those of the chlorido ligands *trans* to each other (223.8(2) pm compared to 227.6(2) pm). The latter Au–Cl distance is comparable to those

Table 1. Reaction enthalpies ΔH of the reaction of [Au($OTeF_5$)$_3$] with different ligands L (cf. Scheme 2), calculated at the RI-BP86/def-SV(P) and RI-B3LYP-D3/def2-TZVPP level of theory, respectively; values in kJ mol^{-1}. The fluoride ion affinity (FIA) was calculated using Me_3SiF as anchor point.[31]

L	[Au($OTeF_5$)$_3$]		[Au_2($OTeF_5$)$_6$]	
	RI-BP86/def-SV(P)	RI-B3LYP-D3/def2-TZVPP	RI-BP86/def-SV(P)	RI-B3LYP-D3/def2-TZVPP
F^- (FIA)	−557	−616	−504	−471
CH3CN	−230	−319	−178	−175
Et_3PO	−219	−307	−166	−162
Ph_3PO	−205	−315	−153	−170

Chemistry–A European Journal | Research Article
doi.org/10.1002/chem.202203634
Chemistry Europe
European Chemical Societies Publishing

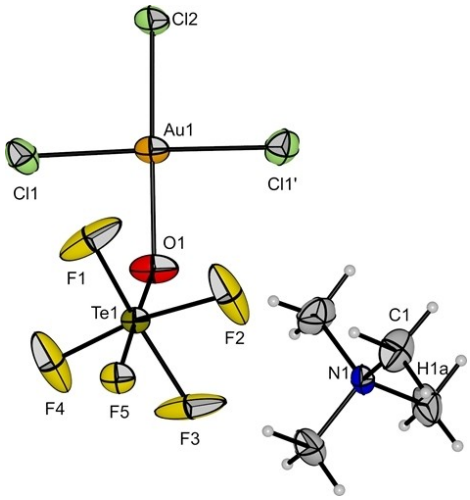

Figure 5. Molecular structure of $[NMe_4][AuCl_3(OTeF_5)]$ in the solid state. Disorders of the basal fluorine atoms (F1–F4) are omitted for clarity (cf. Figure S2). Thermal ellipsoids are shown at 50% probability. Bond lengths [pm] and angles [°] involving the gold atom: 204.1(4) (Au1–O1), 227.6(2) (Au1–Cl1), 223.8(2) (Au1–Cl2); 89.2(3) (O1–Au1–Cl1), 175.3(2) (O1–Au1–Cl2), 178.3(6) (Cl1–Au1–Cl1), 90.8(3) (Cl1–Au1–Cl2).

in $Cs[AuCl_4]$ (227.18(13) pm and 228.38(13) pm).[39] The characterization of the $[AuCl_3(OTeF_5)]^-$ anion supports the postulation of a stepwise substitution going from $[AuCl_4]^-$ to $[Au(OTeF_5)_4]^-$, as indicated by quantum chemical calculations on the RI-B3LYP-D3/def2-TZVPP level, which predict that the first substitution is the most exothermic step with a reaction enthalpy of $\Delta H = -98\ kJ\,mol^{-1}$. For the complete substitution of all chlorides in $[AuCl_4]^-$ by teflate groups yielding $[Au(OTeF_5)_4]^-$, a reaction enthalpy $\Delta H = -317\ kJ\,mol^{-1}$ was calculated (see Scheme S1 and Table S2).

In analogy to the recent preparation of the $[Ni(OTeF_5)_4]^{2-}$ anion by our group, we then changed the approach to using neat $ClOTeF_5$ as shown in Scheme 3.[16] The condensation of $ClOTeF_5$ onto $[NEt_3Me][AuCl_4]$ resulted in a brown slurry that turned into a yellow slurry with a pale yellow gas phase after 3 h. A UV/Vis spectrum of the gas phase confirmed the desired formation of gaseous chlorine (s. Figure S25). Evaporation of all volatile material resulted in a light yellow powder, which was characterized as $[NEt_3Me][Au(OTeF_5)_4]$ (see below).

Single crystals of $[NEt_3Me][Au(OTeF_5)_4]$ suitable for X-ray diffraction were obtained by cooling down a reaction mixture of $[NEt_3Me][AuCl_4]$ and $ClOTeF_5$ in DCM to −16 °C. The salt

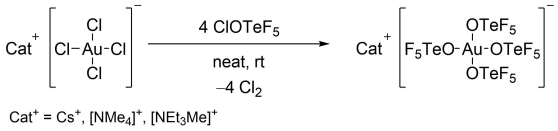

Scheme 3. Synthetic route to the $[Au(OTeF_5)_4]^-$ anion with different cations starting from the corresponding $[AuCl_4]^-$ salt and an excess of $ClOTeF_5$.

$[NEt_3Me][Au(OTeF_5)_4]$ crystallizes in the orthorhombic space group $P2_12_12_1$. The coordination around the gold(III) center is slightly distorted from the typical square planar arrangement (see Figure 6). The angles α(O–Au–O) involving two oxygen atoms in *cis* position are in a range of 89.5(2)°–90.9(2)°, while α(O–Au–O) with *trans*-oriented oxygen atoms are 169.9(2)° and 171.5(2)°. These angles give a value for the geometry index of $\tau_4 = 0.13$,[35] which is still close to the ideal square planar geometry ($\tau_4 = 0$), but shows even a greater distortion than $[Au(OPPh_3)(OTeF_5)_3]$ (see above). The closest distance between two fluorine atoms of adjacent teflate groups is 300.2(7) pm, which is above the sum of their van der Waals radii. This structural motif is also a minimum structure in quantum chemical calculations on the RI-B3LYP-D3/def2-TZVPP level (cf. Figure S27). Interestingly, the structural motif is different to that of similar, structurally characterized teflate complexes, namely $Xe(OTeF_5)_4$[40] and $[I(OTeF_5)_4]^-$,[36] both having a planar $\{EO_4\}$ unit (E=Xe, I) and adjacent –TeF_5 groups that are oriented pairwise above and below the $\{EO_4\}$ plane. A similar structure to $Xe(OTeF_5)_4$ and $[I(OTeF_5)_4]^-$ is calculated to be a local minimum, but about 1 $kJ\,mol^{-1}$ higher in energy than the structure mentioned above.

The Au–O distances in $[NEt_3Me][Au(OTeF_5)_4]$ are between 196.7(3) pm and 197.7(3) pm, which do not deviate significantly from those in $[Au(OPPh_3)(OTeF_5)_3]$ (197.3(3) pm and 197.7(3) pm, see above), which supports the finding from the previous section that the –$OTeF_5$ group and the –$OPPh_3$ group have a similar *trans*-influence. Compared to the $[AuCl_3(OTeF_5)]^-$ anion (204.1(4) pm), the Au–O bond is about 7 pm shorter, due

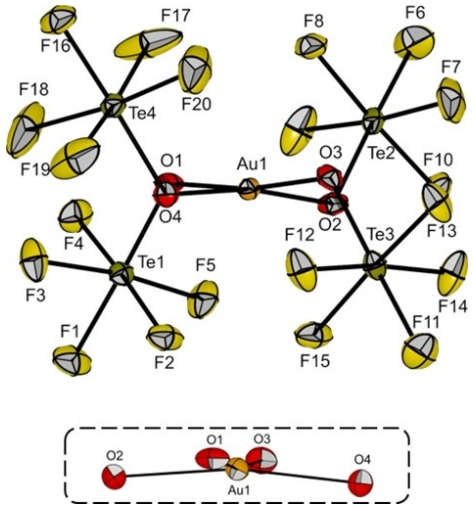

Figure 6. Molecular structure of $[NEt_3Me][Au(OTeF_5)_4]$ in the solid state (top) and excerpt of the $\{AuO_4\}$ unit, highlighting the deviation from a square planar coordination (bottom). The $[NEt_3Me]^+$ cation is omitted for clarity (cf. Figure S1). Thermal ellipsoids are set at 50% probability. Bond lengths [pm] and angles [°] involving the gold atom: 197.4(3) (Au1–O1), 196.7(3) (Au1–O2), 197.7(3) (Au1–O3), 197.2(3) (Au1–O4); 90.8(2) (O1–Au1–O2), 171.5(2) (O1–Au1–O3), 90.9(2) (O1–Au1–O4), 89.5(2) (O2–Au1–O3), 169.9(2) (O2–Au1–O4), 90.2(2) (O3–Au1–O4). The closest F–F distance of two adjacent –$OTeF_5$ groups is 300.2(7) pm (F3–F18).

Chemistry–A European Journal
Research Article
doi.org/10.1002/chem.202203634
Chemistry Europe
European Chemical Societies Publishing

to the stronger *trans*-influence of the chlorido ligand compared to the teflate ligand (see above). The Au–O distances are also in good agreement with those of the literature-known $[Au(ONO_2)_4]^-$ anion (199(1) pm and 202(2) pm).[41] Furthermore, the Au–O distances are significantly shorter than the E–O distances in $[I(OTeF_5)_4]^-$(208.4(9)-217.4(9) pm)[36] and $Xe(OTeF_5)_4$ (202.6(5)-203.9(5) pm).[40]

Compounds containing the $-OTeF_5$ group often give ^{19}F NMR spectra of higher order with an AB_4X pattern, however, the multiplet patterns can at nowadays common field strengths usually be assigned to the two chemically inequivalent types of fluorine atoms even without a detailed analysis.[42] In the case of the $[Au(OTeF_5)_4]^-$ anion, the chemical shifts δ for the fluorine atom F_A and the fluorine atoms F_B are at −38.5 ppm and −39.5 ppm, respectively, with a coupling constant of $^2J(^{19}F,^{19}F) = 183$ Hz, as determined by simulation of the ^{19}F NMR spectrum (cf. Figure 7). Due to this difference of only 1 ppm, the two multiplets overlap yielding an unusual pattern, which resembles the observed one in the series of $[M(OTeF_5)_6]^-$ (M=As, Sb, Bi) anions, but with an inverted order of the F_A and F_B signals.[43] Note that the pattern of the teflate signals in the ^{19}F and ^{125}Te NMR spectra assigned to the $[Au(OTeF_5)_4]^-$ anion are not significantly influenced by the cation (cf. Figures S13, S14, S17 and S18).

The aforementioned proximity in the chemical shifts of the two different types of fluorine atoms also affects the ^{125}Te NMR spectrum of the $[Au(OTeF_5)_4]^-$ anion. Usually, the ^{125}Te NMR spectrum of compounds containing the $-OTeF_5$ group is of first order showing a doublet of quintets. Hence, a direct determination of the $^1J(^{125}Te,^{19}F)$ coupling constant is usually possible. In contrast, the pattern in the ^{125}Te NMR spectrum of $[Au(OTeF_5)_4]^-$ (cf. Figure 8) resembles only vaguely a doublet of quintets, but it is actually a higher order multiplet and the $^1J(^{125}Te,^{19}F)$ coupling constants cannot be straightforwardly assigned. However, by simulation of the spectrum, the $^1J(^{125}Te,^{19}F)$ coupling constants were determined to be 3280 Hz and 3662 Hz for F_A and F_B, respectively (see Figure 8). The chemical shift of $\delta(^{125}Te) = 587$ ppm is by far the most downfield shifted resonance of all $[E(OTeF_5)_4]^{x-}$ (E=B,[44] Al,[13] C,[46] Te,[46] x = 0, 1) complexes that have been characterized by ^{125}Te NMR spectroscopy so far, as they range from 548 ppm to 569 ppm.

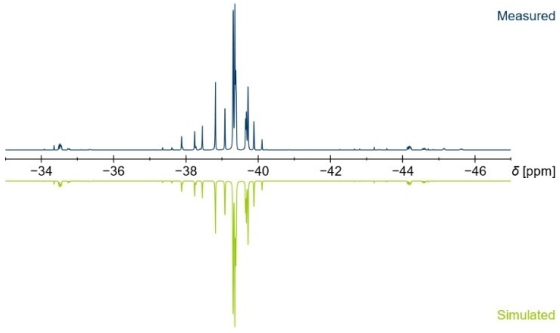

Figure 7. ^{19}F NMR spectrum (377 MHz, DCM-d_2, 17 °C) of $[NEt_3Me][Au(OTeF_5)_4]$ (top, blue) compared to the simulated spectrum (bottom, green). NMR spectroscopical parameters used in the simulation: $\delta(F_A) = -38.5$ ppm, $\delta(F_B) = -39.5$ ppm, $^2J(^{19}F,^{19}F) = 183$ Hz, $^1J(^{19}F_A,^{125}Te) = 3280$ Hz, $^1J(^{19}F_B,^{125}Te) = 3662$ Hz.

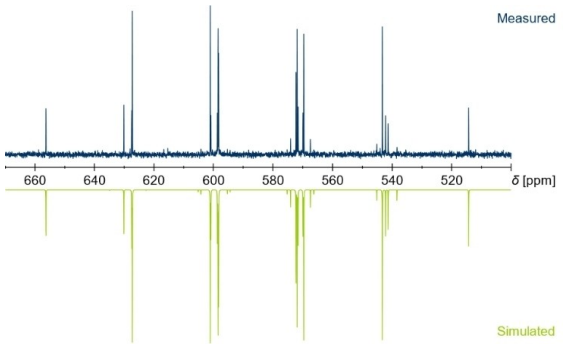

Figure 8. ^{125}Te NMR spectrum (126 MHz, DCM-d_2, 17 °C) of $[NEt_3Me][Au(OTeF_5)_4]$ (top, blue) compared to the simulated spectrum (bottom, green). NMR spectroscopical parameters used in the simulation: $\delta(Te) = 587$ ppm, $^1J(^{125}Te,^{19}F_A) = 3280$ Hz, $^1J(^{125}Te,^{19}F_B) = 3662$ Hz.

In the ESI– mass spectra the parent ion $[Au(OTeF_5)_4]^-$ was not detected, independent of the respective cation, but the gold(I) species $[Au(OTeF_5)_2]^-$ is observed. This anion is an analogue of $[AuF_2]^-$, which has similarly only been detected by mass spectrometry, but never isolated.[47]

The $[Au(OTeF_5)_4]^-$ anion is a rare example of a $\{AuO_4\}$ coordination unit, apart from $[Au(OPPh_3)(OTeF_5)_3]$ (cf. Figure 2), $[Au_2(OTeF_5)_6]$[17] and $[Au(ONO_2)_4]^-$.[41] Solid samples of [Cat] $[Au(OTeF_5)_4]$ stored under inert conditions are stable for more than 6 months at room temperature and DCM solutions are stable for several weeks according to ^{19}F NMR spectroscopic investigation. For comparison, the fluorinated analogue $[AuF_4]^-$ is prepared by reacting Au with [Cat][X] ($[Cat]^+ = K^+$, Cs^+, $[NMe_4]^+$, $[NEt_4]^+$; X=F, Cl, Br) in a Br_2/BrF_3 mixture, which is an ambiguous reaction, especially when using organic cations, as explosions may occur.[48]

Due to the aforementioned stability of the $[Au(OTeF_5)_4]^-$ anion and the known ability of the teflate ligand to stabilize high oxidation states,[7] we considered it a suitable precursor for oxidation reactions in search of the first gold(V) species containing other ligands than fluorides. The only literature-known gold(V) compounds are AuF_5[49–51] and the $[AuF_6]^-$ anion with a series of different cations, namely Li^+,[52] $[NO]^+$,[53] $[O_2]^+$,[50–53,54,55] K^+,[52,53] $[KrF]^+$,[49,51] Ag^+,[52] $[IF_6]^+$,[53] $[XeF_5]^+$,[53] $[Xe_2F_{11}]^+$,[53,56] and Cs^+.[52,53,56] First, the oxidation of $[NMe_4][Au(OTeF_5)_4]$ with $Xe(OTeF_5)_2$ in DCM was investigated, but no reaction was observed. Then, diluted F_2 (10% in Ar) was bubbled through a solution of $[NMe_4][Au(OTeF_5)_4]$ in DCM or MeCN at −40 °C. Although a color change was visible, the desired product was not detected. Treatment of the more robust cesium salt $Cs[Au(OTeF_5)_4]$ with neat F_2 in MeCN at −40 °C only led to decomposition. As none of the attempts starting from $[Au(OTeF_5)_4]^-$ showed any hint of oxidation processes happening, we decided to focus on a different approach, by using $CsAuF_6$ as starting material. The use of different transfer reagents was investigated, but unfortunately neither the reaction with neat $ClOTeF_5$, nor with neat $[B(OTeF_5)_3]$

Chemistry–A European Journal | Research Article doi.org/10.1002/chem.202203634

Chemistry Europe
European Chemical Societies Publishing

at 60 °C, similar to the procedure of *Seppelt* and co-workers for the preparation of $[Au(OTeF_5)_3]$,[17] led to any gold teflate species so far.

Conclusion

In conclusion, the reaction between commercially available and easy-to-handle gold chlorides and $ClOTeF_5$ arises as a new synthetic route to the Lewis acid $[Au(OTeF_5)_3]$ and its related, unprecedented anion $[Au(OTeF_5)_4]^-$. Adducts of the Lewis acid with Et_3PO, Ph_3PO and CD_3CN were prepared and characterized, being the first compounds containing $[Au(OTeF_5)_3]$ in a monomeric form. Investigation of its Lewis acidity using the Gutmann-Beckett method, analysis of the stretching vibration in its acetonitrile adduct and calculation of the fluoride ion affinity resulted in the classification of $[Au(OTeF_5)_3]$ as a Lewis superacid, being the only known gold Lewis superacid apart from AuF_5. In the solid-state structure of $[Au(OPPh_3)(OTeF_5)_3]$, the gold(III) center shows a unique coordination environment, with an arrangement of the ligands in an alternating way above and below the off-planar $\{AuO_4\}$ unit. A similar structural feature is visible in the solid-state structure of $[NEt_3Me][Au(OTeF_5)_4]$. Furthermore, the $[NMe_4]^+$ and Cs^+ salts of this unprecedented anion were also prepared and characterized, with the ^{19}F NMR spectrum showing an interesting pattern which is due to a difference of only 1 ppm in the chemical shift of the F_A and F_B fluorine atoms. Based on the present work, further reactivity studies of $[Au(OTeF_5)_3]$ and potential applications of $[Au(OTeF_5)_4]^-$ as a weakly coordinating anion could be investigated.

Experimental Section

Materials, Chemicals and Procedures

All experiments were conducted under strict exclusion of moisture and air using standard Schlenk techniques. Solid compounds were handled inside an *MBRAUN UNIlab plus* glovebox with an argon atmosphere ($c(O_2) < 0.5$ ppm, $c(H_2O) < 0.5$ ppm). Solvents were dried using an *MBRAUN SPS-800* solvent system and stored over 4 Å molecular sieves. $ClOTeF_5$[23] and $CsAuF_6$[55] were prepared via literature-known procedures. $[NMe_4][AuCl_4]$, $[NEt_3Me][AuCl_4]$ and $Cs[AuCl_4]$ were prepared by adaptation of the literature-known synthesis of $[NR_4][AuCl_4]$ salts (R=Et, Bu).[57] Raman spectra were recorded at room temperature using a *Bruker MultiRAM* FT-Raman spectrometer with an Nd:YAG laser with 1064 nm wavelength. The samples of the isolated powder material were measured in heat-sealed glass capillaries with a laser power of 30 mW and 256 scans with a resolution of 2 cm^{-1}. Raman spectra of single crystals were recorded at −196 °C using a *Bruker RamanScope III* spectrometer with a Laser power of 450 mW and 256 scans with a resolution of 4 cm^{-1}. The samples were measured using a Teflon plate that is cooled by a liquid nitrogen cooled copper block, producing a nitrogen atmosphere that kept the sample inert.[58] IR spectra were measured at room temperature under an argon stream using a *Nicolet iS50* FTIR spectrometer with a diamond ATR attachment with 32 scans and a resolution of 4 cm^{-1}. For the MIR spectra (4000–400 cm^{-1}), a KBr beam splitter was used, while for the FIR spectra (600–50 cm^{-1}), a polyethylene beam splitter was used. Raman and IR spectra were processed using *OPUS 7.5* and *Origin 2022*[59] was used for their graphical representation. NMR spectra were recorded using a *JEOL 400 MHz ECZ-R* or *ECS* spectrometer and all chemical shifts are referenced using the Ξ values given in the *IUPAC* recommendations of 2008 and the ^2H signal of the deuterated solvent as internal reference.[60] For external locking, acetone-d_6 was flame sealed in a glass capillary and the lock oscillator frequency was adjusted to give $\delta(^1H) = 7.26$ ppm for a $CHCl_3$ sample locked on the capillary. For strongly coupled spin systems all chemical shifts and coupling constants are reported as simulated in *gNMR*.[61] *MestReNova 14.2* was used for processing the spectra and for their graphical representation. X-ray diffraction measurements were performed on a *Bruker D8 Venture* diffractometer with MoK_α ($\lambda = 0.71073$ Å) radiation at 100 K and powder X-ray diffraction measurements were performed on a *Bruker D8 Venture* diffractometer with CuK_α ($\lambda = 1.54184$ Å) radiation at 293 K. Single crystals were picked in perfluoroether oil at −40 °C under a nitrogen atmosphere and mounted on a 0.15 mm *Mitegen* micromount. They were solved using the *ShelXT*[62] structure solution program with intrinsic phasing and were refined with the refinement package *ShelXL*[63] using least squares minimizations by using the program *OLEX2*.[64] *Diamond 3* and *POV-Ray 3.7* were used for their graphical representation. UV spectra were measured using a *LAMBDA 465* UV/Vis spectrophotometer. ESI mass spectra were recorded using an *Agilent 6210 ESI-TOF* mass spectrometer, with a flow rate of 4 μL min^{-1} and a spray voltage of 4 kV. The gas for desolvation was set to 1 bar. Elemental analyses (CHN) were performed using a *vario EL* elemental analyzer. Quantum chemical calculations were performed using the functionals B3LYP[65] or BP86 with RI[66] and Grimme-D3[67] corrections where indicated and the basis sets def2-TZVPP[68] or def-SV(P)[69] as incorporated in *TURBOMOLE V7.3*.[70] Reaction enthalpies were calculated by subtraction of the enthalpies of the starting materials from the ones of the products, which were obtained from the calculated SCF energy of geometry optimized minimum structures that were corrected for the enthalpy at standard temperature and pressure using the module *freeh* as incorporated in *TURBOMOLE V7.3* with scaling factors of 0.9614 and 0.9914 for B3LYP and BP86, respectively.[70]

Preparation of $[Au(OTeF_5)_3]$: $ClOTeF_5$ (818 mg, 2.98 mmol, 9 equiv.) was condensed onto a sample of $AuCl_3$ (103 mg, 0.340 mmol, 1 equiv.). The mixture was slowly warmed to room temperature and stirred for 16 h, resulting in an orange-red solution with an orange solid. Volatiles were removed under reduced pressure and afterwards trapped under reduced, static pressure at −80 °C to separate $ClOTeF_5$ from the formed Cl_2. The remaining $ClOTeF_5$ was condensed back onto the reaction mixture and the mixture was stirred for 3 h. All volatiles were removed under reduced pressure and fresh $ClOTeF_5$ (245 mg, 0.894 mmol, 3 equiv.) was condensed onto the reaction mixture and stirred for 3 h. All volatiles were removed under reduced pressure. The product (310 mg, 0.339 mmol, quant.) was obtained as an orange powder. IR (ATR, 25 °C, 4 cm^{-1}): $\tilde{\nu} = 772$ (m, ν_{as}(Au–O)), 691 (vs, ν_{as}(Te–F_B)), 635 (m, ν_{as}(Te–F_A)), 509 (m, $\delta_{ring,oop}(Au_2O_2)$), 297 (vs, δ_{oop}(Te–F_B)), 235 (s, δ_{ip}(Te–F_B)), 156 (m, δ_{ip}(O–Te–F_A)), 92 (m, δ_{oop}(Au–O–Te–F_A)), 81 (m, δ_{ip}(Au–O–Te–F_A)), 73 (m, δ_{ip}(Au–O–Te)), 56 (m) cm^{-1}. FT-Raman (25 °C, 30 mW, 2 cm^{-1}): $\tilde{\nu} = 815$ (m, ν_s(Au–O)), 754 (m, ν_{as}(Au–O)), 732 (m, ν_{as}(Te–F_B)), 725 (m, ν_{as}(Te–F_B)), 715 (m, ν_{as}(Te–F_B)), 702 (s, ν_{as}(Te–F_B)), 669 (vs, ν_s(Te–F_B)), 652 (m, ν_s(Te–F_B)), 637 (m, ν_s(Te–F_B)), 530 (s, $\delta_{ring,ip}(Au_2O_2)$), 493 (m, $\delta_{ring,oop}(Au_2O_2)$), 402 (m, δ_{oop}(Au–O–Au), 326 (m, δ_{oop}(Te–F_B)), 308 (m, δ_{oop}(Te–F_B)), 244 (m, δ_{ip}(Te–F_B)), 228 (m, δ_{ip}(Te–F_B)), 192 (w, δ_{oop}(O–Te–F_B)), 171 (w, δ_{ip}(O–Te–F_A)), 142 (s, δ_{oop}(Au–O–Te–F_A)), 136 (vs, δ_{oop}(Au–O–Te–F_A)), 121 (m, δ_{oop}(O–Te–F_A)), 106 (m, δ_{oop}(O–Te–F_A)), 94 (s, δ_{oop}(Au–O–Te–F_A)), 69 (s) cm^{-1}.

Chemistry–A European Journal | Research Article doi.org/10.1002/chem.202203634 | Chemistry Europe European Chemical Societies Publishing

Preparation of $[Au(OPEt_3)(OTeF_5)_3]$: Et_3PO (12 mg, 0.0894 mmol, 2.3 equiv.) was added to a suspension of $[Au(OTeF_5)_3]$ (36 mg, 0.0394 mmol, 1 equiv.) in DCM-d_2 (1 mL). The mixture was stirred at −40 °C for 2 h, yielding a clear, yellow solution. ^{1}H NMR (400 MHz, DCM-d_2, 21 °C): δ = 2.38 (m, 6H, –CH_2), 1.24 (m, 9H, –CH_3) ppm. ^{19}F NMR (377 MHz, DCM-d_2, 21 °C): δ = −37.8 (m), −38.5 (m) ppm. ^{31}P{^{1}H} NMR (162 MHz, DCM-d_2, 21 °C): δ = 106.1 (s) ppm.

Preparation of $[Au(OPPh_3)(OTeF_5)_3]$: Ph_3PO (9 mg, 0.0323 mmol, 1 equiv.) was added to a suspension of $[Au(OTeF_5)_3]$ (30 mg, 0.0329 mmol, 1 equiv.) in DCM-d_2 (1 mL). The mixture was stirred at room temperature for 10 minutes, yielding a clear, yellow solution. ^{1}H NMR (400 MHz, DCM-d_2, 19 °C): δ = 7.90–7.55 (m, –H_{ar}) ppm. ^{19}F NMR (377 MHz, DCM-d_2, 19 °C): δ = −38.7 (m), −39.3 (m) ppm. ^{31}P{^{1}H} NMR (162 MHz, DCM-d_2, 19 °C): δ = 66.5 (s) ppm.

Preparation of $[Au(CD_3CN)(OTeF_5)_3]$: CD_3CN (2.2 µL, 0.0389 mmol, 1 equiv.) was added to a suspension of $[Au(OTeF_5)_3]$ (35 mg, 0.0383 mmol, 1 equiv.) in DCM-d_2 (1 mL). The mixture was stirred at room temperature for 5 minutes, yielding a clear, bright orange solution. For the IR measurements, all volatiles were pumped off, resulting in a red solid. **^{19}F NMR** (377 MHz, DCM-d_2, 20 °C): δ = −43.5 (m, $1F_{A,c}$, $^2J(^{19}F_{A,c},{}^{19}F_{B,c})$ = 182 Hz, $^1J(^{19}F_{A,c},{}^{125}Te_c)$ = 3501 Hz), −44.5 (m, $2F_{A,t}$, $^2J(^{19}F_{A,t},{}^{19}F_{B,t})$ = 181 Hz, $^1J(^{19}F_{A,t},{}^{125}Te_t)$ = 3535 Hz), −49.1 (m, $8F_{B,c}$, $^1J(^{19}F_{B,c},{}^{125}Te_c)$ = 3751 Hz, $^5J(^{19}F_{B,c},{}^{125}Te_t)$ = 32 Hz), −49.3 (m, $4F_{B,t}$, $^1J(^{19}F_{B,t},{}^{125}Te_t)$ = 3768 Hz, $^5J(^{19}F_{B,t},{}^{125}Te_c)$ = 31 Hz) ppm. ^{125}Te NMR (126 MHz, DCM-d_2, 19 °C): δ = 587 (m, $1Te_t$, $^1J(^{19}F_{A,t},{}^{125}Te_t)$ = 3501 Hz, $^1J(^{19}F_{B,t},{}^{125}Te_t)$ = 3768 Hz, $^5J(^{19}F_{B,c},{}^{125}Te_t)$ = 32 Hz), 586 (m, $2Te_c$, $^1J(^{19}F_{A,c},{}^{125}Te_c)$ = 3535 Hz, $^1J(^{19}F_{B,c},{}^{125}Te_c)$ = 3751 Hz, $^5J(^{19}F_{B,t},{}^{125}Te_c)$ = 31 Hz) ppm. IR (ATR, 25 °C, 4 cm^{-1}): $\tilde{\nu}$ = 2335 (m, ν(N≡C)), 2262 (vw, ν_{as}(C–H)), 2212 (vw, ν_{as}(C–H)), 2115 (vw, ν_s(C–H)), 1670 (vw), 1590 (vw), 1394 (vw), 1245 (vw), 1156 (vw), 1122 (vw), 1083 (w, δ_{oop}(C–H)), 998 (vw, δ_{ip}(C–H)), 816 (m, ν_s(Au–O)), 782 (m, ν_{as}(Au–O)), 670 (vs, ν_{as}(Te–F_B)), 563 (m, $\nu_{as}(\nu_s$(Te–F_B) + ν_s(O–Te–F_A))), 409 (w, δ_{ip}(N–C–C–H)) cm^{-1}.

Reaction between $[Au(OTeF_5)_3]$ and $[PPh_4][SbF_6]$: $[Au(OTeF_5)_3]$ (21 mg, 0.0230 mmol, 1 equiv.) and $[PPh_4][SbF_6]$ (13 mg, 0.0226 mmol, 1 equiv.) were suspended in SO_2ClF (1 mL) at room temperature and agitated for 30 minutes, yielding an orange solution and a colorless solid. The reaction mixture was analyzed by NMR spectroscopy. ^{1}H NMR (400 MHz, SO_2ClF, ext. acetone-d_6, 23 °C): δ = 6.75 (m, 4H, *para*–CH), 6.59 (m, 8H, *meta*–CH), 6.48 (m, 8H, *ortho*–CH), 5.24 (s, 1H, $HOTeF_5$) ppm. ^{19}F NMR (377 MHz, SO_2ClF, ext. acetone-d_6, 22 °C): δ = −40.7 (m, $1F_A$, $[Al(OTeF_5)_4]^-$, $^2J(^{19}F_A,{}^{19}F_B)$ = 181 Hz), −41.8 (m, $4F_B$, $[Al(OTeF_5)_4]^-$), −45.7 (m, $1F_A$, $HOTeF_5$, $^2J(^{19}F_A,{}^{19}F_B)$ = 180 Hz), −49.4 (m, $4F_B$, $HOTeF_5$, $^1J(^{19}F_B,{}^{125}Te)$ = 3583 Hz) ppm. ^{31}P{^{1}H} NMR (162 MHz, SO_2ClF, ext. acetone-d_6, 23 °C): δ = 22.3 (s, 1P, $[PPh_4]^+$) ppm.

Preparation of $[NMe_4][Au(OTeF_5)_4]$: $ClOTeF_5$ (642 mg, 2.34 mmol, 10 equiv.) was condensed onto a sample of $[NMe_4][AuCl_4]$ (98 mg, 0.237 mmol, 1 equiv.). The mixture was slowly warmed to room temperature, resulting in a yellow solution with a light brown solid. The mixture was stirred for 3 h, yielding a light yellow solid with a yellow liquid and a slightly yellow gas phase. All volatiles were removed under reduced pressure. The product (291 mg, 0.234 mmol, quant.) was obtained as a light yellow powder. ^{1}H NMR (400 MHz, DCM-d_2, 19 °C): δ = 3.20 (s, 12H, –CH_3) ppm. ^{13}C{^{1}H} NMR (101 MHz, DCM-d_2, 21 °C): δ = 57.1 (t, 4 C, –CH_3, $^1J(^{13}C,{}^{14}N)$ = 4 Hz) ppm. ^{19}F NMR (377 MHz, DCM-d_2, 20 °C): δ = −38.4 (m, $1F_A$, $^2J(^{19}F,{}^{19}F)$ = 183 Hz, $^1J(^{19}F,{}^{125}Te)$ = 3282 Hz), −39.4 (m, $4F_B$, $^1J(^{19}F,{}^{125}Te)$ = 3663 Hz) ppm. ^{125}Te NMR (126 MHz, DCM-d_2, 19 °C): δ = 586 (m, 1Te, $^1J(^{19}F,{}^{125}Te)$ = 3282 Hz, $^1J(^{19}F,{}^{125}Te)$ = 3663 Hz) ppm. IR (ATR, 25 °C, 4 cm^{-1}): $\tilde{\nu}$ = 1486 (m, δ_{ip}(C–H)), 950 (w, ν_{as}(N–C)), 778 (s, ν_{as}(Au–O)), 692 (vs, ν_{as}(Te–F_B)), 679 (vs, ν(Te–F_A)), 631 (m, ν_{as}(ν_s(Te–F_B) + ν_s(O–Te–F_A))), 514 (w, δ_{oop}(Au–O)), 307 (vs, δ_{oop}(Te–F_B)), 232 (w, δ_{ip}(Te–F_B)), 168 (w, δ_{ip}(O–Te–F_A)), 71 (s, δ_{ip}(Au–O–Te–F_A)), 55 (vs) cm^{-1}. FT-Raman (25 °C, 30 mW, 2 cm^{-1}): $\tilde{\nu}$ = 3047 (m, ν_s(C–H)), 2990 (s, ν_s(C–H)), 2964 (m, ν_s(C–H)), 2931 (m, ν_s(C–H)), 1453 (m, δ_{ip}(C–H)), 755 (m, ν_s(N–C)), 703 (vs, ν_{as}(Te–F)), 688 (s, ν_{as}(Te–F)), 645 (vs, ν_s(Te–F)), 514 (vs, δ_{ip}(Au–O)), 300 (m, δ_{ip}(Te–F)), 235 (s, δ_{ip}(Te–F)), 135 (vs, δ_{oop}(Te–F)), 90 (s, δ_{ip}(Au–O–Te)) cm^{-1}. MS (ESI−): *m/z* = 966.918 (impurity from the spectrometer, 100 %), 674.758 ($[Au(OTeF_5)_2]^-$, 1.7 %), 500.780 ($[Na(OTeF_5)_2]^-$, calc. 500.772, 2.8 %), 240.896 ($[OTeF_5]^-$, calc. 240.891, 75.5 %), 224.901 ($[TeF_5]^-$, calc. 224.896, 56.4 %) Da. Elemental analysis [%]: calculated for $C_4H_{12}AuF_{20}NO_4Te_4$: C 3.92, H 0.99, N 1.14; found: C 4.07, H 1.08, N 1.14.

Preparation of $[NEt_3Me][Au(OTeF_5)_4]$: Following the procedure for the synthesis of $[NMe_4][Au(OTeF_5)_4]$, $[NEt_3Me][Au(OTeF_5)_4]$ was prepared from $ClOTeF_5$ (556 mg, 2.03 mmol, 10 equiv.) and $[NEt_3Me][AuCl_4]$ (92 mg, 0.202 mmol, 1 equiv.) yielding $[NEt_3Me][Au(OTeF_5)_4]$ as a light yellow powder (257 mg, 0.202 mmol, quant.). ^{1}H NMR (400 MHz, DCM-d_2, 18 °C): δ = 3.23 (q, 6H, –CH_2CH_3, $^2J(^1H,{}^1H)$ = 7 Hz), 2.88 (s, 3H, –CH_3), 1.38 (tt, 9H, –CH_2CH_3, $^3J(^1H,{}^{14}N)$ = 2 Hz) ppm. ^{13}C{^{1}H} NMR (101 MHz, DCM-d_2, 19 °C): δ = 57.0 (t, 3 C, –CH_2CH_3, $^1J(^{13}C,{}^{14}N)$ = 3 Hz), 47.6 (t, 1 C, –CH_3, $^1J(^{13}C,{}^{14}N)$ = 4 Hz), 8.0 (s, 3 C, –CH_2CH_3) ppm. ^{19}F NMR (377 MHz, DCM-d_2, 17 °C): δ = −38.5 (m, $1F_A$, $^2J(^{19}F,{}^{19}F)$ = 183 Hz, $^1J(^{19}F,{}^{125}Te)$ = 3280 Hz), −39.5 (m, $4F_B$, $^1J(^{19}F,{}^{125}Te)$ = 3662 Hz) ppm. ^{125}Te NMR (126 MHz, DCM-d_2, 17 °C): δ = 585 (m, 1Te, $^1J(^{19}F,{}^{125}Te)$ = 3280 Hz, $^1J(^{19}F,{}^{125}Te)$ = 3662 Hz) ppm. IR (ATR, 25 °C, 4 cm^{-1}): $\tilde{\nu}$ = 1488 (vw, δ_{ip}(C–H)), 1460 (vw, δ_{oop}(C–H)), 1448 (vw, δ_{oop}(C–H)), 1397 (vw, δ_{oop}(C–H)), 1191 (vw, δ_{ip}(N–C–C)), 998 (vw, ν_{as}(C–C)), 806 (m, δ_{ip}(C–H)), 774 (s, ν_{as}(Au–O)), 695 (vs, ν_{as}(Te–F_B)), 681 (vs, ν(Te–F_A)), 630 (m, $\nu_{as}(\nu_s$(Te–F_B) + ν_s(O–Te–F_A))), 521 (m, δ_{oop}(Au–O)), 307 (vs, δ_{oop}(Te–F_B)), 248 (m), 235 (m, δ_{ip}(Te–F_B)), 168 (m, δ_{ip}(O–Te–F_A)), 142 (w), 67 (m, δ_{ip}(Au–O–Te–F_A)), 61 (m) cm^{-1}. FT-Raman (25 °C, 30 mW, 2 cm^{-1}): $\tilde{\nu}$ = 2991 (m, ν_s(C–H)), 2964 (m, ν_s(C–H)), 1462 (m, δ_{ip}(C–H)), 704 (s, ν_{as}(Te–F)), 691 (s, ν_{as}(Te–F)), 645 (vs, ν_s(Te–F)), 519 (vs, δ_{ip}(Au–O)), 336 (m, δ_{ip}(Te–F)), 299 (m, δ_{ip}(Te–F)), 238 (s, (m, δ_{ip}(Te–F)), 137 (vs, δ_{oop}(Te–F)), 96 (s, δ_{ip}(Au–O–Te)) cm^{-1}. MS (ESI−): *m/z* = 966.918 (impurity from the spectrometer, 93.2 %), 674.756 ($[Au(OTeF_5)_2]^-$, calc. 674.749, 0.6 %), 500.779 ($[Na(OTeF_5)_2]^-$, calc. 500.772, 4.0 %), 240.896 ($[OTeF_5]^-$, calc. 240.891, 100 %), 224.900 ($[TeF_5]^-$, calc. 224.896, 69.0 %) Da. Elemental analysis [%]: calculated for $C_7H_{18}AuF_{20}NO_4Te_4$: C 6.63, H 1.43, N 1.11; found: C 6.77, H 1.60, N 1.34.

Preparation of $Cs[Au(OTeF_5)_4]$: Following the procedure for the synthesis of $[NMe_4][Au(OTeF_5)_4]$, $Cs[Au(OTeF_5)_4]$ was prepared from $ClOTeF_5$ (407 mg, 1.49 mmol, 10 equiv.) and $Cs[AuCl_4]$ (71 mg, 0.151 mmol, 1 equiv.) yielding $Cs[Au(OTeF_5)_4]$ as a light yellow powder (161 mg, 0.125 mmol, 83 %). ^{19}F NMR (377 MHz, DCM-d_2, 19 °C): δ = −37.9 (m, $1F_A$, $^2J(^{19}F,{}^{19}F)$ = 183 Hz, $^1J(^{19}F,{}^{125}Te)$ = 3309 Hz), −38.9 (m, $4F_B$, $^1J(^{19}F,{}^{125}Te)$ = 3662 Hz) ppm. ^{125}Te NMR (126 MHz, DCM-d_2, 19 °C): δ = 585 (m, 1Te, $^1J(^{19}F,{}^{125}Te)$ = 3309 Hz, $^1J(^{19}F,{}^{125}Te)$ = 3662 Hz) ppm. ^{133}Cs NMR (53 MHz, DCM-d_2, 19 °C): δ = 5 (s) ppm. IR (ATR, 25 °C, 4 cm^{-1}): $\tilde{\nu}$ = 872 (m), 825 (m), 792 (m, ν_{as}(Au–O)), 698 (s, ν_{as}(Te–F_B)), 676 (s, ν(Te–F_A)), 635 (s, $\nu_{as}(\nu_s$(Te–F_B) + ν_s(O–Te–F_A))), 525 (w), 501 (m, δ_{oop}(Au–O)), 476 (w), 460 (vw), 386 (vw), 308 (vs, δ_{oop}(Te–F_B)), 234 (m, δ_{ip}(Te–F_B)), 183 (w), 167 (w, δ_{ip}(O–Te–F_A)), 145 (w), 135 (w), 107 (w), 88 (m), 68 (s, δ_{ip}(Au–O–Te–F_A)), 63 (s), 58 (s) cm^{-1}. FT-Raman (25 °C, 30 mW, 2 cm^{-1}): $\tilde{\nu}$ = 871 (w, ν_s(Au–O)), 683 (m, ν_{as}(Te–F)), 650 (m, ν(Te–F)), 579 (w), 388 (s), 352 (vs), 333 (s, δ_{ip}(Te–F)), 323 (vs), 181 (s), 142 (m, δ_{oop}(Te–F)), 108 (m, δ_{ip}(Au–O–Te))), 77 (s) cm^{-1}. MS (ESI−): *m/z* = 966.919 (impurity from the spectrometer, 100 %), 500.780 ($[Na(OTeF_5)_2]^-$, calc. 500.772, 1.5 %), 240.899 ($[OTeF_5]^-$, calc. 240.891, 10.7 %), 224.904 ($[TeF_5]^-$, calc. 224.896, 10.5 %) Da.

Deposition Numbers 2173738, 2156160, 2156159 contain the supplementary crystallographic data for this paper. These data are provided free of charge by the joint Cambridge Crystallographic

Chemistry–A European Journal | Research Article doi.org/10.1002/chem.202203634

Chemistry Europe
European Chemical Societies Publishing

Data Centre and Fachinformationszentrum Karlsruhe Access Structures service.

Acknowledgements

Funded by the ERC project HighPotOx (Grant agreement ID:818862). The authors would like to thank the HPC Service of ZEDAT, Freie Universität Berlin, for computing time and gratefully acknowledge the assistance of the Core Facility BioSupraMol supported by the DFG. M.W. thanks the Dahlem Research School for financial support. A.P.B. and M.A.E. thank the Alexander von Humboldt Foundation for a postdoctoral research fellowship. Open Access funding enabled and organized by Projekt DEAL.

Conflict of Interest

The authors declare no conflict of interest.

Data Availability Statement

The data that support the findings of this study are available from the corresponding author upon reasonable request.

Keywords: gold · lewis acidity · lewis superacid · ligand affinity · pentafluoroorthotellurate

[1] G. N. Lewis, *Valence and the Structure of Atoms and Molecules*, The Chemical Catalog Company, Inc., New York, **1923**.
[2] a) H. Yamamoto, *Lewis Acids in Organic Synthesis*, Wiley-VCH Verlag GmbH, Weinheim, Germany, **2000**; b) A. Corma, H. García, *Chem. Rev.* **2003**, *103*, 4307.
[3] L. O. Müller, D. Himmel, J. Stauffer, G. Steinfeld, J. Slattery, G. Santiso-Quiñones, V. Brecht, I. Krossing, *Angew. Chem. Int. Ed.* **2008**, *47*, 7659; *Angew. Chem.* **2008**, *120*, 7772.
[4] J. F. Kögel, D. A. Sorokin, A. Khvorost, M. Scott, K. Harms, D. Himmel, I. Krossing, J. Sundermeyer, *Chem. Sci.* **2018**, *9*, 245.
[5] L. A. Körte, J. Schwabedissen, M. Soffner, S. Blomeyer, C. G. Reuter, Y. V. Vishnevskiy, B. Neumann, H.-G. Stammler, N. W. Mitzel, *Angew. Chem. Int. Ed.* **2017**, *56*, 8578; *Angew. Chem.* **2017**, *129*, 8701.
[6] L. Greb, *Chem. Eur. J.* **2018**, *24*, 17881.
[7] K. Seppelt, *Angew. Chem. Int. Ed.* **1982**, *21*, 877; *Angew. Chem.* **1982**, *94*, 890.
[8] a) P. K. Hurlburt, D. M. Van Seggen, J. J. Rack, S. H. Strauss in *ACS Symposium Series* (Hrsg.: K. K. Laali), American Chemical Society, Washington, DC, **2007**, S. 338–349; b) M. Gerken, H. P. A. Mercier, G. J. Schrobilgen in *Advanced Inorganic Fluorides; Synthesis, Characterization and Applications* (Hrsg.: T. Nakajima, B. Zemva, A. Tressaud), Elsevier Science S. A. Lausanne, Switzerland, **2000**, S. 117–174.
[9] D. Lentz, K. Seppelt, *Z. Anorg. Allg. Chem.* **1983**, *502*, 83.
[10] M. J. Collins, G. J. Schrobilgen, *Inorg. Chem.* **1985**, *24*, 2608.
[11] F. Sladky, *Monatsh. Chem.* **1970**, *101*, 1559.
[12] a) K. Seppelt, *Chem. Ber.* **1976**, *109*, 1046; b) L. K. Templeton, D. H. Templeton, N. Bartlett, K. Seppelt, *Inorg. Chem.* **1976**, *15*, 2720.
[13] A. Wiesner, T. W. Gries, S. Steinhauer, H. Beckers, S. Riedel, *Angew. Chem. Int. Ed.* **2017**, *56*, 8263; *Angew. Chem.* **2017**, *129*, 8375.
[14] K. F. Hoffmann, A. Wiesner, S. Steinhauer, S. Riedel, *Chem. Eur. J.* **2022**, e202201958.
[15] A. Wiesner, S. Steinhauer, H. Beckers, C. Müller, S. Riedel, *Chem. Sci.* **2018**, *9*, 7169.
[16] A. Pérez-Bitrián, K. F. Hoffmann, K. B. Krause, G. Thiele, C. Limberg, S. Riedel, *Chem. Eur. J.* **2022**, e202202016.
[17] P. Huppmann, H. Hartl, K. Seppelt, *Z. Anorg. Allg. Chem.* **1985**, *524*, 26.
[18] F. W. B. Einstein, P. R. Rao, J. Trotter, N. Bartlett, *J. Chem. Soc. A* **1967**, 478.
[19] D. R. Lide, *ed., CRC Handbook of Chemistry and Physics*, 87. Aufl., Taylor & Francis, Boca Raton, FL., **2006**, p 9–54.
[20] W. J. Wolf, F. D. Toste in *Patai's chemistry of functional groups* (Hrsg.: Z. Rappoport, J. F. Liebman, I. Marek), Wiley, Chichester, **2014**, S. 391–408.
[21] M. A. Ellwanger, C. Von Randow, S. Steinhauer, Y. Zhou, A. Wiesner, H. Beckers, T. Braun, S. Riedel, *Chem. Commun.* **2018**, *54*, 9301.
[22] K. Seppelt, D. Nothe, *Inorg. Chem.* **1973**, *12*, 2727.
[23] C. J. Schack, K. O. Christe, *J. Fluorine Chem.* **1982**, *21*, 393.
[24] a) L. Turowsky, K. Seppelt, *Z. Anorg. Allg. Chem.* **1990**, *590*, 23; b) L. Turowsky, K. Seppelt, *Z. Anorg. Allg. Chem.* **1990**, *590*, 37; c) T. Drews, K. Seppelt, *Z. Anorg. Allg. Chem.* **1991**, *606*, 201; d) A. Vij, W. W. Wilson, V. Vij, R. C. Corley, F. S. Tham, M. Gerken, R. Haiges, S. Schneider, T. Schroer, R. I. Wagner, *Inorg. Chem.* **2004**, *43*, 3189.
[25] U. Mayer, V. Gutmann, W. Gerger, *Monatsh. Chem.* **1975**, *106*, 1235.
[26] M. A. Beckett, G. C. Strickland, J. R. Holland, K. Sukumar Varma, *Polymer* **1996**, *37*, 4629.
[27] D. M. Byler, D. F. Shriver, *Inorg. Chem.* **1973**, *12*, 1412.
[28] D. M. Byler, D. F. Shriver, *Inorg. Chem.* **1974**, *13*, 2697.
[29] B. V. Ahsen, B. Bley, S. Proemmel, R. Wartchow, H. Willner, F. Aubke, *Z. Anorg. Allg. Chem.* **1998**, *624*, 1225.
[30] J. C. Haartz, D. H. McDaniel, *J. Am. Chem. Soc.* **1973**, *95*, 8562.
[31] H. Böhrer, N. Trapp, D. Himmel, M. Schleep, I. Krossing, *Dalton Trans.* **2015**, *44*, 7489.
[32] A. Pérez-Bitrián, M. Baya, J. M. Casas, L. R. Falvello, A. Martín, B. Menjón, *Chem. Eur. J.* **2017**, *23*, 14918.
[33] N. Burford, B. W. Royan, R. E. V. H. Spence, T. S. Cameron, A. Linden, R. D. Rogers, *J. Chem. Soc. Dalton Trans.* **1990**, 1521.
[34] H. Großekappenberg, M. Reißmann, M. Schmidtmann, T. Müller, *Organometallics* **2015**, *34*, 4952.
[35] L. Yang, D. R. Powell, R. P. Houser, *Dalton Trans.* **2007**, 955.
[36] L. Turowsky, K. Seppelt, *Z. Anorg. Allg. Chem.* **1991**, *602*, 79.
[37] W. R. Fawcett, G. Liu, T. E. Kessler, *J. Phys. Chem.* **1993**, *97*, 9293.
[38] K. O. Christe, D. A. Dixon, D. McLemore, W. W. Wilson, J. A. Sheehy, J. A. Boatz, *J. Fluorine Chem.* **2000**, *101*, 151.
[39] F. Kraus, *Z. Naturforsch. B. Chem. Sci.* **2011**, *66*, 871.
[40] L. Turowsky, K. Seppelt, *Z. Anorg. Allg. Chem.* **1992**, *609*, 153.
[41] C. D. Garner, S. C. Wallwork, *J. Chem. Soc. A* **1970**, 3092.
[42] K. Seppelt, *Z. Anorg. Allg. Chem.* **1973**, *399*, 65.
[43] H. P. A. Mercier, J. C. P. Sanders, G. J. Schrobilgen, *J. Am. Chem. Soc.* **1994**, *116*, 2921.
[44] H. Kropshofer, O. Leitzke, P. Peringer, F. Sladky, *Chem. Ber.* **1981**, *114*, 2644.
[45] M. D. Moran, H. P. A. Mercier, G. J. Schrobilgen, *Inorg. Chem.* **2007**, *46*, 5034.
[46] T. Birchall, R. D. Myers, H. D. Waard, G. J. Schrobilgen, *Inorg. Chem.* **1982**, *21*, 1068.
[47] a) N. J. Rijs, R. A. J. O'Hair, *Dalton Trans.* **2012**, *41*, 3395; b) A. Pérez-Bitrián, M. Baya, J. M. Casas, A. Martín, B. Menjón, J. Orduna, *Angew. Chem. Int. Ed.* **2018**, *57*, 6517; *Angew. Chem.* **2018**, *130*, 3425.
[48] a) A. G. Sharpe, *J. Chem. Soc.* **1949**, 2901; b) M. A. Ellwanger, S. Steinhauer, P. Golz, H. Beckers, A. Wiesner, B. Braun-Cula, T. Braun, S. Riedel, *Chem. Eur. J.* **2017**, *23*, 13501.
[49] J. H. Holloway, G. J. Schrobilgen, *J. Chem. Soc. Chem. Commun.* **1975**, 623.
[50] M. J. Vasile, T. J. Richardson, F. A. Stevie, W. E. Falconer, *J. Chem. Soc. Dalton Trans.* **1976**, 351.
[51] I.-C. Hwang, K. Seppelt, *Angew. Chem. Int. Ed.* **2001**, *40*, 3690; *Angew. Chem.* **2001**, *113*, 3803.
[52] O. Graudejus, S. H. Elder, G. M. Lucier, C. Shen, N. Bartlett, *Inorg. Chem.* **1999**, *38*, 2503.
[53] N. Bartlett, *Rev. Chim. Miner.* **1976**, *13*, 82.
[54] a) O. Graudejus, B. G. Müller, *Z. Anorg. Allg. Chem.* **1996**, *622*, 1076; b) J. E. Griffiths, W. A. Sunder, W. E. Falconer, *Spectrochim. Acta Part A* **1975**, *31*, 1207; c) A. J. Edwards, W. E. Falconer, J. E. Griffiths, W. A. Sunder, M. J. Vasile, *J. Chem. Soc. Dalton Trans.* **1974**, 1129; d) Z. Mazej, E. Goreshnik, *Inorg. Chem.* **2020**, *59*, 2092.
[55] Z. Mazej in *Modern Synthesis Processes and Reactivity of Fluorinated Compounds. Progress in Fluorine Science* (Hrsg.: H. Groult, F. Leroux, A. Tressaud), Elsevier Science, San Diego, CA, USA, **2016**, S. 587–607.
[56] K. Leary, N. Bartlett, *J. Chem. Soc. Chem. Commun.* **1972**, 903.

Chemistry–A European Journal
Research Article
doi.org/10.1002/chem.202203634
Chemistry Europe
European Chemical Societies Publishing

[57] P. Braunstein, R. J. H. Clark, *J. Chem. Soc. Dalton Trans.* **1973**, 1845.
[58] P. Voßnacker, T. Keilhack, N. Schwarze, K. Sonnenberg, K. Seppelt, M. Malischewski, S. Riedel, *Eur. J. Inorg. Chem.* **2021**, *2021*, 1034.
[59] OriginLab Corporation, *OriginPro, Version 2022*, Northampton, MA, USA.
[60] R. K. Harris, E. D. Becker, S. M. Cabral de Menezes, P. Granger, R. E. Hoffman, K. W. Zilm, *Pure Appl. Chem.* **2008**, *80*, 59.
[61] Adept Scientific, *gNMR V 5.0*, **2005**.
[62] G. M. Sheldrick, *Acta Crystallogr. Sect. A* **2015**, *71*, 3.
[63] G. M. Sheldrick, *Acta Crystallogr. Sect. C* **2015**, *71*, 3.
[64] O. V. Dolomanov, L. J. Bourhis, R. J. Gildea, J. A. K. Howard, H. Puschmann, *J. Appl. Crystallogr.* **2009**, *42*, 339.
[65] A. D. Becke, *J. Chem. Phys.* **1993**, *98*, 5648.
[66] M. Sierka, A. Hogekamp, R. Ahlrichs, *J. Chem. Phys.* **2003**, *118*, 9136.
[67] S. Grimme, J. Antony, S. Ehrlich, H. Krieg, *J. Chem. Phys.* **2010**, *132*, 154104.
[68] a) F. Weigend, R. Ahlrichs, *Phys. Chem. Chem. Phys.* **2005**, *7*, 3297; b) F. Weigend, M. Häser, H. Patzelt, R. Ahlrichs, *Chem. Phys. Lett.* **1998**, *294*, 143.
[69] A. Schäfer, H. Horn, R. Ahlrichs, *J. Chem. Phys.* **1992**, *97*, 2571.
[70] TURBOMOLE GmbH, *TURBOMOLE V7.3. development of University of Karlsruhe and Forschungszentrum Karlsruhe*, **2018**.

Manuscript received: November 22, 2022
Accepted manuscript online: January 4, 2023
Version of record online: March 3, 2023

4 Conclusion and Outlook

4.1 Conclusion

The first trifluorido organo gold complex, [AuF_3(SIMes)], was reported in 2018.[203] It is soluble in organic solvents and contains a monomeric form of the most stable neutral binary gold fluoride, AuF_3, which is a polymer in the solid state.[127,129] A first reactivity study gave a glimpse of the potential of [AuF_3(SIMes)]: a selective substitution of the fluorido ligand in *trans* position to SIMes yielded *trans*-[AuF_2X(SIMes)] (X = Cl, $OTeF_5$).[204] This reactivity can be explained by the much stronger *trans*-influence of the *N*-heterocyclic carbene SIMes compared to the fluorides, which results in a longer Au–F bond *trans* to SIMes. In this thesis, the reactivity of [AuF_3(SIMes)] was investigated, with the aim of introducing a plethora of ligands with different characteristics and pushing the limits for the use of this unique molecule as a starting material in organo gold chemistry. In most cases, a selective substitution of the *trans*-fluorido ligand is obtained, but a differing reactivity can also be observed, as summarized in Scheme 13.

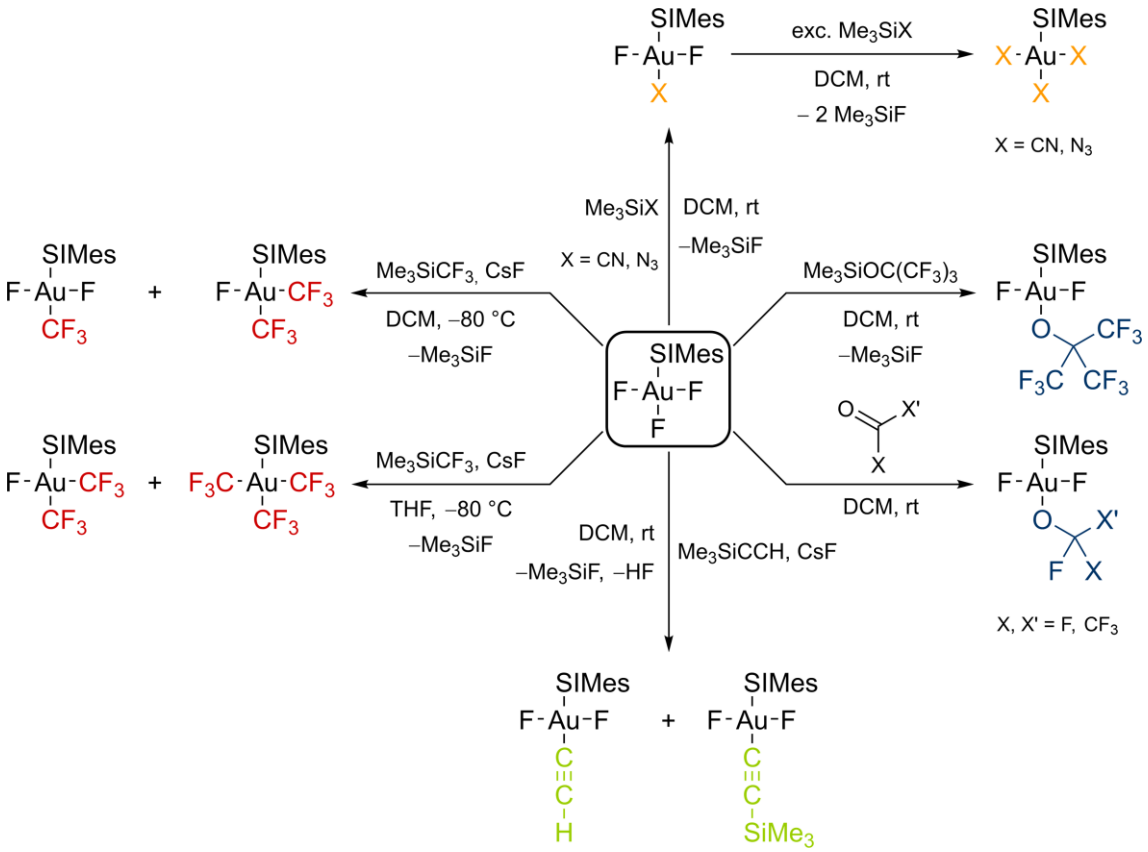

Scheme 13: Overview of the reactivity of [AuF_3(SIMes)] towards a variety of reactants studied in this work.

An important development was the introduction of the trifluoromethyl group. It was not only the first reactivity study to introduce an organic ligand, but also the first synthesis of a series of fluorido trifluoromethyl complexes in which the CF_3 ligand was introduced to a fluorido species and not vice versa. This was achieved by using the *Ruppert-Prakash* reagent Me_3SiCF_3 in combination with CsF as a fluoride source (see Scheme 13, left). Depending on the solvent and the stoichiometry, the whole series $[Au(CF_3)_xF_{3-x}(SIMes)]$ (x = 1–3) was obtained. Substoichiometric use of Me_3SiCF_3 strongly favored the less-substituted product, while the use of a coordinating solvent resulted in a higher degree of substitution.

Based on the well-performing route using trimethylsilyl reagents, additional organic C-donor ligands as well as different N- or O-donor groups with varying electronic properties were introduced to $[AuF_3(SIMes)]$. They ranged from electron donating alkynes, over pseudohalides cyanide and azide, to strongly electron withdrawing perfluorinated alkoxides. In all cases, the expected substitution of the *trans*-fluorido ligand was observed (see Scheme 13). However, in the reaction with Me_3SiCCH, *trans*-$[Au(CCSiMe_3)F_2(SIMes)]$ was obtained as the main product when an excess of Me_3SiCCH was used and CsF was added as a fluoride source. For the cyanide and azide groups, a substitution of all fluorido ligands under the formation of $[AuX_3(SIMes)]$ (X = CN, N_3) was achieved with an excess of Me_3SiX. In neither case, evidence for the doubly substituted complex was found.

Since for the lighter perfluoroalkoxy homologues no trimethylsilyl compounds are known, a new synthetic pathway was developed based on the reaction of the corresponding perfluorinated ketones with $[AuF_3(SIMes)]$. In all cases, the *trans*-$[AuF_2X(SIMes)]$ (X = OCF_3, $OC(CF_3)F_2$, $OC(CF_3)_2F$) species was obtained selectively (see Scheme 13, right). The stability of these compounds strongly increases with the size of the perfluoroalkoxido ligand.

For the aforementioned complexes, a correlation between a high value for the quantum-chemically calculated SIMes affinity and a downfield shift of the carbene carbon atom in the corresponding ^{13}C NMR spectrum was found. Including similar, literature-known complexes,[203,204,267] a total ordering of the *trans*-influences was obtained. It increases in the series $OTeF_5$ < F < OCF_3 ≈ $OC(CF_3)F_2$ ≈ $OC(CF_3)_2F$ ≈ $OC(CF_3)_3$ << Cl < CN ≈ N_3 < CCH ≈ $CCSiMe_3$ < CF_3. A downfield shift of the $^{13}C_{carbene}$ signal also correlates with an elongation of the Au–$C_{carbene}$ bond length for all $[AuF_2X(SIMes)]$ complexes that were characterized by X-ray diffraction.

In the second part of this thesis, the investigation of gold pentafluoroorthotellurates (teflates) was addressed. The only literature-known gold teflate $Au(OTeF_5)_3$ can be regarded as the teflate analogue of AuF_3, due to the similar electron withdrawing properties of the teflate group and the fluoride (see Section 1.6). $Au(OTeF_5)_3$, however, is a dimer in the solid state[62] instead of a polymer like AuF_3, which results in a better solubility and manageability. The reported synthesis of $Au(OTeF_5)_3$ was based on the reaction of AuF_3 with neat, liquid $B(OTeF_5)_3$ at 60 °C for 5 days.[62]

In this work, an improved synthetic procedure was developed, starting from commercially available $AuCl_3$ and using neat $ClOTeF_5$ for the transfer of the teflate group. In this way, $Au(OTeF_5)_3$ was prepared in a quantitative yield at room temperature. By the reaction with Ph_3PO, $[Au(OPPh_3)(OTeF_5)_3]$ was obtained and studied by X-ray diffraction, being the first complex that contains $Au(OTeF_5)_3$ as a monomeric unit in the solid state. The acetonitrile adduct of $Au(OTeF_5)_3$ is stable at room temperature, exceeding the stability of the corresponding AuF_3 complex, which decomposes above −25 °C.[117] An in-depth study of the Lewis acidity of $Au(OTeF_5)_3$ was performed, using the *Gutmann-Beckett* method, the shift of the CN stretching mode in the corresponding acetonitrile complex and a calculation of the FIA. With a higher FIA than SbF_5 and a similar blue shift of the acetonitrile adduct, $Au(OTeF_5)_3$ was classified as a Lewis superacid, being only the second gold-based Lewis superacid after AuF_5.[28] The Lewis superacidity of $Au(OTeF_5)_3$ was experimentally underlined by the fluoride abstraction from an $[SbF_6]^-$ salt.

The hitherto unknown corresponding anion $[Au(OTeF_5)_4]^-$ was also prepared: the reaction of $ClOTeF_5$ with different salts of the $[AuCl_4]^-$ anion quantitatively yielded $[Cat][Au(OTeF_5)_4]$ ($Cat^+ = Cs^+$, $[NMe_4]^+$, $[NEt_3Me]^+$). Attempts to oxidize these salts with $Xe(OTeF_5)_2$ or diluted F_2 as well as the teflate group transfer by $ClOTeF_5$ or $B(OTeF_5)_3$ to $[AuF_6]^-$ did not show any evidence for a gold(V) teflate species.

This thesis paved the way to a better understanding of highly Lewis acidic gold(III) complexes containing the related fluorido and teflato ligands. A variety of organic ligands was introduced to $[AuF_3(SIMes)]$, which combines a decent stability and manageability in organic solvents with a broad reactivity. Furthermore, the teflate analogue of AuF_3, $Au(OTeF_5)_3$, was classified as a Lewis superacid, clearly outperforming AuF_3 in terms of acidity. Moreover, it was possible to synthesize the first complexes of monomeric $Au(OTeF_5)_3$, which showed an unexpected stability.

In a broader perspective, this thesis contributed to the understanding of the chemistry of fluorido organo gold complexes, which has seen several major breakthroughs in the last two decades, including their application in C–C or C–F bond-forming reactions (see Section 1.4). In the literature, the fluorido organo gold complexes were either prepared by (oxidative) fluorination or by halogen exchange, starting from the more stable heavier gold halides.[104,105] Recently, a different approach was taken which made direct use of the most stable binary gold fluorides, i.e. AuF_3 and its fluoroanion $[AuF_4]^-$, and their reactivity towards σ donor ligands was tested.[117,203] This has culminated in the stabilization of $[AuF_3(SIMes)]$, the reactivity of which has been broadly explored in this work. Herein, it was shown to be a monomeric and manageable version of the highly Lewis acidic $\{AuF_3\}$ moiety for the introduction of a variety of ligands. In contrast to the reactivity of literature-known fluorido organo gold complexes, a unique feature of $[AuF_3(SIMes)]$ is the possibility to selectively substitute one instead of all fluorido ligands. In this way, it can be of use in organo gold chemistry as a toolbox for the preparation of gold compounds with a tunable Lewis acidity that contain both fluorido as well as organic ligands. In addition, the scope of highly reactive organo gold(III) complexes was widened by the investigation of the reactivity of $Au(OTeF_5)_3$, resulting in the first teflato gold complexes, which show an increased stability compared to their fluorinated analogues. The study of the Lewis acidity of $Au(OTeF_5)_3$ was the first study of this kind for a transition metal teflate, which shed more light into the relationship between teflate and fluoride in transition metal chemistry. Compared to polymeric AuF_3, $Au(OTeF_5)_3$ combines a better manageability, due to its dimeric structure, which increases the solubility, with a higher Lewis acidity. This thesis has shown that $Au(OTeF_5)_3$ is the first gold-centered Lewis superacid that can be used in synthetic chemistry and further investigations of its reactivity will lead to a new category of organo gold complexes.

4.2 Outlook

As fluorido organo gold complexes were used in the literature for cross-coupling or fluorination reactions,[104,105] the derivatives of [AuF_3(SIMes)] presented in Section 3.1 and 3.2 could be studied for potential applications. However, a detailed investigation of their reactivities is hampered by the scale and yield in which [AuF_3(SIMes)] can be prepared. A major challenge is the handling of AuF_3 in organic solvents, as it tends to decompose even at low temperatures.[117] First attempts for the implementation of a different synthetic route were made by halogen exchange from [AuX_3(SIMes)] (X = Cl, Br) complexes, which proved unsuccessful. Oxidative fluorination of the gold(I) complex [AuF(SIMes)] appears difficult as it is light-sensitive and only moderately stable. While the addition of diluted F_2 was unsuccessful, the reaction with XeF_2 showed small amounts of [AuF_3(SIMes)], but also resulted in side products. An optimization of this route could give a synthetic access to [AuF_3(SIMes)] that avoids the use of binary gold fluorides and thus could be scaled up more easily. If this is achieved, *trans*-[AuF_2X(SIMes)] (X = CF_3, OCF_3) should be tested as CF_3 or OCF_3 group transfer reagents, respectively, which are of high interest in organic chemistry.[84,268] In addition, *trans*-[AuF_2X(SIMes)] (X = CN, N_3) could be investigated in click-type reactions.

An exciting alternative to [AuF_3(SIMes)] could arise from the teflato gold complexes that were studied in Section 3.3, which contain the $Au(OTeF_5)_3$ unit in a monomeric form and significantly exceed the stability of their fluorinated analogues. The so far unknown [$Au(OTeF_5)_3$(SIMes)] could be compared to [AuF_3(SIMes)] regarding stability and reactivity. In addition, it would probably possess a gold center of higher Lewis acidity, as was shown for *trans*-[$AuF_2(OTeF_5)$(SIMes)].[204] The $[Au(OTeF_5)_4]^-$ anion could be studied as a WCA for the stabilization of highly reactive cations, similar to $[Al(OTeF_5)_4]^-$[73,74] or $[Au(CF_3)_4]^-$.[269] In addition, the possible oxidation of $Au(OTeF_5)_3$ or $[Au(OTeF_5)_4]^-$ to a gold(V) teflate species should be investigated in more detail. Even though initial attempts were unsuccessful, the stabilization of a gold(V) compound that contains other ligands than fluoride is a tempting reward and would be another manifestation of the analogy between fluoride and teflate.

5 References

[1] A. F. Holleman, N. Wiberg, *Lehrbuch der Anorganischen Chemie,* 102. Ed., de Gruyter, Berlin, **2007**.

[2] V. Leusch, B. Armbruster, E. Pernicka, V. Slavčev, *Cambridge Archaeol. J.* **2015**, *25*, 353.

[3] L. C. Pauling, *The Nature of the Chemical Bond and the Structure of Molecules and Crystals. An Introduction to Modern Structural Chemistry.,* 3. Ed., Cornell University Press, Ithaca, New York, **1960**.

[4] D. R. Lide, ed., *CRC Handbook of Chemistry and Physics,* 87. Ed., Taylor & Francis, Boca Raton, Florida, **2006**.

[5] a) P. S. Bagus, Y. S. Lee, K. S. Pitzer, *Chem. Phys. Lett.* **1975**, *33*, 408; b) P. Pyykkö, *Adv. Quantum Chem.* **1978**, *11*, 353; c) D. R. McKelvey, *J. Chem. Educ.* **1983**, *60*, 112; d) P. Pyykkö, *Chem. Rev.* **1988**, *88*, 563; e) P. Schwerdtfeger, G. A. Bowmaker, *J. Chem. Phys.* **1994**, *100*, 4487; f) N. Bartlett, *Gold Bull.* **1998**, *31*, 22; g) R. Wesendrup, J. K. Laerdahl, P. Schwerdtfeger, *J. Chem. Phys.* **1999**, *110*, 9457; h) P. Schwerdtfeger, *Heteroat. Chem.* **2002**, *13*, 578; i) P. Pyykkö, *Angew. Chem. Int. Ed.* **2004**, *43*, 4412; *Angew. Chem.* **2004**, *116*, 4512; j) H. Schmidbaur, S. Cronje, B. Djordjevic, O. Schuster, *Chem. Phys.* **2005**, *311*, 151; k) P. Pyykkö, *Inorg. Chim. Acta* **2005**, *358*, 4113; l) P. Pyykkö, *Chem. Soc. Rev.* **2008**, *37*, 1967; m) P. Schwerdtfeger, M. Lein in *Gold Chemistry*. *Applications and Future Directions in the Life Sciences* (Ed.: F. Mohr), Wiley-VCH, Weinheim, **2009**, pp. 183–247; n) P. Pyykkö, *Ann. Rev. Phys. Chem.* **2012**, *63*, 45.

[6] P. Pyykkö, J. P. Desclaux, *Acc. Chem. Res.* **1979**, *12*, 276.

[7] P. Schwerdtfeger, M. Dolg, Schwarz, W. H. Eugen, G. A. Bowmaker, P. D. W. Boyd, *J. Chem. Phys.* **1989**, *91*, 1762.

[8] P. Schwerdtfeger, *J. Am. Chem. Soc.* **1989**, *111*, 7261.

[9] P. Schwerdtfeger, P. D. W. Boyd, A. K. Burrell, W. T. Robinson, M. J. Taylor, *Inorg. Chem.* **1990**, *29*, 3593.

[10] P. Schwerdtfeger, P. D. W. Boyd, S. Brienne, A. K. Burrell, *Inorg. Chem.* **1992**, *31*, 3411.

[11] G. Lucier, C. Shen, W. J. Casteel, L. Chacón, N. Bartlett, *J. Fluorine Chem.* **1995**, *72*, 157.

[12] a) H. Schmidbaur, *Gold Bull.* **2000**, *33*, 3; b) H. Schmidbaur, A. Schier, *Chem. Soc. Rev.* **2008**, *37*, 1931.

[13] H. Schmidbaur, A. Schier, *Chem. Soc. Rev.* **2012**, *41*, 370.

[14] A. N. Chernyshev, M. V. Chernysheva, P. Hirva, V. Y. Kukushkin, M. Haukka, *Dalton Trans.* **2015**, *44*, 14523.

[15] W. Biltz, W. Wein, *Z. Anorg. Allg. Chem.* **1925**, *148*, 192.

[16] S. P. Fricker, *Gold Bull.* **1996**, *29*, 53.

[17] a) P. Wilkinson, *Gold Bull.* **1986**, *19*, 75; b) I. R. Christie, B. P. Cameron, *Gold Bull.* **1994**, *27*, 12.

[18] a) G. Dyker, *Angew. Chem. Int. Ed.* **2000**, *39*, 4237; *Angew. Chem.* **2000**, *112*, 4407; b) A. S. K. Hashmi, *Gold Bull.* **2004**, *37*, 51; c) A. S. K. Hashmi, *Angew. Chem. Int. Ed.* **2005**, *44*, 6990; *Angew. Chem.* **2005**, *117*, 7150; d) M. Haruta, *Nature* **2005**, *437*, 1098; e) A. S. K. Hashmi, G. J. Hutchings, *Angew. Chem. Int. Ed.* **2006**, *45*, 7896; *Angew. Chem.* **2006**, *118*, 8064; f) S. P. Nolan, *Nature* **2007**, *445*, 496; g) M. D. Đurović, Ž. D. Bugarčić, R. van Eldik, *Coord. Chem. Rev.* **2017**, *338*, 186.

[19] H. G. Raubenheimer, H. Schmidbaur, *J. Chem. Educ.* **2014**, *91*, 2024.

[20] M. Joost, A. Amgoune, D. Bourissou, *Angew. Chem. Int. Ed.* **2015**, *54*, 15022; *Angew. Chem.* **2015**, *127*, 15234.

[21] a) N. Kaltsoyannis, *J. Chem. Soc., Dalton Trans.* **1997**, 1; b) D. J. Gorin, F. D. Toste, *Nature* **2007**, *446*, 395; c) A. Leyva-Pérez, A. Corma, *Angew. Chem. Int. Ed.* **2012**, *51*, 614; *Angew. Chem.* **2012**, *124*, 636.

[22] M. Jansen, *Chem. Soc. Rev.* **2008**, *37*, 1826.

[23] K. Heinze, *Angew. Chem. Int. Ed.* **2017**, *56*, 16126; *Angew. Chem.* **2017**, *129*, 16342.

[24] S. Seidel, K. Seppelt, *Science* **2000**, *290*, 117.

[25] S. Dhaif Allah Al Harbi, M. M. Al Mogren, A. Elmarghany, D. Ben Abdallah, B. Mehnen, R. Linguerri, M. Hochlaf, *Phys. Chem. Chem. Phys.* **2019**, *21*, 16120.

[26] J. H. Holloway, G. J. Schrobilgen, *J. Chem. Soc., Chem. Commun.* **1975**, 623.

[27] M. J. Vasile, T. J. Richardson, F. A. Stevie, W. E. Falconer, *J. Chem. Soc., Dalton Trans.* **1976**, 351.

[28] I.-C. Hwang, K. Seppelt, *Angew. Chem. Int. Ed.* **2001**, *40*, 3690; *Angew. Chem.* **2001**, *113*, 3803.

[29] K. Leary, N. Bartlett, *J. Chem. Soc., Chem. Commun.* **1972**, 903.

[30] A. J. Edwards, W. E. Falconer, J. E. Griffiths, W. A. Sunder, M. J. Vasile, *J. Chem. Soc., Dalton Trans.* **1974**, 1129.

[31] J. E. Griffiths, W. A. Sunder, W. E. Falconer, *Spectrochim. Acta, Part A* **1975**, *31*, 1207.

[32] N. Bartlett, *Rev. Chim. Miner.* **1976**, *13*, 82.

[33] O. Graudejus, B. G. Müller, *Z. Anorg. Allg. Chem.* **1996**, *622*, 1076.

[34] O. Graudejus, S. H. Elder, G. M. Lucier, C. Shen, N. Bartlett, *Inorg. Chem.* **1999**, *38*, 2503.

[35] Z. Mazej in *Modern Synthesis Processes and Reactivity of Fluorinated Compounds*. *Progress in Fluorine Science* (Eds.: H. Groult, F. Leroux, A. Tressaud), Elsevier Science, San Diego, California, **2016**, pp. 587–607.

[36] Z. Mazej, E. Goreshnik, *Inorg. Chem.* **2020**, *59*, 2092.

[37] P. Kirsch, *Modern Fluoroorganic Chemistry*. *Synthesis, Reactivity, Applications,* 2. Ed., Wiley-VCH, Weinheim, **2013**.

[38] a) D. B. Harper, D. O'Hagan, *Nat. Prod. Rep.* **1994**, *11*, 123; b) D. O'Hagan, D. B. Harper, *J. Fluorine Chem.* **1999**, *100*, 127.

[39] L. Ma, A. Bartholome, M. H. Tong, Z. Qin, Y. Yu, T. Shepherd, K. Kyeremeh, H. Deng, D. O'Hagan, *Chem. Sci.* **2015**, *6*, 1414.

[40] J. Schmedt auf der Günne, M. Mangstl, F. Kraus, *Angew. Chem. Int. Ed.* **2012**, *51*, 7847; *Angew. Chem.* **2012**, *124*, 7968.

[41] H. Moissan, *C. R. Hebd. Seances Acad. Sci.* **1886**, *102*, 1543.

[42] K. O. Christe, *Inorg. Chem.* **1986**, *25*, 3721.

[43] M. Möbs, D. A. Dixon, G. F. de Melo, M. Vasiliu, T. Graubner, K. O. Christe, F. Kraus, *Angew. Chem. Int. Ed.* **2023**, e202307218; *Angew. Chem.* **2023**, e202307218.

[44] L. E. Forslund, N. Kaltsoyannis, *New J. Chem.* **2003**, *27*, 1108.

[45] a) S. Shaik, D. Danovich, W. Wu, P. C. Hiberty, *Nat. Chem.* **2009**, *1*, 443; b) S. Shaik, D. Danovich, J. M. Galbraith, B. Braïda, W. Wu, P. C. Hiberty, *Angew. Chem. Int. Ed.* **2020**, *59*, 984; *Angew. Chem.* **2020**, *132*, 996.

[46] S. Riedel in *Comprehensive Inorganic Chemistry II*. *From Elements to Applications* (Eds.: J. Reedijk, K. R. Poeppelmeier), Elsevier, Amsterdam, **2013**, pp. 187–221.

[47] E. F. Murphy, R. Murugavel, H. W. Roesky, *Chem. Rev.* **1997**, *97*, 3425.

[48] S. L. Benjamin, W. Levason, G. Reid, *Chem. Soc. Rev.* **2013**, *42*, 1460.

[49] W. Levason, F. M. Monzittu, G. Reid, *Coord. Chem. Rev.* **2019**, *391*, 90.

[50] R. Damerius, P. Huppmann, D. Lentz, K. Seppelt, *J. Chem. Soc., Dalton Trans.* **1984**, 2821.

[51] D. Lentz, K. Seppelt, *Angew. Chem. Int. Ed.* **1978**, *17*, 355; *Angew. Chem.* **1978**, *90*, 390.

[52] T. Birchall, R. D. Myers, H. de Waard, G. J. Schrobilgen, *Inorg. Chem.* **1982**, *21*, 1068.

[53] K. Seppelt, *Angew. Chem. Int. Ed.* **1982**, *21*, 877; *Angew. Chem.* **1982**, *94*, 890.

[54] P. K. Hurlburt, D. M. Van Seggen, J. J. Rack, S. H. Strauss in *Inorganic Fluorine Chemistry: Toward the 21st Century* (Eds.: J. S. Thrasher, S. H. Strauss), American Chemical Society, Washington, **1994**, pp. 338–349.

[55] M. Gerken, H. P. A. Mercier, G. J. Schrobilgen in *Advanced Inorganic Fluorides; Synthesis, Characterization and Applications* (Eds.: T. Nakajima, B. Žemva, A. Tressaud), Elsevier Science S.A., Lausanne, **2000**, pp. 117–174.

[56] a) D. Lentz, K. Seppelt, *Z. Anorg. Allg. Chem.* **1983**, *502*, 83; b) M. J. Collins, G. J. Schrobilgen, *Inorg. Chem.* **1985**, *24*, 2608.

[57] a) K. Seppelt, *Chem. Ber.* **1976**, *109*, 1046; b) L. K. Templeton, D. H. Templeton, N. Bartlett, K. Seppelt, *Inorg. Chem.* **1976**, *15*, 2720.

[58] F. Sladky, *Monatsh. Chem.* **1970**, *101*, 1559.

[59] D. Lentz, K. Seppelt, *Angew. Chem. Int. Ed.* **1978**, *17*, 356; *Angew. Chem.* **1978**, *90*, 391.

[60] E. Jacob, D. Lentz, K. Seppelt, A. Simon, *Z. Anorg. Allg. Chem.* **1981**, *472*, 7.

[61] J. C. P. Sanders, G. J. Schrobilgen, *J. Chem. Soc., Chem. Commun.* **1989**, 1576.

[62] P. Huppmann, H. Hartl, K. Seppelt, *Z. Anorg. Allg. Chem.* **1985**, *524*, 26.

[63] J. R. DeBackere, H. P. A. Mercier, G. J. Schrobilgen, *Inorg. Chem.* **2015**, *54*, 1606.

[64] A. Engelbrecht, F. Sladky, *Angew. Chem. Int. Ed.* **1964**, *3*, 383; *Angew. Chem.* **1964**, *76*, 379.

[65] F. Sladky, H. Kropshofer, O. Leitzke, *J. Chem. Soc., Chem. Commun.* **1973**, 134.

[66] L. Greb, *Chem. Eur. J.* **2018**, *24*, 17881.

[67] H. Kropshofer, O. Leitzke, P. Peringer, F. Sladky, *Chem. Ber.* **1981**, *114*, 2644.

[68] H. P. A. Mercier, J. C. P. Sanders, G. J. Schrobilgen, *J. Am. Chem. Soc.* **1994**, *116*, 2921.

[69] S. H. Strauss, *Chem. Rev.* **1993**, *93*, 927.

[70] H. P. A. Mercier, M. D. Moran, J. C. P. Sanders, G. J. Schrobilgen, R. J. Suontamo, *Inorg. Chem.* **2005**, *44*, 49.

[71] T. S. Cameron, A. Decken, I. Dionne, M. Fang, I. Krossing, J. Passmore, *Chem. Eur. J.* **2002**, *8*, 3386.

[72] D. Aris, J. Beck, A. Decken, I. Dionne, I. Krossing, J. Passmore, E. Rivard, F. Steden, X. Wang, *Phosphorus Sulfur Silicon Relat. Elem.* **2004**, *179*, 859.

[73] A. Wiesner, T. W. Gries, S. Steinhauer, H. Beckers, S. Riedel, *Angew. Chem. Int. Ed.* **2017**, *56*, 8263; *Angew. Chem.* **2017**, *129*, 8375.

[74] A. Wiesner, S. Steinhauer, H. Beckers, C. Müller, S. Riedel, *Chem. Sci.* **2018**, *9*, 7169.

[75] a) A. Pérez-Bitrián, K. F. Hoffmann, K. B. Krause, G. Thiele, C. Limberg, S. Riedel, *Chem. Eur. J.* **2022**, e202202016; b) A. Pérez-Bitrián, J. Munárriz, J. S. Sturm, D. Wegener, K. B. Krause, A. Wiesner, C. Limberg, S. Riedel, *Inorg. Chem.* **2023**, accepted article.

[76] D. O'Hagan, *Chem. Soc. Rev.* **2008**, *37*, 308.

[77] Y. Zhou, J. Wang, Z. Gu, S. Wang, W. Zhu, J. L. Aceña, V. A. Soloshonok, K. Izawa, H. Liu, *Chem. Rev.* **2016**, *116*, 422.

[78] B. E. Smart, *J. Fluorine Chem.* **2001**, *109*, 3.

[79] a) S. Purser, P. R. Moore, S. Swallow, V. Gouverneur, *Chem. Soc. Rev.* **2008**, *37*, 320; b) J. Wang, M. Sánchez-Roselló, J. L. Aceña, C. del Pozo, A. E. Sorochinsky, S. Fustero, V. A. Soloshonok, H. Liu, *Chem. Rev.* **2014**, *114*,

2432; c) H. Mei, J. Han, S. Fustero, M. Medio-Simon, D. M. Sedgwick, C. Santi, R. Ruzziconi, V. A. Soloshonok, *Chem. Eur. J.* **2019**, *25*, 11797.

[80] a) P. Jeschke, *ChemBioChem* **2004**, *5*, 570; b) T. Fujiwara, D. O'Hagan, *J. Fluorine Chem.* **2014**, *167*, 16.

[81] S. Ali, J. Zhou, *Eur. J. Med. Chem.* **2023**, *256*, 115476.

[82] a) S. G. Bratsch, *J. Chem. Educ.* **1985**, *62*, 101; b) J. E. True, T. D. Thomas, R. W. Winter, G. L. Gard, *Inorg. Chem.* **2003**, *42*, 4437.

[83] M. Shimizu, T. Hiyama, *Angew. Chem. Int. Ed.* **2004**, *44*, 214; *Angew. Chem.* **2004**, *117*, 218.

[84] T. Furuya, A. S. Kamlet, T. Ritter, *Nature* **2011**, *473*, 470.

[85] T. Liang, C. N. Neumann, T. Ritter, *Angew. Chem. Int. Ed.* **2013**, *52*, 8214; *Angew. Chem.* **2013**, *125*, 8372.

[86] X. Liu, C. Xu, M. Wang, Q. Liu, *Chem. Rev.* **2015**, *115*, 683.

[87] M. A. García-Monforte, S. Martínez-Salvador, B. Menjón, *Eur. J. Inorg. Chem.* **2012**, *2012*, 4945.

[88] P. v. R. Schleyer, A. J. Kos, *Tetrahedron* **1983**, *39*, 1141.

[89] H. C. Clark, J. H. Tsai, *J. Organomet. Chem.* **1967**, *7*, 515.

[90] T. Leyssens, D. Peeters, A. G. Orpen, J. N. Harvey, *Organometallics* **2007**, *26*, 2637.

[91] P. Sgarbossa, A. Scarso, G. Strukul, R. A. Michelin, *Organometallics* **2012**, *31*, 1257.

[92] A. G. Algarra, V. V. Grushin, S. A. Macgregor, *Organometallics* **2012**, *31*, 1467.

[93] a) T. G. Appleton, M. H. Chisholm, H. C. Clark, L. E. Manzer, *Inorg. Chem.* **1972**, *11*, 1786; b) M. A. Bennett, H.-K. Chee, G. B. Robertson, *Inorg. Chem.* **1979**, *18*, 1061; c) M. A. Bennett, H.-K. Chee, J. C. Jeffery, G. B. Robertson, *Inorg. Chem.* **1979**, *18*, 1071; d) V. V. Grushin, W. J. Marshall, *J. Am. Chem. Soc.* **2006**, *128*, 4632; e) J. Goodman, V. V. Grushin, R. B. Larichev, S. A. Macgregor, W. J. Marshall, D. C. Roe, *J. Am. Chem. Soc.* **2010**, *132*, 12013.

[94] a) J. P. Snyder, *Angew. Chem. Int. Ed.* **1995**, *34*, 986; *Angew. Chem.* **1995**, *107*, 1076; b) M. Kaupp, H. G. von Schnering, *Angew. Chem. Int. Ed.* **1995**, *34*, 986; *Angew. Chem.* **1995**, *107*, 1076.

[95] a) J. P. Snyder, *Angew. Chem. Int. Ed.* **1995**, *34*, 80; *Angew. Chem.* **1995**, *107*, 112; b) R. Hoffmann, S. Alvarez, C. Mealli, A. Falceto, T. J. Cahill, T. Zeng, G. Manca, *Chem. Rev.* **2016**, *116*, 8173.

[96] a) D. Joven-Sancho, M. Baya, A. Martín, B. Menjón, *Chem. Eur. J.* **2018**, *24*, 13098; b) M. Baya, D. Joven-Sancho, P. J. Alonso, J. Orduna, B. Menjón, *Angew. Chem. Int. Ed.* **2019**, *58*, 9954; *Angew. Chem.* **2019**, *131*, 10059.

[97] J. A. Morrison, *Adv. Organomet. Chem.* **1993**, *35*, 211.

[98] a) I. Ruppert, K. Schlich, W. Volbach, *Tetrahedron Lett.* **1984**, *25*, 2195; b) Prakash, G. K. Surya, A. K. Yudin, *Chem. Rev.* **1997**, *97*, 757; c) D. Huang, K. G. Caulton, *J. Am. Chem. Soc.* **1997**, *119*, 3185.

[99] a) R. P. Singh, J. M. Shreeve, *Tetrahedron* **2000**, *56*, 7613; b) G. Prakash, M. Mandal, *J. Fluorine Chem.* **2001**, *112*, 123.

[100] N. Maggiarosa, W. Tyrra, D. Naumann, N. V. Kirij, Y. L. Yagupolskii, *Angew. Chem. Int. Ed.* **1999**, *38*, 2252; *Angew. Chem.* **1999**, *111*, 2392.

[101] T. Umemoto, *Chem. Rev.* **1996**, *96*, 1757.

[102] P. Eisenberger, S. Gischig, A. Togni, *Chem. Eur. J.* **2006**, *12*, 2579.

[103] F. Mohr, *Gold Bull.* **2004**, *37*, 164.

[104] W. J. Wolf, F. D. Toste in *Patai's chemistry of functional groups* (Eds.: Z. Rappoport, J. F. Liebman, I. Marek), Wiley, Chichester, **2014**, pp. 391–408.

[105] J. Miró, C. del Pozo, *Chem. Rev.* **2016**, *116*, 11924.

[106] T. C. Waddington, *Trans. Faraday Soc.* **1959**, *55*, 1531.

[107] R. G. Pearson, *J. Am. Chem. Soc.* **1963**, *85*, 3533.

[108] K. L. Saenger, C. P. Sun, *Phys. Rev. A* **1992**, *46*, 670.

[109] D. Schröder, J. Hrušák, I. C. Tornieporth-Oetting, T. M. Klapötke, H. Schwarz, *Angew. Chem. Int. Ed.* **1994**, *33*, 212; *Angew. Chem.* **1994**, *106*, 223.

[110] C. J. Evans, M. C. L. Gerry, *J. Am. Chem. Soc.* **2000**, *122*, 1560.

[111] X. Wang, L. Andrews, K. Willmann, F. Brosi, S. Riedel, *Angew. Chem. Int. Ed.* **2012**, *51*, 10628; *Angew. Chem.* **2012**, *124*, 10780.

[112] X. Wang, L. Andrews, F. Brosi, S. Riedel, *Chem. Eur. J.* **2013**, *19*, 1397.

[113] C. J. Evans, D. S. Rubinoff, M. C. L. Gerry, *Phys. Chem. Chem. Phys.* **2000**, *2*, 3943.

[114] J. M. Thomas, N. R. Walker, S. A. Cooke, M. C. L. Gerry, *J. Am. Chem. Soc.* **2004**, *126*, 1235.

[115] S. A. Cooke, M. C. L. Gerry, *J. Am. Chem. Soc.* **2004**, *126*, 17000.

[116] X.-G. Xiong, Y.-L. Wang, C.-Q. Xu, Y.-H. Qiu, L.-S. Wang, J. Li, *Dalton Trans.* **2015**, *44*, 5535.

[117] M. A. Ellwanger, S. Steinhauer, P. Golz, H. Beckers, A. Wiesner, B. Braun-Cula, T. Braun, S. Riedel, *Chem. Eur. J.* **2017**, *23*, 13501.

[118] N. J. Rijs, R. A. J. O'Hair, *Dalton Trans.* **2012**, *41*, 3395.

[119] A. Pérez-Bitrián, M. Baya, J. M. Casas, A. Martín, B. Menjón, J. Orduna, *Angew. Chem. Int. Ed.* **2018**, *57*, 6517; *Angew. Chem.* **2018**, *130*, 3425.

[120] V. Lenher, *J. Am. Chem. Soc.* **1903**, *25*, 1136.

[121] O. Ruff, *Ber. Dtsch. Chem. Ges.* **1913**, *46*, 920.

[122] A. G. Sharpe, *J. Chem. Soc.* **1949**, 2901.

[123] M. F. A. Dove, P. Benkič, C. Platte, T. J. Richardson, N. Bartlett, *J. Fluorine Chem.* **2001**, *110*, 83.

[124] L. B. Asprey, F. H. Kruse, K. H. Jack, R. Maitland, *Inorg. Chem.* **1964**, *3*, 602.

[125] U. Engelmann, B. G. Müller, *Z. Anorg. Allg. Chem.* **1992**, *618*, 43.

[126] U. Engelmann, B. G. Müller, *Z. Anorg. Allg. Chem.* **1993**, *619*, 1661.

[127] F. W. B. Einstein, P. R. Rao, J. Trotter, N. Bartlett, *J. Chem. Soc. A* **1967**, 478.

[128] I. C. Tornieporth-Oetting, T. M. Klapötke, *Chem. Ber.* **1995**, *128*, 957.

[129] B. Zemva, K. Lutar, A. Jesih, W. J. Casteel, A. P. Wilkinson, D. E. Cox, R. B. von Dreele, H. Borrmann, N. Bartlett, *J. Am. Chem. Soc.* **1991**, *113*, 4192.

[130] S. S. Batsanov, *Inorg. Mater.* **2001**, *37*, 871.

[131] E. S. Clark, D. H. Templeton, C. H. MacGillavry, *Acta Cryst. A* **1958**, *11*, 284.

[132] J. Strähle, K.-P. Lörcher, *Z. Naturforsch. B* **1974**, *29*, 266.

[133] A. Schulz, M. Hargittai, *Chem. Eur. J.* **2001**, *7*, 3657.

[134] B. Réffy, M. Kolonits, A. Schulz, T. M. Klapötke, M. Hargittai, *J. Am. Chem. Soc.* **2000**, *122*, 3127.

[135] R. D. Peacock, *Chem. Ind.* **1959**, 90.

[136] M. Binnewies, M. Finze, M. Jäckel, P. Schmidt, H. Willner, G. Rayner-Canham, *Allgemeine und Anorganische Chemie,* 3. Ed., Springer Spektrum, Berlin, **2016**.

[137] a) R. Hoppe, W. Klemm, *Z. Anorg. Allg. Chem.* **1952**, *268*, 364; b) R. Hoppe, R. Homann, *Z. Anorg. Allg. Chem.* **1970**, *379*, 193; c) U. Engelmann, B. G. Müller, *Z. Anorg. Allg. Chem.* **1991**, *598*, 103.

[138] B. G. Müller, *Z. Anorg. Allg. Chem.* **1987**, *555*, 57.

[139] R. Fischer, B. G. Müller, *Z. Anorg. Allg. Chem.* **1997**, *623*, 1729.

[140] R. Schmidt, B. G. Müller, *Z. Anorg. Allg. Chem.* **1999**, *625*, 602.

[141] K. Lutar, A. Jesih, I. Leban, B. Žemva, N. Bartlett, *Inorg. Chem.* **1989**, *28*, 3467.

[142] R. Schmidt, B. G. Müller, *Z. Anorg. Allg. Chem.* **2004**, *630*, 2393.

[143] a) S. H. Elder, G. M. Lucier, F. J. Hollander, N. Bartlett, *J. Am. Chem. Soc.* **1997**, *119*, 1020; b) R. Schmidt, B. G. Müller, *Z. Anorg. Allg. Chem.* **1999**, *625*, 605.

[144] A. J. Edwards, G. R. Jones, *J. Chem. Soc. A* **1969**, 1936.

[145] Z. Mazej, *J. Fluorine Chem.* **2004**, *125*, 1723.

[146] C. Shen, B. Zemva, G. M. Lucier, O. Graudejus, J. A. Allman, N. Bartlett, *Inorg. Chem.* **1999**, *38*, 4570.

[147] J. Brunvoll, A. A. Ischenko, A. A. Ivanov, G. V. Romanov, V. B. Sokolov, V. P. Spiridonov, T. G. Strand, *Acta Chem. Scand. A* **1982**, *36*, 705.

[148] J. E. Bloor, R. E. Sherrod, *J. Am. Chem. Soc.* **1980**, *102*, 4333.

[149] R. Craciun, D. Picone, R. T. Long, S. Li, D. A. Dixon, K. A. Peterson, K. O. Christe, *Inorg. Chem.* **2010**, *49*, 1056.

[150] a) N. Bartlett, D. H. Lohmann, *Proc. Chem. Soc.* **1962**, 115; b) N. Bartlett, D. H. Lohmann, *J. Chem. Soc.* **1962**, 5253.

[151] N. Bartlett, *Proc. Chem. Soc.* **1962**, 218.

[152] a) N. Bartlett, S. P. Beaton, N. K. Jha, *Chem. Commun.* **1966**, 168; b) N. Bartlett, *Angew. Chem. Int. Ed.* **1968**, *7*, 433; *Angew. Chem.* **1968**, *80*, 453; c) E. Miyoshi, Y. Sakai, *J. Chem. Phys.* **1988**, *89*, 7363.

[153] a) J. Lin, S. Zhang, W. Guan, G. Yang, Y. Ma, *J. Am. Chem. Soc.* **2018**, *140*, 9545; b) G. Liu, X. Feng, L. Wang, S. A. T. Redfern, X. Yong, G. Gao, H. Liu, *Phys. Chem. Chem. Phys.* **2019**, *21*, 17621.

[154] a) P. Schwerdtfeger, J. S. McFeaters, M. J. Liddell, J. Hrušák, H. Schwarz, *J. Chem. Phys.* **1995**, *103*, 245; b) J. G. Hill, K. A. Peterson, *J. Chem. Theory Comput.* **2012**, *8*, 518; c) X. Li, J. Cai, *Int. J. Quantum Chem.* **2016**, *116*, 1350.

[155] P. Koirala, M. Willis, B. Kiran, A. K. Kandalam, P. Jena, *J. Phys. Chem. C* **2010**, *114*, 16018-16024.

[156] A. A. Timakov, V. N. Prusakov, Y. V. Drobyshevskii, *Dokl. Akad. Nauk SSSR* **1986**, *291*, 125.

[157] S. Riedel, M. Kaupp, *Inorg. Chem.* **2006**, *45*, 1228.

[158] D. Himmel, S. Riedel, *Inorg. Chem.* **2007**, *46*, 5338.

[159] Y.-R. Luo, *Comprehensive Handbook of Chemical Bond Energies*, CRC Press, Boca Raton, Florida, **2007**.

[160] K. G. Caulton, *New J. Chem.* **1994**, *18*, 25.

[161] K. Fagnou, M. Lautens, *Angew. Chem. Int. Ed.* **2002**, *41*, 26; *Angew. Chem.* **2002**, *114*, 26.

[162] M. Kaupp, *J. Comput. Chem.* **2007**, *28*, 320.

[163] S. Ahrland, J. Chatt, N. R. Davies, *Q. Rev., Chem. Soc.* **1958**, *12*, 265.

[164] M. N. Hopkinson, A. D. Gee, V. Gouverneur, *Isr. J. Chem.* **2010**, *50*, 675.

[165] M. N. Hopkinson, A. D. Gee, V. Gouverneur, *Chem. Eur. J.* **2011**, *17*, 8248.

[166] R. P. Herrera, M. C. Gimeno, *Chem. Rev.* **2021**, *121*, 8311.

[167] E. Bernhardt, M. Finze, H. Willner, *J. Fluorine Chem.* **2004**, *125*, 967.

[168] D. S. Laitar, P. Müller, T. G. Gray, J. P. Sadighi, *Organometallics* **2005**, *24*, 4503.

[169] C. M. Wyss, B. K. Tate, J. Bacsa, M. Wieliczko, J. P. Sadighi, *Polyhedron* **2014**, *84*, 87.

[170] J. A. Akana, K. X. Bhattacharyya, P. Müller, J. P. Sadighi, *J. Am. Chem. Soc.* **2007**, *129*, 7736.

[171] N. P. Mankad, F. D. Toste, *Chem. Sci.* **2012**, *3*, 72.

[172] F. Nahra, S. R. Patrick, D. Bello, M. Brill, A. Obled, D. B. Cordes, D. O'Hagan, S. P. Nolan, *ChemCatChem* **2015**, *7*, 240.

[173] M. S. Winston, W. J. Wolf, F. D. Toste, *J. Am. Chem. Soc.* **2015**, *137*, 7921.

[174] S. G. Rachor, R. Müller, P. Wittwer, M. Kaupp, T. Braun, *Inorg. Chem.* **2022**, *61*, 357.

[175] S. G. Rachor, R. Jaeger, T. Braun, *Eur. J. Inorg. Chem.* **2022**, e202200158.

[176] S. G. Rachor, M. Ahrens, T. Braun, *Angew. Chem. Int. Ed.* **2022**, *61*, e202212858; *Angew. Chem.* **2022**, *134*, e202212858.

[177] S. G. Rachor, R. Müller, M. Kaupp, T. Braun, *Eur. J. Inorg. Chem.* **2023**, *26*.

[178] R. M. P. Veenboer, A. Collado, S. Dupuy, T. Lebl, L. Falivene, L. Cavallo, D. B. Cordes, A. M. Z. Slawin, C. S. J. Cazin, S. P. Nolan, *Organometallics* **2017**, *36*, 2861.

[179] A. Pérez-Bitrián, S. Martínez-Salvador, M. Baya, J. M. Casas, A. Martín, B. Menjón, J. Orduna, *Chem. Eur. J.* **2017**, *23*, 6919.

[180] D. Y. Melgarejo, G. M. Chiarella, J. P. Fackler, L. M. Perez, A. Rodrigue-Witchel, C. Reber, *Inorg. Chem.* **2011**, *50*, 4238.

[181] E. Tkatchouk, N. P. Mankad, D. Benitez, W. A. Goddard III, F. D. Toste, *J. Am. Chem. Soc.* **2011**, *133*, 14293.

[182] H. A. Wegner, M. Auzias, *Angew. Chem. Int. Ed.* **2011**, *50*, 8236; *Angew. Chem.* **2011**, *123*, 8386.

[183] R. Dorel, A. M. Echavarren, *Chem. Rev.* **2015**, *115*, 9028.

[184] M. N. Hopkinson, A. Tlahuext-Aca, F. Glorius, *Acc. Chem. Res.* **2016**, *49*, 2261.

[185] L. Rocchigiani, M. Bochmann, *Chem. Rev.* **2021**, *121*, 8364.

[186] A. Corma, A. Leyva-Pérez, M. J. Sabater, *Chem. Rev.* **2011**, *111*, 1657.

[187] K. Chen, S. Zhu, *Synlett* **2017**, *28*, 640.

[188] D. Mulryan, J. Rodwell, N. A. Phillips, M. R. Crimmin, *ACS Catal.* **2022**, *12*, 3411.

[189] P. Garcia, M. Malacria, C. Aubert, V. Gandon, L. Fensterbank, *ChemCatChem* **2010**, *2*, 493.

[190] S. G. Bratsch, *J. Phys. Chem. Ref. Data* **1989**, *18*, 1.

[191] a) R. P. Singh, J. M. Shreeve, *Acc. Chem. Res.* **2004**, *37*, 31; b) S. Stavber, M. Zupan, *Acta Chim. Slov.* **2005**, *52*, 13; c) M. Schuler, F. Silva, C. Bobbio, A. Tessier, V. Gouverneur, *Angew. Chem. Int. Ed.* **2008**, *47*, 7927; *Angew. Chem.* **2008**, *120*, 8045.

[192] a) G. Zhang, Y. Peng, L. Cui, L. Zhang, *Angew. Chem. Int. Ed.* **2009**, *48*, 3112; *Angew. Chem.* **2009**, *121*, 3158; b) Y. Peng, L. Cui, G. Zhang, L. Zhang, *J. Am. Chem. Soc.* **2009**, *131*, 5062; c) G. Zhang, L. Cui, Y. Wang, L. Zhang, *J. Am. Chem. Soc.* **2010**, *132*, 1474; d) L. T. Ball, M. Green, G. C. Lloyd-Jones, C. A. Russell, *Org. Lett.* **2010**, *12*, 4724; e) W. E. Brenzovich Jr., J.-F. Brazeau, F. D. Toste, *Org. Lett.* **2010**, *12*, 4728; f) A. D. Melhado, W. E. Brenzovich Jr., A. D. Lackner, F. D. Toste, *J. Am. Chem. Soc.* **2010**, *132*, 8885; g) W. E. Brenzovich Jr., D. Benitez, A. D. Lackner, H. P. Shunatona, E. Tkatchouk, W. A. Goddard III, F. D. Toste, *Angew. Chem. Int. Ed.* **2010**, *49*, 5519-5522; *Angew. Chem.* **2010**, *122*, 5651.

[193] N. P. Mankad, F. D. Toste, *J. Am. Chem. Soc.* **2010**, *132*, 12859.

[194] M. S. Winston, W. J. Wolf, F. D. Toste, *J. Am. Chem. Soc.* **2014**, *136*, 7777.

[195] R. Bhattacharjee, A. Nijamudheen, A. Datta, *Chem. Eur. J.* **2017**, *23*, 4169.

[196] R. Kumar, A. Linden, C. Nevado, *Angew. Chem. Int. Ed.* **2015**, *54*, 14287; *Angew. Chem.* **2015**, *127*, 14495.

[197] R. Kumar, A. Linden, C. Nevado, *J. Am. Chem. Soc.* **2016**, *138*, 13790.

[198] A. Genoux, M. Biedrzycki, E. Merino, E. Rivera-Chao, A. Linden, C. Nevado, *Angew. Chem. Int. Ed.* **2021**, *60*, 4164; *Angew. Chem.* **2021**, *133*, 4210.

[199] G. Kleinhans, A. K.-W. Chan, M.-Y. Leung, D. C. Liles, M. A. Fernandes, V. W.-W. Yam, I. Fernández, D. I. Bezuidenhout, *Chem. Eur. J.* **2020**, *26*, 6993.

[200] M. Albayer, R. Corbo, J. L. Dutton, *Chem. Commun.* **2018**, *54*, 6832.

[201] M. Albayer, L. Sharp-Bucknall, N. Withanage, G. Armendariz-Vidales, C. F. Hogan, J. L. Dutton, *Inorg. Chem.* **2020**, *59*, 2765.

[202] L. Sharp-Bucknall, L. Barwise, J. D. Bennetts, M. Albayer, J. L. Dutton, *Organometallics* **2020**, *39*, 3344.

[203] M. A. Ellwanger, S. Steinhauer, P. Golz, T. Braun, S. Riedel, *Angew. Chem. Int. Ed.* **2018**, *57*, 7210; *Angew. Chem.* **2018**, *130*, 7328–7332.

[204] M. A. Ellwanger, C. von Randow, S. Steinhauer, Y. Zhou, A. Wiesner, H. Beckers, T. Braun, S. Riedel, *Chem. Commun.* **2018**, *54*, 9301.

[205] M. B. Smith, J. March, *March's Advanced Organic Chemistry*. *Reactions, Mechanisms, and Structure,* 6. Ed., John Wiley & Sons, Inc, Hoboken, New Jersey, **2006**.

[206] J. B. Dumas, E. Péligot, *Ann. Chim. Phys.* **1835**, *58*, 5.

[207] D. Bourissou, O. Guerret, F. P. Gabbaï, G. Bertrand, *Chem. Rev.* **2000**, *100*, 39.

[208] A. J. Arduengo III, R. Krafczyk, *Chem. Unserer Zeit* **1998**, *32*, 6.

[209] D. L. S. Brahms, W. P. Dailey, *Chem. Rev.* **1996**, *96*, 1585.

[210] W. von E. Doering, A. K. Hoffmann, *J. Am. Chem. Soc.* **1954**, *76*, 6162.

[211] E. O. Fischer, A. Maasböl, *Angew. Chem. Int. Ed.* **1964**, *3*, 580; *Angew. Chem.* **1964**, *76*, 571.

[212] H.-W. Wanzlick, H.-J. Schönherr, *Angew. Chem. Int. Ed.* **1968**, *7*, 141; *Angew. Chem.* **1968**, *80*, 154.

[213] K. Öfele, *J. Organomet. Chem.* **1968**, *12*, P42.

[214] M. N. Hopkinson, C. Richter, M. Schedler, F. Glorius, *Nature* **2014**, *510*, 485.

[215] A. J. Arduengo III, R. L. Harlow, M. Kline, *J. Am. Chem. Soc.* **1991**, *113*, 361.

[216] A. J. Arduengo III, J. R. Goerlich, W. J. Marshall, *J. Am. Chem. Soc.* **1995**, *117*, 11027.

[217] A. J. Arduengo III, R. Krafczyk, R. Schmutzler, H. A. Craig, J. R. Goerlich, W. J. Marshall, M. Unverzagt, *Tetrahedron* **1999**, *55*, 14523.

[218] M. Melaimi, M. Soleilhavoup, G. Bertrand, *Angew. Chem. Int. Ed.* **2010**, *49*, 8810; *Angew. Chem.* **2010**, *122*, 8992.

[219] M. Melaimi, R. Jazzar, M. Soleilhavoup, G. Bertrand, *Angew. Chem. Int. Ed.* **2017**, *56*, 10046; *Angew. Chem.* **2017**, *129*, 10180.

[220] R. Maity, B. Sarkar, *JACS Au* **2022**, *2*, 22.

[221] a) T. Dröge, F. Glorius, *Angew. Chem. Int. Ed.* **2010**, *49*, 6940; *Angew. Chem.* **2010**, *122*, 7094; b) D. J. Nelson, S. P. Nolan, *Chem. Soc. Rev.* **2013**, *42*, 6723; c) H. V. Huynh, S. Guo, W. Wu, *Organometallics* **2013**, *32*, 4591.

[222] a) N. Marion, S. Díez-González, S. P. Nolan, *Angew. Chem. Int. Ed.* **2007**, *46*, 2988; *Angew. Chem.* **2007**, *119*, 3046; b) D. Enders, O. Niemeier, A. Henseler, *Chem. Rev.* **2007**, *107*, 5606.

[223] T. Scattolin, S. P. Nolan, *Trends Chem.* **2020**, *2*, 721.

[224] J. Cheng, L. Wang, P. Wang, L. Deng, *Chem. Rev.* **2018**, *118*, 9930.

[225] S. Díez-González, N. Marion, S. P. Nolan, *Chem. Rev.* **2009**, *109*, 3612.

[226] K. M. Hindi, M. J. Panzner, C. A. Tessier, C. L. Cannon, W. J. Youngs, *Chem. Rev.* **2009**, *109*, 3859.

[227] J. L. Hickey, R. A. Ruhayel, P. J. Barnard, M. V. Baker, S. J. Berners-Price, A. Filipovska, *J. Am. Chem. Soc.* **2008**, *130*, 12570.

[228] R. Rubbiani, I. Kitanovic, H. Alborzinia, S. Can, A. Kitanovic, L. A. Onambele, M. Stefanopoulou, Y. Geldmacher, W. S. Sheldrick, G. Wolber, A. Prokop, S. Wölfl, I. Ott, *J. Med. Chem.* **2010**, *53*, 8608.

[229] M. Gil-Moles, U. Basu, R. Büssing, H. Hoffmeister, S. Türck, A. Varchmin, I. Ott, *Chem. Eur. J.* **2020**.

[230] a) H. V. Huynh, Y. Han, R. Jothibasu, J. A. Yang, *Organometallics* **2009**, *28*, 5395; b) Q. Teng, H. V. Huynh, *Dalton Trans.* **2017**, *46*, 614.

[231] a) J. Vícha, C. Foroutan-Nejad, T. Pawlak, M. L. Munzarová, M. Straka, R. Marek, *J. Chem. Theory Comput.* **2015**, *11*, 1509; b) J. Novotný, J. Vícha, P. L. Bora, M. Repisky, M. Straka, S. Komorovsky, R. Marek, *J. Chem. Theory Comput.* **2017**, *13*, 3586; c) A. H. Greif, P. Hrobárik, M. Kaupp, *Chem. Eur. J.* **2017**, *23*, 9790.

[232] S. Arrhenius, *Z. Phys. Chem.* **1887**, *1*, 631.

[233] J. N. Brönsted, *Recl. Trav. Chim. Pays-Bas* **1923**, *42*, 718.

[234] T. M. Lowry, *J. Chem. Technol. Biotechnol.* **1923**, *42*, 43.

[235] G. N. Lewis, *Valence and the Structure of Atoms and Molecules*, The Chemical Catalog Company, Inc., New York, **1923**.

[236] a) H. Yamamoto, *Lewis Acids in Organic Synthesis*, Wiley-VCH, Weinheim, **2000**; b) A. Corma, H. García, *Chem. Rev.* **2003**, *103*, 4307.

[237] a) C. Friedel, J. M. Crafts, *J. Chem. Soc.* **1877**, *32*, 725; b) G. A. Olah, *Friedel-Crafts Chemistry*, John Wiley & Sons, Inc, Hoboken, New Jersey, **1973**; c) M. Rueping, B. J. Nachtsheim, *Beilstein J. Org. Chem.* **2010**, *6*, No 6.

[238] J. S. Panek, P. F. Cirillo, *J. Org. Chem.* **1993**, *58*, 999.

[239] G. Cappozzi, G. Romeo, F. Marcuzzi, *J. Chem. Soc., Chem. Commun.* **1982**, 959.

[240] P. H. Kasai, P. Wheeler, *Appl. Surf. Sci.* **1991**, *52*, 91.

[241] D. A. Evans, A. R. Muci, R. Stuermer, *J. Org. Chem.* **1993**, *58*, 5307.

[242] L. P. Hammett, A. J. Deyrup, *J. Am. Chem. Soc.* **1932**, *54*, 2721.

[243] D. Himmel, V. Radtke, B. Butschke, I. Krossing, *Angew. Chem. Int. Ed.* **2018**, *57*, 4386; *Angew. Chem.* **2018**, *130*, 4471.

[244] P. Muller, *Pure Appl. Chem.* **1994**, *66*, 1077.

[245] a) D. P. N. Satchell, R. S. Satchell, *Q. Rev., Chem. Soc.* **1971**, *25*, 171; b) R. S. Drago, *Coord. Chem. Rev.* **1980**, *33*, 251.

[246] P. Erdmann, L. Greb, *Angew. Chem. Int. Ed.* **2022**, *61*, e202114550; *Angew. Chem.* **2022**, *134*, e202114550.

[247] H. Böhrer, N. Trapp, D. Himmel, M. Schleep, I. Krossing, *Dalton Trans.* **2015**, *44*, 7489.

[248] R. G. Parr, L. v. Szentpály, S. Liu, *J. Am. Chem. Soc.* **1999**, *121*, 1922.

[249] a) K. Müther, P. Hrobárik, V. Hrobáriková, M. Kaupp, M. Oestreich, *Chem. Eur. J.* **2013**, *19*, 16579; b) M. González Martínez, C. Cárdenas Valencia, J. I. Rodríguez, S. Liu, F. Heidar Zadeh, R. A. Miranda Quintana, P. W. Ayers, *Acta Phys. Chim. Sin.* **2018**, *34*, 662.

[250] a) D. M. Byler, D. F. Shriver, *Inorg. Chem.* **1973**, *12*, 1412; b) D. M. Byler, D. F. Shriver, *Inorg. Chem.* **1974**, *13*, 2697; c) B. v. Ahsen, B. Bley, S. Proemmel, R. Wartchow, H. Willner, F. Aubke, *Z. Anorg. Allg. Chem.* **1998**, *624*, 1225.

[251] S. Fukuzumi, K. Ohkubo, *Chem. Eur. J.* **2000**, *6*, 4532.

[252] a) S. Fukuzumi, K. Ohkubo, *J. Am. Chem. Soc.* **2002**, *124*, 10270; b) J. R. Gaffen, J. N. Bentley, L. C. Torres, C. Chu, T. Baumgartner, C. B. Caputo, *Chem* **2019**, *5*, 1567.

[253] U. Mayer, V. Gutmann, W. Gerger, *Monatsh. Chem.* **1975**, *106*, 1235.

[254] J. Ramler, C. Lichtenberg, *Chem. Eur. J.* **2020**, *26*, 10250.

[255] R. F. Childs, D. L. Mulholland, A. Nixon, *Can. J. Chem.* **1982**, *60*, 809.

[256] A. E. Ashley, T. J. Herrington, G. G. Wildgoose, H. Zaher, A. L. Thompson, N. H. Rees, T. Krämer, D. O'Hare, *J. Am. Chem. Soc.* **2011**, *133*, 14727.

[257] a) J. C. Haartz, D. H. McDaniel, *J. Am. Chem. Soc.* **1973**, *95*, 8562; b) T. E. Mallouk, G. L. Rosenthal, G. Mueller, R. Brusasco, N. Bartlett, *Inorg. Chem.* **1984**, *23*, 3167.

[258] P. Erdmann, J. Leitner, J. Schwarz, L. Greb, *ChemPhysChem* **2020**, *21*, 987.

[259] K. O. Christe, D. A. Dixon, D. McLemore, W. W. Wilson, J. A. Sheehy, J. A. Boatz, *J. Fluorine Chem.* **2000**, *101*, 151.

[260] G. A. Olah, G. K. Prakash, J. Sommer, *Science* **1979**, *206*, 13.

[261] L. O. Müller, D. Himmel, J. Stauffer, G. Steinfeld, J. Slattery, G. Santiso-Quiñones, V. Brecht, I. Krossing, *Angew. Chem. Int. Ed.* **2008**, *47*, 7659; *Angew. Chem.* **2008**, *120*, 7772.

[262] G. A. Olah, G. K. Surya Prakash, Q. Wang, X. Li in *Encyclopedia of Reagents for Organic Synthesis* (Ed.: L. A. Paquette), Wiley, Chichester, **1995**.

[263] H. Heaney in *Encyclopedia of Reagents for Organic Synthesis* (Ed.: L. A. Paquette), Wiley, Chichester, **1995**.

[264] L. A. Körte, J. Schwabedissen, M. Soffner, S. Blomeyer, C. G. Reuter, Y. V. Vishnevskiy, B. Neumann, H.-G. Stammler, N. W. Mitzel, *Angew. Chem. Int. Ed.* **2017**, *56*, 8578; *Angew. Chem.* **2017**, *129*, 8701.

[265] J. F. Kögel, D. A. Sorokin, A. Khvorost, M. Scott, K. Harms, D. Himmel, I. Krossing, J. Sundermeyer, *Chem. Sci.* **2018**, *9*, 245.

[266] K. F. Hoffmann, A. Wiesner, S. Steinhauer, S. Riedel, *Chem. Eur. J.* **2022**, e202201958.

[267] S. Gaillard, A. M. Z. Slawin, A. T. Bonura, E. D. Stevens, S. P. Nolan, *Organometallics* **2010**, *29*, 394.

[268] T. Besset, P. Jubault, X. Pannecoucke, T. Poisson, *Org. Chem. Front.* **2016**, *3*, 1004.

[269] U. Preiss, I. Krossing, *Z. Anorg. Allg. Chem.* **2007**, *633*, 1639.

6 Publications and Conference Contributions

6.1 Publications

(1) **Reactivity of [AuF_3(SIMes)]: Pathway to Unprecedented Structural Motifs**

Marlon Winter, Mathias A. Ellwanger, Niklas Limberg, Alberto Pérez-Bitrián, Patrick Voßnacker, Simon Steinhauer, Sebastian Riedel, *Chem. Eur. J.* **2023**, e202301684, https://doi.org/10.1002/chem.202301684

(2) **Gold Teflates Revisited: From the Lewis Superacid [$Au(OTeF_5)_3$] to the Anion [$Au(OTeF_5)_4$]$^-$**

Marlon Winter, Natallia Peshkur, Mathias A. Ellwanger, Alberto Pérez-Bitrián, Patrick Voßnacker, Simon Steinhauer, Sebastian Riedel, *Chem. Eur. J.* **2023**, *29*, e202203634, https://doi.org/10.1002/chem.202203634

(3) **Trifluoromethylation of [AuF_3(SIMes)]: Preparation and Characterization of [$Au(CF_3)_xF_{3-x}$(SIMes)] (x =1–3) Complexes**

Marlon Winter, Niklas Limberg, Mathias A. Ellwanger, Alberto Pérez-Bitrián, Karsten Sonnenberg, Simon Steinhauer, Sebastian Riedel, *Chem. Eur. J.* **2020**, *26*, 16089, https://doi.org/10.1002/chem.202002940

6.2 Conference Contributions

(1) **Synthesis of Fluorido Organo Gold(III) Complexes from [AuF_3(SIMes)]**
Marlon Winter, Niklas Limberg, Mathias A. Ellwanger, Alberto Pérez-Bitrián, Sebastian Riedel, *19. Deutscher Fluortag*, Schmitten, Germany, **2022** (Oral Presentation)

(2) **Synthesis of Fluorido Organo Gold(III) Complexes from [AuF_3(SIMes)] – Introduction of –CF_3 and –C≡CR Groups**
Marlon Winter, Niklas Limberg, Mathias A. Ellwanger, Alberto Pérez-Bitrián, Sebastian Riedel, *21st Conference on Inorganic Chemistry (Wöhler-Tagung)*, Marburg, Germany, **2022** (Poster Presentation)

(3) **Synthesis of Fluorido Organo Gold(III) Complexes from [AuF_3(SIMes)] – Introduction of –CF_3 and –C≡CR Groups**
Marlon Winter, Niklas Limberg, Mathias A. Ellwanger, Alberto Pérez-Bitrián, Sebastian Riedel, *20th European Symposium on Fluorine Chemistry*, Berlin, Germany, **2022** (Poster Presentation)

(4) **Synthesis of Fluorido Organo Gold(III) Complexes from [AuF_3(SIMes)] – Introduction of –CF_3 and –C≡CR Groups**
Marlon Winter, Niklas Limberg, Mathias A. Ellwanger, Alberto Pérez-Bitrián, Sebastian Riedel, *XXIV Virtual Conference on Organometallic Chemistry*, Madrid, Spain (online), **2021** (Poster Presentation)

(5) **Substitution Reactions on Fluoridogold(III) Complexes – Introduction of –CF_3 and –$OTeF_5$ Groups to [AuF_3(SIMes)] and [AuF_4]$^-$**
Marlon Winter, Niklas Limberg, Lucia Anghileri, Rickesh Rajamenon, Sebastian Riedel, *7. Tag der Anorganischen Chemie, Freie Universität Berlin*, Berlin, Germany, **2019** (Poster Presentation)

7 Curriculum Vitae

The curriculum vitae is not included for reasons of data protection.

8 Appendix

8.1 Supporting Information of ‘Trifluoromethylation of [AuF_3(SIMes)]: Preparation and Characterization of [$Au(CF_3)_xF_{3-x}$(SIMes)] (x = 1–3) Complexes’

Chemistry–A European Journal

Supporting Information

Trifluoromethylation of $[AuF_3(SIMes)]$: Preparation and Characterization of $[Au(CF_3)_xF_{3-x}(SIMes)]$ ($x = 1–3$) Complexes

Marlon Winter,[a] Niklas Limberg,[a] Mathias A. Ellwanger,[a] Alberto Pérez-Bitrián,[a, b] Karsten Sonnenberg,[a] Simon Steinhauer,[a] and Sebastian Riedel*[a]

Table of Contents

X-Ray Crystallography

Crystallographic Data

Table S1: Crystal data and refinement details for the analysis of the molecular structures in the solid state of *trans*-[Au(CF_3)F_2(SIMes)] (**1**), [Au(CF_3)$_3$(SIMes)]·0.5 CH_2Cl_2 (**3a**) and [Au(CF_3)$_3$(SIMes)]·0.5 $CHCl_3$ (**3b**). For **1**, the largest diffraction peak of 2.6 e Å^{-3} is close to the gold center and can be explained by the reduced precision of the crystal face determination due to large twin contributions and respective deviations of the numerical absorption correction.

	trans-[Au(CF_3)F_2(SIMes)] (**1**)	[Au(CF_3)$_3$(SIMes)]·0.5 CH_2Cl_2 (**3a**)	[Au(CF_3)$_3$(SIMes)]·0.5 $CHCl_3$ (**3b**)
Empirical formula	$C_{22}H_{26}AuF_5N_2$	$C_{49}H_{52}Au_2Cl_2F_{18}N_4$	$C_{49}H_{53}Au_2Cl_3F_{18}N_4$
Formula weight	610.41	1503.78	1540.23
Temperature/K	100.07	99.98	100.07
Crystal system	orthorhombic	monoclinic	monoclinic
Space group	*Pnma*	$P2_1/c$	$P2_1/c$
a/Å	15.183(6)	18.669(4)	19.0487(19)
b/Å	19.914(5)	9.174(2)	9.0163(8)
c/Å	7.540(3)	17.106(3)	17.3412(17)
α/°	90	90	90
β/°	90	116.201(7)	116.330(4)
γ/°	90	90	90
Volume/Å^3	2279.7(13)	2628.6(9)	2669.3(4)
Z	4	2	2
ρ_{calc}g/cm^3	1.779	1.900	1.916
μ/mm^{-1}	6.504	5.779	5.742
F(000)	1184.0	1456.0	1492.0
Crystal size/mm^3	0.546 × 0.252 × 0.195	0.12 × 0.11 × 0.1	0.45 × 0.39 × 0.32
Radiation	MoK_α (λ = 0.71073)	MoK_α (λ = 0.71073)	MoK_α (λ = 0.71073)
2Θ range for data collection/°	5.366 to 54.482	4.764 to 56.718	4.698 to 56.656
Index ranges	-19 ≤ h ≤ 19, -25 ≤ k ≤ 25, -9 ≤ l ≤ 9	-24 ≤ h ≤ 24, -12 ≤ k ≤ 12, -22 ≤ l ≤ 22	-25 ≤ h ≤ 25, -12 ≤ k ≤ 12, -23 ≤ l ≤ 23
Reflections collected	108341	106844	54535
Independent reflections	2618 [R_{int} = 0.0626, R_{sigma} = 0.0144]	6557 [R_{int} = 0.0574, R_{sigma} = 0.0195]	6623 [R_{int} = 0.0935, R_{sigma} = 0.0486]
Data/restraints/ parameters	2618/360/250	6557/7/351	6623/0/371
Goodness-of-fit on F^2	1.235	1.061	1.040
Final R indexes [I>=2σ (I)]	R_1 = 0.0329, wR_2 = 0.0726	R_1 = 0.0198, wR_2 = 0.0423	R_1 = 0.0300, wR_2 = 0.0644
Final R indexes [all data]	R_1 = 0.0430, wR_2 = 0.0814	R_1 = 0.0242, wR_2 = 0.0436	R_1 = 0.0391, wR_2 = 0.0679
Largest diff. peak/hole / e Å^{-3}	2.62/-1.94	1.53/-1.37	1.01/-1.85
CCDC deposition number	2001090	2000997	2000994

Table S2: Crystal data and refinement details for the analysis of the molecular structures in the solid state of [$Au(CF_3)_3$(SIMes)]·C_3H_6O (**3c**) and [$Au(CF_3)_3$(SIMes)]·C_5H_8O (**3d**).

	[$Au(CF_3)_3$(SIMes)]·0.5 C_3H_6O (**3c**)	[$Au(CF_3)_3$(SIMes)]·0.5 C_5H_8O (**3d**)
Empirical formula	$C_{51}H_{58}Au_2F_{18}N_4O$	$C_{52}H_{60}Au_2F_{18}N_4O$
Formula weight	1478.94	1492.97
Temperature/K	100.01	100.02
Crystal system	monoclinic	monoclinic
Space group	$P2_1/c$	$P2_1/c$
a/Å	18.8838(13)	19.016(4)
b/Å	9.0553(5)	9.0238(13)
c/Å	17.2002(11)	17.301(4)
α/°	90	90
β/°	116.683(2)	115.892(5)
γ/°	90	90
Volume/Å^3	2628.0(3)	2670.8(9)
Z	2	2
ρ_{calc}g/cm^3	1.869	1.856
μ/mm^{-1}	5.682	5.592
F(000)	1440.0	1456.0
Crystal size/mm^3	0.24 × 0.24 × 0.08	0.2 × 0.11 × 0.04
Radiation	MoK_α (λ = 0.71073)	MoK_α (λ = 0.71073)
2Θ range for data collection/°	4.736 to 56.638	4.71 to 54.902
Index ranges	-25 ≤ h ≤ 25, -12 ≤ k ≤ 12, -22 ≤ l ≤ 22	-24 ≤ h ≤ 24, -11 ≤ k ≤ 11, -22 ≤ l ≤ 22
Reflections collected	60698	74712
Independent reflections	6520 [R_{int} = 0.0665, R_{sigma} = 0.0326]	6097 [R_{int} = 0.1016, R_{sigma} = 0.0393]
Data/restraints/ parameters	6520/6/369	6097/0/376
Goodness-of-fit on F^2	1.046	1.032
Final R indexes [I>=2σ (I)]	R_1 = 0.0225, wR_2 = 0.0490	R_1 = 0.0281, wR_2 = 0.0464
Final R indexes [all data]	R_1 = 0.0298, wR_2 = 0.0514	R_1 = 0.0431, wR_2 = 0.0498
Largest diff. peak/hole / e Å^{-3}	0.65/-1.73	1.02/-0.89
CCDC deposition number	2000995	2000996

Molecular Structure of *trans*-[Au(CF$_3$)F$_2$(SIMes)] (1) in the Solid State

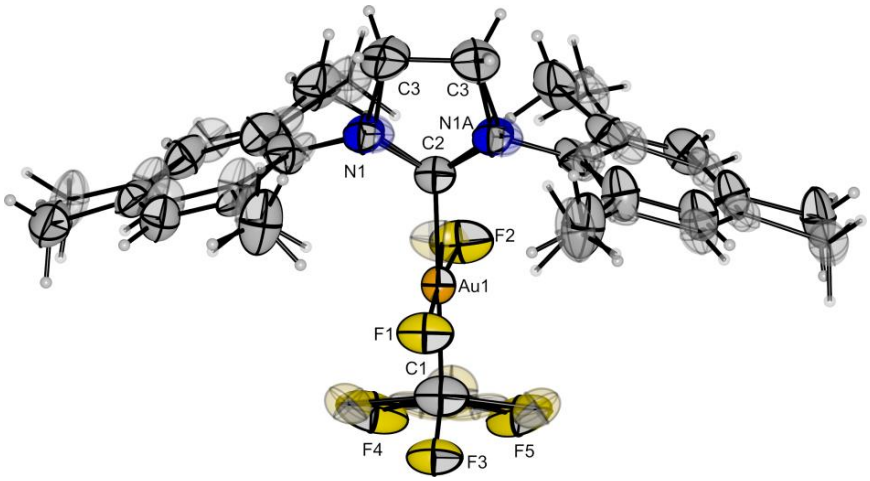

Figure S1: Molecular structure of *trans*-[Au(CF$_3$)F$_2$(SIMes)] (**1**) in the solid state. The second position of disordered atoms in the CF$_3$ and the SIMes ligand is shown as transparent ellipsoids. Thermal ellipsoids are set at 50 % probability. Bond lengths [pm] to the central gold atom: 193.2(5) (F1-Au1), 193.2(10) (F2-Au1), 203.6(10) (C1-Au1), 203.5(9) (C2-Au1).

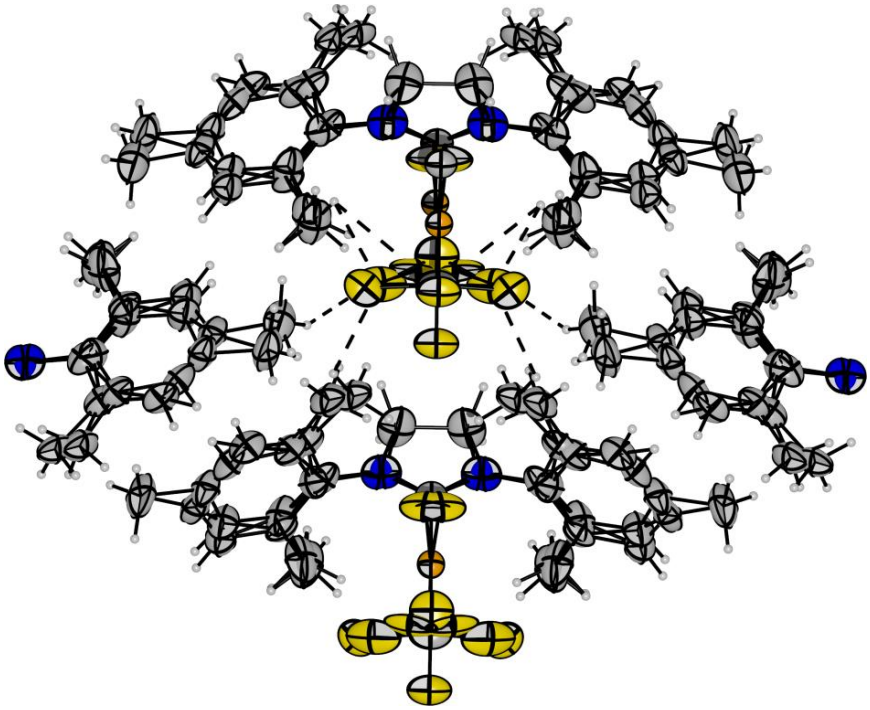

Figure S2: Crystal packing via intermolecular H-F contacts (r[C(H)-F] < 300 pm; dashed bonds), shown exemplarily for one entity of *trans*-[Au(CF$_3$)F$_2$(SIMes)] (**1**), including disorders. Thermal ellipsoids are set at 50 % probability.

Molecular Structure of [Au(CF$_3$)$_3$(SIMes)]·0.5 CH$_2$Cl$_2$ (3a) in the Solid State

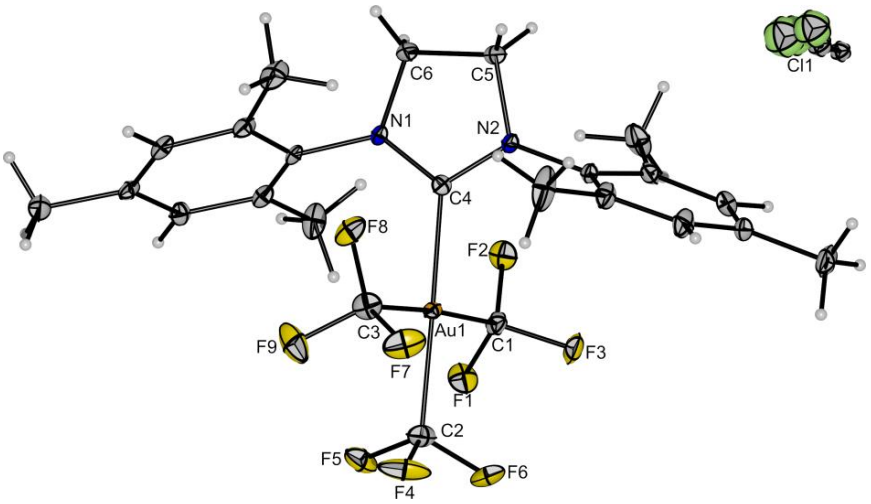

Figure S3: Molecular structure of [Au(CF$_3$)$_3$(SIMes)]·0.5 CH$_2$Cl$_2$ (**3a**) in the solid state. Thermal ellipsoids are set at 50 % probability. Bond lengths [pm] to the central gold atom: 208.6(3) (C1-Au1), 207.8(3) (C2-Au1), 208.3(3) (C3-Au1), 208.1(2) (C4-Au1).

Molecular Structure of [Au(CF$_3$)$_3$(SIMes)]·0.5 CHCl$_3$ (3b) in the Solid State

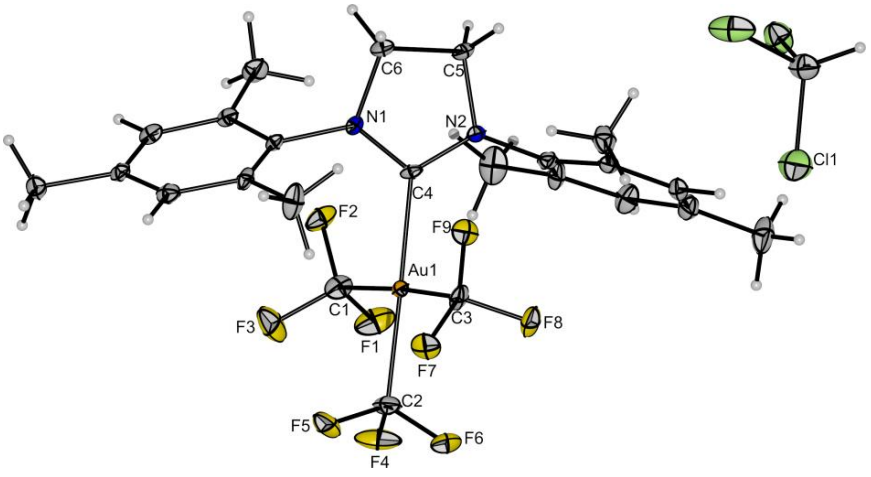

Figure S4: Molecular structure of [Au(CF$_3$)$_3$(SIMes)]·0.5 CHCl$_3$ (**3b**) in the solid state. Thermal ellipsoids are set at 50 % probability. Bond lengths [pm] to the central gold atom: 208.9(4) (C1-Au1), 207.7(4) (C2-Au1), 209.4(4) (C3-Au1), 208.5(3) (C4-Au1).

Molecular Structure of $[Au(CF_3)_3(SIMes)]\cdot 0.5\ C_3H_6O$ (3c) in the Solid State

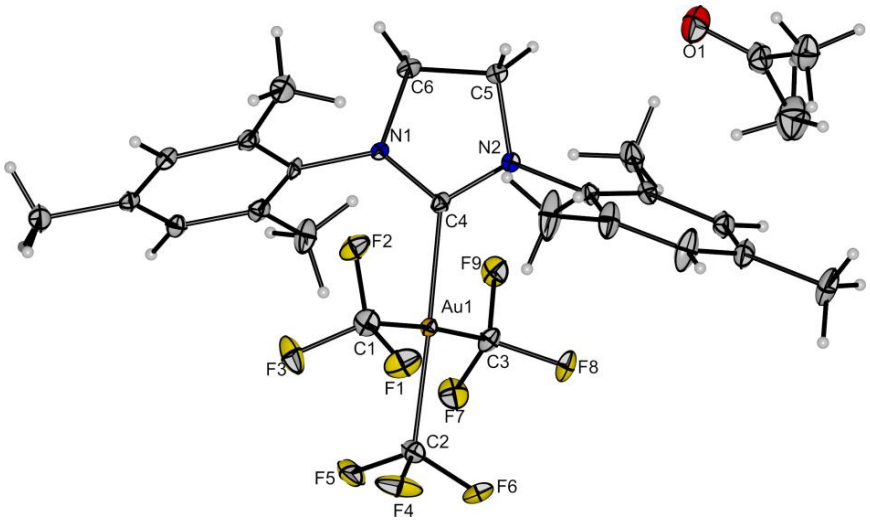

Figure S5: Molecular structure of $[Au(CF_3)_3(SIMes)]\cdot 0.5\ C_3H_6O$ (**3c**) in the solid state. Thermal ellipsoids are set at 50 % probability. Bond lengths [pm] to the central gold atom: 208.5(3) (C1-Au1), 207.3(3) (C2-Au1), 208.7(3) (C3-Au1), 207.7(3) (C4-Au1).

Molecular Structure of $[Au(CF_3)_3(SIMes)]\cdot 0.5\ C_5H_8O$ (3d) in the Solid State

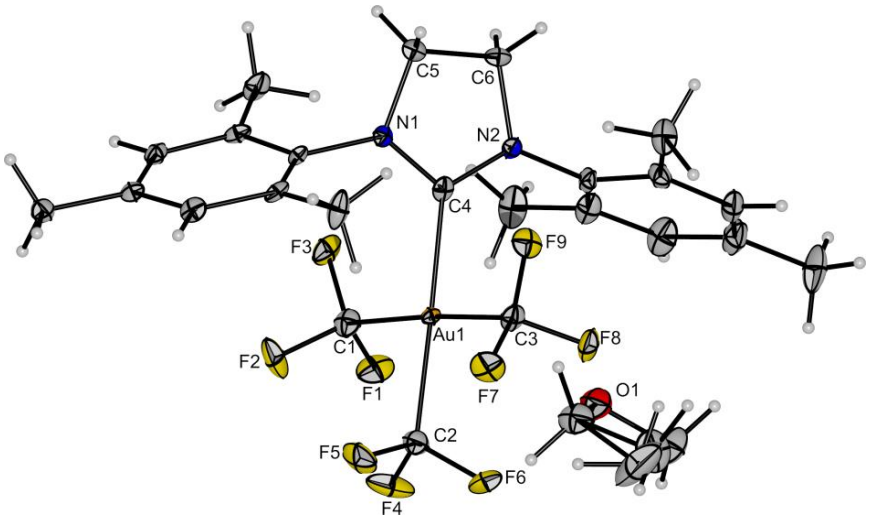

Figure S6: Molecular structure of $[Au(CF_3)_3(SIMes)]\cdot 0.5\ C_5H_8O$ (**3d**) in the solid state. Thermal ellipsoids are set at 50 % probability. Bond lengths [pm] to the central gold atom: 208.8(4) (C1-Au1), 207.5(4) (C2-Au1), 208.4(4) (C3-Au1), 207.4(3) (C4-Au1).

NMR Spectroscopy

Summary of Products Identified by NMR Spectroscopy

Figure S7 shows the products that have been identified by ^{19}F NMR spectroscopy. Their assignment in the following spectra is done using the numbers written in bold.[1] For compounds **1** - **3**, which incorporate different fluorine-containing groups, the different groups will be denoted by F for fluorine atoms and CF_3 for trifluoromethyl groups. Furthermore, c for ligands *cis* to the SIMes ligand (cf. Figure S8) and t for *trans* to SIMes are used as subscripts in case of chemically inequivalent ligands of the same type (compound **2** and **3**). Figure S8 depicts the structure of SIMes denoting the chemically inequivalent hydrogen and carbon atoms, which can be distinguished in the ^1H and ^{13}C NMR spectra that are shown below.

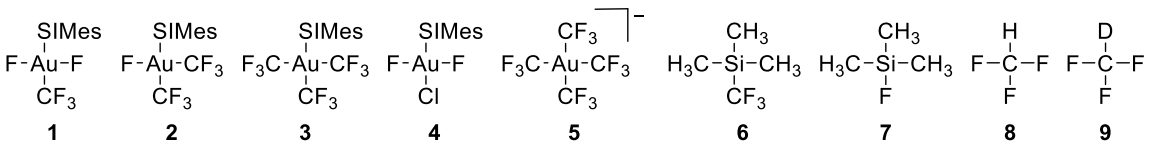

Figure S7: List of products that have been detected in the ^{19}F NMR spectra of the reactions that are presented in this work. The numbers in bold are used for their assignment in the following ^{19}F NMR spectra.

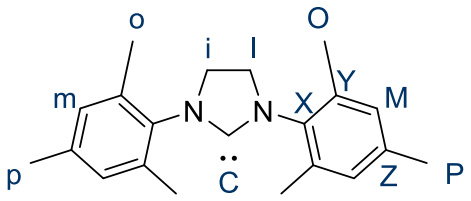

Figure S8: Structure of the NHC 1,3-bis(2,4,6-trimethylphenyl)-4,5-dihydroimidazol-2-ylidene (SIMes), which is present in products **1**-**4** (cf. Figure S7). The positions of chemically inequivalent hydrogen atoms are denoted in blue small letters, those of the chemically inequivalent carbon atoms by blue capital letters. C = carbene, I = imidazolidine, M = *meta* C, O = *ortho* CH_3, P = *para* CH_3, X = *ipso* C, Y = *ortho* C, Z = *para* C, i = imidazolidine H, m = *meta* H, o = *ortho* H, p = *para* H.

NMR Spectra of the Reaction Between [AuF_3(SIMes)] and $TMSCF_3$ in DCM

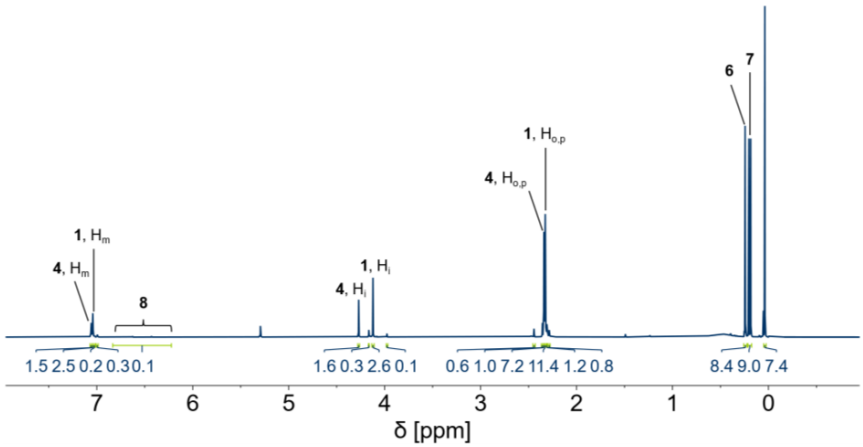

Figure S9: ^{1}H NMR spectrum (400 MHz, CD_2Cl_2, 22 °C) of the reaction between 1 eq. of [AuF_3(SIMes)] and 0.5 eq. of $TMSCF_3$ in DCM including assignments to the compounds shown in Figure S7. The integrals were referenced to TMSF (**7**) with an integral of 9.0.

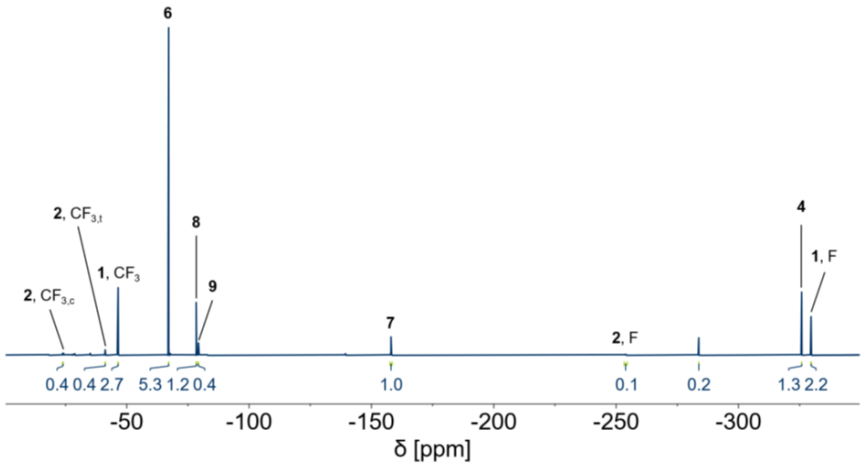

Figure S10: ^{19}F NMR spectrum (377 MHz, CD_2Cl_2, 22 °C) of the reaction between 1 eq. of [AuF_3(SIMes)] and 0.5 eq. of $TMSCF_3$ in DCM including assignments to the compounds shown in Figure S7. The integrals were referenced to TMSF (**7**) with an integral of 1.0.

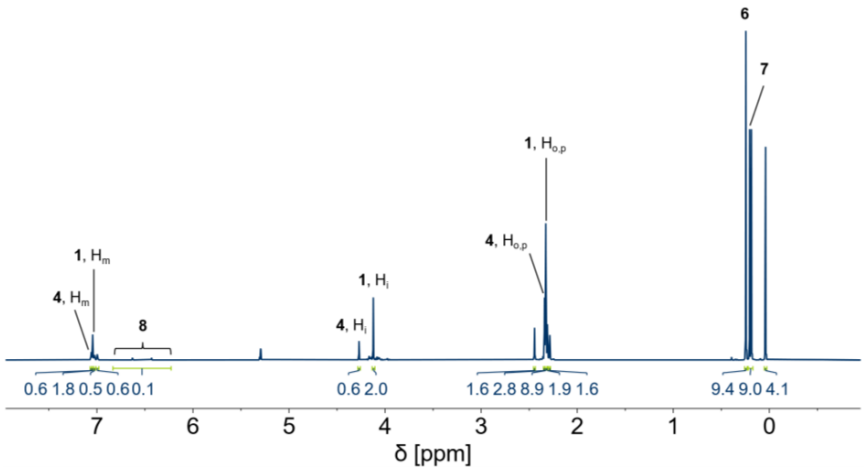

Figure S11: ^{1}H NMR spectrum (400 MHz, CD_2Cl_2, 20 °C) of the reaction between 1 eq. of [AuF_3(SIMes)] and 1 eq. of $TMSCF_3$ in DCM including assignments to the compounds shown in Figure S7. The integrals were referenced to TMSF (**7**) with an integral of 9.0.

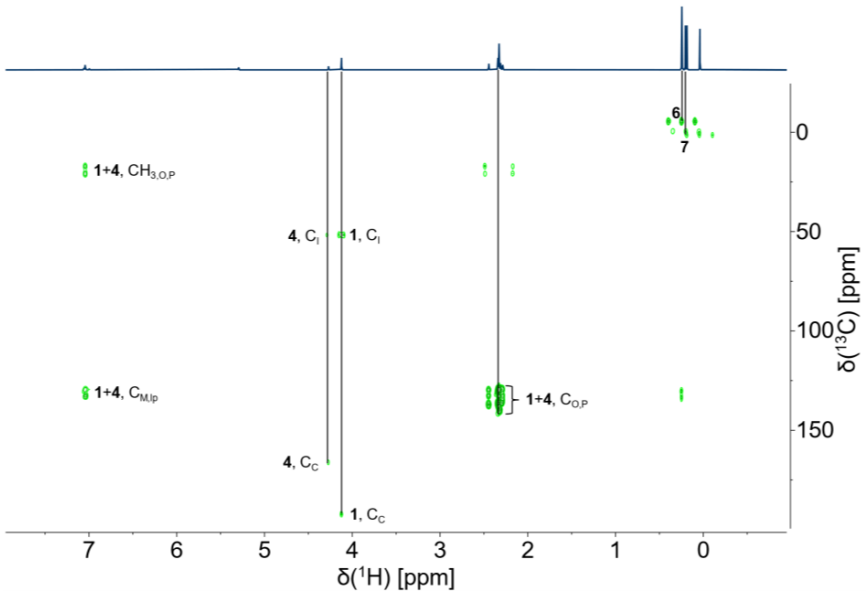

Figure S12: $^{1}H,^{13}C$ HMBC NMR spectrum (400 MHz, CD_2Cl_2, 20 °C) of the reaction between 1 eq. of [AuF_3(SIMes)] and 1 eq. of $TMSCF_3$ in DCM including assignments to the compounds shown in Figure S7.

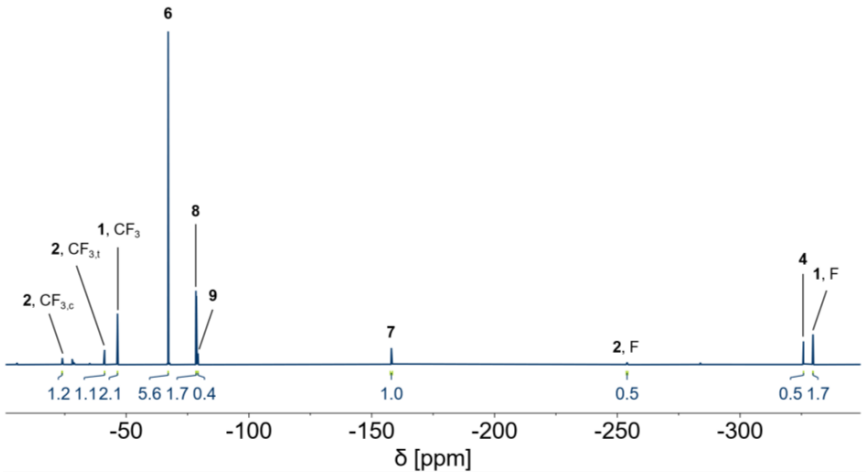

Figure S13: ^{19}F NMR spectrum (377 MHz, CD_2Cl_2, 20 °C) of the reaction between 1 eq. of [AuF_3(SIMes)] and 1 eq. of $TMSCF_3$ in DCM including assignments to the compounds shown in Figure S7. The integrals were referenced to TMSF (**7**) with an integral of 1.0.

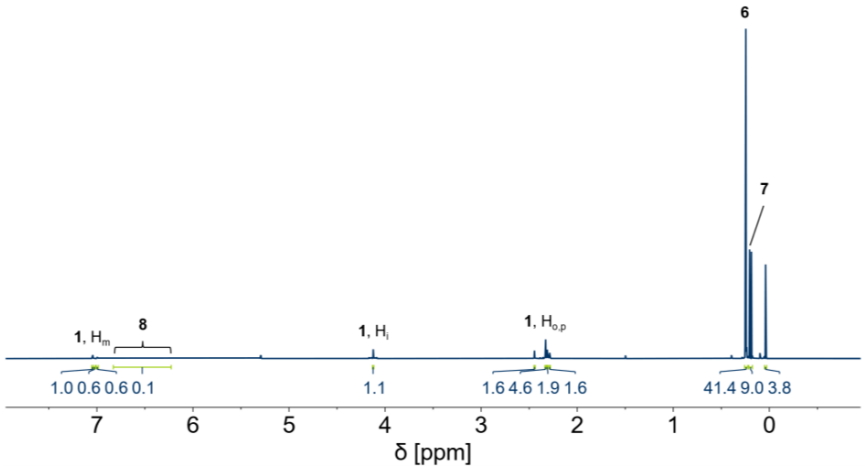

Figure S14: ^{1}H NMR spectrum (400 MHz, CD_2Cl_2, 21 °C) of the reaction between 1 eq. of [AuF_3(SIMes)] and 5 eq. of $TMSCF_3$ in DCM including assignments to the compounds shown in Figure S7. The integrals were referenced to TMSF (**7**) with an integral of 9.0.

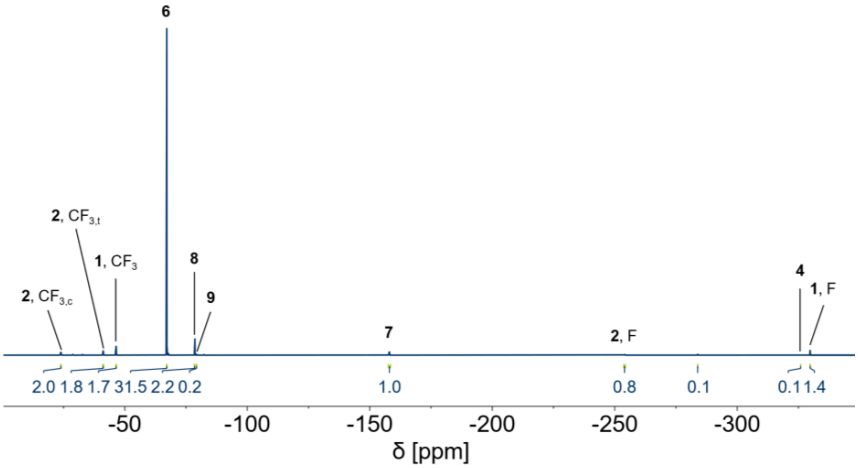

Figure S15: ^{19}F NMR spectrum (377 MHz, CD_2Cl_2, 21 °C) of the reaction between 1 eq. of [AuF_3(SIMes)] and 5 eq. of $TMSCF_3$ in DCM including assignments to the compounds shown in Figure S7. The integrals were referenced to TMSF (**7**) with an integral of 1.0.

NMR Spectra of the Reaction Between [AuF_3(SIMes)] and $TMSCF_3$ in THF

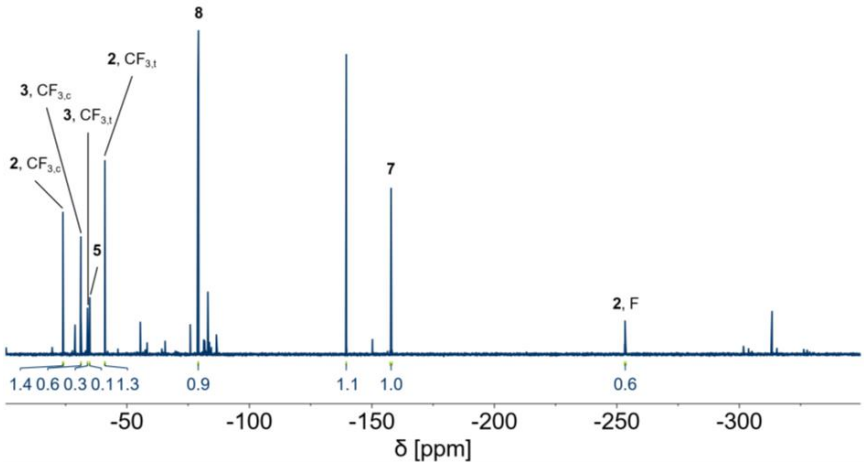

Figure S16: ^{19}F NMR spectrum (377 MHz, ext.$(CD_3)_2CO$, 20 °C) of the reaction between 1 eq. of [AuF_3(SIMes)] and 0.5 eq. of $TMSCF_3$ in THF including assignments to the compounds shown in Figure S7. The integrals were referenced to TMSF (**7**) with an integral of 1.0.

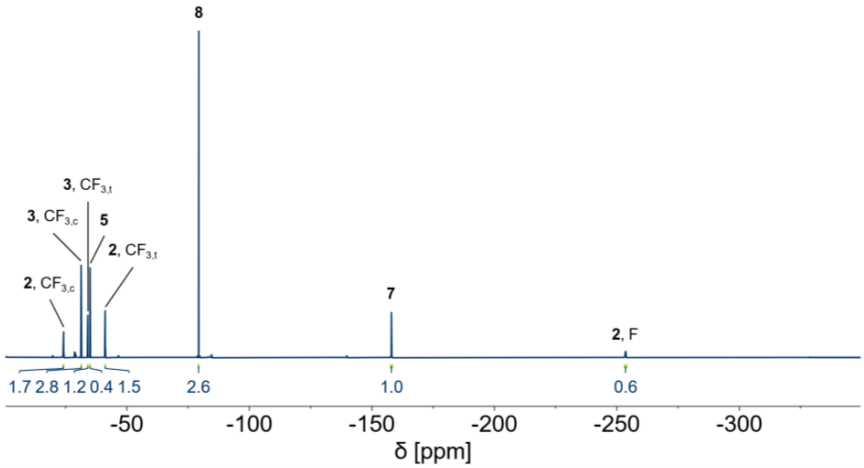

Figure S17: ^{19}F NMR spectrum (377 MHz, ext.$(CD_3)_2CO$, 21 °C) of the reaction between 1 eq. of [AuF_3(SIMes)] and 1 eq. of $TMSCF_3$ in THF including assignments to the compounds shown in Figure S7. The integrals were referenced to TMSF (**7**) with an integral of 1.0.

NMR Spectra of [Au(CF$_3$)$_3$(SIMes)] (3)

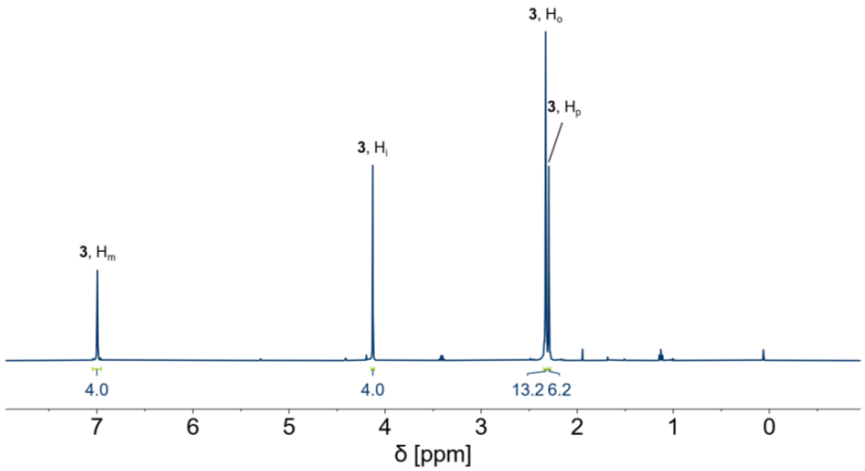

Figure S18: ^{1}H NMR spectrum (400 MHz, CD_2Cl_2, 21 °C) of [Au(CF$_3$)$_3$(SIMes)] (**3**). The integrals were referenced to the signal of the hydrogen atoms in *meta* position of the SIMes ligand in compound **3** with an integral of 4.0.

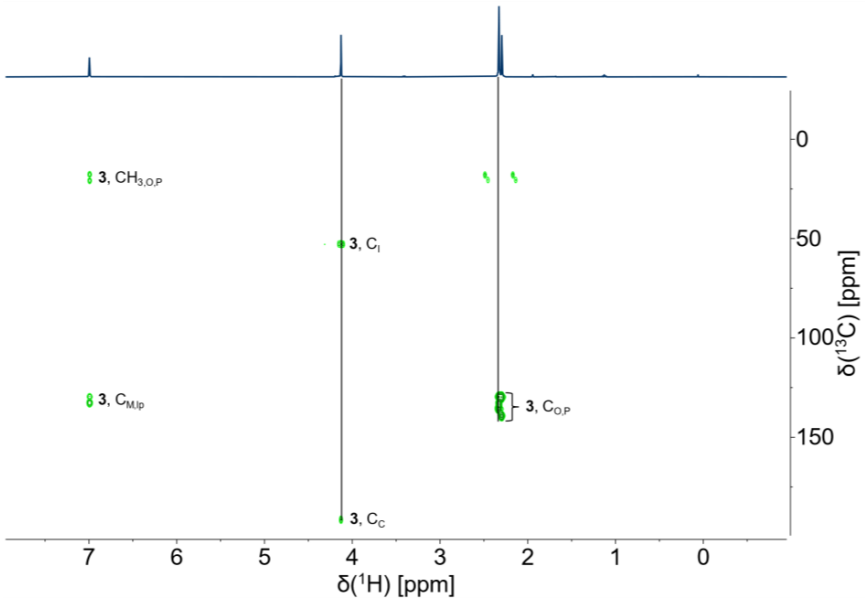

Figure S19: ^{1}H,^{13}C HMBC NMR spectrum (400 MHz, CD_2Cl_2, 21 °C) of [Au(CF$_3$)$_3$(SIMes)] (**3**).

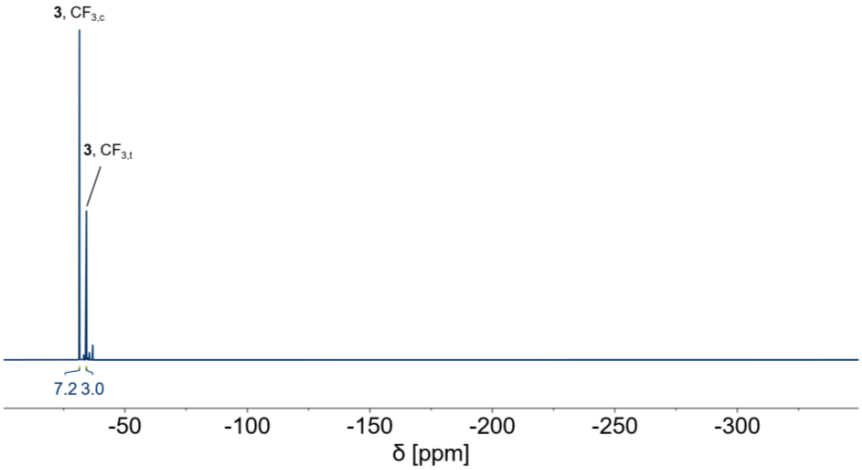

Figure S20: ^{19}F NMR spectrum (377 MHz, CD_2Cl_2, 21 °C) of [$Au(CF_3)_3$(SIMes)] (**3**). The integrals were referenced to the signal of the CF_3 group *trans* to the SIMes ligand of compound **3** with an integral of 3.0.

Vibrational Spectroscopy

IR and Raman Spectra of $[Au(CF_3)_3(SIMes)]$ (3)

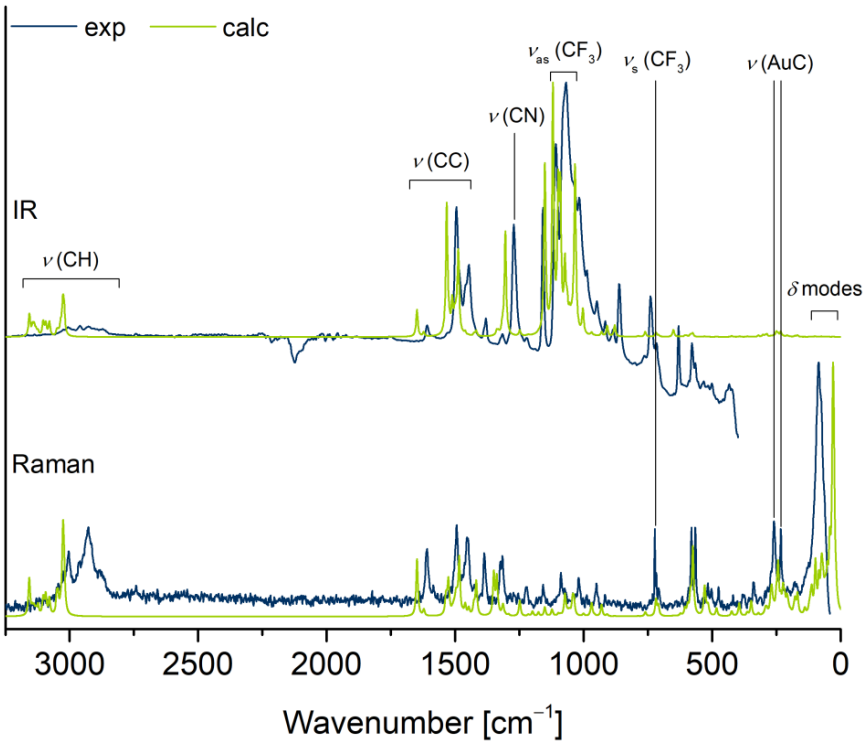

Figure S21: IR (top) and Raman (bottom) spectra of $[Au(CF_3)_3(SIMes)]$ (**3**) taken at room temperature (blue lines) compared to the respective calculated spectra at the RI-B3LYP-D3/def2-TZVPP level of theory (green lines) including assignments of the most pronounced bands. The shift of the baseline in the experimental IR spectrum is due to pressure changes inside the glovebox during the measurement.

Quantum-Chemical Calculations

Coordinates of *trans*-[Au(CF$_3$)F$_2$(SIMes)] (1) on RI-B3LYP-D3/def2-TZVPP Level

xyz-Coordinates [Å] of the optimized minimum structure of *trans*-[Au(CF$_3$)F$_2$(SIMes)].

56

N	0.50168306269757	-1.99122569872415	-2.12674790065973	7
N	-0.53866790244528	1.99417766254798	-2.11469340933680	7
C	-0.00050843175022	0.00186820955035	-0.69750370189893	6
C	-0.41745073832938	1.41036752815574	-4.84178197020148	6
C	0.30920768434604	-1.40956954244729	-4.85017826708545	6
C	1.15076290440180	-4.44868491982770	-1.19161674601552	6
C	3.69680902373326	-5.02510470133836	-0.77870610839879	6
C	4.27987890025913	-7.42781924324619	0.12162929786223	6
C	2.41037217375334	-9.21318692508954	0.62293583024689	6
C	-0.10482084694442	-8.55486521803787	0.20622738506014	6
C	-0.78527893213047	-6.17728673257122	-0.69280731603043	6
C	5.72547658674054	-3.07525258524604	-1.19009384574451	6
C	3.08764063371387	-11.76942324496073	1.67457684340703	6
C	-3.51621593647022	-5.45222279185808	-1.01419838874388	6
C	-1.16068880760291	4.45295638494358	-1.16476069667449	6
C	-3.69317731372968	5.02926584373529	-0.67540512080850	6
C	-4.24924024968166	7.43322503302532	0.23849699837034	6
C	-2.36608185227799	9.22007468499799	0.67940700994380	6
C	0.13550329546140	8.56206618015286	0.18682557520825	6
C	0.78899735012571	6.18309053372043	-0.72841151140417	6
C	-5.73304339504958	3.07839485500967	-1.02095037577768	6
C	-3.01263215633849	11.77748010556034	1.74737652670983	6
C	3.50894168664886	5.45807515581372	-1.13275172272562	6
H	0.98896647981425	2.60435420968756	-5.75613772800017	1
H	-2.24332304001492	1.77169399662858	-5.72201321239048	1
H	-1.12089413125999	-2.60434598167944	-5.72605813196994	1
H	2.11115699132340	-1.77168830331241	-5.77801725045623	1
H	6.24164417562138	-7.90654629278944	0.45957294659886	1
H	-1.57915955581735	-9.91669800343994	0.61059318974417	1
H	5.63853375898020	-2.25832345242663	-3.08302502977390	1
H	7.59384756922415	-3.90135180420294	-0.94649335254790	1
H	5.51762602551024	-1.53057131868024	0.16246119657307	1
H	3.10976011847519	-11.71950917546080	3.73943773670095	1
H	4.95698100884999	-12.37100843054102	1.05153208233453	1
H	1.72339125010672	-13.20500141350158	1.10668902638181	1
H	-4.03947812349837	-4.00058604824113	0.35626788290813	1
H	-4.74271223277539	-7.07946437976664	-0.73082199491879	1
H	-3.89704889962521	-4.69395466263632	-2.89511403340183	1
H	-6.19983924845516	7.91160490899969	0.63613996653767	1
H	1.62092370435065	9.92535441769685	0.54297223967289	1
H	-5.69351387952116	2.24614414944257	-2.90871911930926	1
H	-7.59403427712362	3.90834387154591	-0.73732370480068	1
H	-5.49378636564970	1.54417258388353	0.33839779749260	1
H	-4.89264842551322	12.38569356597990	1.16399247617064	1
H	-1.65593147579187	13.20925990046959	1.15260757736794	1
H	-2.99257183574096	11.72525263030292	3.81219959633269	1
H	4.06892058409079	3.99595282121731	0.21169335112899	1
H	4.74476275446736	7.08226005732116	-0.87326102767513	1
H	3.83517907811662	4.71344351228417	-3.02939227712221	1
Au	0.03955147933681	-0.00025138550749	3.28530808048718	79
F	-3.54478598360196	-0.89488101465213	3.33514697724602	9
F	3.62067770578321	0.89673633616878	3.20885389990659	9
C	-0.00251992748870	-0.02170267647272	7.22137731499415	6
F	-0.75109191128513	-2.29494275877852	8.12617171691594	9
F	-1.64535973597762	1.71448957593359	8.13705313461235	9
F	2.25930962595822	0.47966999066129	8.27104028695687	9

E_{tot} = −1598.31784268855 H

Coordinates of [Au(CF$_3$)$_3$(SIMes)] (3) on RI-B3LYP-D3/def2-TZVPP Level

xyz-Coordinates [Å] of the optimized minimum structure of [Au(CF$_3$)$_3$(SIMes)].

62

N	0.42943905835783	-1.96054738023150	-2.30572899438743	7
N	-0.67536248845823	2.01380214861782	-2.24376125395314	7
C	-0.05821176523399	0.02332027581897	-0.82579031109381	6
C	-0.33170287743976	1.47556922051452	-4.96181679450861	6
C	-0.15897511694741	-1.40463209339656	-4.97802368155276	6
C	1.25086243073304	-4.42152361215396	-1.51944955036556	6
C	3.72282257370981	-5.17620639348333	-2.12342328281884	6
C	4.54057279738046	-7.52971137994382	-1.29300593667418	6
C	2.98534662749340	-9.14206498041803	0.08917828997449	6
C	0.52275439415313	-8.37165771081662	0.57306220964121	6
C	-0.40014005548471	-6.03639521742287	-0.22567580215325	6
C	5.49376605056994	-3.55888680104508	-3.65870808921555	6
C	3.96705164132246	-11.62478177115899	1.07010876320245	6
C	-3.11230616441070	-5.37561651306191	0.32344510166653	6
C	-1.33896728907114	4.48943310712141	-1.36693774916851	6
C	-3.82339710688553	5.34278777186383	-1.73769454285146	6
C	-4.46714543513667	7.72023986489721	-0.82452229275919	6
C	-2.72925998066087	9.25913069912863	0.41512091112369	6
C	-0.26424303329753	8.38935827953514	0.66820901992457	6
C	0.48719352036343	6.02684986602159	-0.22242413290507	6
C	-5.79004941288518	3.81101477718016	-3.11418093591607	6
C	-3.51602731285537	11.77226492074174	1.49016791467428	6
C	3.20943932982291	5.25276383981805	0.06869338447574	6
H	1.40620597762873	2.38295120479088	-5.61132644079736	1
H	-1.90440992470172	2.20416392491663	-6.06084365245889	1
H	-1.94984672789450	-2.30654127477299	-5.47164061222460	1
H	1.30552824340536	-2.12650914041006	-6.22110157219446	1
H	6.45934723339690	-8.10760831663938	-1.71536505377037	1
H	-0.73637961854007	-9.61794278707549	1.60016402168918	1
H	5.42116852189644	-4.09029917446694	-5.65498414054972	1
H	7.43392512307407	-3.81834204771115	-3.02439914838259	1
H	5.05841659961981	-1.55883573399346	-3.50651078388328	1
H	4.90947566078509	-11.35706915151400	2.88841104544557	1
H	5.34163833931879	-12.45662190694973	-0.22034065316263	1
H	2.44340620172536	-12.98114049405513	1.35589616292112	1
H	-3.36227811750808	-4.81085612812854	2.29053713183204	1
H	-4.31519150735771	-7.01880566742463	0.01111215475341	1
H	-3.80937506399038	-3.83529896048284	-0.83946475093177	1
H	-6.39203239572923	8.37615026170602	-1.06647371760398	1
H	1.13240544317937	9.57931511876093	1.57788541659890	1
H	-5.39694182428749	1.79827539882528	-3.05919069480241	1
H	-5.91397900338623	4.39857422785116	-5.09217143987651	1
H	-7.64453226188016	4.09957171121638	-2.27000512033550	1
H	-4.97861411331775	12.66049246063270	0.34204514311908	1
H	-1.92184760769221	13.06981960910173	1.62531547653890	1
H	-4.28436809270072	11.53229826625171	3.39230311911736	1
H	3.62038184401762	4.67771665441428	2.00342309668617	1
H	4.44547847795731	6.84286394160396	-0.36588749472411	1
H	3.73107989541632	3.68232616977397	-1.14685842720923	1
Au	0.02778432612641	-0.07750485160451	3.17158222885068	79
C	-0.04158315522507	-0.40729901054580	7.15088102359845	6
F	-0.98440090196304	-2.70659650220305	7.80460309690130	9
F	-1.53780440065124	1.34406388721716	8.26700951304712	9
F	2.22076506253274	-0.22408014304978	8.31343920492982	9
C	-3.96605239688926	0.51303213683859	3.33754166457242	6
F	-5.18897031983288	0.14288354148524	1.07602773824589	9
F	-4.54093210892378	2.91450291347810	4.01851409313150	9
F	-5.18622165196947	-1.02266393351948	4.98177694880986	9
C	4.02855936470347	-0.57793634414143	3.20940600897762	6
F	5.13578788750245	-0.46980707384836	0.86520837628902	9
F	5.25741423757663	1.21802629525339	4.56938983949151	9
F	4.73353236943844	-2.83977999970802	4.17724895300116	9

E_{tot} = −2073.93400595089 H

Coordinates of SIMes on RI-B3LYP-D3/def2-TZVPP Level

xyz-Coordinates [Å] of the optimized minimum structure of SIMes.

49

N	-0.2150429	-1.0038805	-0.6330203	7
N	0.5837386	0.9751496	-0.4064118	7
C	-0.0719539	0.0014631	0.2444842	6
C	0.8385285	0.6949789	-1.8417560	6
C	0.4477449	-0.7800335	-1.9421970	6
C	-0.7856218	-2.2721692	-0.3190063	6
C	-0.0385732	-3.2073218	0.4077555	6
C	-0.6104343	-4.4478597	0.6791185	6
C	-1.8931269	-4.7766786	0.2452920	6
C	-2.6142920	-3.8209128	-0.4653608	6
C	-2.0821033	-2.5658033	-0.7552681	6
C	1.3393066	-2.8644599	0.9073603	6
C	-2.4747961	-6.1390938	0.5211980	6
C	-2.8952840	-1.5374977	-1.4960017	6
C	0.8557706	2.2651506	0.1366482	6
C	-0.1739412	3.2100941	0.2268971	6
C	0.1247351	4.4711309	0.7365881	6
C	1.4113354	4.8110903	1.1501521	6
C	2.4103720	3.8458568	1.0579284	6
C	2.1542800	2.5700013	0.5582962	6
C	-1.5761466	2.8569185	-0.1912927	6
C	1.7144611	6.1949357	1.6636683	6
C	3.2437870	1.5321524	0.5019681	6
H	1.8801328	0.8811831	-2.1003087	1
H	0.2139050	1.3397770	-2.4654913	1
H	-0.2314963	-0.9884222	-2.7678091	1
H	1.3138330	-1.4396500	-2.0408552	1
H	-0.0407484	-5.1743174	1.2474763	1
H	-3.6219153	-4.0513538	-0.7922432	1
H	1.9933223	-2.5468696	0.0925220	1
H	1.8014010	-3.7197891	1.3986163	1
H	1.2941511	-2.0350330	1.6148786	1
H	-2.1823686	-6.8520485	-0.2545999	1
H	-3.5645924	-6.1106487	0.5442619	1
H	-2.1254267	-6.5358262	1.4752073	1
H	-2.8628010	-0.5744440	-0.9856509	1
H	-3.9350776	-1.8506197	-1.5815034	1
H	-2.5161842	-1.3763030	-2.5083906	1
H	-0.6687782	5.2055365	0.8160643	1
H	3.4125879	4.0857177	1.3944114	1
H	-1.6085195	2.4982410	-1.2222596	1
H	-2.2369256	3.7192117	-0.1120906	1
H	-1.9704050	2.0535938	0.4330156	1
H	1.9188487	6.8810521	0.8371814	1
H	2.5894660	6.1968919	2.3141800	1
H	0.8735542	6.6045372	2.2248156	1
H	2.9099321	0.5937321	0.9459461	1
H	4.1326910	1.8708916	1.0326363	1
H	3.5386695	1.3117480	-0.5270511	1

E_{tot} = −925.15875713139 H

Coordinates of [Au(CF$_3$)F$_2$] on RI-B3LYP-D3/def2-TZVPP Level

xyz-Coordinates [Å] of the optimized minimum structure of [Au(CF$_3$)F$_2$].

7

Au	2.20755188580994	-1.19969376545462	0.00000000000000	79
F	0.41105050860525	-4.36929996693524	0.00000000000000	9
F	4.31337790822559	1.76345663419263	0.00000000000000	9
C	-1.21257449415516	0.67574610062594	0.00000000000000	6
F	-0.80137650969151	3.12502431304880	0.00000000000000	9
F	-2.45901464939702	0.00238334226124	-2.04713663284360	9
F	-2.45901464939702	0.00238334226124	2.04713663284360	9

E_{tot} = −673.04056490330 H

Coordinates of [Au(CF$_3$)$_3$] on RI-B3LYP-D3/def2-TZVPP Level

xyz-Coordinates [Å] of the optimized minimum structure of [Au(CF$_3$)$_3$].

13

Au	0.04719566441461	-1.12233322931971	0.03028927353388	79
C	-3.95033446217129	-1.37469420800382	-0.00872322407669	6
C	-0.06832374671078	2.81381072796679	-0.11518311269927	6
C	4.03074957445271	-1.46396478353996	0.10920220984482	6
F	-4.47788327211836	-3.84613964812156	0.55461107074308	9
F	-5.19385000458658	0.04463627360978	1.70600355067283	9
F	-5.02534037356166	-0.90704606747568	-2.27606697154130	9
F	-1.56053017339052	3.51262337321273	-1.99264397200624	9
F	-0.96976458490633	3.64844169890046	2.05916304044270	9
F	2.22491171582116	3.72355723121026	-0.48326464487953	9
F	5.23608929968403	-0.73325664413322	-2.01955388842153	9
F	5.20229233274008	-0.29621263509404	2.05304199557828	9
F	4.50478803033292	-3.99942208921198	0.38312467280897	9

E_{tot} = −1148.65383085260 H

Literature

[1] a) D. J. Adams, J. H. Clark, L. B. Hansen, V. C. Sanders, S. J. Tavener, *J. Fluorine Chem.* **1998**, *92*, 123; b) E. Schnell, E. G. Rochow, *J. Inorg. Nucl. Chem.* **1958**, *6*, 303; c) I. Ruppert, K. Schlich, W. Volbach, *Tetrahedron Lett.* **1984**, *25*, 2195; d) S. Martinez-Salvador, L. R. Falvello, A. Martin, B. Menjon, *Chem. Eur. J.* **2013**, *19*, 14540; e) M. A. Ellwanger, C. von Randow, S. Steinhauer, Y. Zhou, A. Wiesner, H. Beckers, T. Braun, S. Riedel, *Chem. Commun.* **2018**, *54*, 9301.

8.2 Supporting Information of ‘Reactivity of [AuF_3(SIMes)]: Pathway to Unprecedented Structural Motifs’

Chemistry–A European Journal

Supporting Information

Reactivity of [AuF_3(SIMes)]: Pathway to Unprecedented Structural Motifs

Marlon Winter, Mathias A. Ellwanger, Niklas Limberg, Alberto Pérez-Bitrián, Patrick Voßnacker, Simon Steinhauer, and Sebastian Riedel*

Table of Contents

X-Ray Crystallography

Crystallographic Data

Table S1: Crystal data and refinement details for the analysis of the molecular structures in the solid state of *trans*-[Au(CCH)F_2(SIMes)] (**1**), *trans*-[Au(CN)F_2(SIMes)] (**3**) and [Au(CN)$_3$(SIMes)]·CH_2Cl_2 (**4**·CH_2Cl_2).

	trans-[Au(CCH)F_2(SIMes)] (**1**)[a]	*trans*-[Au(CN)F_2(SIMes)] (**3**)[b]	[Au(CN)$_3$(SIMes)]·CH_2Cl_2 (**4**·CH_2Cl_2)[c]
Empirical formula	$C_{22.89}H_{26.95}AuCl_{0.06}F_2N_2$	$C_{22}H_{26}AuF_2N_3$	$C_{25}H_{28}AuCl_2N_5$
Formula weight	567.00	567.42	666.39
Temperature/K	100.00	125.00	100.00
Crystal system	orthorhombic	orthorhombic	monoclinic
Space group	*Pnma*	*Pnma*	$P2_1/n$
a/Å	14.8728(10)	15.0867(6)	10.5865(16)
b/Å	19.8494(12)	19.8520(7)	19.855(3)
c/Å	7.3625(5)	7.1526(2)	12.2404(18)
α/°	90	90	90
β/°	90	90	91.834(5)
γ/°	90	90	90
Volume/Å^3	2173.5(2)	2142.21(13)	2571.6(6)
Z	4	4	4
ρ_{calc}g/cm^3	1.733	1.759	1.721
μ/mm^{-1}	6.802	6.896	5.951
F(000)	1105.0	1104.0	1304.0
Crystal size/mm^3	0.601 × 0.247 × 0.22	0.18 × 0.136 × 0.089	0.334 × 0.142 × 0.104
Radiation	MoK$_\alpha$ (λ = 0.71073)	MoK$_\alpha$ (λ = 0.71073)	MoK$_\alpha$ (λ = 0.71073)
2Θ range for data collection/°	5.478 to 56.566	5.4 to 52.752	5.008 to 56.652
Index ranges	-19 ≤ h ≤ 19, -26 ≤ k ≤ 26, -9 ≤ l ≤ 9	-18 ≤ h ≤ 18, -24 ≤ k ≤ 24, -8 ≤ l ≤ 8	-14 ≤ h ≤ 14, -26 ≤ k ≤ 25, -16 ≤ l ≤ 16
Reflections collected	40805	34243	39398
Independent reflections	2770 [R_{int} = 0.0292, R_{sigma} = 0.0116]	2250 [R_{int} = 0.0375, R_{sigma} = 0.0133]	6348 [R_{int} = 0.0772, R_{sigma} = 0.0593]
Data/restraints/ parameters	2770/1/142	2250/0/139	6348/7/304
Goodness-of-fit on F^2	1.151	1.365	1.061
Final R indexes [I>=2σ (I)]	R_1 = 0.0152, wR_2 = 0.0364	R_1 = 0.0379, wR_2 = 0.0871	R_1 = 0.0413, wR_2 = 0.0812
Final R indexes [all data]	R_1 = 0.0162, wR_2 = 0.0371	R_1 = 0.0425, wR_2 = 0.0900	R_1 = 0.0669, wR_2 = 0.0884
Largest diff. peak/hole / e Å^{-3}	1.42/-0.99	2.48/-2.06	4.03/-1.87
CCDC deposition number	2262531	2262543	2262544

[a] Compound **1** contains about 6 % of *trans*-[AuClF$_2$(SIMes)], which crystallizes in the same space group with similar lattice parameters.[1] [b] Q_max (2.94 e/A^3) without void as an artefact from numerical absorption correction (Z_max = 79) with bias of face indexing due to superposition of three

additional composites (rotation approx. –7°, 8°, –11°). Treatment as pseudo-merohedral twins did not improve refinement and prohibited numerical absorption correction. Lower symmetry space groups clearly indicate missed symmetry; *Pna*2(1) yields NPD ADP; no indication of superstructure reflexes. Semi-empirical absorption correction results in large Q_max (4 e/Å^3) in close proximity to Au. [c] Maximum residual density located in close proximity to heaviest atom (Au01): 4.09 e/Å^3 with Z = 79. No twinning is observed, no superstructure reflexes are present, space group type assignment is unambiguous. Different absorption correction methods (psi-scans, SADABS, numerical) were attempted resulting in different spacial distributions of max. residual density around Au01 with numerical absorption correction yielding best refinement values. DELU restraint (C009, N007) was employed to prevent artificial elongation of C009 ADP towards residual density. OMIT was employed for (2 0 0) due to superposition with parasitic Debye diffraction in the very low theta range.

Table S2: Crystal data and refinement details for the analysis of the molecular structures in the solid state of *trans*-[$AuF_2(N_3)(SIMes)]\cdot 0.5\ CH_2Cl_2$ (**5**·0.5 CH_2Cl_2) and [$Au(N_3)_3$(SIMes)] (**6**).

	trans-[$AuF_2(N_3)$(SIMes)]·0.5 CH_2Cl_2 (**5**·0.5 CH_2Cl_2)	[$Au(N_3)_3$(SIMes)] (**6**)
Empirical formula	$C_{21.5}H_{27}AuClF_2N_5$	$C_{21}H_{26}AuN_{11}$
Formula weight	625.90	629.49
Temperature/K	100.00	100.00
Crystal system	triclinic	triclinic
Space group	$P\bar{1}$	$P\bar{1}$
a/Å	7.7781(4)	8.4626(3)
b/Å	8.2686(5)	16.2949(9)
c/Å	18.2201(10)	17.1279(9)
α/°	83.102(2)	91.741(2)
β/°	89.249(2)	93.416(2)
γ/°	82.312(2)	95.156(2)
Volume/Å^3	1152.86(11)	2346.6(2)
Z	2	4
ρ_{calc}g/cm^3	1.803	1.782
μ/mm^{-1}	6.530	6.302
F(000)	610.0	1232.0
Crystal size/mm^3	0.429 × 0.199 × 0.089	0.508 × 0.143 × 0.109
Radiation	MoK_α (λ = 0.71073)	MoK_α (λ = 0.71073)
2Θ range for data collection/°	5.006 to 56.67	4.768 to 56.648
Index ranges	-10 ≤ h ≤ 10, -11 ≤ k ≤ 11, -24 ≤ l ≤ 24	-10 ≤ h ≤ 11, -21 ≤ k ≤ 21, -22 ≤ l ≤ 22
Reflections collected	82498	61872
Independent reflections	5738 [R_{int} = 0.0469, R_{sigma} = 0.0178]	11595 [R_{int} = 0.0720, R_{sigma} = 0.0446]
Data/restraints/ parameters	5738/25/295	11595/0/607
Goodness-of-fit on F^2	1.153	1.093
Final R indexes [I>=2σ (I)]	R_1 = 0.0188, wR_2 = 0.0447	R_1 = 0.0337, wR_2 = 0.0558
Final R indexes [all data]	R_1 = 0.0196, wR_2 = 0.0450	R_1 = 0.0481, wR_2 = 0.0600
Largest diff. peak/hole / e Å^{-3}	0.97/-1.64	1.81/-1.73
CCDC deposition number	2262532	2262533

Table S3: Crystal data and refinement details for the analysis of the molecular structures in the solid state of *trans*-$[AuF_2(OC(CF_3)_3)(SIMes)]\cdot 2\ CH_2Cl_2$ (**7**·2 CH_2Cl_2) and *trans*-$[AuF_2(OC(CF_3)_2F)(SIMes)]\cdot CH_2Cl_2$ (**10**·CH_2Cl_2).

	trans-$[AuF_2(OC(CF_3)_3)(SIMes)]\cdot 2\ CH_2Cl_2$ (**7**·2 CH_2Cl_2)[a]	*trans*-$[AuF_2(OC(CF_3)_2F)(SIMes)]\cdot CH_2Cl_2$ (**10**·CH_2Cl_2)
Empirical formula	$C_{27}H_{30}AuCl_4F_{11}N_2O$	$C_{25}H_{28}AuCl_2F_9N_2O$
Formula weight	946.29	811.36
Temperature/K	100.18	100.00
Crystal system	monoclinic	triclinic
Space group	$P2_1/n$	$P\bar{1}$
a/Å	13.1522(9)	9.7053(7)
b/Å	14.5331(10)	10.0848(6)
c/Å	17.8095(12)	16.8733(12)
α/°	90	97.846(2)
β/°	90.985(2)	91.615(2)
γ/°	90	116.951(2)
Volume/Å^3	3403.6(4)	1450.74(17)
Z	4	2
ρ_{calc}g/cm^3	1.847	1.857
μ/mm^{-1}	4.722	5.335
F(000)	1840.0	788.0
Crystal size/mm^3	0.212 × 0.18 × 0.073	0.319 × 0.219 × 0.128
Radiation	MoK_α (λ = 0.71073)	MoK_α (λ = 0.71073)
2Θ range for data collection/°	4.574 to 50.832	4.596 to 56.638
Index ranges	-15 ≤ h ≤ 15, -17 ≤ k ≤ 17, -21 ≤ l ≤ 21	-12 ≤ h ≤ 12, -13 ≤ k ≤ 13, -22 ≤ l ≤ 22
Reflections collected	196635	98562
Independent reflections	6268 [R_{int} = 0.0709, R_{sigma} = 0.0162]	7222 [R_{int} = 0.0323, R_{sigma} = 0.0129]
Data/restraints/ parameters	6268/6/421	7222/208/458
Goodness-of-fit on F^2	1.042	1.084
Final R indexes	R_1 = 0.0394,	R_1 = 0.0158,
[I>=2σ (I)]	wR_2 = 0.0971	wR_2 = 0.0387
Final R indexes	R_1 = 0.0450,	R_1 = 0.0167,
[all data]	wR_2 = 0.1005	wR_2 = 0.0394
Largest diff. peak/hole / e Å^{-3}	7.43/-1.51	0.85/-0.92
CCDC deposition number	2262545	2262534

[a] Max. residual density (7.46 e/A^3) in close proximity to heaviest atom (Au, Z = 79).

Molecular Structure of *trans*-[Au(CCH)F_2(SIMes)] (1) in the Solid State

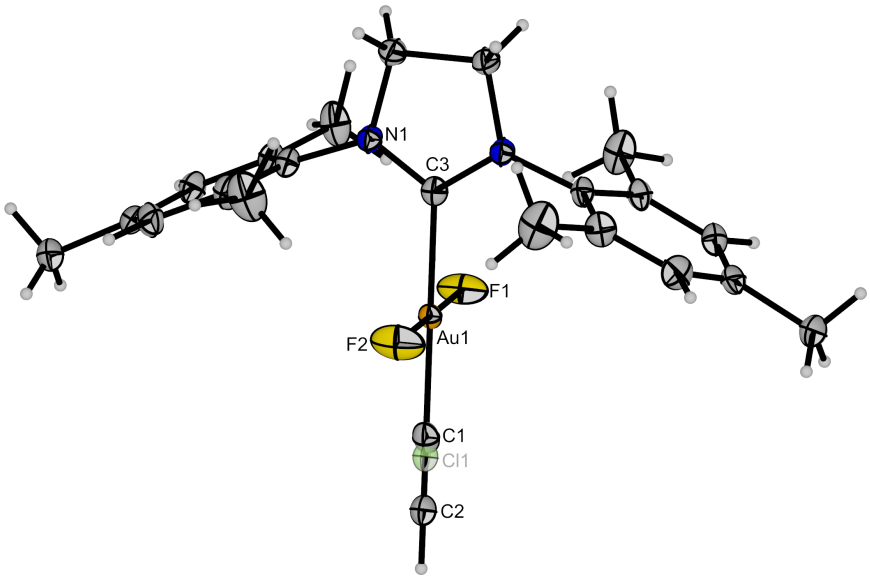

Figure S1: Molecular structure of *trans*-[Au(CCH)F_2(SIMes)] (**1**) in the solid state. About 6 % of *trans*-[AuClF_2(SIMes)] are co-crystallized and shown as transparent ellipsoid. Thermal ellipsoids are set at 50 % probability. Selected bond lengths [pm]: 198.5(7) (C1–Au1), 204.8(3) (C3–Au1), 193.4(2) (F1–Au1), 193.6(2) (F2–Au1), 119.2(8) (C1–C2). Note, that the refinement was done with a fixed bond length *r*(Cl1–Au1) = 230.2 pm taken from the solid state structure of *trans*-[AuClF_2(SIMes)].[1]

Molecular Structure of [Au$(CN)_3$(SIMes)]·CH_2Cl_2 (4·CH_2Cl_2) in the Solid State

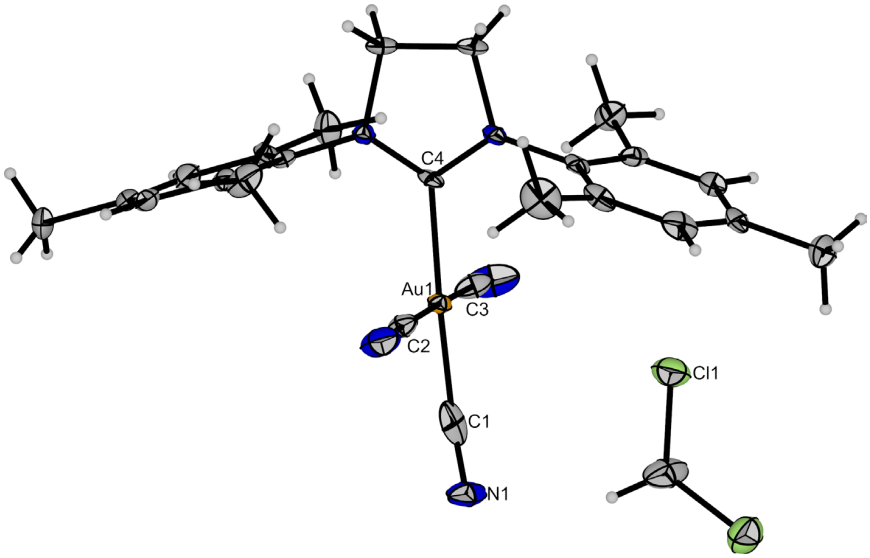

Figure S2: Molecular structure of [Au$(CN)_3$(SIMes)]·CH_2Cl_2 (**4**) in the solid state. Thermal ellipsoids are set at 50 % probability. Bond lengths [pm] to the central gold atom: 197.7(8) (C1–Au1), 198.8(6) (C2–Au1), 199.5(6) (C3–Au1), 206.1(5) (C4–Au1).

Molecular Structure of *trans*-[$AuF_2(N_3)$(SIMes)]·0.5 CH_2Cl_2 (5·0.5 CH_2Cl_2) in the Solid State

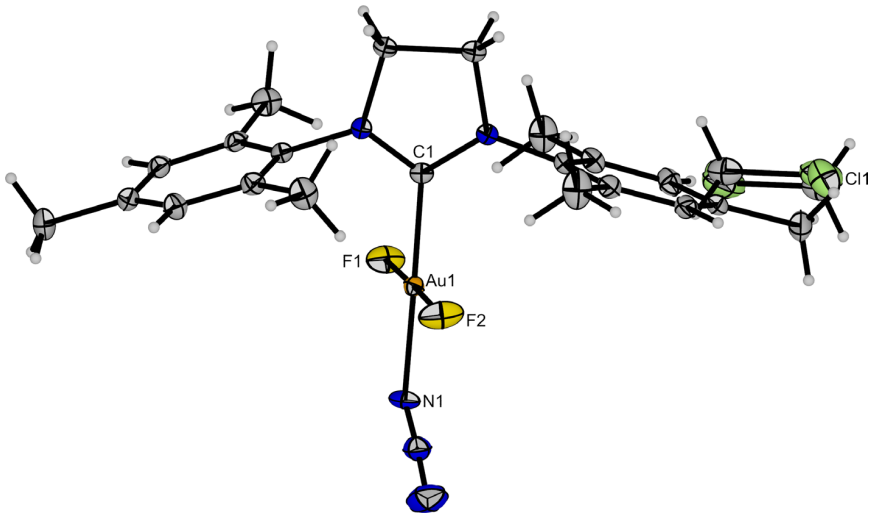

Figure S3: Molecular structure of *trans*-[$AuF_2(N_3)$(SIMes)]·0.5 CH_2Cl_2 (**5**) in the solid state. The co-crystallized solvent molecule shows a disorder. Thermal ellipsoids are set at 50 % probability. Bond lengths [pm] to the central gold atom: 200.9(2) (C1–Au1), 193.4(2) (F1–Au1), 192.4(2) (F2–Au1), 203.5(2) (N1–Au1).

Molecular Structure of [$Au(N_3)_3$(SIMes)] (6) in the Solid State

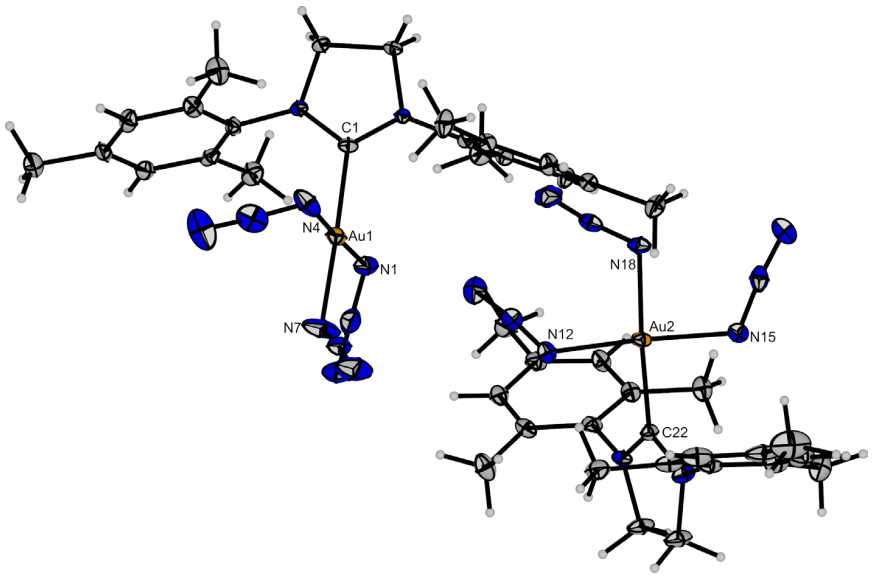

Figure S4: Molecular structure of [$Au(N_3)_3$(SIMes)] (**6**) in the solid state, showing the two crystallographically independent molecules in the unit cell. Thermal ellipsoids are set at 50 % probability. Bond lengths [pm] to the central gold atoms: 202.3(4) (C1–Au1), 203.2(4) (N1–Au1), 203.1(4) (N4–Au1), 203.7(4) (N7–Au1); 202.3(4) (C22–Au2), 203.1(4) (N12–Au2), 204.6(4) (N15–Au2), 204.3(3) (N18–Au2).

Molecular Structure of *trans*-[$AuF_2(OC(CF_3)_3)(SIMes)$]·2 CH_2Cl_2 (7·2 CH_2Cl_2) in the Solid State

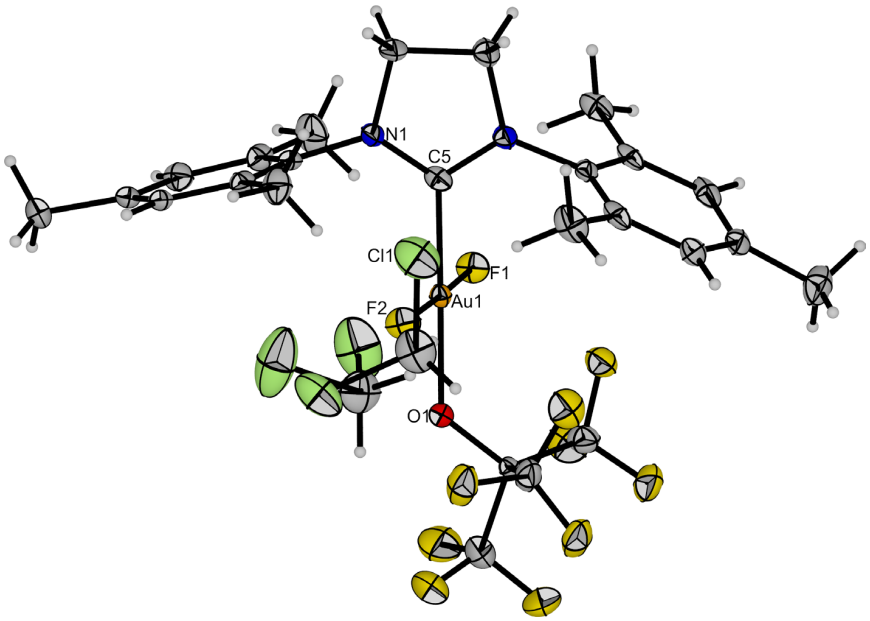

Figure S5: Molecular structure of *trans*-[$AuF_2(OC(CF_3)_3)(SIMes)$]·2 CH_2Cl_2 (**7**) in the solid state. Thermal ellipsoids are set at 50 % probability. Selected bond lengths to the central gold atom [pm]: 198.4(6) (C5–Au1), 192.5(3) (F1–Au1), 192.1(3) (F2–Au1), 202.7(4) (O1–Au1).

Molecular Structure of *trans*-[$AuF_2(OC(CF_3)_2F)(SIMes)$]·$CH_2Cl_2$ (10·CH_2Cl_2) in the Solid State

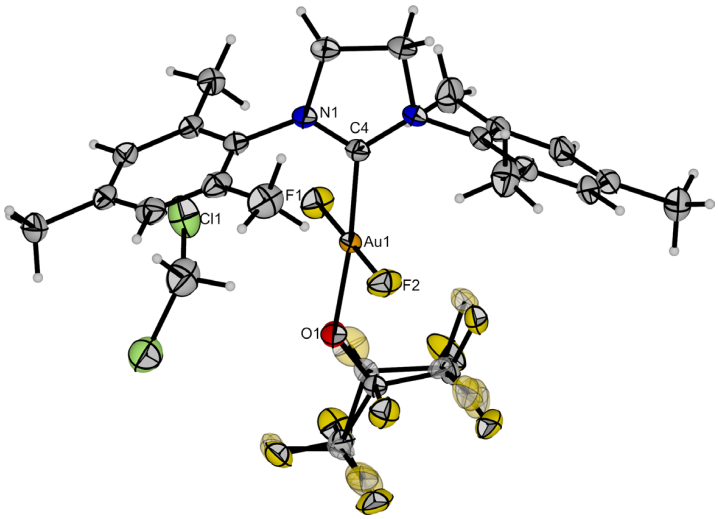

Figure S6: Molecular structure of *trans*-[$AuF_2(OC(CF_3)_2F)(SIMes)$]·$CH_2Cl_2$ (**10**) in the solid state. The second position of disordered atoms in the heptafluoroisopropyl group is shown as transparent ellipsoids. Thermal ellipsoids are set at 50 % probability. Bond lengths [pm] to the central gold atom: 197.8(2) (C4–Au1), 192.3(2) (F1–Au1), 192.2(2) (F2–Au1), 201.3(2) (O1–Au1).

NMR Spectroscopy

Summary of Products Identified by NMR Spectroscopy

Figure S7 gives an overview of the products, starting materials and side products that have been identified by NMR spectroscopy in the spectra shown in this paragraph. Their assignment is done using the numbers written in bold.[1,2] For compounds **7** - **10** and **19**, which incorporate different fluorine-containing groups, the different groups will be denoted by F for fluorine atoms and CF_3 for trifluoromethyl groups, with the former having a subscript C or Au for fluorine atoms connected to a carbon or gold atom, respectively. For compound **13**, which contains two chemically inequivalent fluorine atoms, they will be denoted with a subscript c and t for fluorine atoms *cis* or *trans* to the SIMes ligand, respectively. Figure S8 shows the structure of SIMes highlighting the chemically inequivalent hydrogen and carbon atoms, which can be assigned in the ^{1}H and ^{1}H,^{13}C-HMBC NMR spectra that are shown in this paragraph.

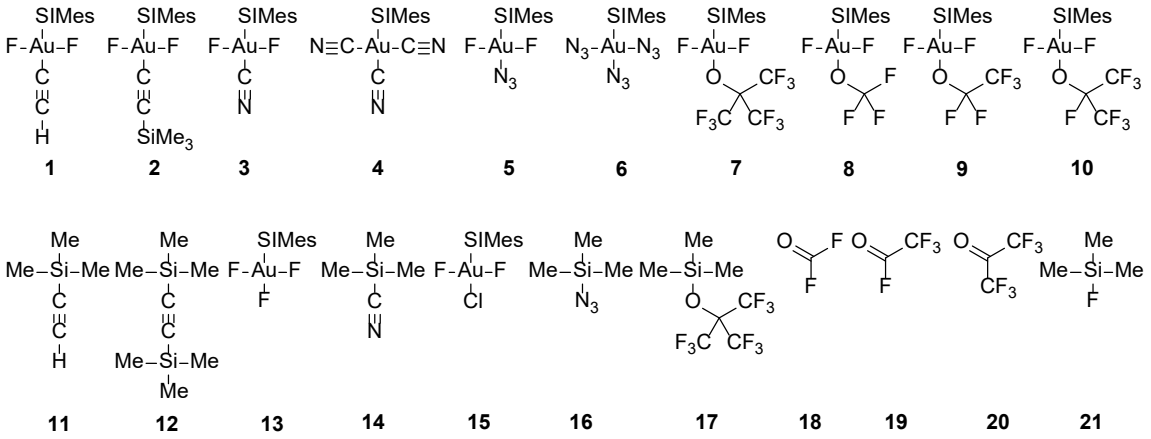

Figure S7: Overview of detected products (top, **1** - **10**), starting materials (middle, **11** - **14, 16** - **20**) and side products (bottom, **15**, **21**) in the ^{19}F NMR spectra of the reactions that are presented in this work. The numbers in bold are used for their assignment in the following ^{19}F NMR spectra.

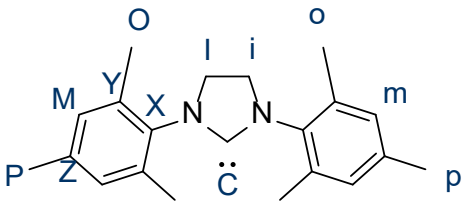

Figure S8: Structure of the NHC 1,3-bis(2,4,6-trimethylphenyl)-4,5-dihydroimidazol-2-ylidene (SIMes), which is present in products **1** – **10**, starting material **13** and side product **15** (cf. Figure S7). The positions of chemically inequivalent carbon atoms are denoted in blue capital letters, those of the chemically inequivalent hydrogen atoms by blue small letters. C = carbene, I = imidazolidine, M = *meta* C, O = *ortho* CH_3, P = *para* CH_3, X = *ipso* C, Y = *ortho* C, Z = *para* C, i = imidazolidine H, m = *meta* H, o = *ortho* H, p = *para* H.

NMR Spectra of the Reaction Between [AuF_3(SIMes)] and Me_3SiCCH

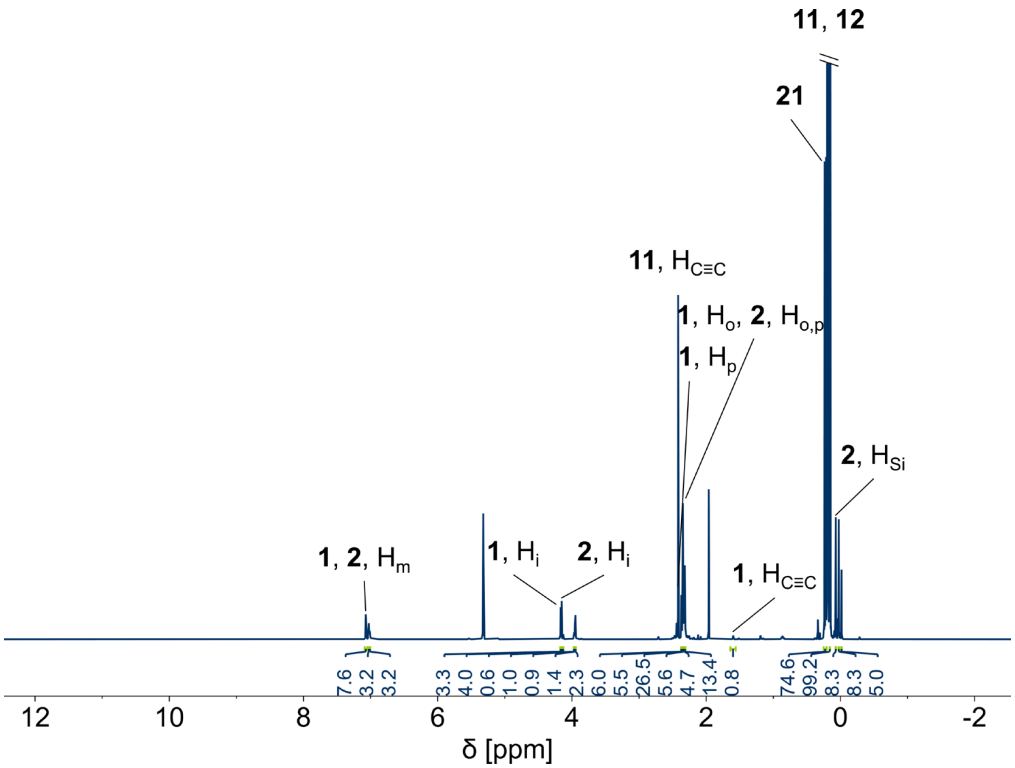

Figure S9: ^{1}H NMR spectrum (400 MHz, CD_2Cl_2, 21 °C) of the reaction between [AuF_3(SIMes)] and Me_3SiCCH in DCM including assignments to the compounds shown in Figure S7.

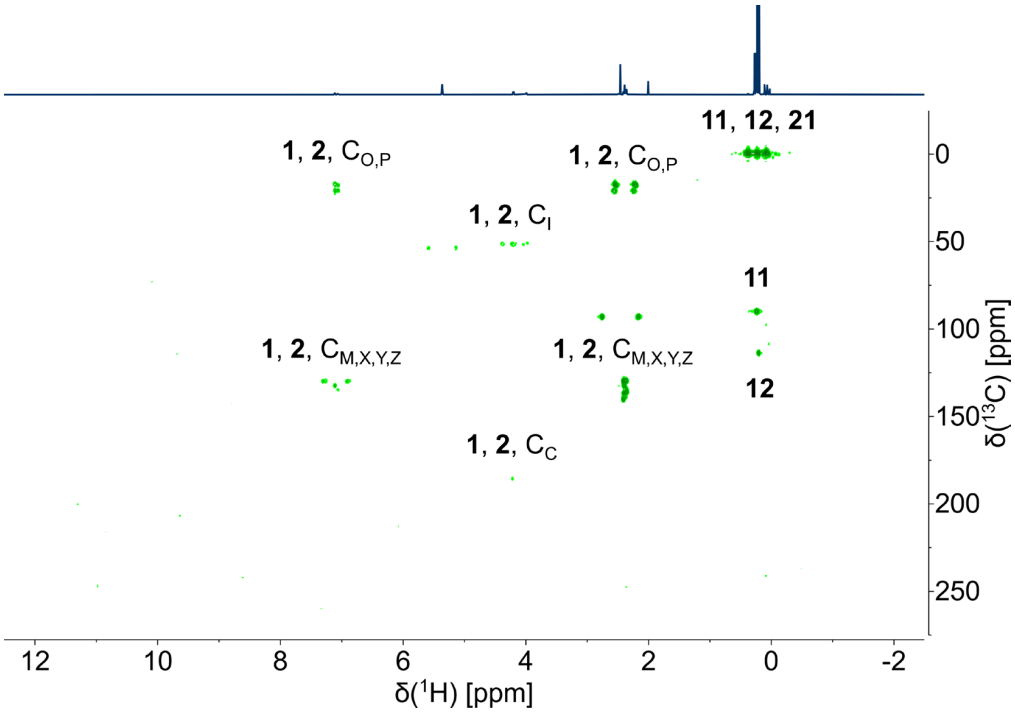

Figure S10: ^{1}H,^{13}C-HMBC NMR spectrum (400 MHz, CD_2Cl_2, 21 °C) of the reaction between [AuF_3(SIMes)] and Me_3SiCCH in DCM including assignments to the compounds shown in Figure S7.

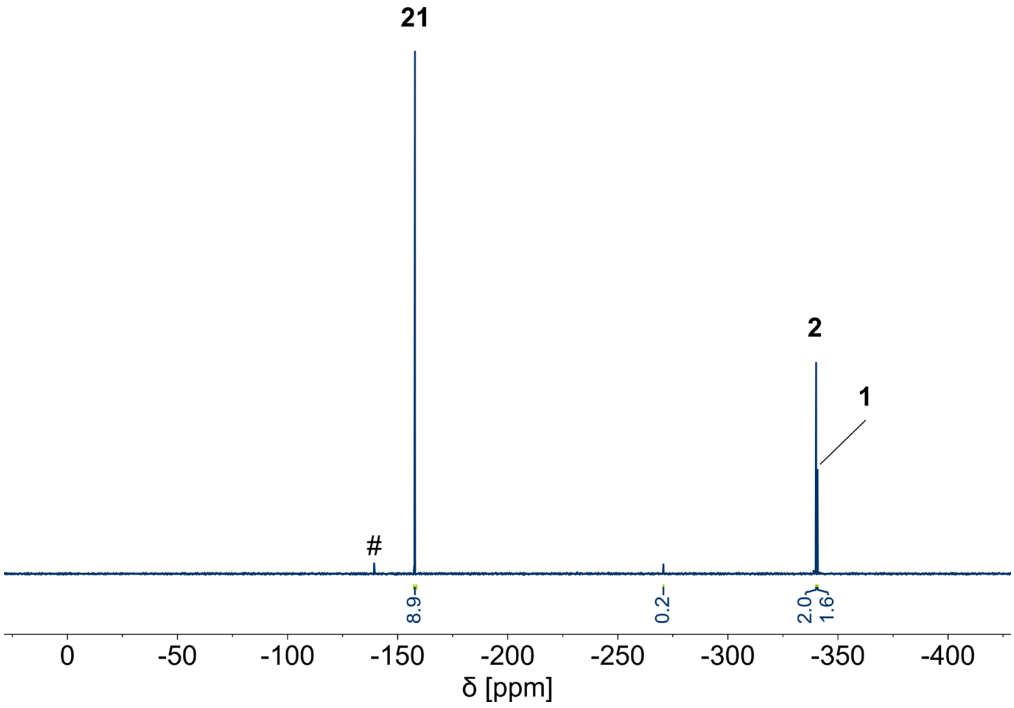

Figure S11: ^{19}F NMR spectrum (377 MHz, CD_2Cl_2, 20 °C) of the reaction between [AuF_3(SIMes)] and Me_3SiCCH in DCM including assignments to the compounds shown in Figure S7. The signal marked with a hash (#) belongs to traces of *ortho*-difluorobenzene from the synthesis of the starting material [AuF_3(SIMes)].

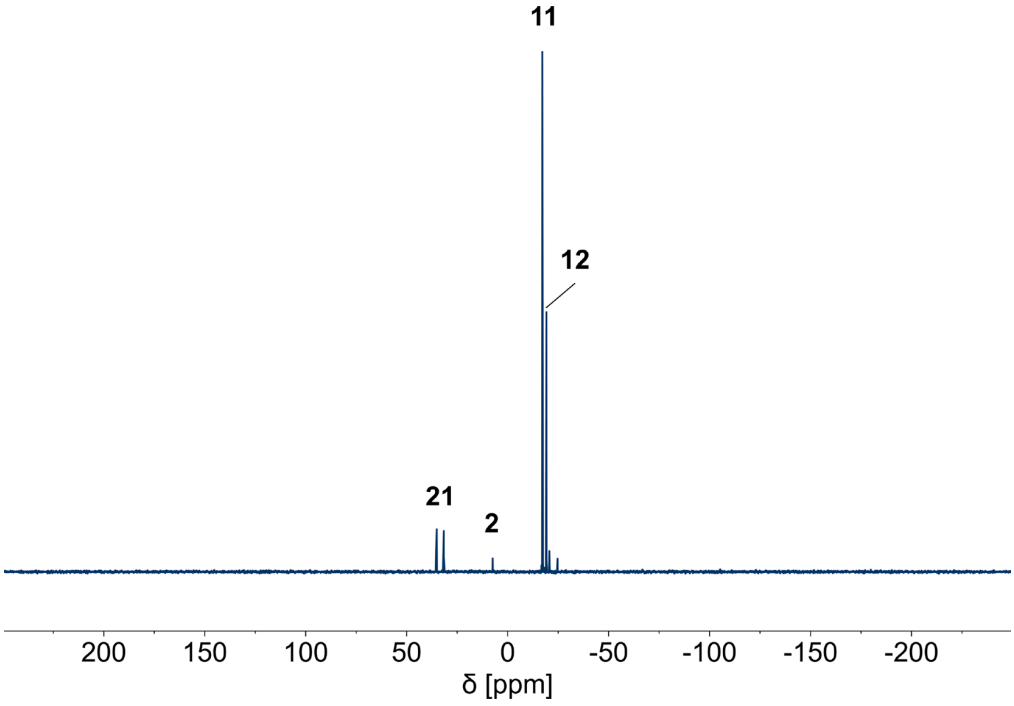

Figure S12: $^{29}Si\{^1H\}$-DEPT NMR spectrum (80 MHz, CD_2Cl_2, 21 °C) of the reaction between [AuF_3(SIMes)] and Me_3SiCCH in DCM including assignments to the compounds shown in Figure S7.

Table S4: Summary of the product ratios in the reaction between [AuF_3(SIMes)] and Me_3SiCCH in DCM (see Scheme 2) depending on the equivalents (eq.) of Me_3SiCCH and the presence of CsF.

eq. (Me_3SiCCH)[a,b]	eq. (CsF)[a]	*trans*-[Au(CCH)F_2(SIMes)] (**1**) : *trans*-[Au(CC$SiMe_3$)F_2(SIMes)] (**2**)[c]		
1	0	23	:	1
exc.	0	14	:	1
1	1	3	:	1
exc.	1	0.4	:	1

[a] Equivalents relative to [AuF_3(SIMes)]. [b] The amount of Me_3SiCCH can slightly deviate due to an inherent uncertainty in the manometer used for determining the pressure of Me_3SiCCH for its condensation. [c] The product ratio is determined by integration of the corresponding signals in the ^{19}F NMR spectra (see Figure S13), referenced to the integral of compound **2**.

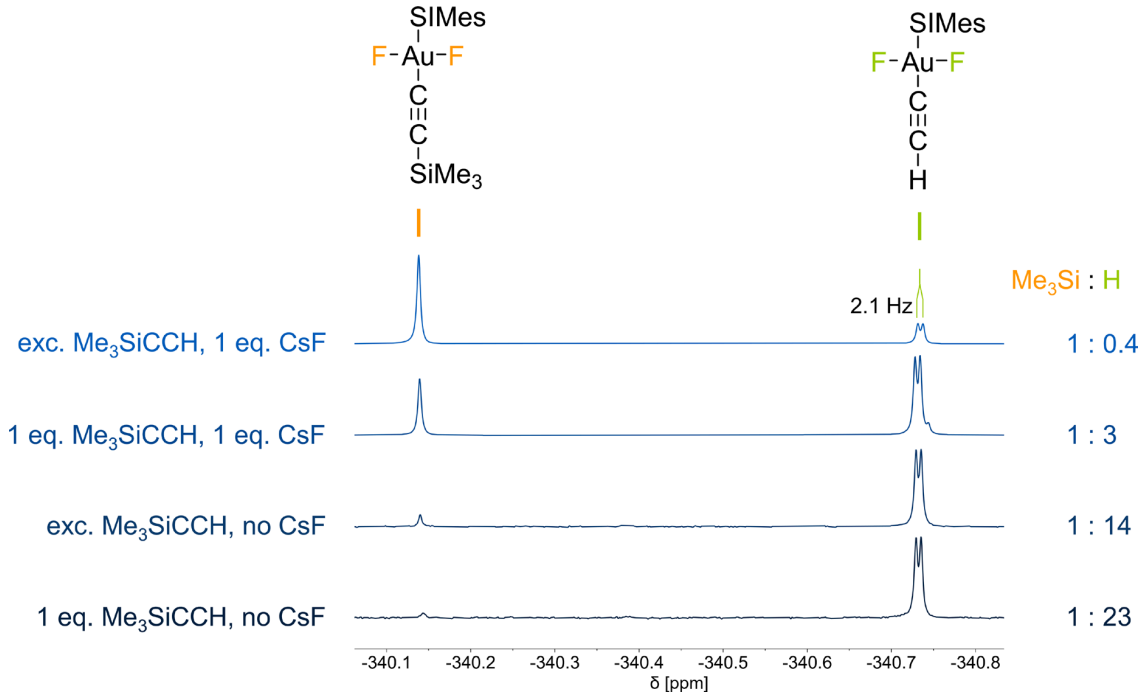

Figure S13: ^{19}F NMR spectra (377 MHz, CD_2Cl_2, 21 °C) of the reaction between [AuF_3(SIMes)] and Me_3SiCCH in DCM using different amounts of Me_3SiCCH and CsF to study the conditions favoring the formation of the desired product *trans*-[Au(CCH)F_2(SIMes)] (**1**, green). The product ratios given on the right are determined by integration of the respective signals, referenced to the integral of compound **2** (orange) (cf. Table S4).

NMR Spectra of the Reaction Between [AuF_3(SIMes)] and $Me_3SiCCSiMe_3$

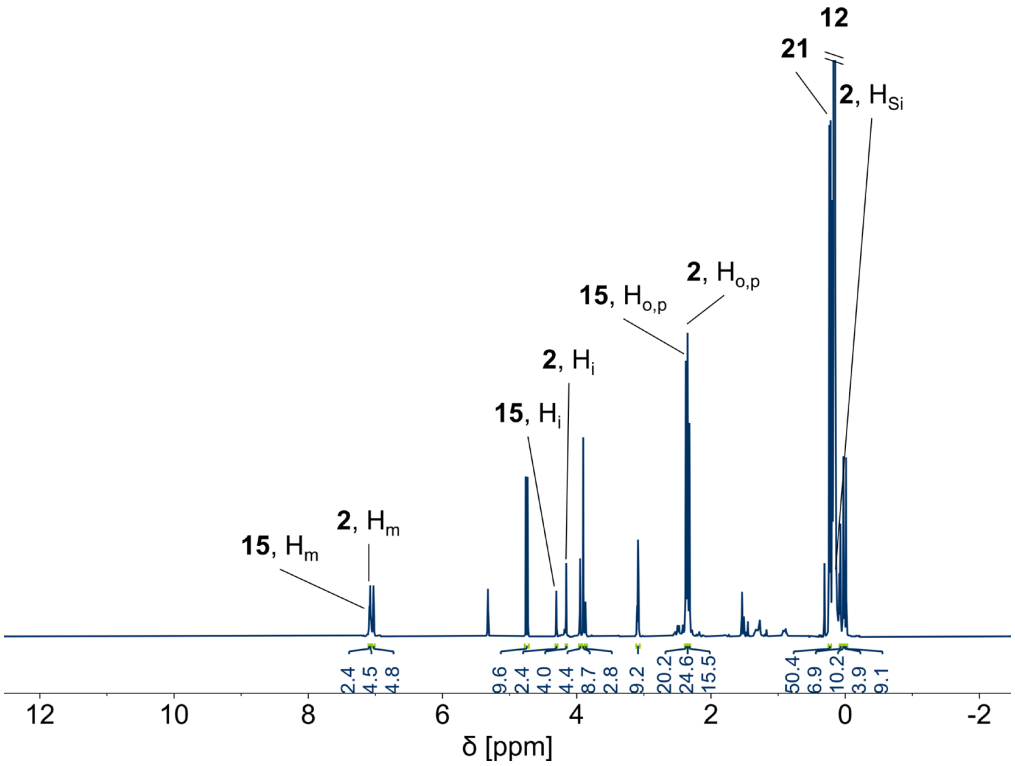

Figure S14: ^{1}H NMR spectrum (400 MHz, CD_2Cl_2, 21 °C) of the reaction between [AuF_3(SIMes)] and $Me_3SiCCSiMe_3$ in DCM including assignments to the compounds shown in Figure S7.

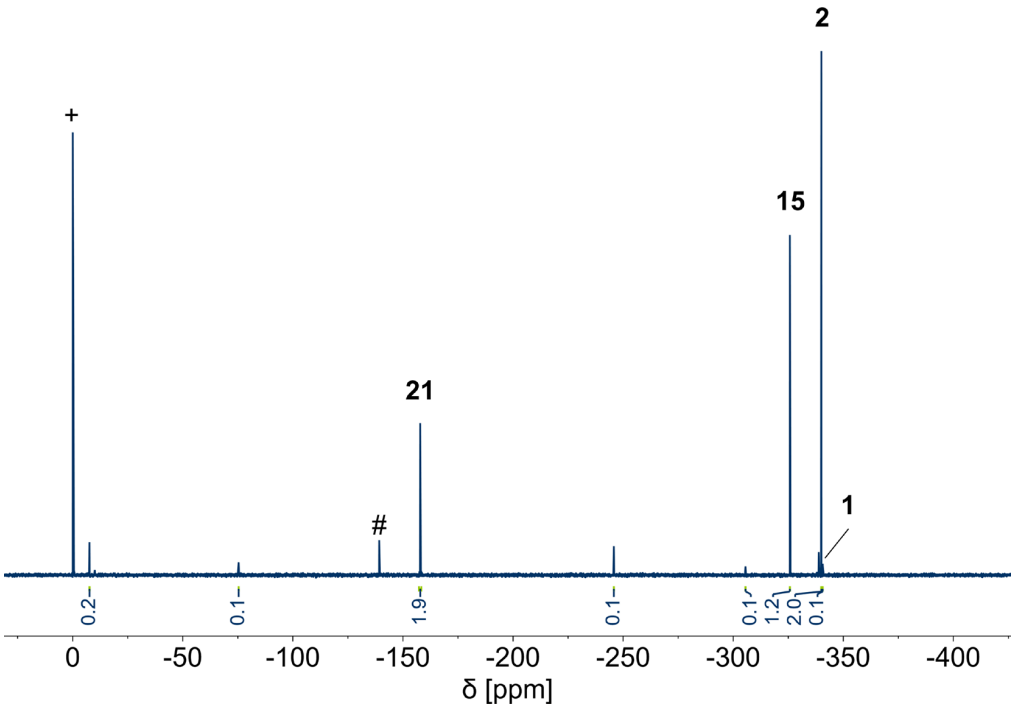

Figure S15: ^{19}F NMR spectrum (377 MHz, CD_2Cl_2, 21 °C) of the reaction between [AuF_3(SIMes)] and Me_3SiCCH in DCM including assignments to the compounds shown in Figure S7. The signal marked with a hash (#) belongs to traces of *ortho*-difluorobenzene from the synthesis of the starting material [AuF_3(SIMes)] and the signal marked with a plus sign (+) belongs to $CFCl_3$ used as a reference inside a glass capillary.

NMR Spectra of the Reaction Between [AuF_3(SIMes)] and Me_3SiCN

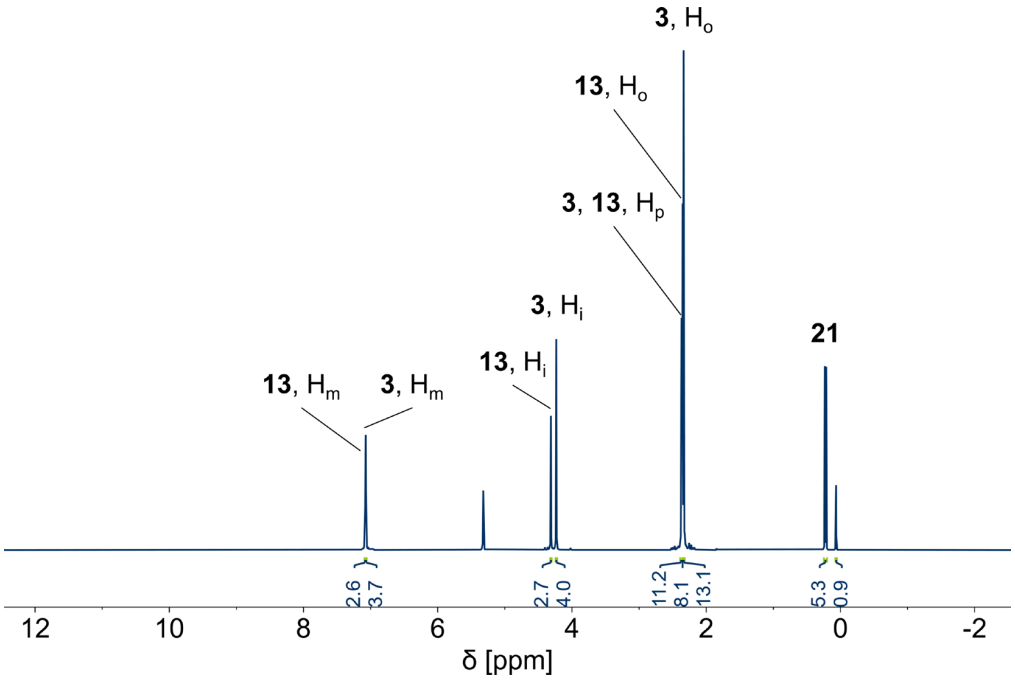

Figure S16: ^{1}H NMR spectrum (400 MHz, CD_2Cl_2, 16 °C) of the reaction between [AuF_3(SIMes)] and 1 eq. of Me_3SiCN in DCM including assignments to the compounds shown in Figure S7.

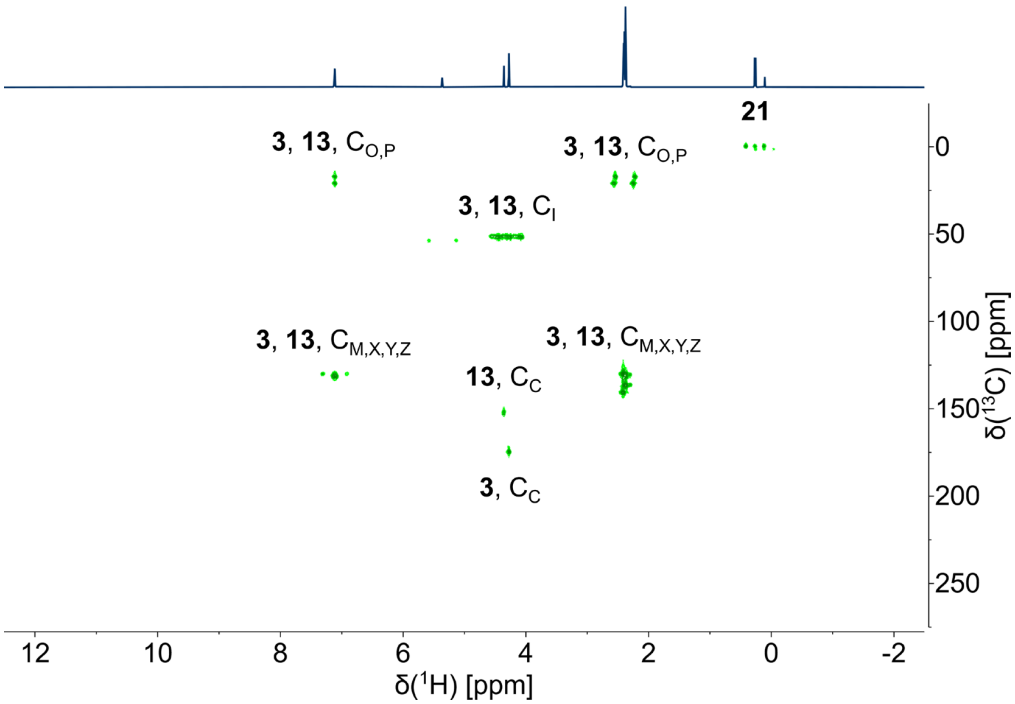

Figure S17: ^{1}H,^{13}C-HMBC NMR spectrum (400 MHz, CD_2Cl_2, 16 °C) of the reaction between [AuF_3(SIMes)] and 1 eq. of Me_3SiCN in DCM including assignments to the compounds shown in Figure S7.

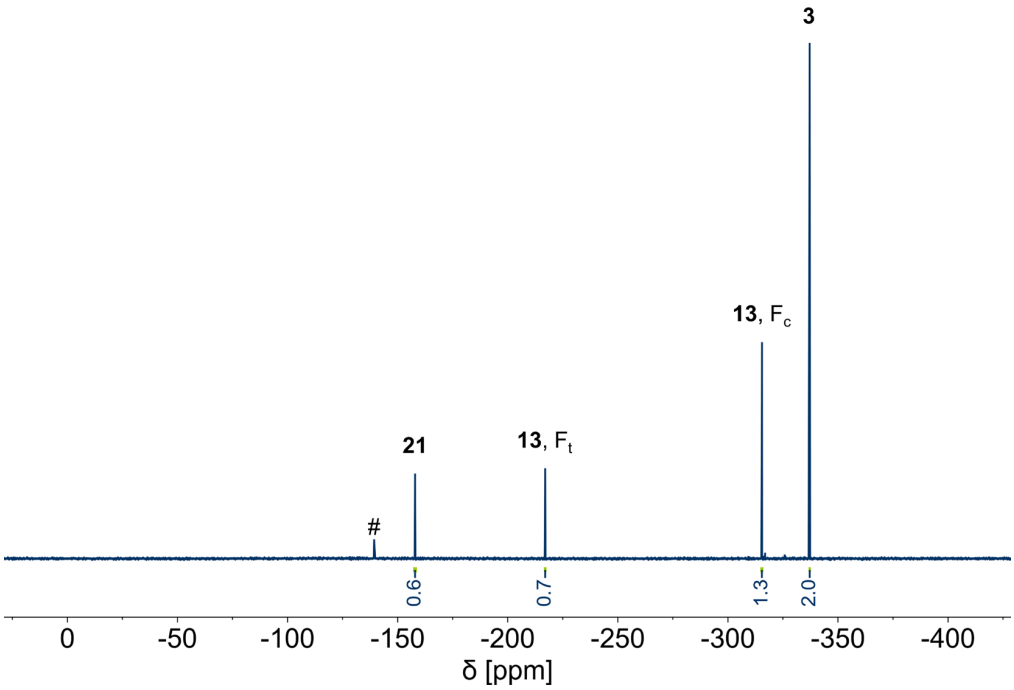

Figure S18: ^{19}F NMR spectrum (377 MHz, CD_2Cl_2, 16 °C) of the reaction between [AuF_3(SIMes)] and 1 eq. of Me_3SiCN in DCM including assignments to the compounds shown in Figure S7. The signal marked with a hash (#) belongs to traces of *ortho*-difluorobenzene from the synthesis of the starting material [AuF_3(SIMes)].

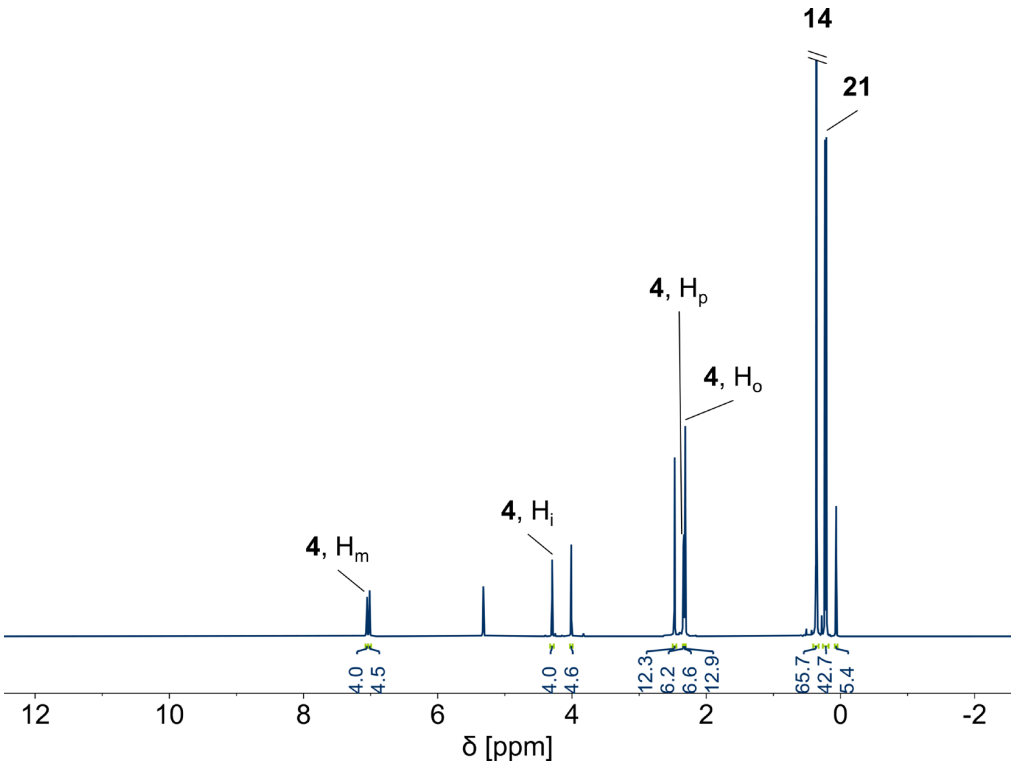

Figure S19: ^1H NMR spectrum (400 MHz, CD_2Cl_2, 15 °C) of the reaction between [AuF_3(SIMes)] and an excess of Me_3SiCN in DCM including assignments to the compounds shown in Figure S7.

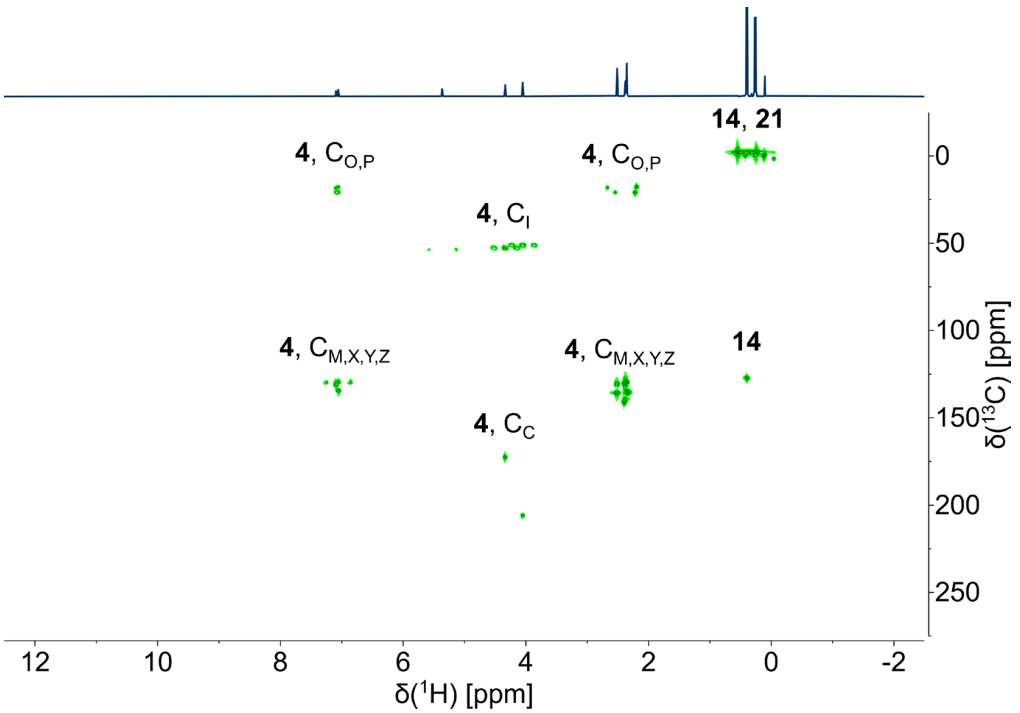

Figure S20: ^{1}H,^{13}C-HMBC NMR spectrum (400 MHz, CD_2Cl_2, 15 °C) of the reaction between [AuF_3(SIMes)] and an excess of Me_3SiCN in DCM including assignments to the compounds shown in Figure S7.

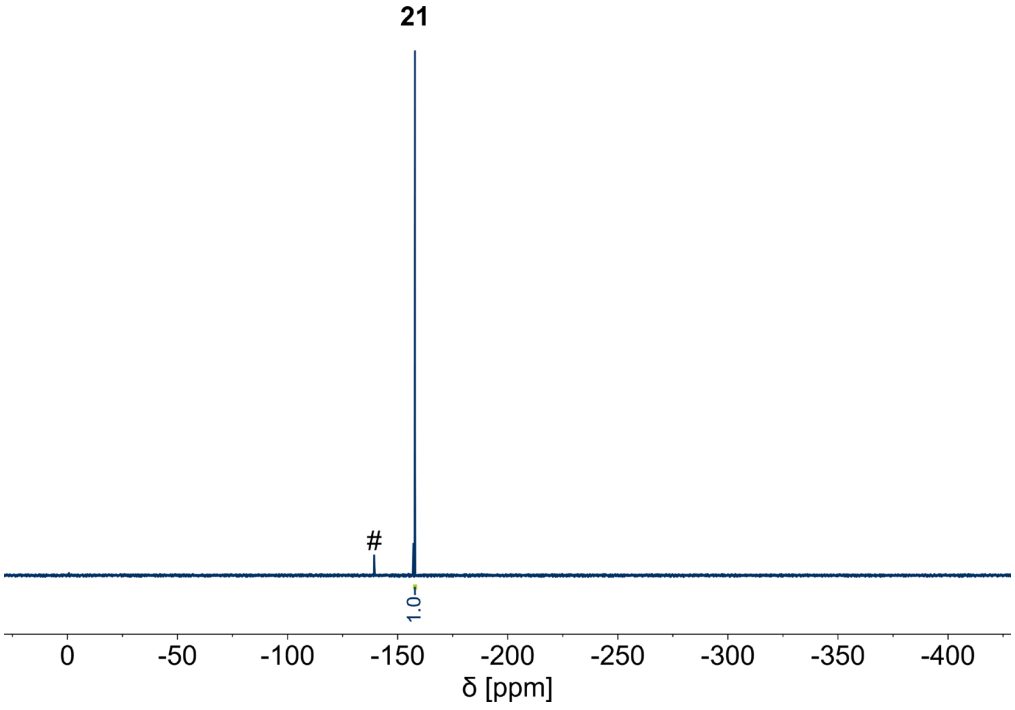

Figure S21: ^{19}F NMR spectrum (377 MHz, CD_2Cl_2, 15 °C) of the reaction between [AuF_3(SIMes)] and an excess of Me_3SiCN in DCM including assignments to the compounds shown in Figure S7. The signal marked with a hash (#) belongs to traces of *ortho*-difluorobenzene from the synthesis of the starting material [AuF_3(SIMes)].

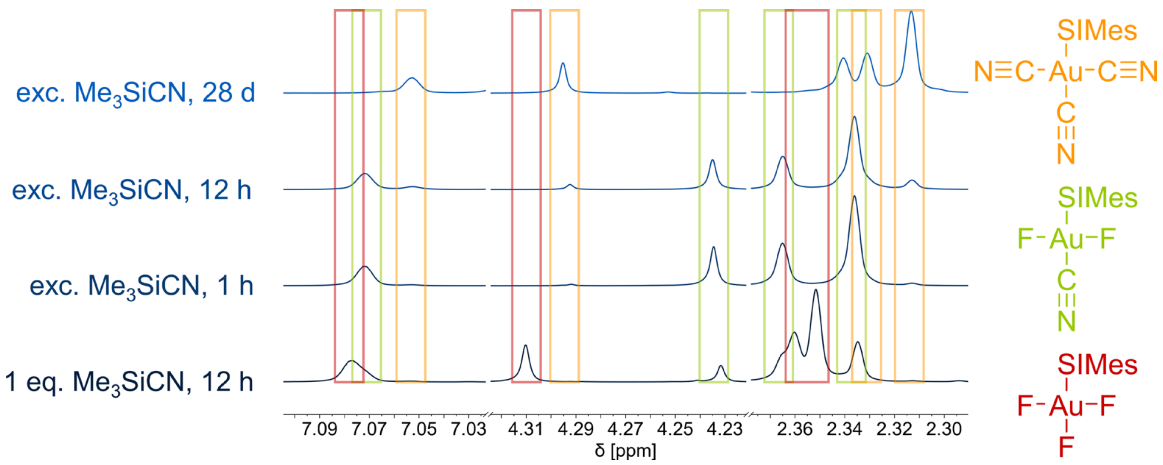

Figure S22: ^{1}H NMR spectra (400 MHz, CD_2Cl_2, 16 °C) at different times of the reaction between [AuF_3(SIMes)] (red) and Me_3SiCN in DCM including a color-coded assignment to the products *trans*-[Au(CN)F_2(SIMes)] (**3**, green) and [Au(CN)$_3$(SIMes)] (**4**, orange).

NMR Spectra of Reaction Between [AuF$_3$(SIMes)] and Me$_3$SiN$_3$

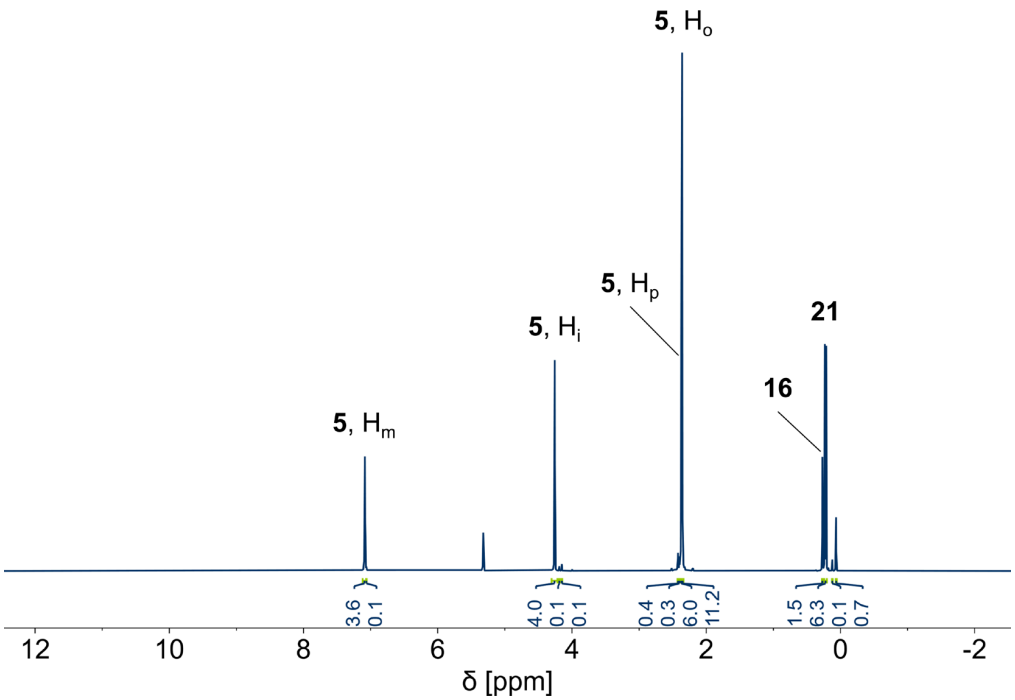

Figure S23: ^{1}H NMR spectrum (400 MHz, CD_2Cl_2, 16 °C) of the reaction between [AuF_3(SIMes)] and 1 eq. of Me_3SiN_3 in DCM including assignments to the compounds shown in Figure S7.

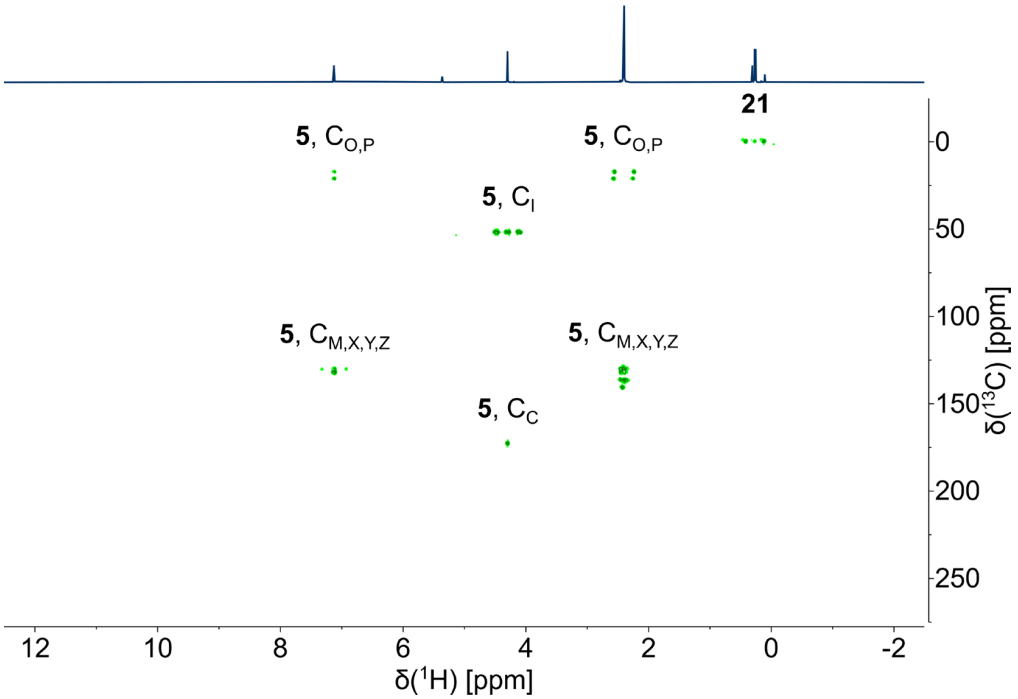

Figure S24: $^{1}H,^{13}C$-HMBC NMR spectrum (400 MHz, CD_2Cl_2, 16 °C) of the reaction between [AuF_3(SIMes)] and 1 eq. of Me_3SiN_3 in DCM including assignments to the compounds shown in Figure S7.

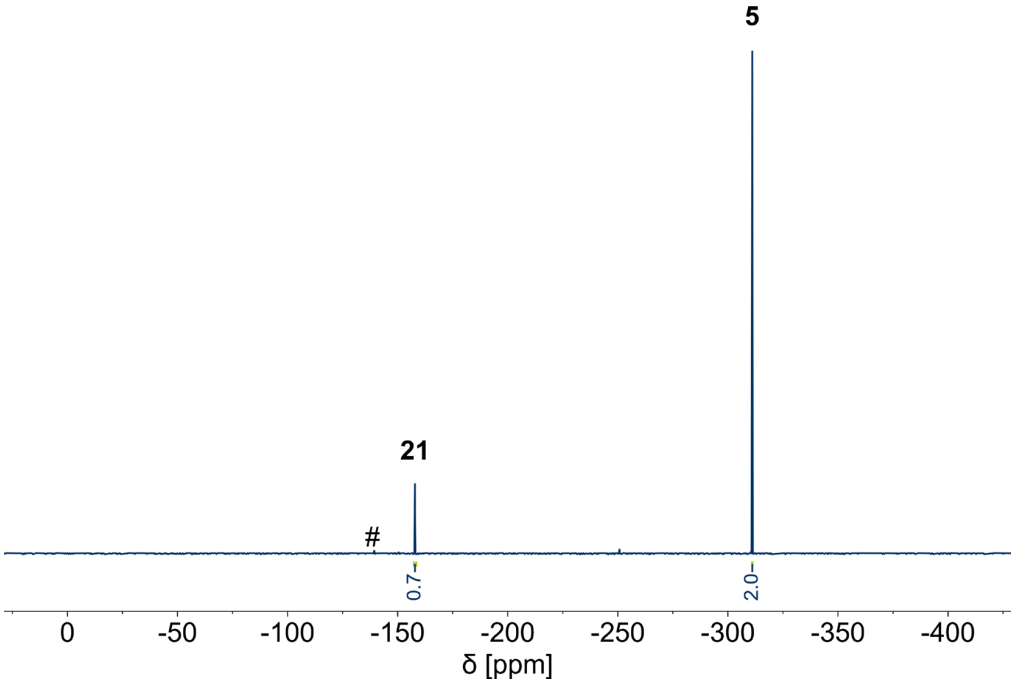

Figure S25: ^{19}F NMR spectrum (377 MHz, CD_2Cl_2, 16 °C) of the reaction between [AuF_3(SIMes)] and 1 eq. of Me_3SiN_3 in DCM including assignments to the compounds shown in Figure S7. The signal marked with a hash (#) belongs to traces of *ortho*-difluorobenzene from the synthesis of the starting material [AuF_3(SIMes)].

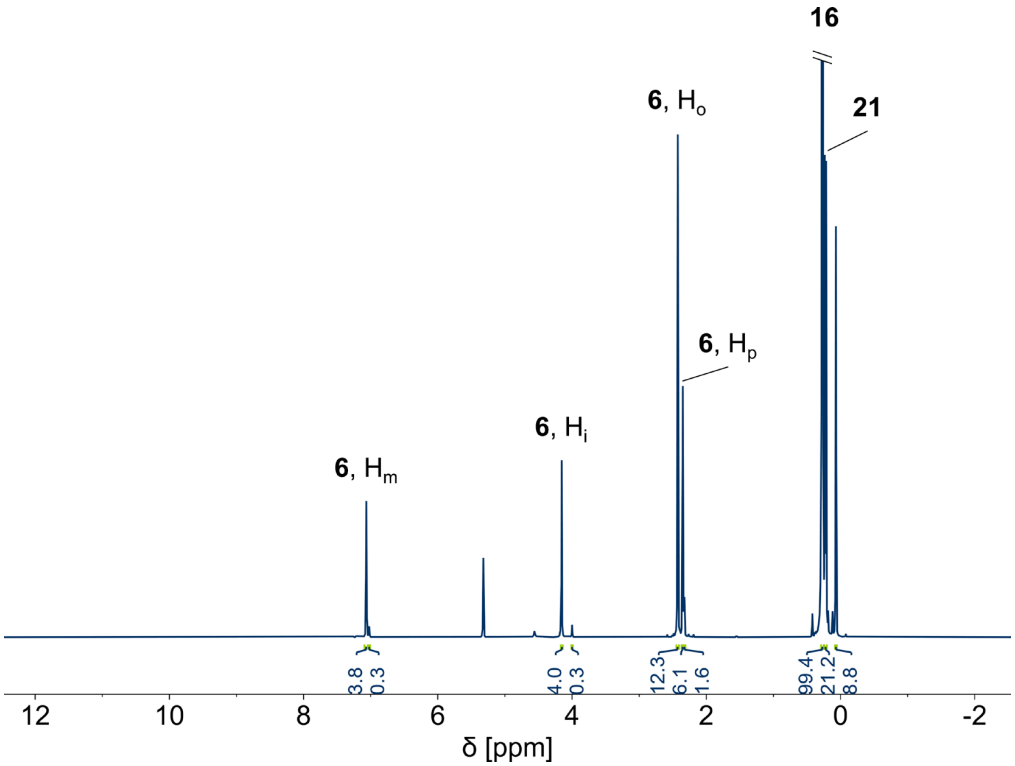

Figure S26: ^{1}H NMR spectrum (400 MHz, CD_2Cl_2, 15 °C) of the reaction between [AuF_3(SIMes)] and an excess of Me_3SiN_3 in DCM including assignments to the compounds shown in Figure S7.

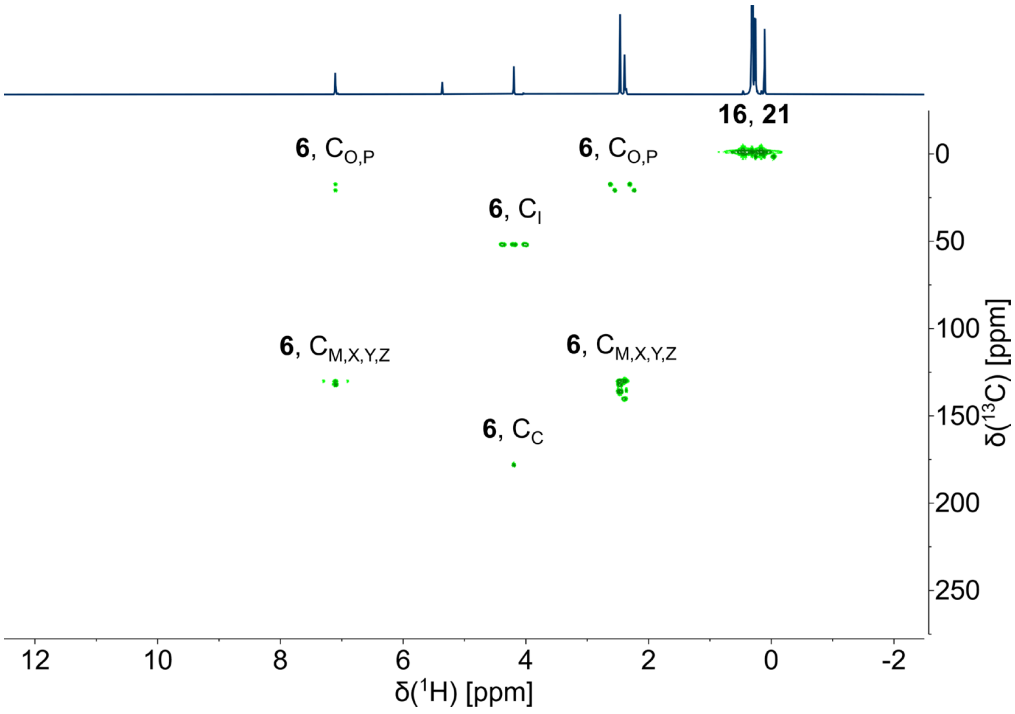

Figure S27: ^{1}H,^{13}C-HMBC NMR spectrum (400 MHz, CD_2Cl_2, 15 °C) of the reaction between [AuF_3(SIMes)] and an excess of Me_3SiN_3 in DCM including assignments to the compounds shown in Figure S7.

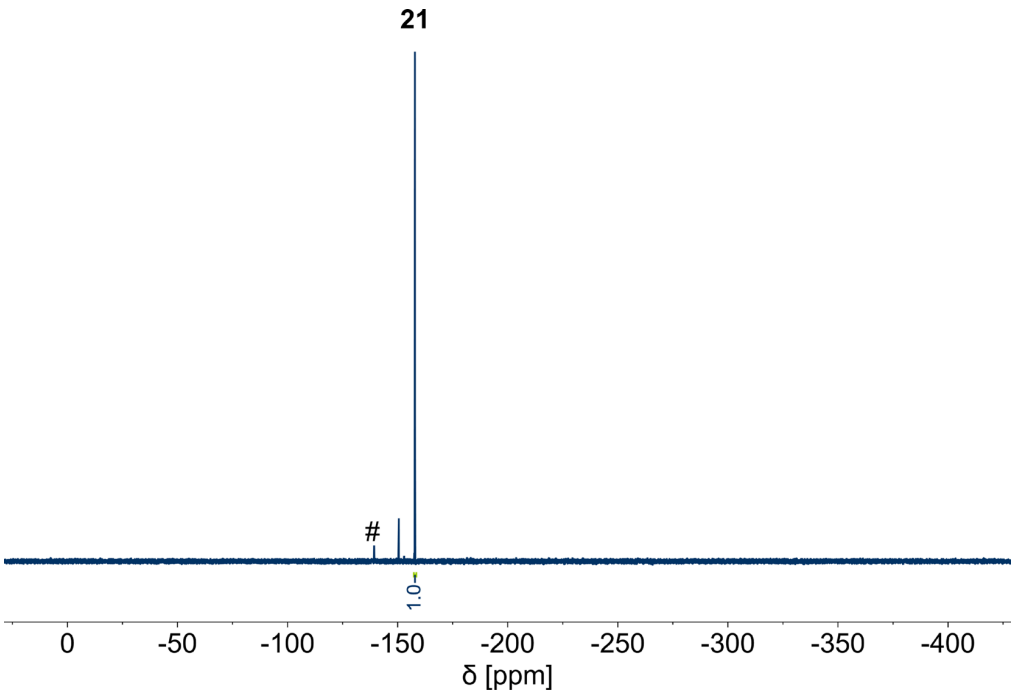

Figure S28: ^{19}F NMR spectrum (377 MHz, CD_2Cl_2, 15 °C) of the reaction between [AuF_3(SIMes)] and an excess of Me_3SiN_3 in DCM including assignments to the compounds shown in Figure S7. The signal marked with a hash (#) belongs to traces of *ortho*-difluorobenzene from the synthesis of the starting material [AuF_3(SIMes)].

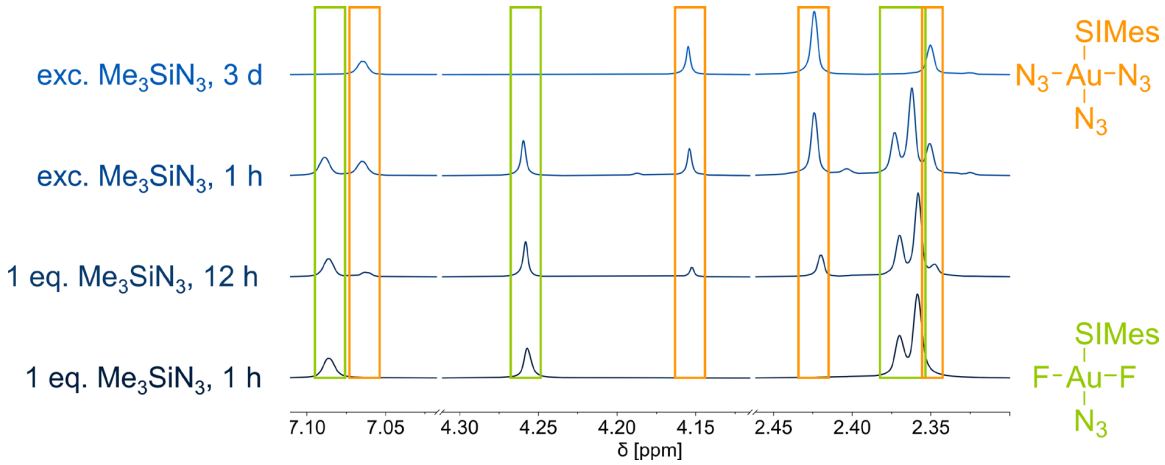

Figure S29: ^1H NMR spectra (400 MHz, CD_2Cl_2, 16 °C) at different times of the reaction between [AuF_3(SIMes)] (red) and Me_3SiN_3 in DCM including a color-coded assignment to the products *trans*-[$AuF_2(N_3)$(SIMes)] (**5**, green) and [$Au(N_3)_3$(SIMes)] (**6**, orange).

NMR Spectra of the Reaction Between [AuF_3(SIMes)] and $Me_3SiOC(CF_3)_3$

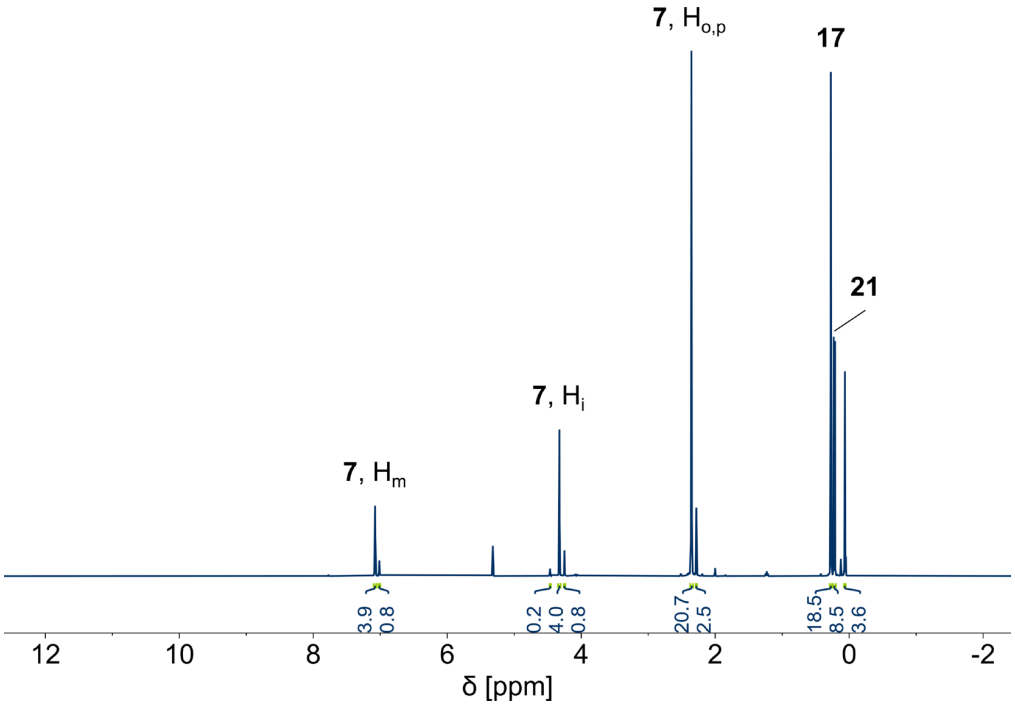

Figure S30: ^{1}H NMR spectrum (400 MHz, CD_2Cl_2, 18 °C) of the reaction between [AuF_3(SIMes)] and $Me_3SiOC(CF_3)_3$ in DCM including assignments to the compounds shown in Figure S7.

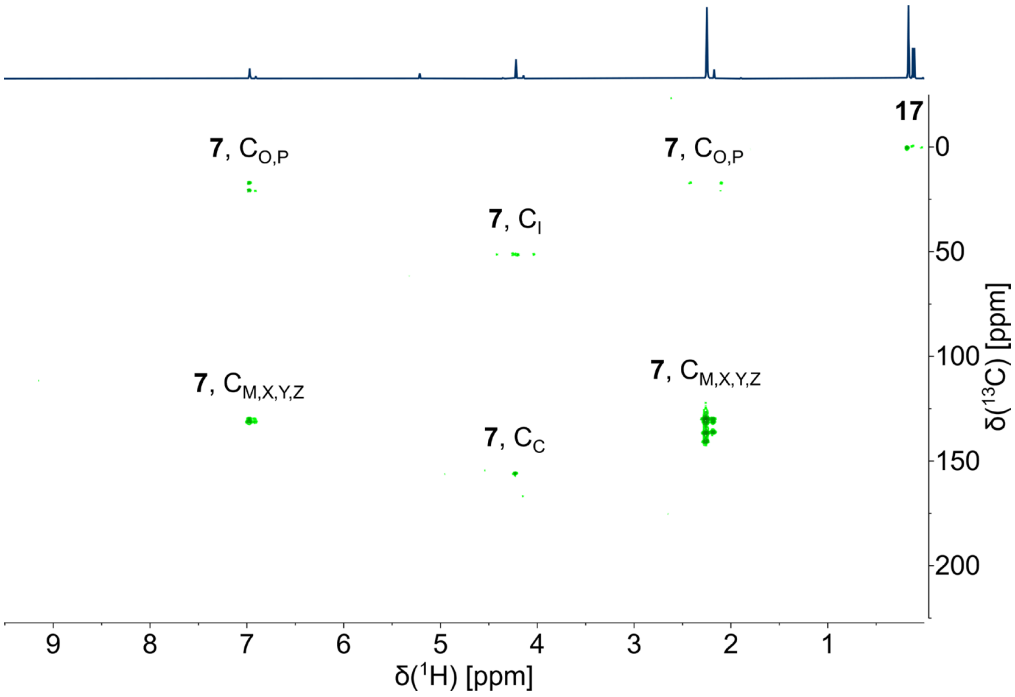

Figure S31: ^{1}H,^{13}C-HMBC NMR spectrum (400 MHz, CD_2Cl_2, 18 °C) of the reaction between [AuF_3(SIMes)] and $Me_3SiOC(CF_3)_3$ in DCM including assignments to the compounds shown in Figure S7.

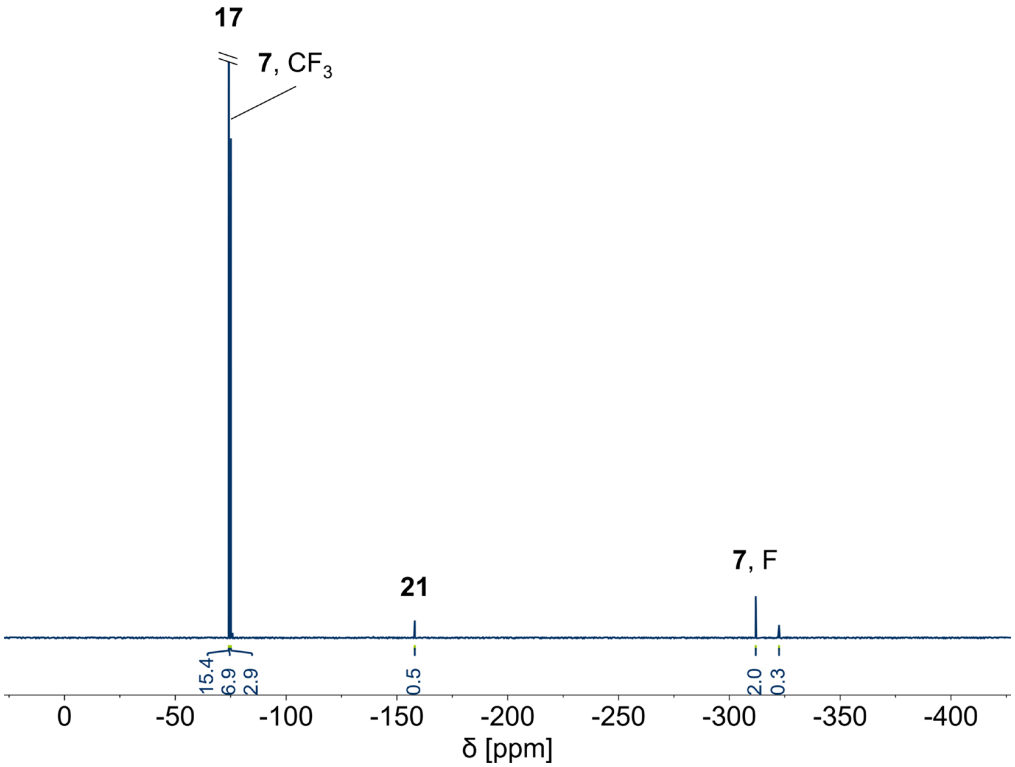

Figure S32: ^{19}F NMR spectrum (377 MHz, CD_2Cl_2, 18 °C) of the reaction between $[AuF_3(SIMes)]$ and $Me_3SiOC(CF_3)_3$ in DCM including assignments to the compounds shown in Figure S7.

NMR Spectra of Reaction Between $[AuF_3(SIMes)]$ and COF_2

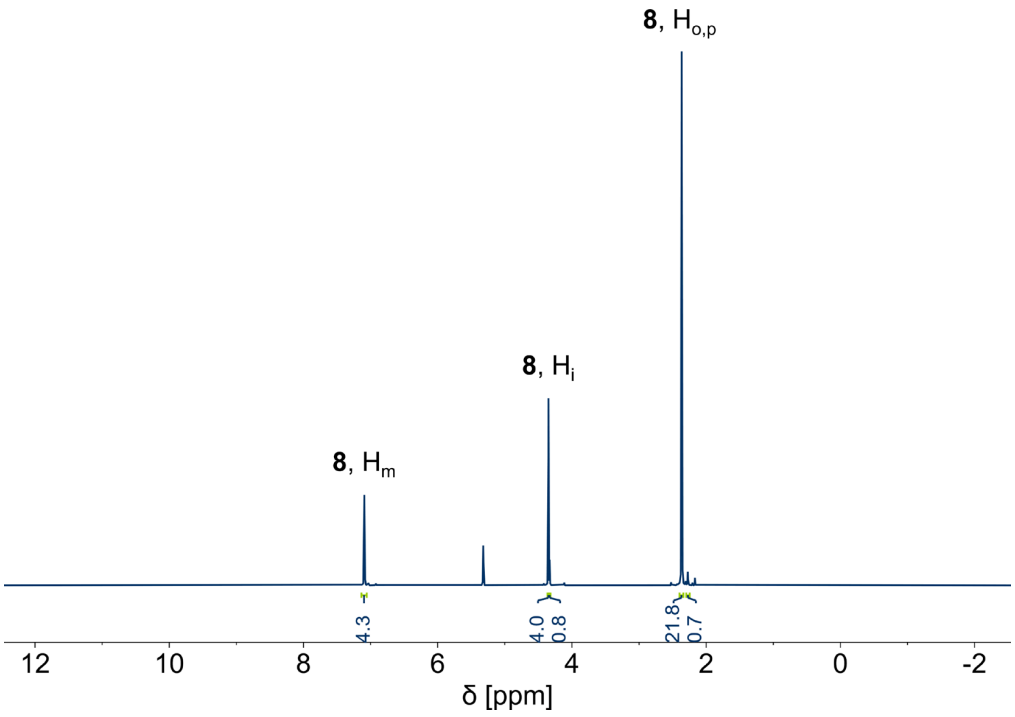

Figure S33: ^1H NMR spectrum (400 MHz, CD_2Cl_2, 18 °C) of the reaction between $[AuF_3(SIMes)]$ and COF_2 in DCM including assignments to the compounds shown in Figure S7.

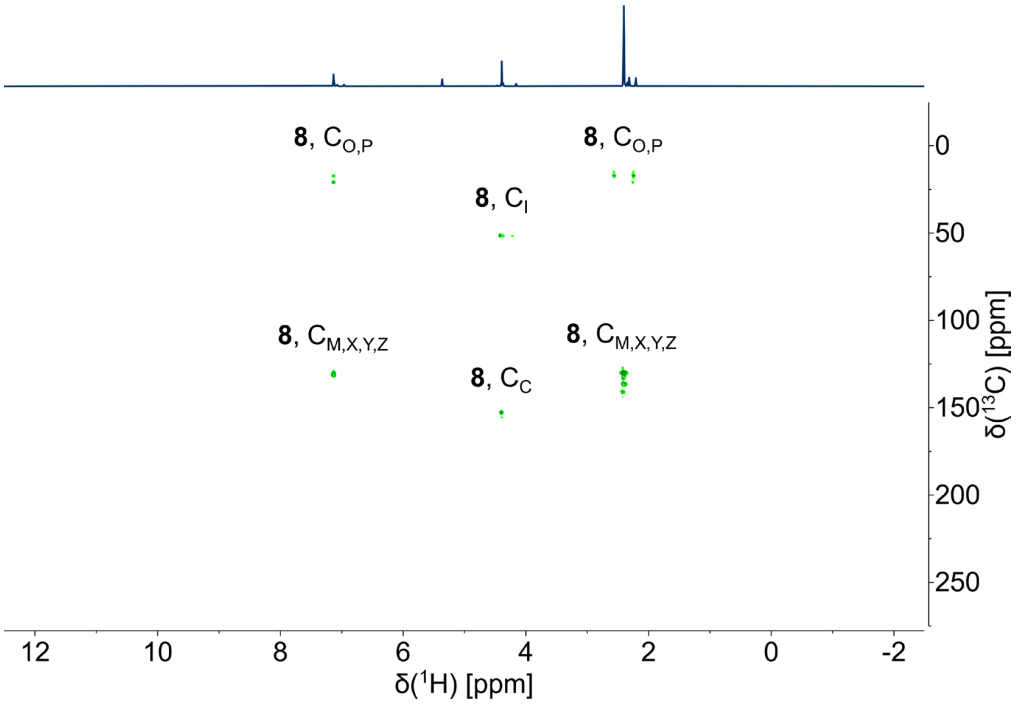

Figure S34: ^{1}H,^{13}C-HMBC NMR spectrum (400 MHz, CD_2Cl_2, 18 °C) of the reaction between [AuF_3(SIMes)] and COF_2 in DCM including assignments to the compounds shown in Figure S7.

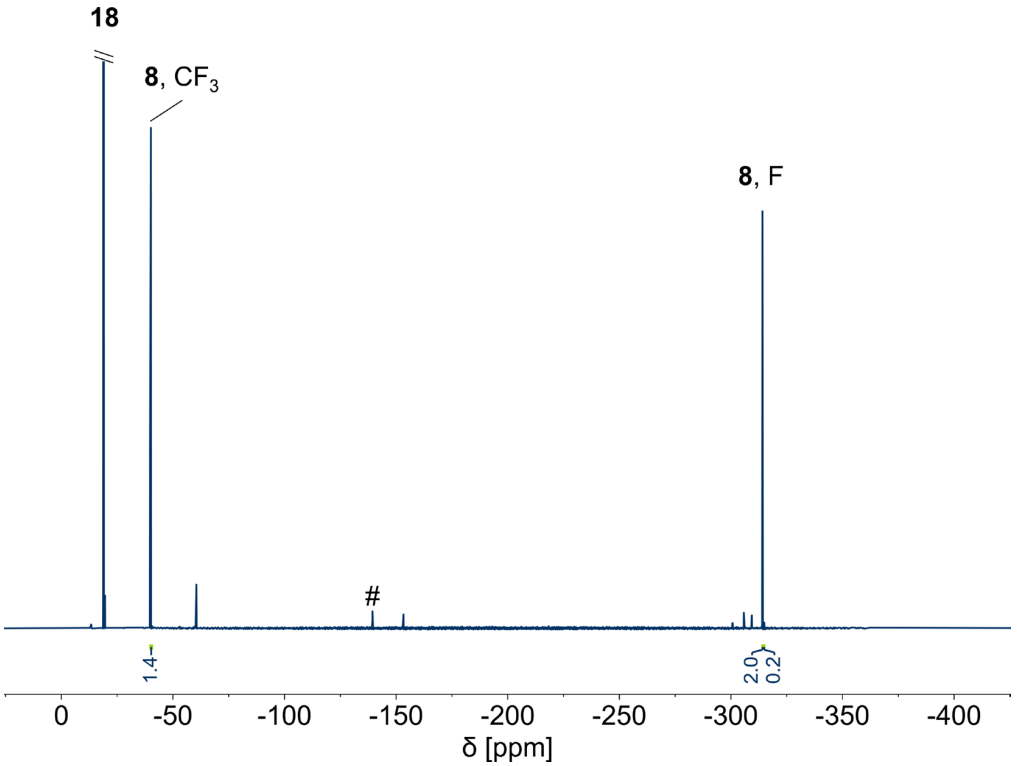

Figure S35: ^{19}F NMR spectrum (377 MHz, CD_2Cl_2, 18 °C) of the reaction between [AuF_3(SIMes)] and COF_2 in DCM including assignments to the compounds shown in Figure S7. The signal marked with a hash (#) belongs to traces of *ortho*-difluorobenzene from the synthesis of the starting material [AuF_3(SIMes)].

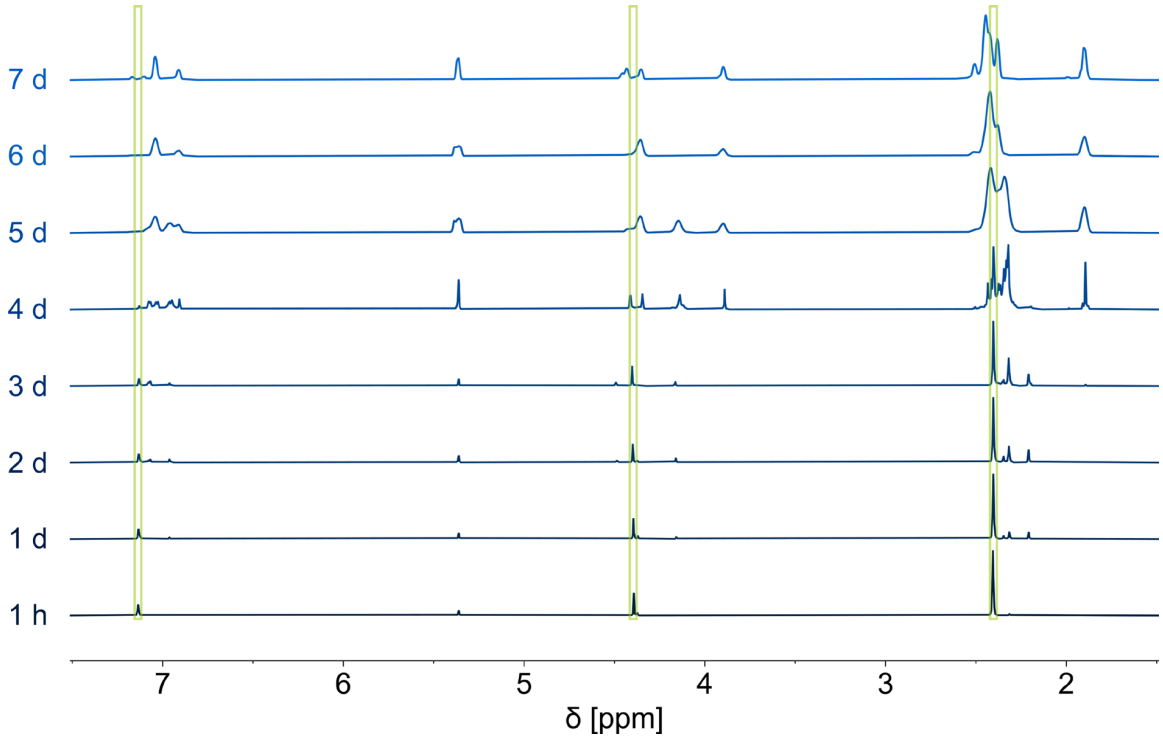

Figure S36: ^{1}H NMR spectra (400 MHz, CD_2Cl_2, 18 °C) at different times of the reaction between [AuF_3(SIMes)] and COF_2. The signals that are assigned to the desired product *trans*-[$AuF_2(OCF_3)$(SIMes)] (**8**) are highlighted in green.

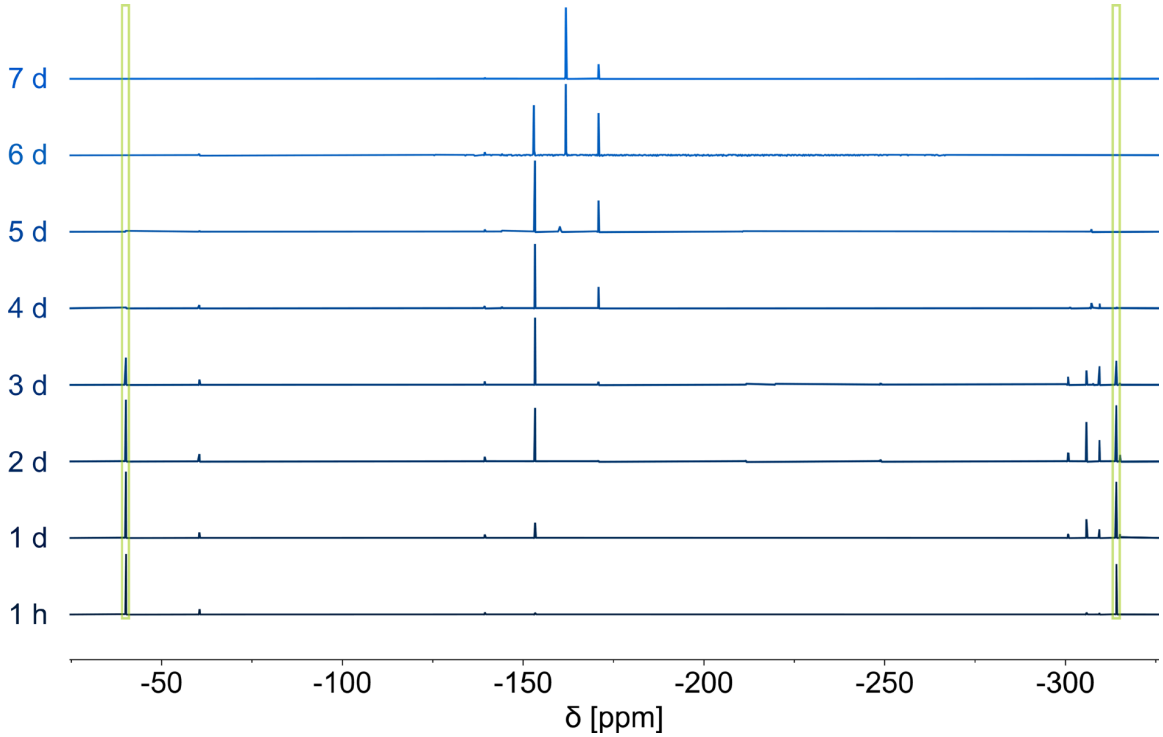

Figure S37: ^{19}F NMR spectra (377 MHz, CD_2Cl_2, 18 °C) at different times of the reaction between [AuF_3(SIMes)] and COF_2. The signals that are assigned to the desired product *trans*-[$AuF_2(OCF_3)$(SIMes)] (**8**) are highlighted in green.

NMR Spectra of Reaction Between [AuF_3(SIMes)] and $CO(CF_3)F$

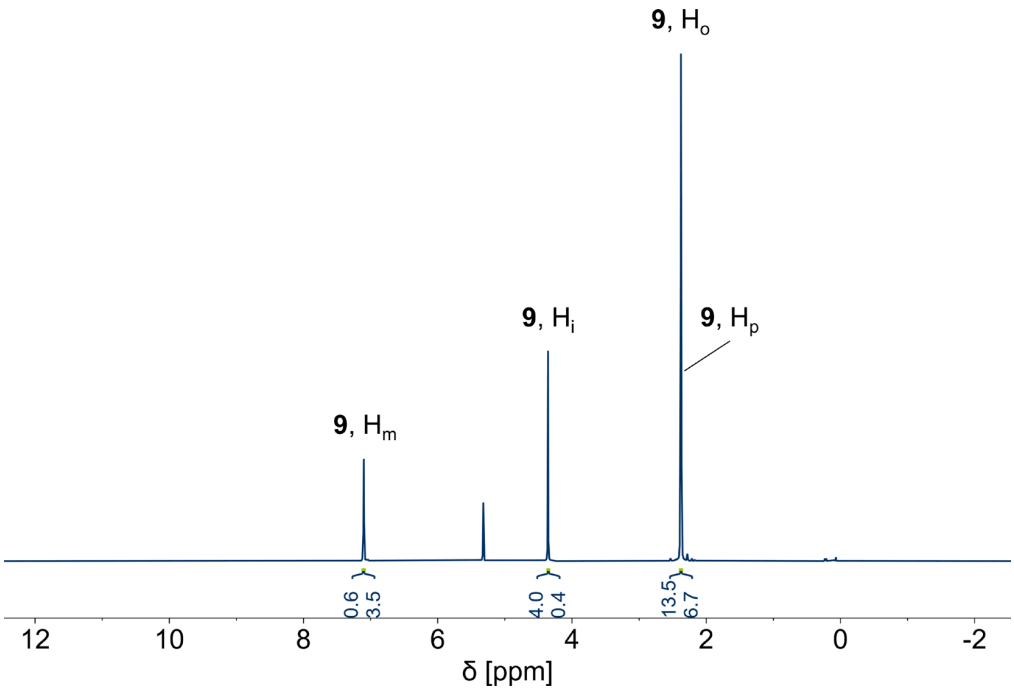

Figure S38: ^{1}H NMR spectrum (400 MHz, CD_2Cl_2, 17 °C) of the reaction between [AuF_3(SIMes)] and $CO(CF_3)F$ in DCM including assignments to the compounds shown in Figure S7.

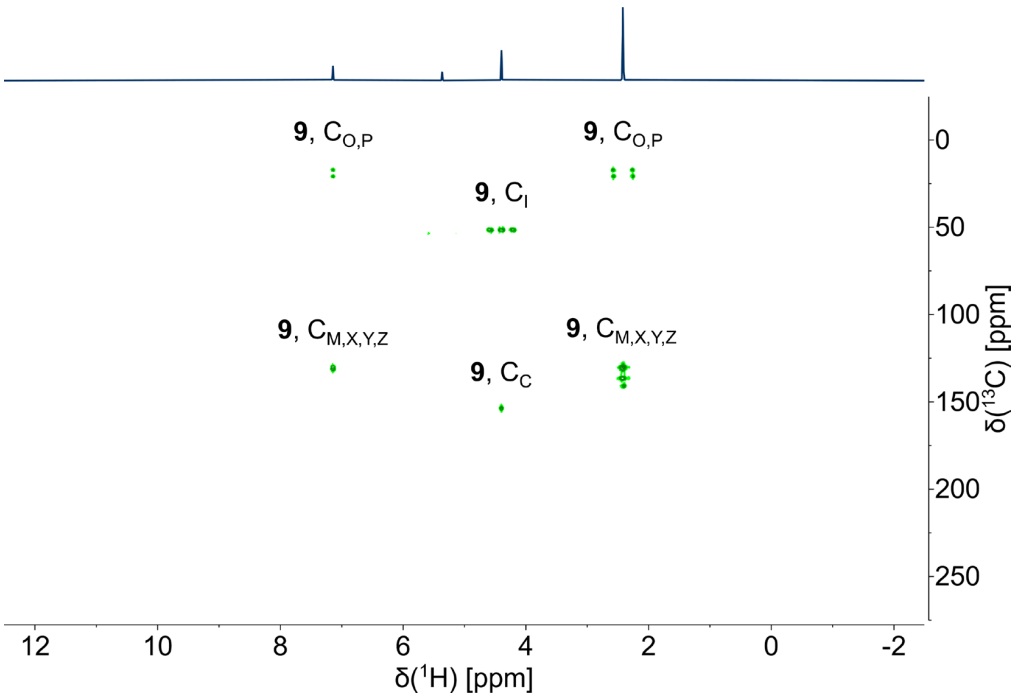

Figure S39: ^{1}H,^{13}C-HMBC NMR spectrum (400 MHz, CD_2Cl_2, 17 °C) of the reaction between [AuF_3(SIMes)] and $CO(CF_3)F$ in DCM including assignments to the compounds shown in Figure S7.

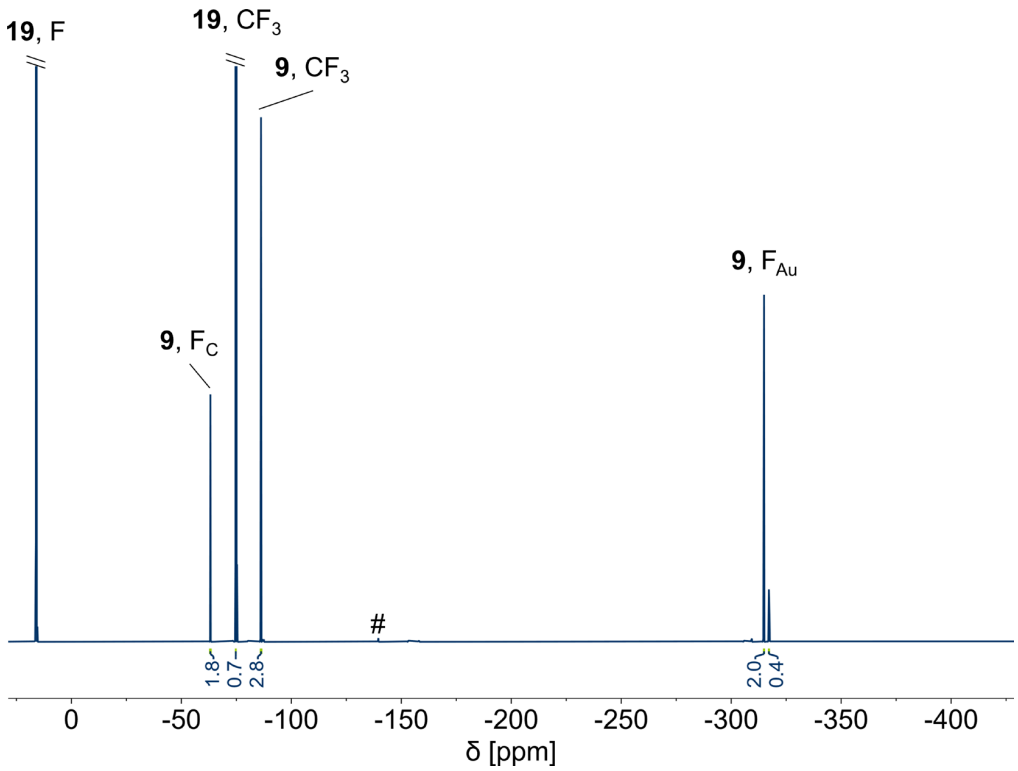

Figure S40: ^{19}F NMR spectrum (377 MHz, CD_2Cl_2, 17 °C) of the reaction between [AuF_3(SIMes)] and $CO(CF_3)F$ in DCM including assignments to the compounds shown in Figure S7. The signal marked with a hash (#) belongs to traces of *ortho*-difluorobenzene from the synthesis of the starting material [AuF_3(SIMes)].

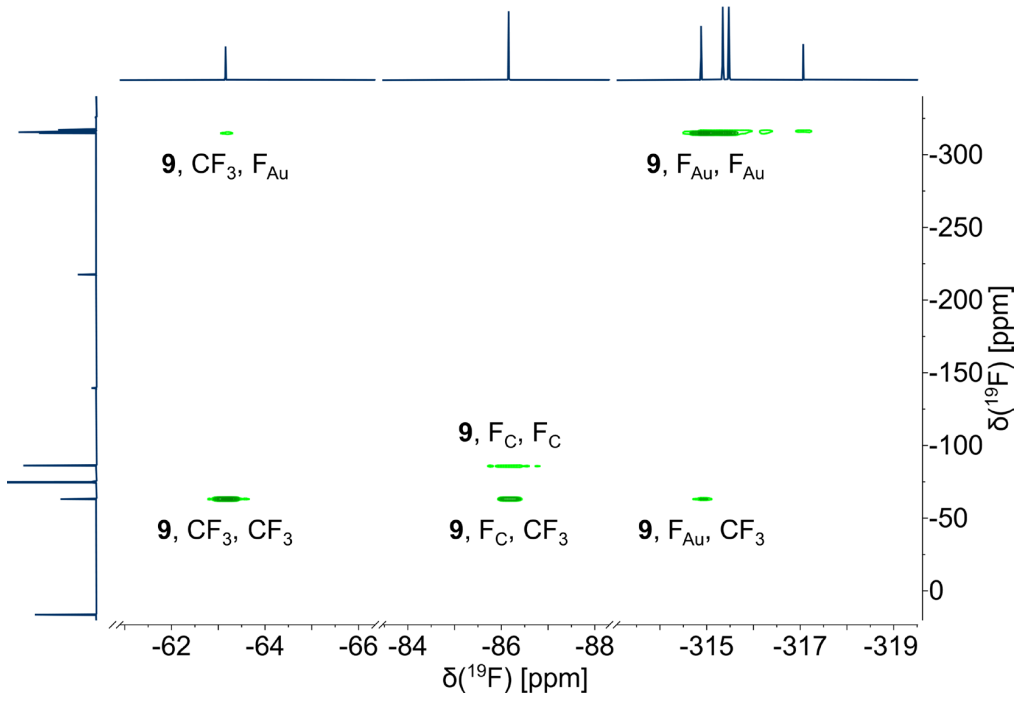

Figure S41: ^{19}F,^{19}F-COSY NMR spectrum (377 MHz, CD_2Cl_2, 22 °C) of the reaction between [AuF_3(SIMes)] and $CO(CF_3)F$ in DCM including assignments to the compounds shown in Figure S7, showing the cross-couplings between the three different signals assigned to compound **9**.

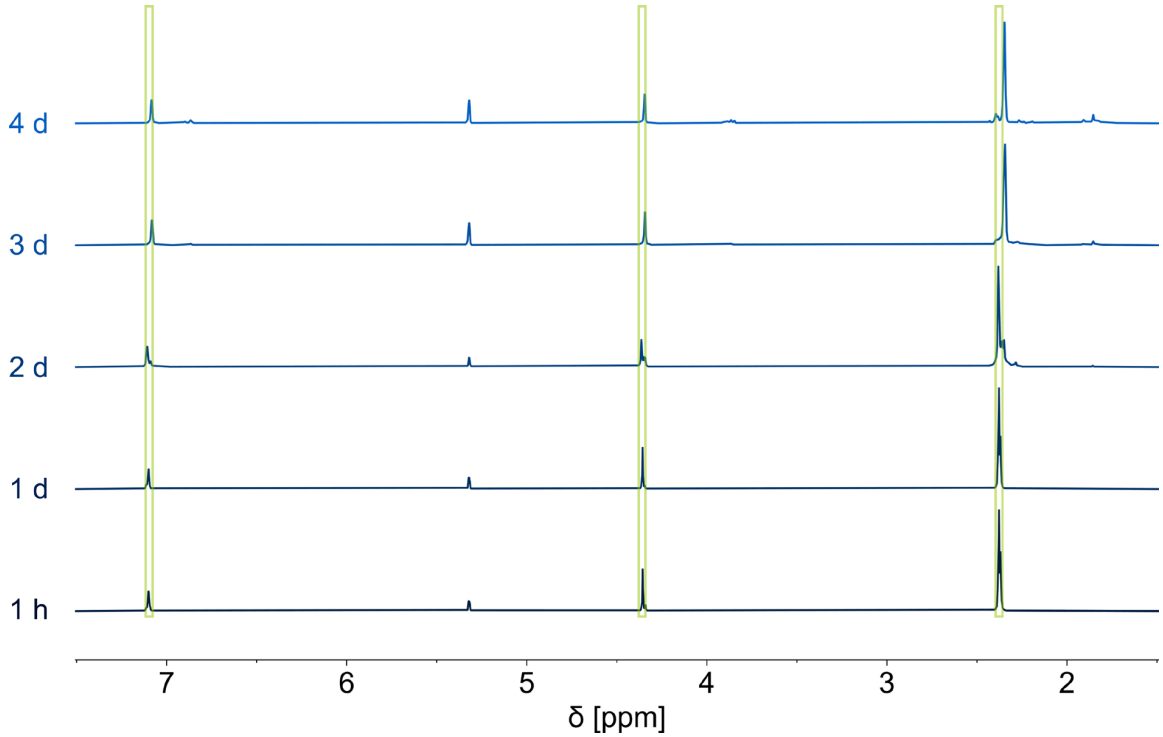

Figure S42: ^{1}H NMR spectra (400 MHz, CD_2Cl_2, 17 °C) at different times of the reaction between [AuF_3(SIMes)] and $COFCF_3$. The signals that are assigned to the desired product *trans*-[AuF_2($OC(CF_3)F_2$)(SIMes)] (**9**) are highlighted in green.

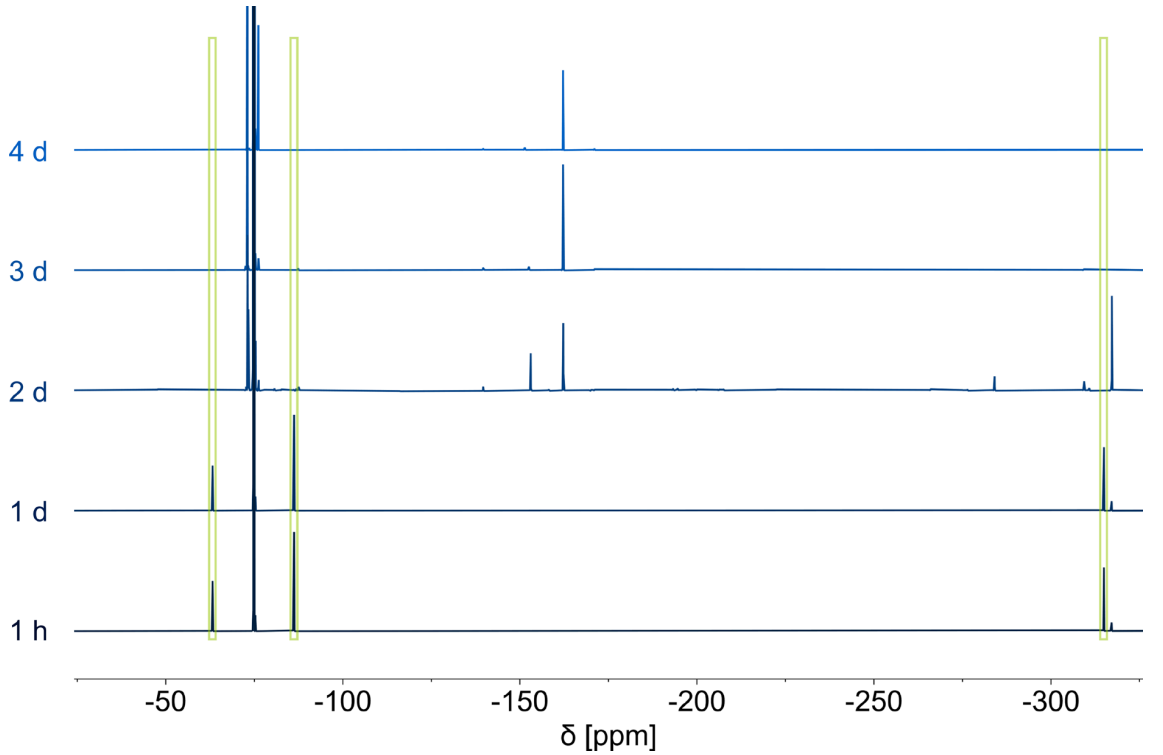

Figure S43: ^{19}F NMR spectra (377 MHz, CD_2Cl_2, 17 °C) at different times of the reaction between [AuF_3(SIMes)] and $COFCF_3$. The signals that are assigned to the desired product *trans*-[AuF_2($OC(CF_3)F_2$)(SIMes)] (**9**) are highlighted in green.

NMR Spectra of Reaction Between [AuF_3(SIMes)] and $CO(CF_3)_2$

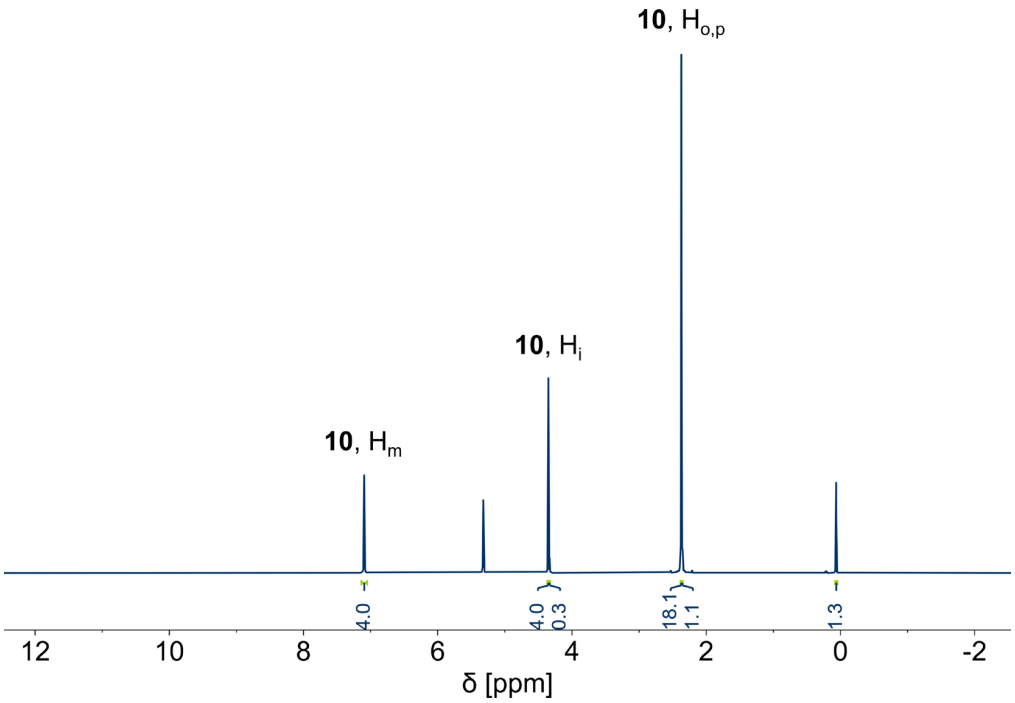

Figure S44: ^{1}H NMR spectrum (400 MHz, CD_2Cl_2, 16 °C) of the reaction between [AuF_3(SIMes)] and $CO(CF_3)_2$ in DCM including assignments to the compounds shown in Figure S7.

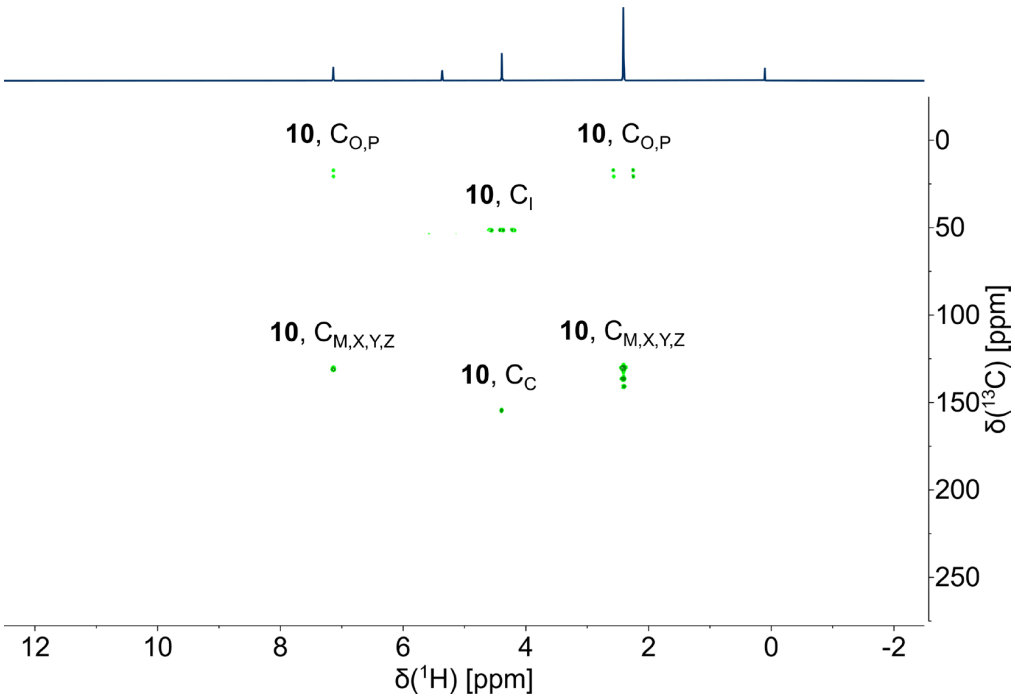

Figure S45: ^{1}H,^{13}C-HMBC NMR spectrum (400 MHz, CD_2Cl_2, 17 °C) of the reaction between [AuF_3(SIMes)] and $CO(CF_3)_2$ in DCM including assignments to the compounds shown in Figure S7.

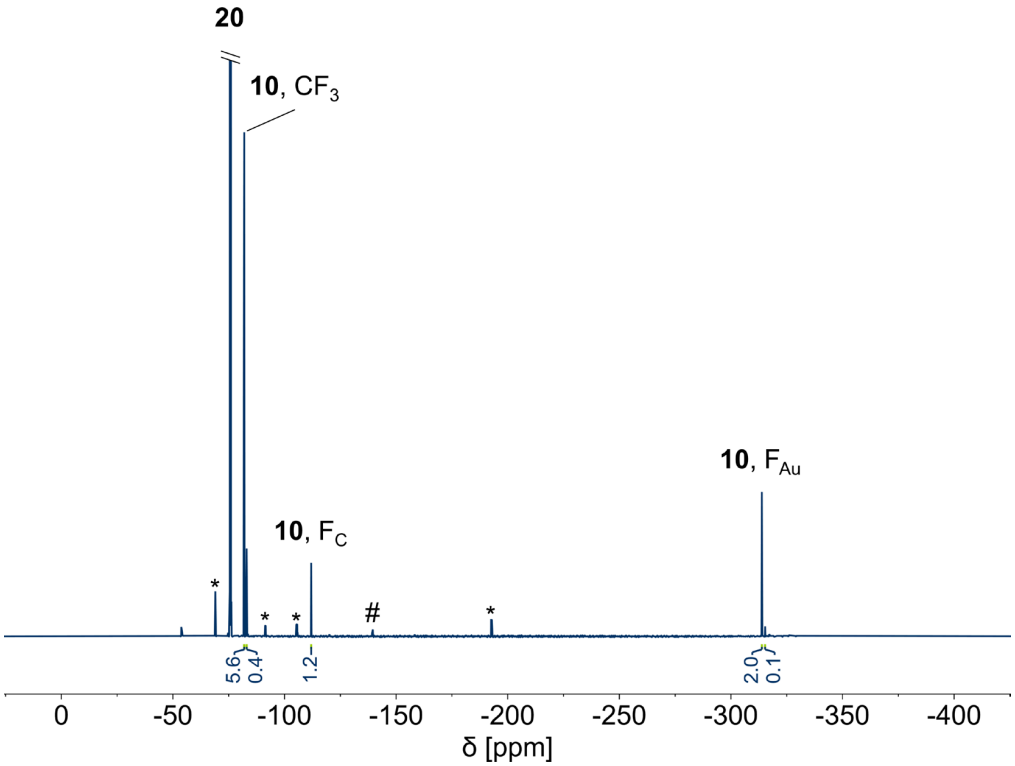

Figure S46: ^{19}F NMR spectrum (377 MHz, CD_2Cl_2, 16 °C) of the reaction between [AuF_3(SIMes)] and $CO(CF_3)_2$ in DCM including assignments to the compounds shown in Figure S7. The signal marked with a hash (#) belongs to traces of *ortho*-difluorobenzene from the synthesis of the starting material [AuF_3(SIMes)] and the signals marked with an asterisk (*) belong to $CO(C_2F_5)F$, which was an impurity of the used $CO(CF_3)_2$

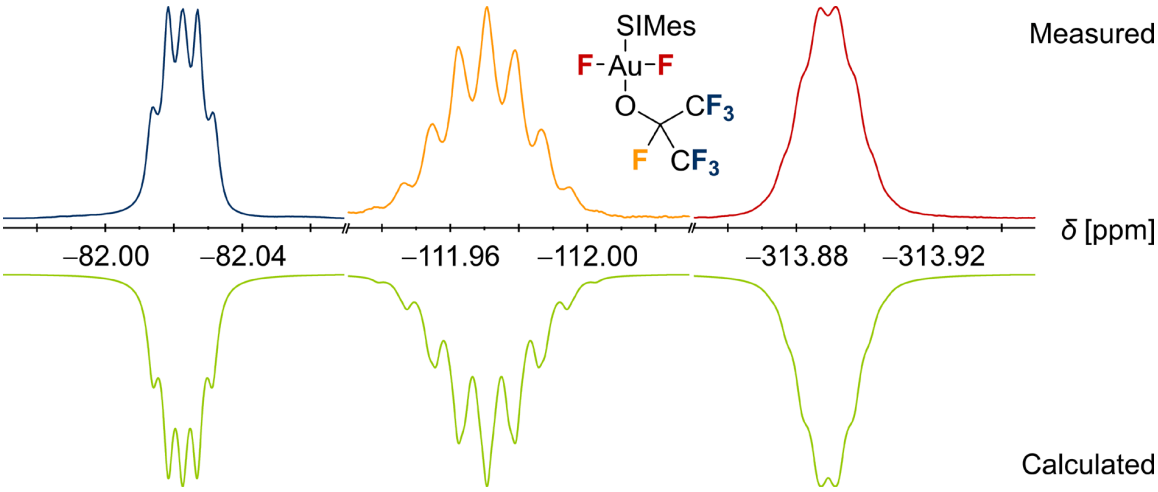

Figure S47: ^{19}F NMR spectrum (377 MHz, DCM-d_2, 16 °C) of [AuF_2($OC(CF_3)_2F$)(SIMes)] (**10**) (top, multicolored) compared to the simulated spectrum (bottom, green). NMR spectroscopical parameters used in the simulation: $\delta(F_{CF3})$ = −82.02 ppm, $\delta(F_C)$ = −111.97 ppm, $\delta(F_C)$ = −313.89 ppm, $^3J(^{19}F_{CF3},^{19}F_C)$ = 3.20 Hz, $^5J(^{19}F_{CF3},^{19}F_{Au})$ = 1.70 Hz, $^4J(^{19}F_C,^{19}F_{Au})$ = 2.42 Hz.

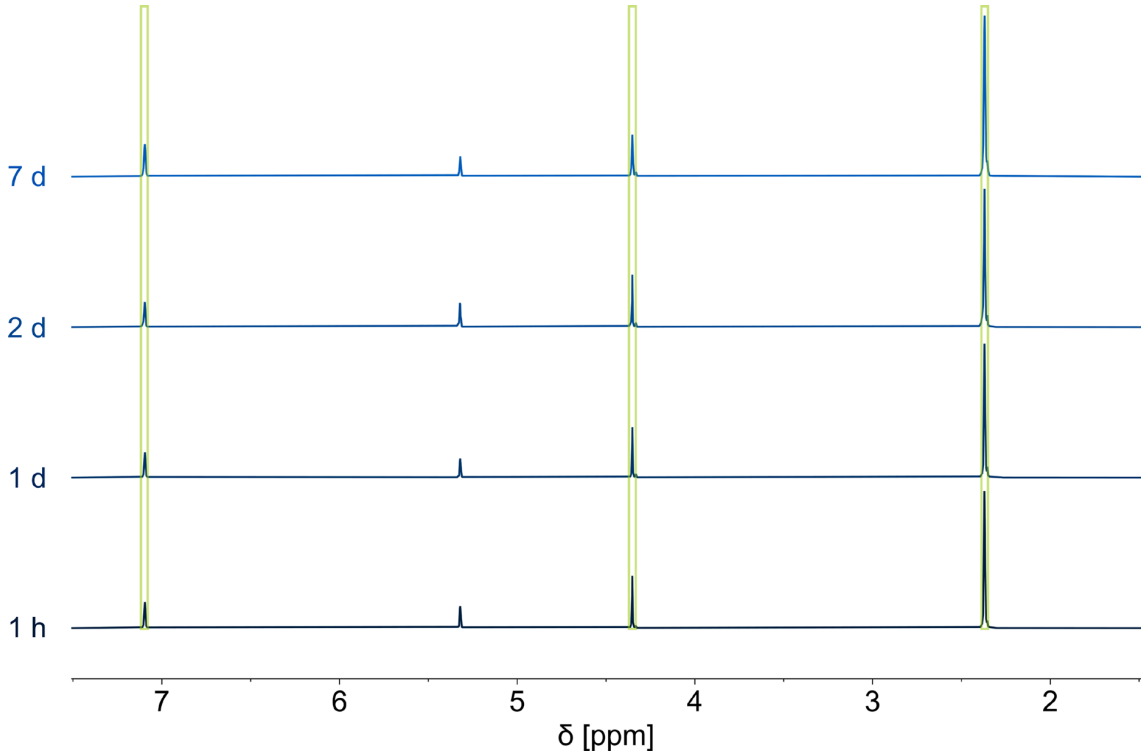

Figure S48: ^{1}H NMR spectra (400 MHz, CD_2Cl_2, 16 °C) at different times of the reaction between [AuF_3(SIMes)] and $CO(CF_3)_2$. The signals that are assigned to the desired product *trans*-[$AuF_2(OC(CF_3)_2F)$(SIMes)] (**10**) are highlighted in green.

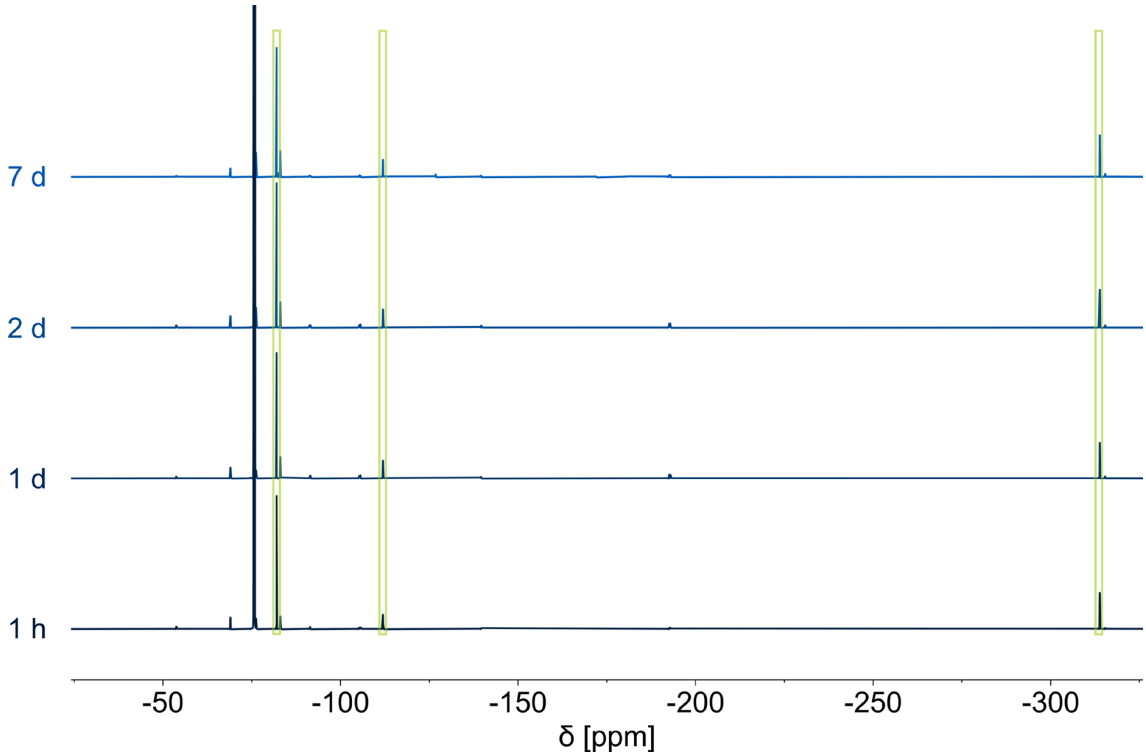

Figure S49: ^{19}F NMR spectra (377 MHz, CD_2Cl_2, 16 °C) at different times of the reaction between [AuF_3(SIMes)] and $CO(CF_3)_2$. The signals that are assigned to the desired product *trans*-[$AuF_2(OC(CF_3)_2F)$(SIMes)] (**10**) are highlighted in green.

Correlation Between Au–C Distance and ^{13}C Chemical Shift

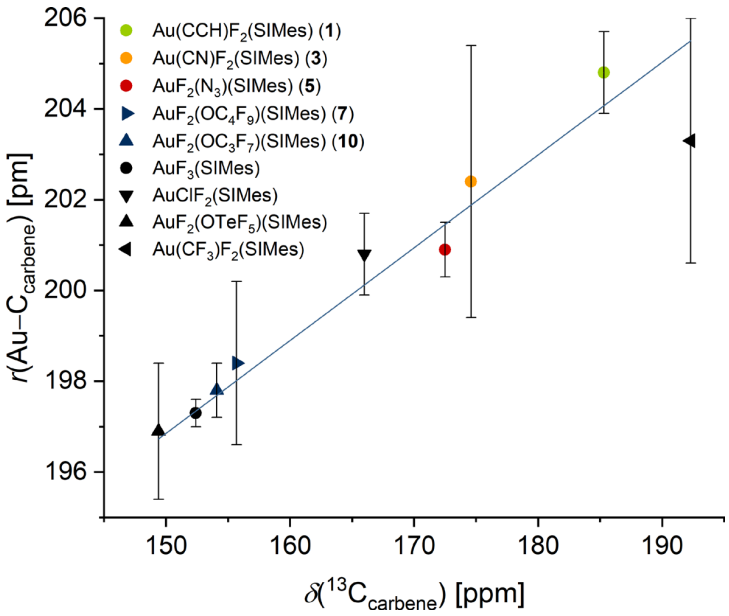

Figure S50: Correlation between the gold carbon distances (r(Au-$C_{carbene}$)) in the molecular structures in the solid state with the chemical shifts of the carbene carbon atoms in the ^{13}C NMR spectra (δ($^{13}C_{carbene}$)) of *trans*-[AuF_2X(SIMes)] complexes prepared in this work (green: alkynido complexes, orange: cyanido complexes, red: azido complexes, blue: perfluoroalkoxido complexes) and similar, literature-known compounds (black).[1,3] The error bars of the y-axis equal three times the estimated standard deviation in both directions.

Vibrational Spectroscopy

IR and Raman Spectrum of *trans*-[Au(CCH)F_2(SIMes)] (1)

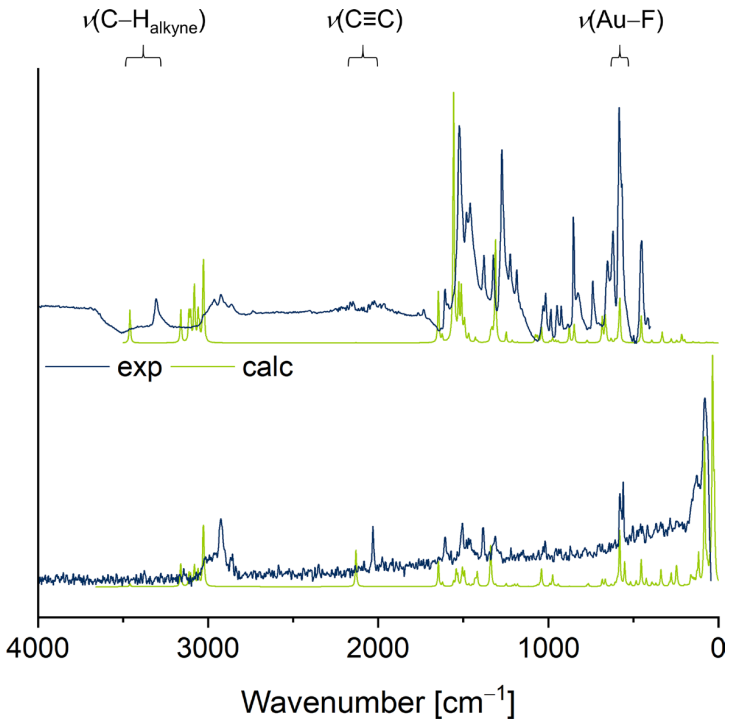

Figure S51: IR (top) and Raman (bottom) spectrum of *trans*-[Au(CCH)F_2(SIMes)] (**1**) (blue) compared to the calculated spectrum (green; RI-B3LYP-D3/def2-TZVPP level).

IR Spectrum of *trans*-[Au(CN)F_2(SIMes)] (3)

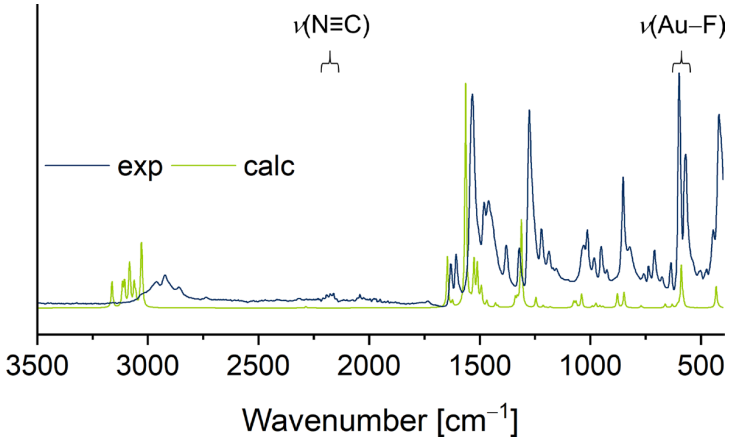

Figure S52: IR spectrum of *trans*-[Au(CN)F_2(SIMes)] (**3**) (blue) compared to the calculated spectrum (green; RI-B3LYP-D3/def2-TZVPP level).

IR Spectrum of [Au(CN)$_3$(SIMes)] (4)

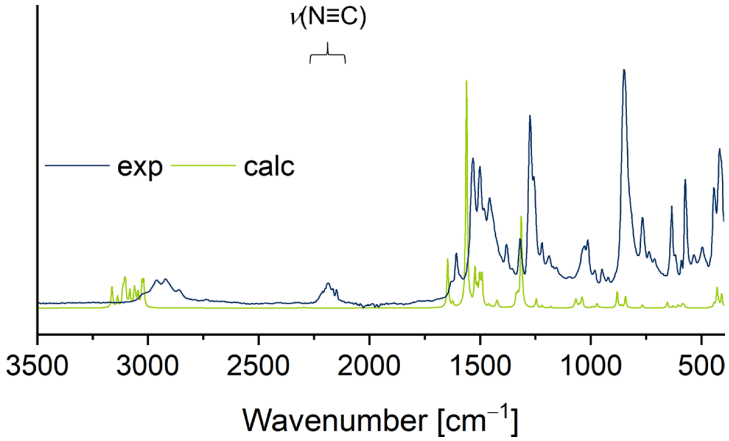

Figure S53: IR spectrum of [Au(CN)$_3$(SIMes)] (**4**) (blue) compared to the calculated spectrum (green; RI-B3LYP-D3/def2-TZVPP level).

IR Spectrum of *trans*-[AuF$_2$(N$_3$)(SIMes)] (5)

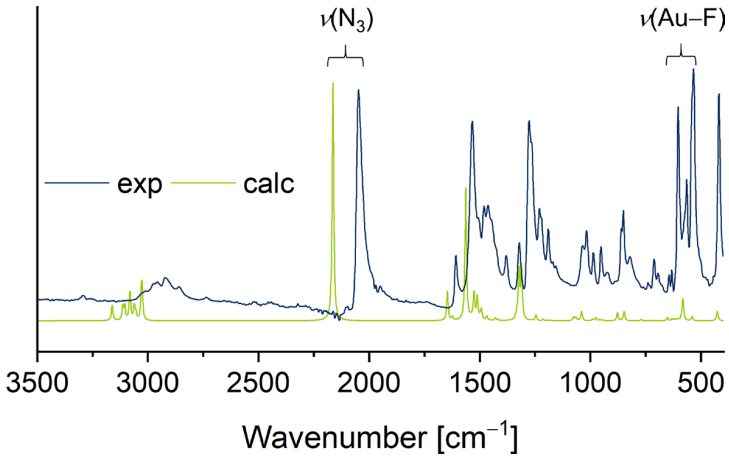

Figure S54: IR spectrum of *trans*-[AuF$_2$(N$_3$)(SIMes)] (**5**) (blue) compared to the calculated spectrum (green; RI-B3LYP-D3/def2-TZVPP level).

IR and Raman Spectrum of $[Au(N_3)_3(SIMes)]$ (6)

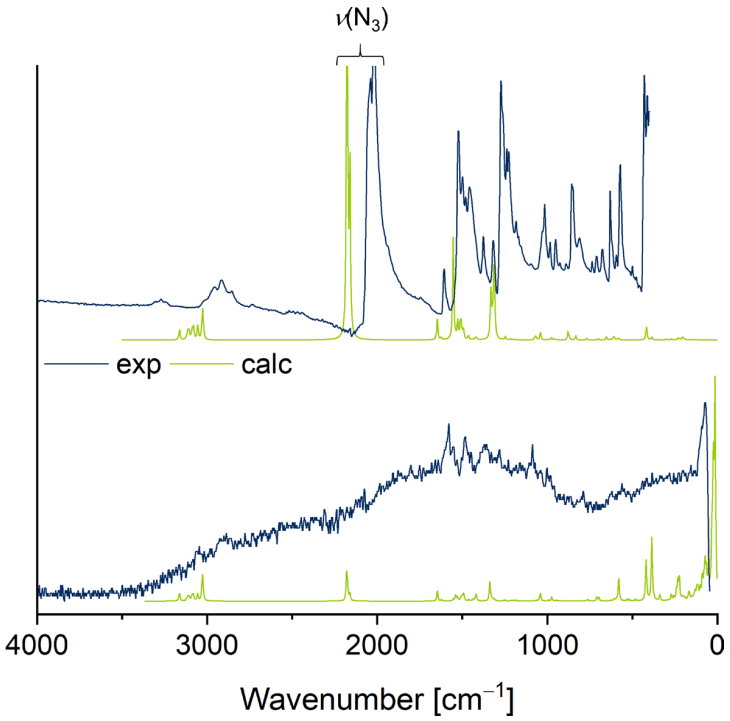

Figure S55: IR (top) and Raman (bottom) spectrum of $[Au(N_3)_3(SIMes)]$ (**6**) (blue) compared to the calculated spectrum (green; RI-B3LYP-D3/def2-TZVPP level).

IR and Raman Spectrum of *trans*-$[AuF_2(OC(CF_3)_3)(SIMes)]$ (7)

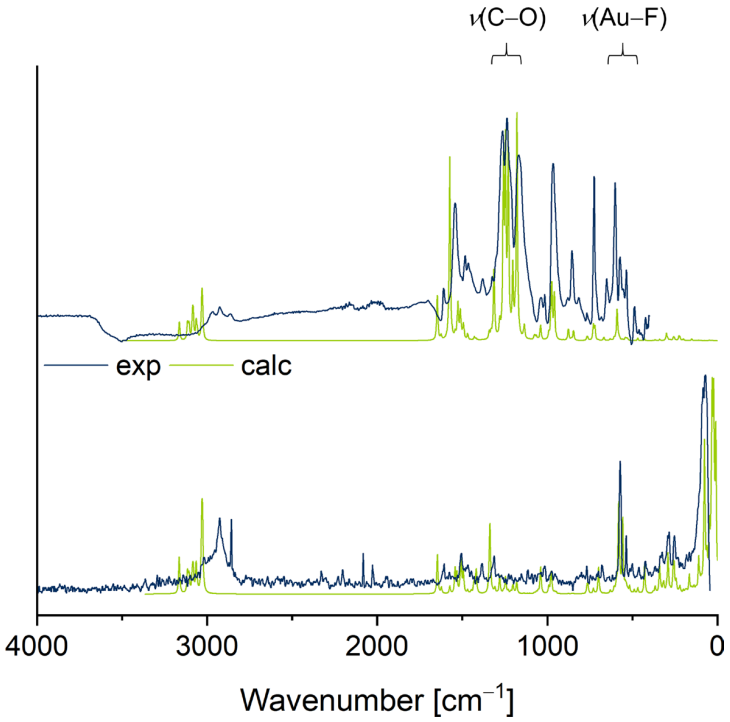

Figure S56: IR (top) and Raman (bottom) spectrum of *trans*-$[AuF_2(OC(CF_3)_3(SIMes)]$ (**7**) (blue) compared to the calculated spectrum (green; RI-B3LYP-D3/def2-TZVPP level).

Raman Spectrum of *trans*-[$AuF_2(OC(CF_3)_2F)$(SIMes)] (10)

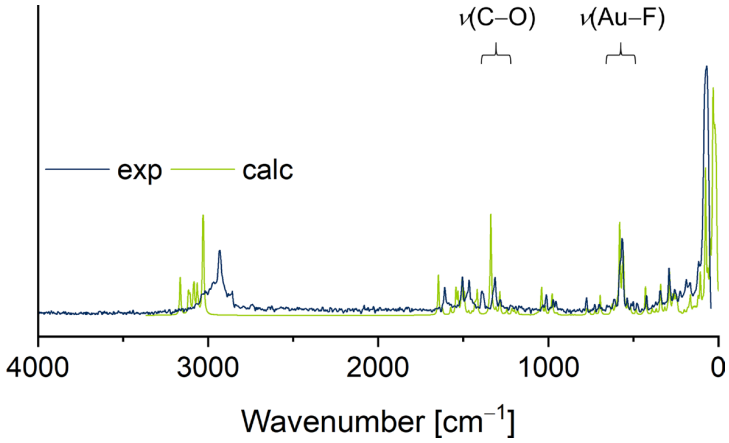

Figure S57: Raman spectrum of *trans*-[$AuF_2(OC(CF_3)_2F)$(SIMes)] (**10**) (blue) compared to the calculated spectrum (green; RI-B3LYP-D3/def2-TZVPP level).

Quantum Chemical Calculations

Coordinates of SIMes on RI-B3LYP-D3/def2-TZVPP Level

xyz-Coordinates [Å] of the optimized minimum structure of SIMes.

49

N	-0.341498	-0.954689	-0.655530	7
C	-0.046845	-0.007084	0.247471	6
C	0.116387	-0.659696	-2.036364	6
C	-0.901240	-2.226587	-0.336126	6
N	0.532726	0.992222	-0.434763	7
C	0.588123	0.790014	-1.904222	6
H	-0.695605	-0.782399	-2.752580	1
H	0.922197	-1.341450	-2.319275	1
C	-0.074497	-3.241678	0.159140	6
C	-2.269195	-2.441225	-0.534884	6
C	0.934299	2.233961	0.139531	6
H	1.597367	0.948370	-2.283290	1
H	-0.076228	1.497318	-2.406701	1
C	-0.641079	-4.483369	0.437525	6
C	1.385779	-2.981106	0.414966	6
C	-2.794717	-3.699133	-0.246216	6
C	-3.156629	-1.324595	-1.016953	6
C	-0.022021	3.227751	0.377464	6
C	2.283572	2.441233	0.445495	6
C	-1.996486	-4.734172	0.234538	6
H	-0.008594	-5.272441	0.828196	1
H	1.897217	-2.639395	-0.487403	1
H	1.888306	-3.880941	0.767367	1
H	1.508247	-2.195694	1.162511	1
H	-3.855602	-3.869998	-0.389459	1
H	-3.035021	-0.437603	-0.393924	1
H	-4.204266	-1.622098	-0.997580	1
H	-2.914680	-1.029449	-2.040751	1
C	0.400820	4.441861	0.913902	6
C	-1.477318	2.972230	0.090045	6
C	2.664182	3.671208	0.978253	6
C	3.292918	1.344154	0.234762	6
C	-2.578541	-6.096698	0.509054	6
C	1.739342	4.685696	1.213720	6
H	-0.335088	5.213975	1.107673	1
H	-1.638226	2.694610	-0.953809	1
H	-2.079065	3.855327	0.300880	1
H	-1.846538	2.143593	0.696446	1
H	3.706650	3.835680	1.226156	1
H	2.968984	0.422367	0.719592	1
H	4.265306	1.625413	0.636982	1
H	3.426063	1.115759	-0.825380	1
H	-2.495103	-6.740542	-0.370814	1
H	-3.635925	-6.034139	0.768144	1
H	-2.057565	-6.595231	1.327272	1
C	2.177799	6.020046	1.759545	6
H	2.423160	6.711180	0.948477	1
H	3.066120	5.922954	2.384611	1
H	1.392010	6.484490	2.356306	1

E_{tot} = −925.15878592856 H

Coordinates of [AuF_3(SIMes)] on RI-B3LYP-D3/def2-TZVPP Level

xyz-Coordinates [Å] of the optimized minimum structure of [AuF_3(SIMes)].

53

C	1.868365	-1.228257	-2.444050	6
C	1.694870	-0.003025	-1.795279	6
C	1.877784	1.222709	-2.446447	6
C	2.254497	1.193250	-3.784882	6
C	2.441056	-0.006927	-4.470427	6
C	2.245462	-1.202808	-3.785563	6
N	1.313211	-0.000181	-0.412077	7
C	0.071191	0.001966	0.049571	6
N	0.047318	0.005369	1.374255	7
C	1.409583	0.008307	1.942151	6
C	2.300626	-0.001244	0.684695	6
C	-1.129944	0.004449	2.194477	6
C	-1.678009	-1.222849	2.584984	6
C	-2.811477	-1.197199	3.390974	6
C	-3.397609	0.000816	3.797984	6
C	-2.822721	1.198865	3.382641	6
C	-1.686726	1.228056	2.576084	6
C	-1.091644	-2.523634	2.107388	6
C	-4.645502	-0.010719	4.640701	6
C	-1.110669	2.531353	2.092805	6
C	1.625363	2.525435	-1.737132	6
C	2.818996	0.002798	-5.928028	6
C	1.606892	-2.529817	-1.735826	6
H	-3.254769	-2.136532	3.699349	1
H	-3.272829	2.137029	3.683624	1
H	2.394499	2.131097	-4.309197	1
H	2.377250	-2.142463	-4.307930	1
H	-1.588212	-3.368161	2.581951	1
H	-1.208506	-2.619221	1.026222	1
H	-0.024969	-2.596618	2.330455	1
H	-4.839215	0.965385	5.084422	1
H	-5.514847	-0.278575	4.035288	1
H	-4.573264	-0.743705	5.445671	1
H	-0.043614	2.611504	2.311390	1
H	-1.231814	2.623869	1.011815	1
H	-1.610664	3.373916	2.567311	1
H	2.167941	-2.605874	-0.801946	1
H	0.547252	-2.623585	-1.490706	1
H	1.889741	-3.373818	-2.362484	1
H	1.904504	3.368210	-2.367096	1
H	0.568075	2.621583	-1.483034	1
H	2.195104	2.601099	-0.808411	1
H	3.090149	-0.992175	-6.279247	1
H	1.985578	0.356702	-6.539339	1
H	3.661961	0.670968	-6.112887	1
H	2.938795	0.878254	0.609591	1
H	2.928915	-0.888484	0.616078	1
H	1.551158	-0.870507	2.569905	1
H	1.552120	0.896189	2.556985	1
Au	-1.556804	0.001647	-1.107916	79
F	-1.541222	1.946940	-1.109178	9
F	-1.554712	-1.943456	-1.091740	9
F	-3.138515	0.002064	-2.237946	9

E_{tot} = −1360.50818584245 H

Coordinates of *trans*-[$AuF_2(OCF_3)$(SIMes)] on RI-B3LYP-D3/def2-TZVPP Level

xyz-Coordinates [Å] of the optimized minimum structure of *trans*-[$AuF_2(OCF_3)$(SIMes)].

57

C	-1.485071	1.227849	2.846049	6
C	-0.926371	0.001317	2.472803	6
C	-1.485136	-1.223896	2.851326	6
C	-2.635670	-1.194594	3.634430	6
C	-3.225228	0.004565	4.030174	6
C	-2.635968	1.201826	3.629346	6
N	0.264306	-0.000392	1.671707	7
C	0.308703	-0.000210	0.349620	6
N	1.551553	-0.000276	-0.103447	7
C	2.527195	-0.001603	1.004686	6
C	1.622269	0.000298	2.253597	6
C	1.933421	-0.000078	-1.488524	6
C	2.101697	-1.225885	-2.140961	6
C	2.448677	-1.197532	-3.488498	6
C	2.620253	0.000680	-4.178313	6
C	2.452052	1.198433	-3.486977	6
C	2.105054	1.226026	-2.139417	6
C	1.864764	-2.529978	-1.428737	6
C	1.871231	2.529826	-1.425678	6
C	2.934274	0.001003	-5.650349	6
Au	-1.290930	-0.001016	-0.854081	79
O	-2.936159	-0.001482	-2.028407	8
C	-0.890750	-2.527086	2.390172	6
C	-4.495231	0.004950	4.838907	6
C	-0.890838	2.529329	2.379805	6
F	-1.282312	1.941779	-0.834865	9
F	-1.287652	-1.943729	-0.823690	9
H	-3.087244	-2.132651	3.933897	1
H	-3.087492	2.141174	3.924694	1
H	2.577539	2.137172	-4.012596	1
H	2.571594	-2.135961	-4.015328	1
H	-1.403502	-3.369491	2.850871	1
H	-0.977149	-2.624356	1.306437	1
H	0.168798	-2.603951	2.643725	1
H	-4.580910	0.904514	5.448526	1
H	-5.366966	-0.029466	4.180487	1
H	-4.549408	-0.862126	5.497585	1
H	0.169278	2.606277	2.630885	1
H	-0.979293	2.623683	1.295969	1
H	-1.402117	3.373395	2.839102	1
H	2.433336	-2.596905	-0.498713	1
H	0.808283	-2.640914	-1.178671	1
H	2.156033	-3.370003	-2.056691	1
H	2.164878	3.369893	-2.052445	1
H	0.814876	2.642817	-1.176122	1
H	2.439493	2.594210	-0.495302	1
H	3.506103	-0.881537	-5.937771	1
H	2.010139	-0.002062	-6.233819	1
H	3.500879	0.886605	-5.938576	1
H	3.162083	0.880765	0.938797	1
H	3.158839	-0.886372	0.939262	1
H	1.756986	-0.882305	2.877257	1
H	1.757042	0.884829	2.874569	1
C	-2.765530	-0.009467	-3.319553	6
F	-3.954625	-0.001851	-3.962102	9
F	-2.060129	1.066429	-3.797854	9
F	-2.079941	-1.102476	-3.787197	9

E_{tot} = −1673.56494040770 H

Coordinates of *trans*-[$AuF_2(OC_2F_5)$(SIMes)] on RI-B3LYP-D3/def2-TZVPP Level

xyz-Coordinates [Å] of the optimized minimum structure of *trans*-[$AuF_2(OC_2F_5)$(SIMes)].

60

C	-1.276209	1.227306	3.052300	6
C	-0.713060	0.000860	2.685543	6
C	-1.273903	-1.224484	3.060581	6
C	-2.431535	-1.195371	3.833126	6
C	-3.025972	0.003706	4.221882	6
C	-2.434206	1.201064	3.825069	6
N	0.483989	-0.000689	1.893891	7
C	0.538269	-0.000190	0.572400	6
N	1.783928	0.000607	0.127720	7
C	2.751786	-0.001133	1.242824	6
C	1.837952	0.001475	2.485391	6
C	2.174084	0.001169	-1.255159	6
C	2.344653	-1.224436	-1.907394	6
C	2.697393	-1.195581	-3.253420	6
C	2.872473	0.002856	-3.941959	6
C	2.702150	1.200379	-3.250700	6
C	2.349327	1.227524	-1.904660	6
C	2.103931	-2.528828	-1.196962	6
C	2.112729	2.531162	-1.191513	6
C	3.192358	0.003802	-5.412703	6
Au	-1.053161	-0.002249	-0.643782	79
O	-2.692055	-0.002501	-1.834086	8
C	-0.674016	-2.527657	2.606547	6
C	-4.303440	0.003674	5.018738	6
C	-0.678956	2.528889	2.590174	6
F	-1.045447	1.940364	-0.628039	9
F	-1.053202	-1.944640	-0.609052	9
H	-2.884875	-2.133509	4.129659	1
H	-2.889313	2.140305	4.115166	1
H	2.830457	2.139299	-3.775323	1
H	2.822103	-2.133801	-3.780159	1
H	-1.190029	-3.369995	3.063686	1
H	-0.750670	-2.626475	1.522244	1
H	0.383264	-2.603104	2.869765	1
H	-4.397009	0.905013	5.624529	1
H	-5.168878	-0.035105	4.352306	1
H	-4.361666	-0.861383	5.679721	1
H	0.379009	2.606632	2.849878	1
H	-0.758615	2.622812	1.505625	1
H	-1.194481	3.372894	3.044783	1
H	2.666391	-2.595582	-0.263245	1
H	1.045931	-2.640750	-0.953875	1
H	2.399864	-3.368516	-1.823155	1
H	2.411215	3.371276	-1.815927	1
H	1.054944	2.645245	-0.948588	1
H	2.675245	2.594372	-0.257589	1
H	3.763361	-0.879718	-5.698681	1
H	2.270503	0.003314	-5.999768	1
H	3.762002	0.888437	-5.697882	1
H	3.387672	0.880798	1.181288	1
H	3.383216	-0.886372	1.181923	1
H	1.968800	-0.880349	3.110910	1
H	1.967655	0.886808	3.106282	1
C	-2.513446	-0.020189	-3.124742	6
C	-3.876375	0.002756	-3.878261	6
F	-1.776232	1.049955	-3.602708	9
F	-1.825181	-1.131405	-3.580123	9
F	-3.691375	-0.015303	-5.207454	9
F	-4.616325	-1.063482	-3.547202	9
F	-4.567023	1.108044	-3.569840	9

E_{tot} = –-1911.37010627796 H

Coordinates of *trans*-[$AuF_2(OC_3F_7)$(SIMes)] on RI-B3LYP-D3/def2-TZVPP Level

xyz-Coordinates [Å] of the optimized minimum structure of *trans*-[$AuF_2(OC_3F_7)$(SIMes)].

63

C	-1.233588	1.318822	3.212379	6
C	-0.640630	0.101542	2.862537	6
C	-1.179169	-1.132138	3.242569	6
C	-2.345012	-1.120992	4.003503	6
C	-2.968043	0.068427	4.376294	6
C	-2.397799	1.274728	3.974543	6
N	0.563838	0.119202	2.082584	7
C	0.631914	0.070305	0.762634	6
N	1.881933	0.085486	0.330021	7
C	2.837037	0.168399	1.452902	6
C	1.911492	0.162756	2.686755	6
C	2.285178	0.043410	-1.048596	6
C	2.521715	-1.201096	-1.641795	6
C	2.880276	-1.218009	-2.985794	6
C	2.992692	-0.046530	-3.731236	6
C	2.758943	1.171886	-3.098168	6
C	2.401860	1.244992	-1.754635	6
C	2.332913	-2.481354	-0.874610	6
C	2.101727	2.568322	-1.104171	6
C	3.308603	-0.101642	-5.201603	6
Au	-0.942535	-0.011957	-0.470665	79
O	-2.573727	-0.100537	-1.665875	8
C	-0.547295	-2.426626	2.806805	6
C	-4.252928	0.049356	5.160916	6
C	-0.660787	2.627904	2.741114	6
F	-1.031481	1.928878	-0.447494	9
F	-0.850204	-1.953660	-0.449406	9
H	-2.781203	-2.065968	4.303993	1
H	-2.875846	2.206524	4.251511	1
H	2.839834	2.090194	-3.666840	1
H	3.052613	-2.172596	-3.467800	1
H	-1.043497	-3.274750	3.275056	1
H	-0.618815	-2.544230	1.723891	1
H	0.511117	-2.472811	3.072022	1
H	-4.357976	0.942150	5.777526	1
H	-5.111791	0.014425	4.485815	1
H	-4.311835	-0.824562	5.809948	1
H	0.390591	2.735598	3.016557	1
H	-0.725951	2.702055	1.654135	1
H	-1.204180	3.465536	3.174561	1
H	2.883063	-2.480061	0.068687	1
H	1.276936	-2.629065	-0.642200	1
H	2.676216	-3.334037	-1.457628	1
H	2.374912	3.391105	-1.762343	1
H	1.037337	2.651919	-0.878084	1
H	2.648274	2.695843	-0.167376	1
H	3.953627	-0.947424	-5.440977	1
H	2.388399	-0.216748	-5.780041	1
H	3.798110	0.811079	-5.541408	1
H	3.425668	1.081053	1.368441	1
H	3.515363	-0.682894	1.426165	1
H	2.057548	-0.709290	3.323030	1
H	2.013839	1.057192	3.299175	1
C	-2.509247	0.086081	-2.974163	6
C	-3.973005	0.222448	-3.512664	6
F	-1.870135	1.278827	-3.342460	9
C	-1.696110	-1.020289	-3.734594	6
F	-4.003868	0.521958	-4.820951	9
F	-4.657754	-0.917196	-3.334929	9
F	-4.604604	1.199405	-2.854879	9
F	-1.690247	-0.839165	-5.064475	9
F	-0.410933	-0.993596	-3.324842	9
F	-2.183372	-2.238582	-3.483367	9

E_{tot} = −2149.17250496802 H

Coordinates of *trans*-[$AuF_2(OC_4F_9)$(SIMes)] on RI-B3LYP-D3/def2-TZVPP Level

xyz-Coordinates [Å] of the optimized minimum structure of *trans*-[$AuF_2(OC_4F_9)$(SIMes)].

66

C	-1.136906	1.234379	3.377348	6
C	-0.573129	0.003537	3.026332	6
C	-1.150093	-1.217169	3.390963	6
C	-2.323916	-1.179131	4.138473	6
C	-2.918818	0.024455	4.511960	6
C	-2.311346	1.217261	4.124985	6
N	0.640267	-0.007202	2.260412	7
C	0.721569	0.012928	0.940617	6
N	1.976715	0.009688	0.521500	7
C	2.921096	-0.025848	1.655593	6
C	1.981933	-0.016697	2.879404	6
C	2.390162	0.037239	-0.854770	6
C	2.545506	-1.173036	-1.538350	6
C	2.902009	-1.114011	-2.882469	6
C	3.097788	0.098796	-3.538515	6
C	2.950087	1.279898	-2.814907	6
C	2.590783	1.277003	-1.470899	6
C	2.281025	-2.492885	-0.866395	6
C	2.362268	2.565372	-0.728406	6
C	3.409069	0.135093	-5.010439	6
Au	-0.832189	0.027414	-0.321425	79
O	-2.439475	0.064776	-1.547631	8
C	-0.549651	-2.524632	2.950389	6
C	-4.213137	0.035284	5.281132	6
C	-0.522631	2.531040	2.923517	6
F	-0.810636	1.972224	-0.316338	9
F	-0.855576	-1.915711	-0.268132	9
H	-2.789793	-2.113749	4.426548	1
H	-2.766910	2.159996	4.402899	1
H	3.093829	2.230227	-3.314373	1
H	3.009386	-2.039818	-3.434257	1
H	-1.086675	-3.363467	3.389441	1
H	-0.595795	-2.618562	1.863973	1
H	0.498752	-2.610958	3.244181	1
H	-4.302014	0.927276	5.901449	1
H	-5.064474	0.026599	4.595718	1
H	-4.302881	-0.840173	5.924540	1
H	0.532215	2.600295	3.197771	1
H	-0.586015	2.625790	1.837840	1
H	-1.037767	3.379326	3.370569	1
H	2.818585	-2.585073	0.079578	1
H	1.216905	-2.605890	-0.653106	1
H	2.589272	-3.318247	-1.505597	1
H	2.688335	3.416142	-1.324002	1
H	1.300854	2.690021	-0.507332	1
H	2.904135	2.595110	0.219144	1
H	3.941810	-0.760601	-5.330079	1
H	2.483553	0.191401	-5.589168	1
H	4.011829	1.005311	-5.271162	1
H	3.578449	0.841448	1.617842	1
H	3.533106	-0.925024	1.597480	1
H	2.093397	-0.899468	3.507088	1
H	2.105820	0.867662	3.503191	1
C	-2.423765	-0.076576	-2.898963	6
C	-3.927082	0.063186	-3.354064	6
C	-1.574175	1.045461	-3.613298	6
C	-1.884661	-1.491003	-3.343816	6
F	-4.048198	0.205367	-4.686422	9
F	-4.629834	-1.021042	-2.996082	9

F	-4.498294	1.123744	-2.779911	9
F	-2.154596	-1.770925	-4.631682	9
F	-0.543363	-1.545143	-3.196456	9
F	-2.411961	-2.457302	-2.597503	9
F	-1.422636	0.827192	-4.931855	9
F	-2.143950	2.244541	-3.457953	9
F	-0.338168	1.116863	-3.086120	9

E_{tot} = −2386.97677114289 H

Coordinates of *trans*-[$AuF_2(N_3)$(SIMes)] on RI-B3LYP-D3/def2-TZVPP Level

xyz-Coordinates [Å] of the optimized minimum structure of *trans*-[$AuF_2(N_3)$(SIMes)].

55

C	2.010127	1.262201	-2.359573	6
C	1.827275	0.040013	-1.704975	6
C	1.974085	-1.188134	-2.357775	6
C	2.329265	-1.167374	-3.703848	6
C	2.527465	0.027511	-4.392848	6
C	2.364770	1.228655	-3.705573	6
N	1.470135	0.045953	-0.315912	7
C	0.235024	0.059551	0.161231	6
N	0.231406	0.054662	1.485359	7
C	1.601635	0.039110	2.036438	6
C	2.474954	0.031567	0.766482	6
C	-0.938009	0.061154	2.315739	6
C	-1.500265	-1.161295	2.697403	6
C	-2.630578	-1.128484	3.509622	6
C	-3.198660	0.072656	3.929648	6
C	-2.609963	1.267688	3.521255	6
C	-1.479125	1.289177	2.709124	6
C	-0.934778	-2.465580	2.203793	6
C	-0.891113	2.587704	2.227401	6
C	-4.447591	0.078613	4.770888	6
Au	-1.448558	0.065592	-0.996362	79
N	-3.128084	0.160796	-2.151878	7
N	-3.627575	-0.896927	-2.484879	7
N	-4.163567	-1.833440	-2.844135	7
C	1.705944	-2.485601	-1.644108	6
C	2.867619	0.021176	-5.859735	6
C	1.779231	2.567349	-1.647388	6
F	-1.489226	-1.885228	-1.008470	9
F	-1.405966	2.020966	-0.982933	9
H	2.506437	2.165069	-4.231633	1
H	2.443284	-2.108356	-4.228473	1
H	-3.083706	-2.064903	3.812111	1
H	-3.046980	2.208782	3.832736	1
H	2.055389	3.407805	-2.281769	1
H	0.726297	2.671399	-1.377691	1
H	2.362852	2.638657	-0.727055	1
H	3.434290	-0.868691	-6.134605	1
H	1.956517	0.028526	-6.463515	1
H	3.451341	0.898734	-6.138362	1
H	2.279427	-2.568639	-0.718528	1
H	0.648825	-2.565937	-1.383200	1
H	1.967086	-3.334131	-2.274034	1
H	0.177412	2.656291	2.442567	1
H	-1.015383	2.683152	1.146796	1
H	-1.381072	3.434425	2.704961	1
H	-1.433603	-3.307840	2.680007	1
H	-1.068790	-2.554719	1.123923	1
H	0.134169	-2.551356	2.409985	1
H	-4.501452	0.967161	5.400170	1
H	-5.336730	0.072762	4.135192	1
H	-4.500315	-0.800292	5.413821	1
H	1.742800	-0.846580	2.654736	1
H	1.761734	0.920052	2.656870	1

H	3.117520	0.907602	0.687510	1
H	3.096772	-0.859008	0.683489	1

E_{tot} = −1424.84057734394 H

Coordinates of [Au(N_3)$_3$(SIMes)] on RI-B3LYP-D3/def2-TZVPP Level

xyz-Coordinates [Å] of the optimized minimum structure of [Au(N_3)$_3$(SIMes)].

59

C	-1.189749	-1.289304	3.020891	6
C	-0.785406	-0.074526	2.456067	6
C	-1.459306	1.125166	2.708937	6
C	-2.587314	1.076359	3.525157	6
C	-3.038299	-0.115792	4.085875	6
C	-2.321023	-1.283288	3.831242	6
N	0.369267	-0.057679	1.604980	7
C	0.358853	-0.043961	0.278180	6
N	1.591950	0.037877	-0.204745	7
C	2.603895	0.043575	0.870092	6
C	1.738988	0.079035	2.142118	6
C	1.943471	0.040051	-1.594697	6
C	2.005278	-1.178680	-2.280090	6
C	2.319443	-1.144439	-3.636178	6
C	2.571600	0.052496	-4.303147	6
C	2.526795	1.240294	-3.577376	6
C	2.218855	1.260770	-2.220566	6
C	1.729506	-2.483836	-1.582793	6
C	2.182486	2.560842	-1.462256	6
C	2.847357	0.069648	-5.782828	6
Au	-1.341647	-0.113099	-0.884374	79
N	-1.502760	-2.114157	-0.368797	7
C	-0.996100	2.429143	2.115915	6
C	-4.288866	-0.149547	4.923578	6
C	-0.439439	-2.564932	2.750885	6
N	-1.153658	1.911592	-1.257881	7
N	-3.009494	-0.292009	-2.063384	7
N	-3.631942	0.708379	-2.362474	7
N	-4.274935	1.586914	-2.689749	7
H	2.713650	2.179249	-4.083505	1
H	2.361438	-2.077276	-4.185426	1
H	-2.655432	-2.216997	4.267196	1
H	-3.125998	1.994713	3.725379	1
H	2.138383	3.403626	-2.149066	1
H	1.315863	2.615297	-0.804562	1
H	3.078190	2.684427	-0.847338	1
H	3.248948	-0.883391	-6.126995	1
H	1.925711	0.259963	-6.338532	1
H	3.554734	0.856024	-6.047677	1
H	2.334098	-2.591903	-0.679620	1
H	0.684444	-2.563684	-1.278806	1
H	1.956204	-3.324115	-2.236697	1
H	0.071924	2.588693	2.277851	1
H	-1.164438	2.465400	1.039055	1
H	-1.528099	3.265230	2.566520	1
H	-0.945532	-3.413571	3.207838	1
H	-0.368754	-2.747169	1.678871	1
H	0.574020	-2.529898	3.158329	1
H	-4.467677	0.807317	5.414185	1
H	-5.160245	-0.366512	4.300446	1
H	-4.235443	-0.923072	5.690089	1
H	1.957472	-0.736502	2.828414	1
H	1.824732	1.019727	2.686562	1
H	3.251924	0.912287	0.771331	1
H	3.217109	-0.855174	0.799516	1
N	-0.937726	2.243633	-2.408255	7
N	-0.721837	2.653692	-3.446706	7
N	-2.496702	-2.705406	-0.753028	7

N -3.388765 -3.331505 -1.067955 7

E_{tot} = −1553.50892252747 H

Coordinates of *trans*-[Au(CN)F_2(SIMes)] on RI-B3LYP-D3/def2-TZVPP Level

xyz-Coordinates [Å] of the optimized minimum structure of *trans*-[Au(CN)F_2(SIMes)].

54
C 1.952208 -1.227769 -2.379751 6
C 1.780687 -0.001904 -1.728370 6
C 1.952922 1.222864 -2.381589 6
C 2.315730 1.194496 -3.725461 6
C 2.498619 -0.004137 -4.412098 6
C 2.315166 -1.201639 -3.723610 6
N 1.408864 -0.000741 -0.342786 7
C 0.167817 0.000004 0.118542 6
N 0.147889 0.000905 1.442383 7
C 1.511250 0.000832 2.010846 6
C 2.400377 -0.000379 0.752073 6
C -1.033539 0.002027 2.256203 6
C -1.590184 1.227853 2.635565 6
C -2.734984 1.201701 3.427540 6
C -3.322054 0.004200 3.831251 6
C -2.736097 -1.194426 3.429205 6
C -1.591297 -1.222761 2.637338 6
C -1.000754 2.529650 2.163832 6
C -1.003068 -2.525752 2.167419 6
C -4.586668 0.005298 4.648450 6
Au -1.518215 -0.000307 -1.073145 79
F -1.482939 1.947815 -1.050341 9
C 1.707121 2.525876 -1.670000 6
C 2.845170 -0.005403 -5.877327 6
C 1.705570 -2.529555 -1.666205 6
C -3.161413 -0.000674 -2.235620 6
F -1.484585 -1.948416 -1.046816 9
H 2.447865 2.132817 -4.250522 1
H 2.447157 -2.140826 -4.247157 1
H -3.186363 -2.132758 3.729858 1
H -3.184256 2.140880 3.727035 1
H 1.978264 3.368745 -2.303235 1
H 0.652790 2.622684 -1.404505 1
H 2.286756 2.602302 -0.747638 1
H 3.422438 -0.888850 -6.150684 1
H 1.936276 -0.007216 -6.484408 1
H 3.420336 0.878766 -6.152739 1
H 2.285225 -2.604988 -0.743774 1
H 0.651198 -2.625285 -1.400495 1
H 1.976112 -3.373546 -2.298198 1
H 0.062565 2.605367 2.400959 1
H -1.103562 2.625087 1.081329 1
H -1.505746 3.373660 2.630261 1
H -1.509141 -3.368655 2.634674 1
H -1.105567 -2.622395 1.084998 1
H 0.060073 -2.602312 2.405077 1
H -4.652556 0.890233 5.281684 1
H -5.463069 0.003783 3.995337 1
H -4.651963 -0.877365 5.284922 1
H 1.653743 -0.882097 2.632678 1
H 1.654353 0.884563 2.631404 1
H 3.033898 0.882652 0.678393 1
H 3.033188 -0.884020 0.679601 1
N -4.103606 -0.000881 -2.902382 7

E_{tot} = −1353.48116081317 H

Coordinates of [$Au(CN)_3$(SIMes)] on RI-B3LYP-D3/def2-TZVPP Level

xyz-Coordinates [Å] of the optimized minimum structure of [$Au(CN)_3$(SIMes)].

56

C	-1.679323	-1.156523	2.536572	6
C	-0.996964	0.041328	2.288451	6
C	-1.413442	1.262062	2.832901	6
C	-2.576037	1.266642	3.598134	6
C	-3.306285	0.105121	3.837009	6
C	-2.834901	-1.095513	3.310925	6
N	0.176714	0.015133	1.463920	7
C	0.196658	-0.000111	0.138795	6
N	1.439035	-0.015204	-0.322686	7
C	2.428837	0.005728	0.773348	6
C	1.540486	-0.005616	2.030676	6
C	1.823624	-0.041120	-1.704516	6
C	2.197733	-1.261716	-2.279258	6
C	2.528843	-1.266284	-3.631099	6
C	2.508267	-0.104870	-4.399352	6
C	2.170255	1.095667	-3.778974	6
C	1.828144	1.156668	-2.430645	6
C	2.271373	-2.535426	-1.480667	6
C	1.473991	2.476145	-1.797109	6
C	2.816569	-0.150668	-5.871949	6
Au	-1.502599	-0.000506	-1.062845	79
C	-1.164411	-1.929650	-1.531969	6
C	-0.636798	2.535944	2.633993	6
C	-4.590049	0.150755	4.621629	6
C	-1.200664	-2.476004	1.990999	6
C	-1.833629	1.928444	-0.587856	6
C	-3.146597	-0.000884	-2.226752	6
N	-4.087627	-0.001079	-2.893381	7
H	2.171031	2.011365	-4.357968	1
H	2.798536	-2.206573	-4.096586	1
H	-3.379846	-2.011280	3.506223	1
H	-2.924389	2.207003	4.007922	1
H	1.919129	3.298095	-2.355545	1
H	0.396582	2.640371	-1.776284	1
H	1.821286	2.543062	-0.765764	1
H	3.521620	-0.947770	-6.108223	1
H	1.905411	-0.338893	-6.445430	1
H	3.234711	0.792999	-6.222573	1
H	3.276428	-2.672679	-1.070779	1
H	1.559408	-2.549249	-0.659592	1
H	2.046633	-3.395008	-2.108416	1
H	0.085970	2.674004	3.443634	1
H	-0.101568	2.549384	1.688152	1
H	-1.303902	3.395254	2.631924	1
H	-1.580456	-3.298152	2.595494	1
H	-1.538734	-2.638966	0.967594	1
H	-0.112551	-2.543982	1.976286	1
H	-4.576709	0.948786	5.364105	1
H	-5.436275	0.337333	3.955591	1
H	-4.779094	-0.792441	5.134405	1
H	1.669953	-0.901875	2.636988	1
H	1.689397	0.866287	2.665116	1
H	3.043489	0.902030	0.692783	1
H	3.076635	-0.866128	0.701833	1
N	-1.970162	3.038639	-0.305507	7
N	-0.943737	-3.040076	-1.753676	7

E_{tot} = −1339.44625759901 H

Coordinates of *trans*-[Au(CCH)F_2(SIMes)] on RI-B3LYP-D3/def2-TZVPP Level

xyz-Coordinates [Å] of the optimized minimum structure of *trans*-[Au(CCH)F_2(SIMes)].

55
C 2.044508 -1.226525 -2.314348 6
C 1.871328 -0.001249 -1.662653 6
C 2.045830 1.223013 -2.315864 6
C 2.419083 1.195195 -3.657001 6
C 2.608250 -0.003306 -4.341948 6
C 2.417775 -1.200759 -3.655531 6
N 1.495165 -0.000210 -0.279359 7
C 0.250630 0.000129 0.177090 6
N 0.236242 0.000873 1.502591 7
C 1.598301 0.001237 2.072279 6
C 2.487213 0.000140 0.814029 6
C -0.941771 0.001444 2.319480 6
C -1.498612 -1.222999 2.702324 6
C -2.637637 -1.195616 3.502767 6
C -3.220173 0.002644 3.910328 6
C -2.637472 1.200324 3.501167 6
C -1.498469 1.226522 2.700709 6
C -0.916954 -2.524602 2.220907 6
C -4.478114 0.003316 4.738310 6
C -0.916640 2.527439 2.217686 6
C 1.786770 2.524815 -1.607036 6
C 2.967433 -0.004316 -5.804444 6
C 1.784061 -2.527214 -1.603992 6
H -3.086125 -2.134297 3.805354 1
H -3.085833 2.139471 3.802521 1
H 2.554095 2.133707 -4.181210 1
H 2.551748 -2.140076 -4.178562 1
H -1.419636 -3.369240 2.689041 1
H -1.030378 -2.613761 1.138650 1
H 0.148586 -2.603490 2.446836 1
H -4.537282 0.886784 5.374436 1
H -5.360655 0.004431 4.093400 1
H -4.538847 -0.880631 5.373594 1
H 0.148808 2.606683 2.443943 1
H -1.029667 2.615154 1.135264 1
H -1.419494 3.372691 2.684517 1
H 2.353046 -2.605734 -0.675180 1
H 0.726041 -2.615229 -1.349138 1
H 2.056549 -3.372657 -2.233458 1
H 2.058960 3.369278 -2.237946 1
H 0.729088 2.613713 -1.351154 1
H 2.356850 2.604288 -0.678970 1
H 3.544303 -0.889416 -6.073616 1
H 2.064324 -0.002205 -6.420218 1
H 3.548480 0.878007 -6.073779 1
H 3.121384 0.883089 0.741152 1
H 3.120831 -0.883306 0.742255 1
H 1.741876 -0.881468 2.694637 1
H 1.742027 0.884915 2.693228 1
Au -1.445772 -0.000093 -1.021963 79
C -3.075328 -0.000186 -2.174507 6
F -1.407335 1.951398 -0.996924 9
F -1.409349 -1.951570 -0.993868 9
C -4.060337 -0.000246 -2.871176 6
H -4.927703 -0.000302 -3.484651 1

E_{tot} = −1337.36931192370 H

Coordinates of *trans*-[Au(CCSiMe$_3$)F$_2$(SIMes)] on RI-B3LYP-D3/def2-TZVPP Level

xyz-Coordinates [Å] of the optimized minimum structure of *trans*-[Au(CCSiMe$_3$)F$_2$(SIMes)].

67

C	-0.384259	1.223608	3.484875	6
C	0.175264	-0.000339	3.104146	6
C	-0.379636	-1.225842	3.486500	6
C	-1.519332	-1.200679	4.286092	6
C	-2.104561	-0.003553	4.693141	6
C	-1.523825	1.195245	4.284455	6
N	1.352661	0.001338	2.286424	7
C	1.364407	-0.000734	0.960882	6
N	2.608158	0.000826	0.502316	7
C	3.602379	0.004844	1.593777	6
C	2.715736	0.004383	2.853765	6
C	2.980302	-0.000296	-0.882029	6
C	3.154451	-1.225578	-1.533418	6
C	3.522141	-1.199941	-2.876157	6
C	3.706013	-0.002556	-3.564484	6
C	3.515920	1.195991	-2.879851	6
C	3.148158	1.223874	-1.537193	6
C	2.900224	-2.526329	-0.820939	6
C	2.887371	2.525518	-0.828715	6
C	4.059151	-0.003807	-5.028461	6
Au	-0.336555	-0.005474	-0.236484	79
F	-0.295718	-1.957451	-0.210969	9
C	0.204515	-2.526315	3.005064	6
C	-3.363194	-0.005176	5.520083	6
C	0.195020	2.525575	3.001632	6
C	-1.965953	-0.008947	-1.383845	6
C	-2.960183	-0.008511	-2.083833	6
F	-0.305945	1.946785	-0.211556	9
H	-1.966192	-2.140238	4.588385	1
H	-1.974283	2.133523	4.585394	1
H	3.645795	2.134430	-3.405491	1
H	3.656940	-2.139338	-3.398848	1
H	-0.296167	-3.371952	3.473541	1
H	0.090701	-2.615912	1.922862	1
H	1.270322	-2.602942	3.230431	1
H	-3.423189	0.876804	6.158191	1
H	-4.245226	-0.002718	4.874465	1
H	-3.424261	-0.890603	6.153255	1
H	1.260384	2.606817	3.227510	1
H	0.081412	2.612781	1.919221	1
H	-0.309307	3.369996	3.468392	1
H	3.472604	-2.602352	0.105971	1
H	1.843310	-2.616924	-0.562404	1
H	3.172793	-3.371669	-1.450520	1
H	3.155899	3.370254	-1.460834	1
H	1.830004	2.611822	-0.570546	1
H	3.459220	2.607160	0.098046	1
H	4.637895	-0.887206	-5.299184	1
H	3.153524	-0.005359	-5.640543	1
H	4.636041	0.880220	-5.301107	1
H	4.233892	0.889572	1.519096	1
H	4.238435	-0.876813	1.521592	1
H	2.862211	-0.878003	3.475936	1
H	2.859008	0.888381	3.474368	1
Si	-4.453817	0.000690	-3.136545	14
C	-4.981840	-1.770848	-3.481385	6
C	-5.832332	0.913143	-2.239562	6
C	-4.059442	0.874296	-4.754805	6
H	-5.874914	-1.797881	-4.110560	1
H	-4.189009	-2.319839	-3.992583	1
H	-5.204805	-2.297530	-2.551763	1
H	-6.741793	0.940536	-2.844741	1
H	-6.069410	0.424585	-1.292704	1

H	-5.538392	1.941138	-2.020328	1
H	-4.934684	0.900483	-5.408526	1
H	-3.739660	1.901891	-4.573018	1
H	-3.254378	0.363148	-5.285879	1

E_{tot} = −1746.00846648550 H

Coordinates of *trans*-[Au(CF$_3$)F$_2$(SIMes)] on RI-B3LYP-D3/def2-TZVPP Level

xyz-Coordinates [Å] of the optimized minimum structure of *trans*-[Au(CF$_3$)F$_2$(SIMes)].

56

N	0.265434	-1.053720	-1.125435	7
N	-0.285073	1.055271	-1.119050	7
C	-0.000294	0.000983	-0.369108	6
C	-0.220940	0.746332	-2.562163	6
C	0.163584	-0.745915	-2.566609	6
C	0.608936	-2.354146	-0.630585	6
C	1.956254	-2.659146	-0.412083	6
C	2.264828	-3.930594	0.064369	6
C	1.275545	-4.875389	0.329662	6
C	-0.055442	-4.527050	0.109144	6
C	-0.415553	-3.268902	-0.366619	6
C	3.029762	-1.627311	-0.629781	6
C	1.633971	-6.228072	0.886190	6
C	-1.860708	-2.885241	-0.536696	6
C	-0.614208	2.356405	-0.616364	6
C	-1.954340	2.661395	-0.357403	6
C	-2.248573	3.933520	0.126211	6
C	-1.252034	4.879068	0.359522	6
C	0.071742	4.530844	0.098855	6
C	0.417534	3.271937	-0.385466	6
C	-3.033802	1.629052	-0.540256	6
C	-1.594158	6.232389	0.924672	6
C	1.856860	2.888254	-0.599442	6
H	0.523302	1.378161	-3.046026	1
H	-1.187153	0.937542	-3.027955	1
H	-0.593203	-1.378157	-3.030101	1
H	1.117127	-0.937547	-3.057612	1
H	3.302954	-4.183899	0.243208	1
H	-0.835614	-5.247715	0.323133	1
H	2.983709	-1.194961	-1.631453	1
H	4.018469	-2.064464	-0.500935	1
H	2.919792	-0.809934	0.086002	1
H	1.645717	-6.201632	1.978866	1
H	2.623174	-6.546418	0.556461	1
H	0.912037	-6.987762	0.585723	1
H	-2.137629	-2.117107	0.188557	1
H	-2.509730	-3.746358	-0.386785	1
H	-2.062233	-2.483942	-1.532017	1
H	-3.280780	4.186685	0.336645	1
H	0.857806	5.252252	0.287313	1
H	-3.012932	1.188701	-1.539247	1
H	-4.018590	2.068230	-0.390094	1
H	-2.907165	0.817138	0.179031	1
H	-2.588902	6.554379	0.615719	1
H	-0.876054	6.989993	0.610172	1
H	-1.583838	6.204680	2.017330	1
H	2.153173	2.114510	0.111990	1
H	2.510842	3.747721	-0.462107	1
H	2.029494	2.494228	-1.603109	1
Au	0.020899	-0.000149	1.738499	79
F	-1.875844	-0.473591	1.764844	9
F	1.915952	0.474517	1.698070	9
C	-0.001375	-0.011536	3.821374	6
F	-0.397444	-1.214519	4.300135	9
F	-0.870792	0.907158	4.305943	9
F	1.195506	0.253833	4.376858	9

E_{tot} = −1598.31784268855 H

Coordinates of [Au(CF_3)$_3$(SIMes)] on RI-B3LYP-D3/def2-TZVPP Level

62

N	0.227237	-1.037488	-1.220156	7
N	-0.357379	1.065655	-1.187347	7
C	-0.030808	0.012328	-0.436997	6
C	-0.175505	0.780848	-2.625679	6
C	-0.084135	-0.743294	-2.634271	6
C	0.661916	-2.339778	-0.804076	6
C	1.970022	-2.739137	-1.123696	6
C	2.402765	-3.984552	-0.684250	6
C	1.579784	-4.837770	0.047182	6
C	0.276640	-4.430092	0.303250	6
C	-0.211746	-3.194330	-0.119421	6
C	2.907155	-1.883288	-1.936146	6
C	2.099308	-6.151539	0.566308	6
C	-1.646960	-2.844657	0.171176	6
C	-0.708560	2.375688	-0.723328	6
C	-2.023264	2.827260	-0.919523	6
C	-2.363925	4.085348	-0.436287	6
C	-1.444285	4.899684	0.219733	6
C	-0.139858	4.439413	0.353687	6
C	0.257796	3.189244	-0.117656	6
C	-3.063950	2.016698	-1.647974	6
C	-1.860613	6.229603	0.788575	6
C	1.698354	2.779626	0.036363	6
H	0.744173	1.260997	-2.969364	1
H	-1.007728	1.166426	-3.207269	1
H	-1.031834	-1.220545	-2.895482	1
H	0.690840	-1.125307	-3.292083	1
H	3.418145	-4.290345	-0.907739	1
H	-0.389650	-5.089590	0.846789	1
H	2.868725	-2.164493	-2.992534	1
H	3.933847	-2.020590	-1.600496	1
H	2.676781	-0.824903	-1.855599	1
H	2.598019	-6.009831	1.528504	1
H	2.826714	-6.591736	-0.116556	1
H	1.293047	-6.869304	0.717566	1
H	-1.779237	-2.545815	1.212123	1
H	-2.283502	-3.714191	0.005884	1
H	-2.015836	-2.029548	-0.444199	1
H	-3.382520	4.432461	-0.564353	1
H	0.599217	5.069108	0.835074	1
H	-2.855960	0.951596	-1.618843	1
H	-3.129463	2.327599	-2.694692	1
H	-4.045322	2.169429	-1.201313	1
H	-2.634561	6.699624	0.180984	1
H	-1.016997	6.916226	0.860077	1
H	-2.267218	6.102666	1.795142	1
H	1.915848	2.475319	1.060174	1
H	2.352428	3.621075	-0.193621	1
H	1.974383	1.948595	-0.606895	1
Au	0.014702	-0.041020	1.678322	79
C	-0.022014	-0.215511	3.784078	6
F	-0.521016	-1.432207	4.130034	9
F	-0.813716	0.711332	4.374689	9
F	1.175174	-0.118629	4.399275	9
C	-2.098735	0.271547	1.766137	6
F	-2.745874	0.075649	0.569393	9
F	-2.402911	1.542370	2.126451	9
F	-2.744460	-0.541058	2.636246	9
C	2.131819	-0.305880	1.698330	6
F	2.717724	-0.248641	0.457824	9
F	2.782131	0.644465	2.418018	9
F	2.504850	-1.502816	2.210460	9

E_{tot} = −2073.93400595089 H

Coordinates of *trans*-[AuClF$_2$(SIMes)] on RI-B3LYP-D3/def2-TZVPP Level

xyz-Coordinates [Å] of the optimized minimum structure of *trans*-[AuClF$_2$(SIMes)].

53

C	1.148350	-4.348343	-2.377650	6
C	0.421444	-4.385923	-1.189689	6
C	-0.184349	-3.248176	-0.662929	6
C	-0.046213	-2.051095	-1.372620	6
C	0.675995	-1.968052	-2.567628	6
C	1.261743	-3.134239	-3.052009	6
N	-0.665503	-0.863861	-0.856765	7
C	-0.110382	-0.003450	-0.018148	6
N	-0.931676	0.993661	0.270525	7
C	-2.222531	0.854483	-0.433995	6
C	-2.041211	-0.462118	-1.214580	6
Au	1.759737	-0.203396	0.752430	79
F	2.465236	0.749368	-0.794310	9
C	-0.628636	2.109682	1.119924	6
C	-0.946519	2.029858	2.479451	6
C	-0.645079	3.128549	3.279590	6
C	-0.041682	4.272413	2.760611	6
C	0.259326	4.309152	1.400737	6
C	-0.021794	3.237402	0.557540	6
C	-1.546356	0.780942	3.066369	6
C	-0.920680	-3.296201	0.648515	6
C	0.359833	3.272908	-0.897745	6
C	0.857516	-0.654364	-3.278110	6
C	0.317525	5.426447	3.658698	6
C	1.833335	-5.583296	-2.900120	6
F	0.971793	-1.147749	2.264803	9
Cl	3.880280	-0.440948	1.642839	17
H	-0.840773	-0.048773	2.993890	1
H	-0.395791	-2.708421	1.403988	1
H	1.150520	2.548619	-1.102894	1
H	-1.795994	0.928627	4.115618	1
H	-2.459606	0.483607	2.546177	1
H	-1.931736	-2.892009	0.562829	1
H	-1.002414	-4.320539	1.007778	1
H	0.720435	4.261056	-1.178022	1
H	-0.484226	3.030271	-1.546983	1
H	-2.743331	-1.236782	-0.908489	1
H	-2.121206	-0.332204	-2.293080	1
H	-2.383520	1.714447	-1.082977	1
H	-3.036334	0.811339	0.288540	1
H	-0.877017	3.083379	4.336815	1
H	0.331043	-5.321943	-0.651830	1
H	0.735336	5.189328	0.985537	1
H	1.830284	-3.089282	-3.973063	1
H	1.360664	-0.797506	-4.232820	1
H	1.459290	0.024091	-2.670648	1
H	-0.097117	-0.161920	-3.476003	1
H	-0.373192	5.509442	4.497971	1
H	0.312981	6.371845	3.115891	1
H	1.320263	5.290474	4.072044	1
H	2.852468	-5.647969	-2.510296	1
H	1.900270	-5.572861	-3.988244	1
H	1.309200	-6.489972	-2.597465	1

E_{tot} = −1720.84412759482 H

Coordinates of [$AuCl_3$(SIMes)] on RI-B3LYP-D3/def2-TZVPP Level

xyz-Coordinates [Å] of the optimized minimum structure of [$AuCl_3$(SIMes)].

53

C	-1.882742	1.148367	2.393383	6
C	-1.163056	-0.032732	2.185899	6
C	-1.510761	-1.232910	2.820634	6
C	-2.636902	-1.236142	3.635263	6
C	-3.405104	-0.090477	3.835849	6
C	-3.005099	1.089615	3.218634	6
N	-0.009725	-0.019224	1.333206	7
C	0.006356	0.000192	0.004272	6
N	1.254059	0.018377	-0.453690	7
C	2.233957	-0.085494	0.646076	6
C	1.353833	0.083149	1.890701	6
C	1.673218	0.032043	-1.825392	6
C	1.627173	-1.148681	-2.573424	6
C	2.029476	-1.089732	-3.907233	6
C	2.478163	0.090215	-4.490143	6
C	2.547377	1.235473	-3.698484	6
C	2.156566	1.231987	-2.364756	6
C	1.155774	-2.453915	-1.991782	6
C	2.270114	2.484787	-1.538442	6
C	2.855272	0.141038	-5.946680	6
Au	-1.667070	0.002570	-1.179980	79
Cl	-3.566384	0.005274	-2.525902	17
C	-0.695391	-2.486353	2.649733	6
C	-4.651752	-0.140147	4.678313	6
C	-1.491694	2.453794	1.755317	6
Cl	-1.177954	2.187537	-1.819066	17
Cl	-2.112655	-2.181938	-0.508196	17
H	-2.929194	-2.161651	4.116900	1
H	-3.578192	1.994796	3.380473	1
H	2.904289	2.160859	-4.134698	1
H	1.989390	-1.994604	-4.501819	1
H	-1.294005	-3.366330	2.878594	1
H	-0.331546	-2.590818	1.630059	1
H	0.163620	-2.491800	3.327352	1
H	-4.898740	0.839966	5.086290	1
H	-5.503732	-0.471122	4.078995	1
H	-4.545530	-0.839911	5.507943	1
H	-0.417384	2.529552	1.590682	1
H	-1.962469	2.575802	0.779687	1
H	-1.799564	3.289823	2.382280	1
H	1.363474	-2.531421	-0.925054	1
H	0.078282	-2.573740	-2.105788	1
H	1.640430	-3.290248	-2.494217	1
H	2.284092	3.365315	-2.178417	1
H	1.432509	2.588805	-0.852459	1
H	3.197443	2.489570	-0.957801	1
H	3.135864	-0.842812	-6.322509	1
H	2.012694	0.494540	-6.546402	1
H	3.687495	0.824259	-6.119884	1
H	2.992744	0.687226	0.550779	1
H	2.722540	-1.060360	0.600328	1
H	1.516188	-0.690053	2.637495	1
H	1.474254	1.057682	2.367081	1

E_{tot} = −2441.52318938263 H

Coordinates of *trans*-[$AuF_2(OTeF_5)$(SIMes)] on RI-B3LYP-D3/def2-TZVPP Level

xyz-Coordinates [Å] of the optimized minimum structure of *trans*-[$AuF_2(OTeF_5)$(SIMes)].

59

N	-0.361214	-1.384895	-1.275677	7
N	-0.318135	0.804304	-1.451793	7
C	-0.178343	-0.235953	-0.649003	6
C	-0.641516	0.373611	-2.826949	6
C	-0.670560	-1.164935	-2.704250	6
C	-0.276952	-2.687185	-0.677606	6
C	0.959432	-3.340828	-0.659315	6
C	1.014938	-4.599605	-0.067293	6
C	-0.110728	-5.197273	0.496327	6
C	-1.322555	-4.510479	0.454427	6
C	-1.432294	-3.249543	-0.125234	6
C	2.195464	-2.688245	-1.216849	6
C	-0.010630	-6.537941	1.173867	6
C	-2.736707	-2.499284	-0.114487	6
C	-0.182949	2.178977	-1.050398	6
C	-1.310747	2.852882	-0.570602	6
C	-1.139394	4.159675	-0.124543	6
C	0.104823	4.785524	-0.144050	6
C	1.195500	4.086033	-0.655067	6
C	1.079652	2.777576	-1.112554	6
C	-2.651864	2.175498	-0.484912	6
C	0.279260	6.166973	0.425147	6
C	2.284802	2.018745	-1.598028	6
H	0.123910	0.730166	-3.514381	1
H	-1.599801	0.793460	-3.128685	1
H	-1.644264	-1.591603	-2.940128	1
H	0.080088	-1.654370	-3.322934	1
H	1.964255	-5.120432	-0.036783	1
H	-2.204135	-4.961463	0.893559	1
H	2.055039	-2.366337	-2.250914	1
H	3.038044	-3.376892	-1.196025	1
H	2.461075	-1.806368	-0.631194	1
H	0.230039	-6.412632	2.232645	1
H	0.773562	-7.152095	0.731054	1
H	-0.950676	-7.086688	1.115226	1
H	-2.663780	-1.613754	0.519405	1
H	-3.539503	-3.126722	0.268227	1
H	-3.023385	-2.165738	-1.114057	1
H	-1.996038	4.693044	0.268878	1
H	2.168657	4.560979	-0.674418	1
H	-2.939803	1.717083	-1.433386	1
H	-3.426720	2.890376	-0.214282	1
H	-2.635756	1.389986	0.272090	1
H	-0.639173	6.749782	0.354238	1
H	1.074016	6.712963	-0.083585	1
H	0.548977	6.102275	1.482254	1
H	2.550756	1.232887	-0.889515	1
H	3.140266	2.683336	-1.703634	1
H	2.109026	1.546736	-2.566969	1
Au	0.269363	-0.041434	1.283380	79
F	-1.621926	0.009898	1.712103	9
F	2.157026	-0.116383	0.843625	9
O	0.727188	0.123260	3.266949	8
Te	1.180909	1.723719	4.067353	52
F	1.370735	0.899147	5.728028	9
F	3.012674	1.523882	3.753737	9
F	1.029254	2.727991	2.476650	9
F	-0.587446	2.169261	4.485001	9
F	1.638263	3.329047	4.905329	9

E_{tot} = −2103.21081882496 H

Coordinates of *trans*-[$AuF_2(OC(CH_3)_2F)$(SIMes)] on RI-B3LYP-D3/def2-TZVPP Level

xyz-Coordinates [Å] of the optimized minimum structure of *trans*-[$AuF_2(OC(CH_3)_2F)$(SIMes)].

63

C	2.320928	1.276764	-1.765501	6
C	2.239267	0.073362	-1.056786	6
C	2.475856	-1.166321	-1.659259	6
C	2.798983	-1.177897	-3.013237	6
C	2.879183	-0.003593	-3.758494	6
C	2.645958	1.210372	-3.117101	6
N	1.857017	0.104568	0.326931	7
C	0.605750	0.107639	0.763900	6
N	0.557568	0.151343	2.086491	7
C	1.909859	0.154862	2.680288	6
C	2.823485	0.185806	1.438566	6
C	-0.638058	0.116895	2.876849	6
C	-1.211321	1.325338	3.284517	6
C	-2.366424	1.265120	4.059338	6
C	-2.949528	0.050726	4.415826	6
C	-2.350709	-1.129798	3.981068	6
C	-1.193988	-1.123578	3.205689	6
C	-0.630152	2.643668	2.851775	6
C	-0.591108	-2.405981	2.698273	6
C	-4.224419	0.016767	5.216709	6
Au	-0.982395	0.065184	-0.488294	79
F	-0.852837	-1.882178	-0.584825	9
C	2.325027	-2.448881	-0.886965	6
C	3.163475	-0.045733	-5.236180	6
C	2.009369	2.594129	-1.109302	6
O	-2.561070	0.083953	-1.707442	8
C	-2.348750	-0.031620	-3.048896	6
C	-1.754794	-1.361798	-3.500095	6
H	-2.407974	-2.175856	-3.189500	1
F	-1.109000	2.004147	-0.333198	9
C	-3.647524	0.320688	-3.759851	6
H	-3.971596	1.305866	-3.430416	1
F	-1.386178	0.960174	-3.463839	9
H	-3.497803	0.327370	-4.839185	1
H	-4.414838	-0.409981	-3.506493	1
H	-1.644357	-1.374485	-4.584223	1
H	-0.779622	-1.515380	-3.043036	1
H	-2.798625	-2.080783	4.243413	1
H	-2.828324	2.190845	4.380991	1
H	2.697371	2.130270	-3.686686	1
H	2.974312	-2.129646	-3.500205	1
H	-1.087896	-3.267661	3.140882	1
H	-0.688856	-2.475102	1.612753	1
H	0.472842	-2.477225	2.933910	1
H	-4.294987	0.870184	5.891540	1
H	-5.093332	0.050712	4.554407	1
H	-4.300268	-0.895303	5.809089	1
H	0.424558	2.732857	3.121078	1
H	-0.704529	2.748285	1.767620	1
H	-1.162531	3.472216	3.315720	1
H	2.924695	-2.450401	0.025663	1
H	1.281988	-2.593401	-0.600713	1
H	2.636219	-3.300820	-1.489229	1
H	2.284829	3.422455	-1.759759	1
H	0.941946	2.670583	-0.893020	1
H	2.544594	2.716890	-0.165577	1
H	3.712719	-0.945436	-5.513922	1
H	2.227974	-0.041391	-5.801324	1
H	3.741412	0.821719	-5.556556	1
H	3.399004	1.108075	1.360209	1
H	3.514544	-0.654711	1.397925	1

H 2.048506 -0.740703 3.285935 1
H 2.034554 1.025832 3.321751 1

E_{tot} = −1553.6468600743 H

Coordinates of [AuF_3] on RI-B3LYP-D3/def2-TZVPP Level

xyz-Coordinates [Å] of the optimized minimum structure of [AuF_3].

4
Au 0.000000 0.000000 -0.404157 79
F 0.000000 0.000000 1.484944 9
F 1.903390 0.000000 -0.540393 9
F -1.903390 0.000000 -0.540393 9

E_{tot} = −435.16803891981 H

Coordinates of [$AuF_2(OCF_3)$] on RI-B3LYP-D3/def2-TZVPP Level

xyz-Coordinates [Å] of the optimized minimum structure of [$AuF_2(OCF_3)$].

8
Au 1.483364 0.903886 0.000000 79
F 1.612103 0.924185 1.906720 9
F 1.612103 0.924185 -1.906720 9
O -0.460247 0.731873 0.000000 8
C -0.928543 -0.552329 0.000000 6
F -2.255202 -0.437824 0.000000 9
F -0.547507 -1.246988 -1.079079 9
F -0.547507 -1.246988 1.079079 9

E_{tot} = −748.22821570542 H

Coordinates of [$AuF_2(OC_2F_5)$] on RI-B3LYP-D3/def2-TZVPP Level

xyz-Coordinates [Å] of the optimized minimum structure of [$AuF_2(OC_2F_5)$].

11
Au 2.299398 1.059180 -0.016893 79
F 2.437798 1.082191 1.889545 9
F 2.409834 1.082397 -1.925141 9
O 0.349181 0.844082 -0.001831 8
C -0.090089 -0.427619 0.001553 6
C -1.667564 -0.351858 0.011330 6
F 0.295837 -1.130374 -1.084892 9
F 0.309339 -1.129173 1.083933 9
F -2.148234 -1.595090 0.018347 9
F -2.090778 0.286648 1.098969 9
F -2.104721 0.279617 -1.074921 9

E_{tot} = −986.03433015012 H

Coordinates of [$AuF_2(OC_3F_7)$] on RI-B3LYP-D3/def2-TZVPP Level

xyz-Coordinates [Å] of the optimized minimum structure of [$AuF_2(OC_3F_7)$].

```
14
Au   2.246230    1.344837    0.450567  79
F    1.320785    2.381400    1.767430   9
F    3.374534    0.375381   -0.752024   9
O    0.579288    0.915973   -0.505281   8
C   -0.019651   -0.278046   -0.285026   6
C   -0.491902   -0.516328    1.193276   6
C   -1.231056   -0.273441   -1.315675   6
F    0.768923   -1.342508   -0.612481   9
F   -1.171277   -1.657137    1.303676   9
F    0.588217   -0.599852    1.989261   9
F   -1.252796    0.490408    1.610045   9
F   -1.862766   -1.445466   -1.270704   9
F   -2.094973    0.697660   -1.029673   9
F   -0.753556   -0.092880   -2.543391   9
```

E_{tot} = −1223.83606141208 H

Coordinates of [$AuF_2(OC_4F_9)$] on RI-B3LYP-D3/def2-TZVPP Level

xyz-Coordinates [Å] of the optimized minimum structure of [$AuF_2(OC_4F_9)$].

```
17
Au   2.067588   -1.814885    0.128039  79
F    2.321609   -1.495304    1.997544   9
F    2.053983   -2.239080   -1.738952   9
O    0.165148   -1.311676    0.083709   8
C   -0.249566    0.005549   -0.001197   6
C   -1.838431   -0.164937   -0.020371   6
C    0.168495    0.856837    1.257694   6
C    0.211330    0.711696   -1.331733   6
F   -2.425105    0.985299   -0.355617   9
F   -2.198200   -1.096008   -0.897577   9
F   -2.271966   -0.530381    1.185272   9
F   -0.560982    1.972822    1.355225   9
F    0.015075    0.148273    2.369041   9
F    1.459790    1.211103    1.157372   9
F   -0.129668    2.002766   -1.338409   9
F    1.545073    0.641305   -1.459626   9
F   -0.334174    0.116622   -2.390413   9
```

E_{tot} = −1461.64053310010 H

Coordinates of [$AuF_2(N_3)$] on RI-B3LYP-D3/def2-TZVPP Level

xyz-Coordinates [Å] of the optimized minimum structure of [$AuF_2(N_3)$].

```
6
Au   1.214382   -0.383689    0.434501  79
F    1.518508   -0.717954    2.299074   9
F    1.108972   -0.097760   -1.470472   9
N   -0.720459    0.115014    0.598371   7
N   -1.248312    0.399260   -0.482808   7
N   -1.873090    0.685129   -1.378667   7
```

E_{tot} = −499.53673036487 H

Coordinates of [Au(N$_3$)$_3$] on RI-B3LYP-D3/def2-TZVPP Level

xyz-Coordinates [Å] of the optimized minimum structure of [Au(N$_3$)$_3$].

```
10
Au   0.796532   -0.690622    0.350958   79
N    0.766902   -0.928226    2.346921   7
N    1.347403   -0.795009   -1.581760   7
N   -0.985260    0.331400    0.287631   7
N   -1.205644    0.873214   -0.788074   7
N   -1.510005    1.417007   -1.739081   7
N    1.109726    0.038015   -2.423225   7
N    0.891209    0.784563   -3.256968   7
N   -0.180169   -0.641724    3.046886   7
N   -1.030693   -0.388617    3.756713   7
```

E_{tot} = –628.22170257207 H

Coordinates of [Au(CN)F$_2$] on RI-B3LYP-D3/def2-TZVPP Level

xyz-Coordinates [Å] of the optimized minimum structure of [Au(CN)F$_2$].

```
5
Au   0.000000    0.000000    0.938454   79
F   -1.905423    0.000000    1.082696   9
F    1.905423    0.000000    1.082696   9
C    0.000000    0.000000   -0.975362   6
N    0.000000    0.000000   -2.128485   7
```

E_{tot} = –428.17338172176 H

Coordinates of [Au(CN)$_3$] on RI-B3LYP-D3/def2-TZVPP Level

xyz-Coordinates [Å] of the optimized minimum structure of [Au(CN)$_3$].

```
7
Au   0.000000    0.000000    0.630932   79
C   -1.998357    0.000000    0.713298   6
C    1.998357    0.000000    0.713298   6
C    0.000000    0.000000   -1.298125   6
N    0.000000    0.000000   -2.451223   7
N    3.147027    0.000000    0.845909   7
N   -3.147027    0.000000    0.845909   7
```

E_{tot} = –414.12193232221 H

Coordinates of [Au(CCH)F$_2$] on RI-B3LYP-D3/def2-TZVPP Level

xyz-Coordinates [Å] of the optimized minimum structure of [Au(CCH)F$_2$].

```
6
C    0.000000    0.000000    1.622441   6
C    0.000000    0.000000    0.424716   6
H    0.000000    0.000000    2.685719   1
Au   0.000000    0.000000   -1.482133   79
F   -1.908531    0.000000   -1.625463   9
F    1.908531    0.000000   -1.625463   9
```

E_{tot} = –412.07604954601 H

Coordinates of [Au(CCSiMe$_3$)F$_2$] on RI-B3LYP-D3/def2-TZVPP Level

xyz-Coordinates [Å] of the optimized minimum structure of [Au(CCSiMe$_3$)F$_2$].

18
C 0.892806 1.546336 -1.245638 6
Si -0.001429 0.000391 -0.679146 14
C -1.786253 0.000126 -1.247636 6
C -0.000664 0.000215 1.174019 6
C -0.000720 -0.000138 2.383658 6
Au 0.001532 -0.000667 4.290877 79
F 1.901553 0.198894 4.433491 9
F -1.898034 -0.200368 4.438869 9
C 0.892810 -1.546032 -1.244622 6
H 0.921631 1.590002 -2.336915 1
H 0.391761 2.446087 -0.884763 1
H 1.920265 1.562657 -0.878886 1
H 0.921152 -1.590464 -2.335880 1
H 1.920519 -1.561855 -0.878525 1
H 0.391910 -2.445501 -0.882862 1
H -1.839484 -0.000751 -2.339023 1
H -2.314760 -0.881976 -0.882666 1
H -2.314594 0.883045 -0.884350 1

E_{tot} = −820.71875296558 H

Coordinates of [Au(CF$_3$)F$_2$] on RI-B3LYP-D3/def2-TZVPP Level

xyz-Coordinates [Å] of the optimized minimum structure of [Au(CF$_3$)F$_2$].

7
Au 1.167985 -0.634706 0.000000 79
F 0.217359 -2.311926 0.000000 9
F 2.282774 0.932884 0.000000 9
C -0.641469 0.357619 0.000000 6
F -0.424611 1.653991 0.000000 9
F -1.301019 0.001069 -1.083347 9
F -1.301019 0.001069 1.083347 9

E_{tot} = −673.04056490330 H

Coordinates of [Au(CF$_3$)$_3$] on RI-B3LYP-D3/def2-TZVPP Level

xyz-Coordinates [Å] of the optimized minimum structure of [Au(CF$_3$)$_3$].

13
Au 0.04719566441461 -1.12233322931971 0.03028927353388 79
C -3.95033446217129 -1.37469420800382 -0.00872322407669 6
C -0.06832374671078 2.81381072796679 -0.11518311269927 6
C 4.03074957445271 -1.46396478353996 0.10920220984482 6
F -4.47788327211836 -3.84613964812156 0.55461107074308 9
F -5.19385000458658 0.04463627360978 1.70600355067283 9
F -5.02534037356166 -0.90704606747568 -2.27606697154130 9
F -1.56053017339052 3.51262337321273 -1.99264397200624 9
F -0.96976458490633 3.64844169890046 2.05916304044270 9
F 2.22491171582116 3.72355723121026 -0.48326464487953 9
F 5.23608929968403 -0.73325664413322 -2.01955388842153 9
F 5.20229233274008 -0.29621263509404 2.05304199557828 9
F 4.50478803033292 -3.99942208921198 0.38312467280897 9

E_{tot} = −1148.65383085260 H

Coordinates of [AuClF$_2$] on RI-B3LYP-D3/def2-TZVPP Level

xyz-Coordinates [Å] of the optimized minimum structure of [AuClF$_2$].

```
4
Au   0.325232    0.001550    0.000000  79
F   -1.552545   -0.292117    0.000000   9
Cl   0.690881    2.204228    0.000000  17
F    0.536432   -1.913661    0.000000   9
```

E_{tot} = −795.52955539208 H

Coordinates of [AuCl$_3$] on RI-B3LYP-D3/def2-TZVPP Level

xyz-Coordinates [Å] of the optimized minimum structure of [AuCl$_3$].

```
4
Au   0.000000    0.000000   -0.409283  79
Cl  -2.255015    0.000000   -0.691754  17
Cl   0.000000    0.000000    1.844024  17
Cl   2.255015    0.000000   -0.691754  17
```

E_{tot} = −1516.22032821777 H

Coordinates of [AuF$_2$(OTeF$_5$)] on RI-B3LYP-D3/def2-TZVPP Level

xyz-Coordinates [Å] of the optimized minimum structure of [AuF$_2$(OTeF$_5$)].

```
10
Au  -1.442880   -1.853039   -0.034763  79
O   -1.149549    0.071372   -0.005801   8
Te   0.626404    0.814057    0.009950  52
F   -0.207518    2.465799   -0.062357   9
F    0.620729    0.886052    1.863693   9
F    1.452558   -0.854601    0.102973   9
F    0.745804    0.778386   -1.837000   9
F    2.281050    1.635469    0.043333   9
F   -0.779842   -2.021240   -1.817764   9
F   -2.146756   -1.922255    1.737736   9
```

E_{tot} = −1177.86166662549 H

Coordinates of OC$_3$H$_6$ on RI-B3LYP-D3/def2-TZVPP Level

xyz-Coordinates [Å] of the optimized minimum structure of OC$_3$H$_6$.

```
10
C    1.281462   -0.116872   -0.154880   6
C   -0.008844   -0.090367    0.637658   6
C   -1.277084    0.160510   -0.151335   6
O   -0.025698   -0.260324    1.834550   8
H    1.234604   -0.890613   -0.925157   1
H    1.424647    0.835028   -0.671893   1
H    2.122534   -0.306537    0.507152   1
H   -1.211254    1.116500   -0.676427   1
H   -1.403904   -0.611656   -0.913989   1
H   -2.136464    0.164331    0.514320   1
```

E_{tot} = −193.12755561607 H

Coordinates of OC_3F_6 on RI-B3LYP-D3/def2-TZVPP Level

xyz-Coordinates [Å] of the optimized minimum structure of OC_3F_6.

```
10
C    1.321394   -0.082427   -0.133236   6
C   -0.008915   -0.106493    0.681218   6
O   -0.022950   -0.287995    1.855272   8
C   -1.318510    0.123438   -0.134174   6
F    1.164342   -0.676419   -1.324139   9
F    1.687952    1.192735   -0.337079   9
F    2.285979   -0.704845    0.534976   9
F   -1.139835    1.071613   -1.064007   9
F   -1.660158   -1.019611   -0.749748   9
F   -2.309299    0.490005    0.670917   9
```

E_{tot} = −788.63167093967 H

Coordinates of OC_2F_4 on RI-B3LYP-D3/def2-TZVPP Level

xyz-Coordinates [Å] of the optimized minimum structure of OC_2F_4.

```
7
C    0.751146   -0.022598    0.529385   6
O    0.867951   -0.343641    1.652592   8
F    1.763509    0.398817   -0.237606   9
C   -0.558724   -0.012423   -0.298524   6
F   -0.433223   -0.819098   -1.360210   9
F   -1.576303   -0.430126    0.445320   9
F   -0.814355    1.229069   -0.730957   9
```

E_{tot} = −550.83915072430 H

Coordinates of OCF_2 on RI-B3LYP-D3/def2-TZVPP Level

xyz-Coordinates [Å] of the optimized minimum structure of OCF_2.

```
4
C    0.000000    0.000000    0.096460   6
O    0.000000    0.000000    1.267300   8
F    1.065451    0.000000   -0.681880   9
F   -1.065451    0.000000   -0.681880   9
```

E_{tot} = −313.03805412601 H

Literature

[1] M. A. Ellwanger, C. von Randow, S. Steinhauer, Y. Zhou, A. Wiesner, H. Beckers, T. Braun, S. Riedel, *Chem. Commun.* **2018**, *54*, 9301.

[2] E. Schnell, E. G. Rochow, *J. Inorg. Nucl. Chem.* **1958**, *6*, 303.

[3] a) M. Winter, N. Limberg, M. A. Ellwanger, A. Pérez-Bitrián, K. Sonnenberg, S. Steinhauer, S. Riedel, *Chem. Eur. J.* **2020**, *26*, 16089; b) M. A. Ellwanger, S. Steinhauer, P. Golz, T. Braun, S. Riedel, *Angew. Chem. Int. Ed.* **2018**, *57*, 7210.

8.3 Supporting Information of ‘Gold Teflates Revisited: From the Lewis Superacid $[Au(OTeF_5)_3]$ to the Anion $[Au(OTeF_5)_4]^-$’

Chemistry–A European Journal

Supporting Information

Gold Teflates Revisited: From the Lewis Superacid $[Au(OTeF_5)_3]$ to the Anion $[Au(OTeF_5)_4]^-$

Marlon Winter, Natallia Peshkur, Mathias A. Ellwanger, Alberto Pérez-Bitrián, Patrick Voßnacker, Simon Steinhauer, and Sebastian Riedel*

Table of Contents

X-Ray Crystallography

Crystallographic Data

Table S1: Crystal data and refinement details for the analysis of the molecular structures in the solid state of $[Au(OPPh_3)(OTeF_5)_3]$, $[NEt_3Me][Au(OTeF_5)_4]$ and $[NMe_4][AuCl_3(OTeF_5)]$.

	$[Au(OPPh_3)(OTeF_5)_3]$	$[NEt_3Me][Au(OTeF_5)_4]$	$[NMe_4][AuCl_3(OTeF_5)]$
Empirical formula	$C_{18}H_{15}AuF_{15}O_4PTe_3$	$C_7H_{18}AuF_{20}NO_4Te_4$	$C_4H_{12}AuCl_3F_5NOTe$
Formula weight	1191.04	1267.59	616.065
Temperature/K	100.00	100.00	100.00
Crystal system	monoclinic	orthorhombic	monoclinic
Space group	$P2_1/n$	$P2_12_12_1$	$C2/m$
a/Å	9.1239(5)	9.2412(5)	15.0187(9)
b/Å	17.507(1)	12.4290(6)	14.4319(9)
c/Å	17.5756(8)	23.303(1)	7.0557(4)
α/°	90	90	90
β/°	91.588(2)	90	112.085(2)
γ/°	90	90	90
Volume/Å^3	2806.4(3)	2676.5(2)	1417.1(2)
Z	4	4	4
ρ_{calc}g/cm^3	2.819	3.146	2.888
μ/mm^{-1}	8.482	9.925	13.001
F(000)	2160.0	2264.0	1107.4
Crystal size/mm^3	0.237 × 0.113 × 0.105	0.337 × 0.182 × 0.17	0.151 × 0.121 × 0.052
Radiation	MoKα (λ = 0.71073)	MoK_α (λ = 0.71073)	MoK_α (λ = 0.71073)
2Θ range for data collection/°	5.036 to 56.616	4.742 to 56.606	4.06 to 56.6
Index ranges	-12 ≤ h ≤ 12, 0 ≤ k ≤ 23, 0 ≤ l ≤ 23	-12 ≤ h ≤ 12, -16 ≤ k ≤ 16, -31 ≤ l ≤ 30	-19 ≤ h ≤ 20, -19 ≤ k ≤ 19, -9 ≤ l ≤ 9
Reflections collected	13467	74744	15922
Independent reflections	13467 [R_{int} = -, R_{sigma} = 0.0187]	6659 [R_{int} = 0.0495, R_{sigma} = 0.0251]	1833 [R_{int} = 0.0382, R_{sigma} = 0.0215]
Data/restraints/parameters	13467/0/380	6659/0/339	1833/103/95
Goodness-of-fit on F^2	1.117	1.087	1.026
Final R indexes [I>=2σ (I)]	R_1 = 0.0209, wR_2 = 0.0504	R_1 = 0.0173, wR_2 = 0.0357	R_1 = 0.0227, wR_2 = 0.0547
Final R indexes [all data]	R_1 = 0.0225, wR_2 = 0.0515	R_1 = 0.0182, wR_2 = 0.0359	R_1 = 0.0237, wR_2 = 0.0552
Largest diff. peak/hole / e Å^{-3}	1.28/-0.91	0.58/-0.80	1.17/-1.77
Flack parameter		0.275(3)	
CCDC deposition number	2173738	2156160	2156159

Molecular Structure of $[NEt_3Me][Au(OTeF_5)_4]$ in the Solid State

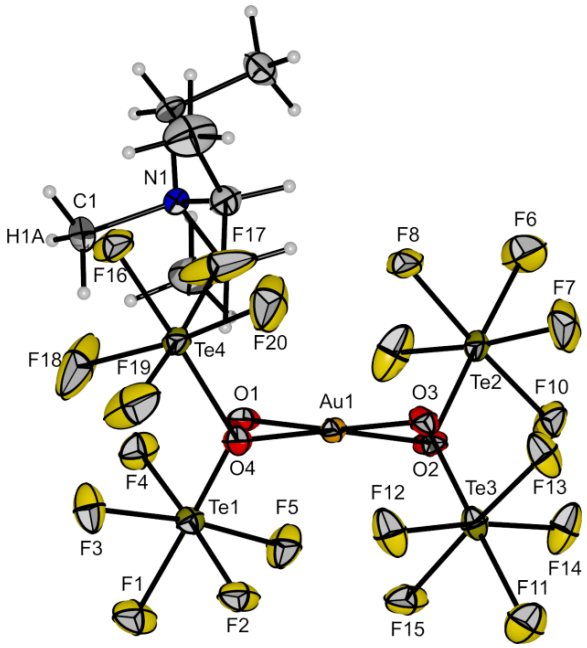

Figure S1: Molecular structure of $[NEt_3Me][Au(OTeF_5)_4]$ in the solid state. Thermal ellipsoids are set at 50 % probability. Bond lengths to the central gold atom [pm]: 197.4(3) (O1–Au1), 196.7(3) (O2–Au1), 197.7(3) (O3–Au1), 197.2(3) (O4–Au1).

Molecular Structure of $[NMe_4][AuCl_3(OTeF_5)]$ in the Solid State

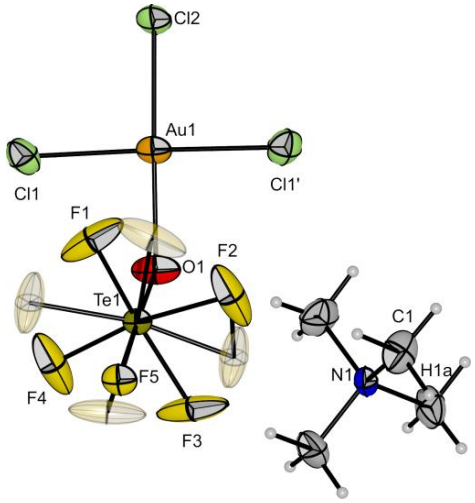

Figure S2: Molecular structure of $[NMe_4][AuCl_3(OTeF_5)]$ in the solid state. The second position of disordered atoms in the $OTeF_5$ ligand is shown as transparent ellipsoids. Thermal ellipsoids are set at 50 % probability. Bond lengths [pm] to the central gold atom: 204.2(4) (O1-Au1), 227.7(2) (Cl1-Au1), 223.8(2) (Cl2-Au1).

Powder X-Ray Diffraction

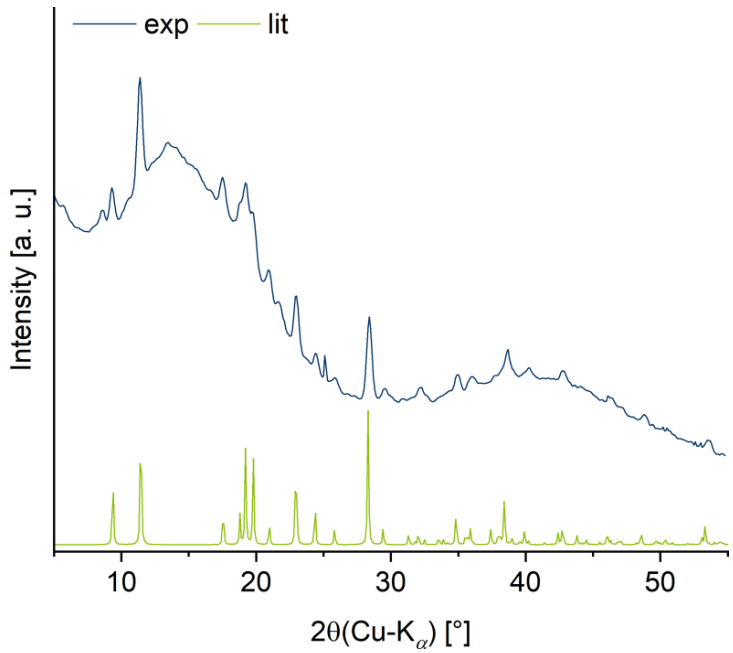

Figure S3: Powder X-ray diffractogram (Cu-K_α) of $[Au(OTeF_5)_3]$ measured in this work (blue line) compared to the one obtained from the literature-known solid state structure (green line).[1]

NMR Spectroscopy

NMR Spectra of $[Au(OPEt_3)(OTeF_5)_3]$

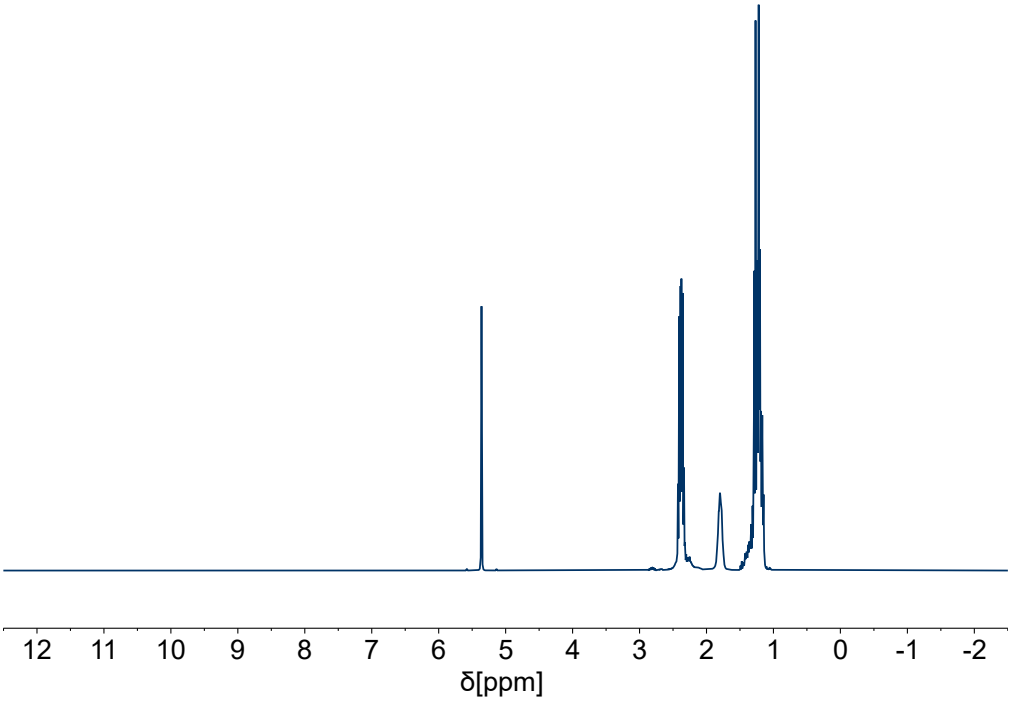

Figure S4: ^{1}H NMR spectrum (400 MHz, DCM-d_2, 21 °C) of $[Au(OPEt_3)(OTeF_5)_3]$.

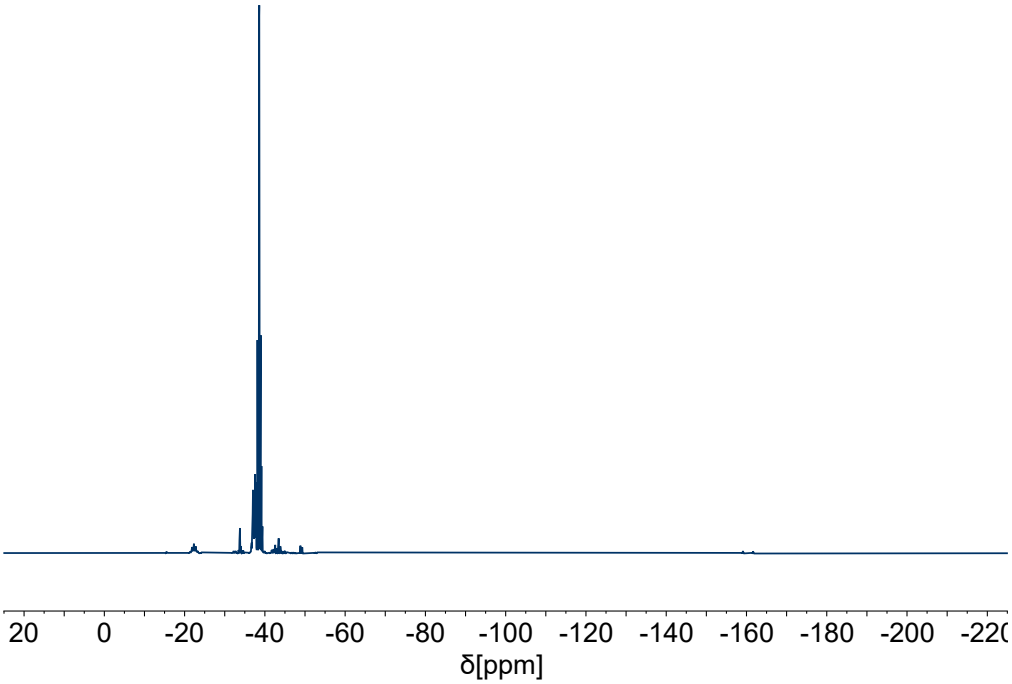

Figure S5: ^{19}F NMR spectrum (377 MHz, DCM-d_2, 21 °C) of $[Au(OPEt_3)(OTeF_5)_3]$.

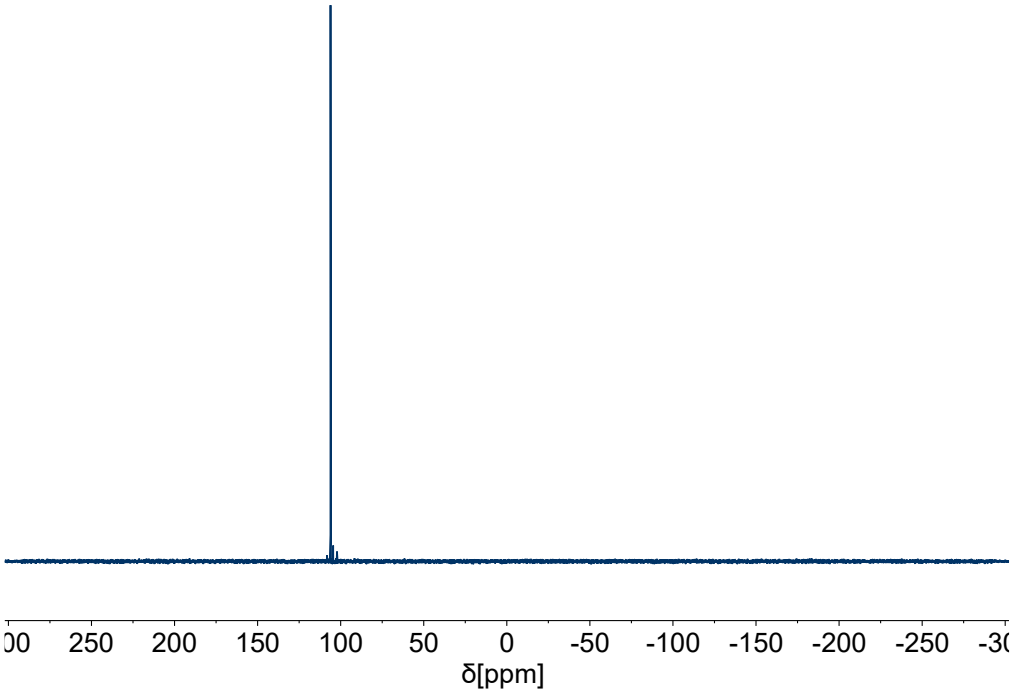

Figure S6: $^{31}P\{^{1}H\}$ NMR spectrum (162 MHz, DCM-d_2, 21 °C) of $[Au(OPEt_3)(OTeF_5)_3]$.

NMR Spectra of $[Au(OPPh_3)(OTeF_5)_3]$

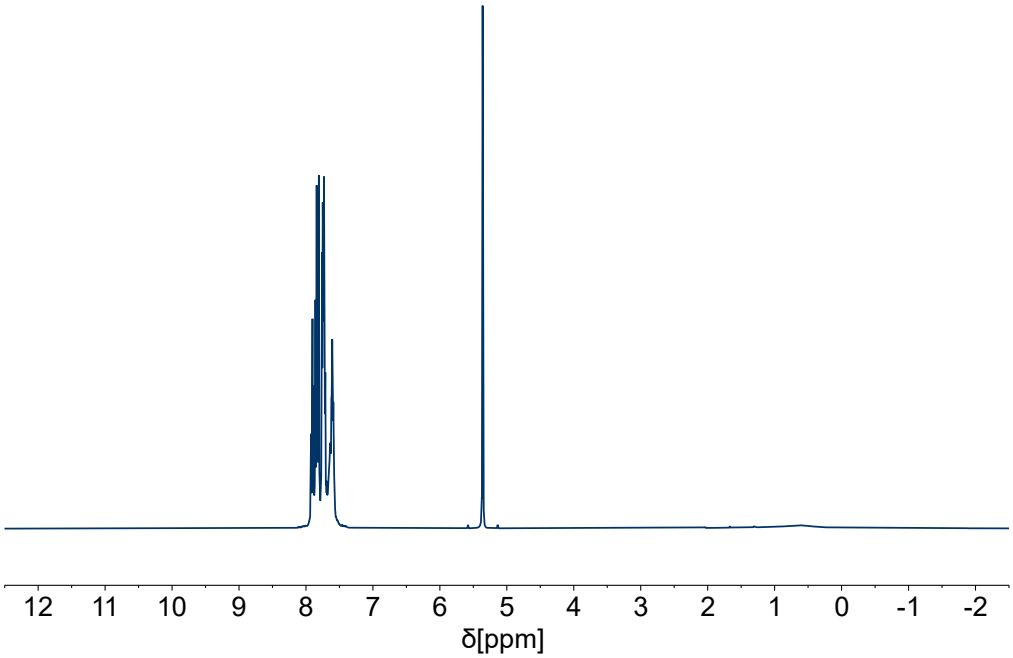

Figure S7: ^{1}H NMR spectrum (400 MHz, DCM-d_2, 19 °C) of $[Au(OPPh_3)(OTeF_5)_3]$.

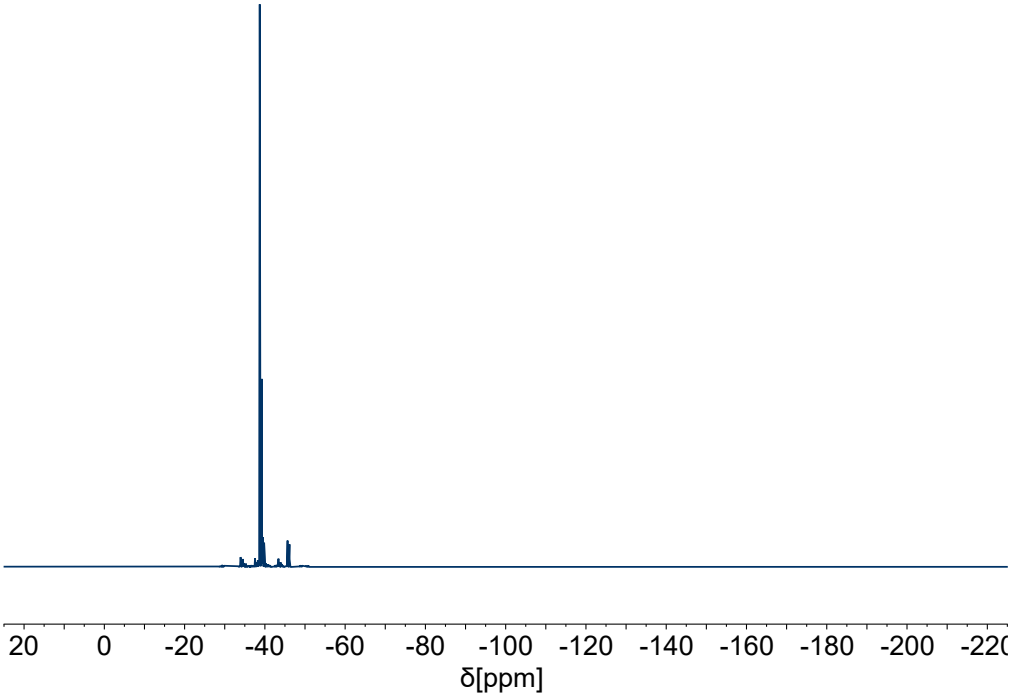

Figure S8: ^{19}F NMR spectrum (377 MHz, DCM-d_2, 19 °C) of $[Au(OPPh_3)(OTeF_5)_3]$.

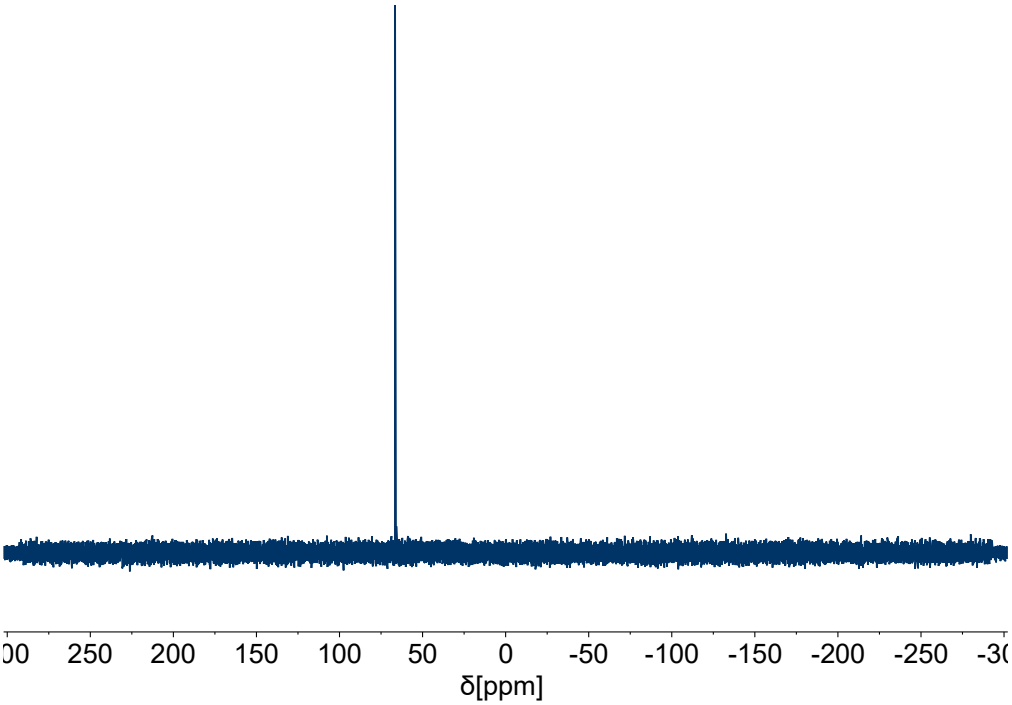

Figure S9: $^{31}P\{^1H\}$ NMR spectrum (162 MHz, DCM-d_2, 19 °C) of $[Au(OPPh_3)(OTeF_5)_3]$.

NMR Spectra of $[Au(CD_3CN)(OTeF_5)_3]$

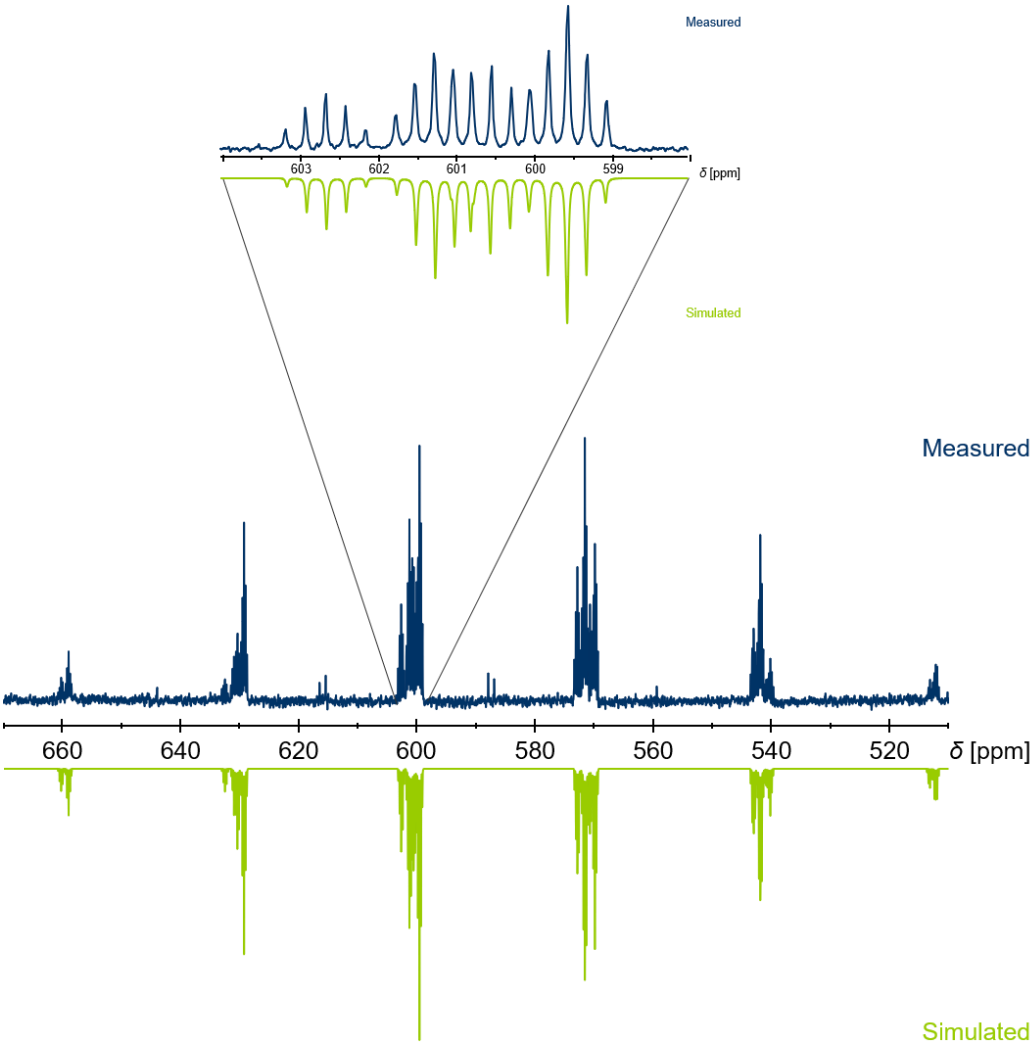

Figure S10: ^{125}Te NMR spectrum (126 MHz, DCM-d_2, 19 °C) of $[Au(CD_3CN)(OTeF_5)_3]$ (top, blue) compared to the simulated spectrum (bottom, green) with a zoom to show the splitting pattern. NMR spectroscopical parameters used in the simulation for the two $-OTeF_5$ ligands in *cis* position to CD_3CN: $\delta(Te_c)$ = 586 ppm, $^1J(^{125}Te_c,^{19}F_{A,c})$ = 3535 Hz, $^1J(^{125}Te_c,^{19}F_{B,c})$ = 3751 Hz, $^5J(^{125}Te_c,^{19}F_{B,t})$ = 31 Hz. NMR spectroscopical parameters used in the simulation for the $-OTeF_5$ ligand in *trans* position to CD_3CN: $\delta(Te_t)$ = 587 ppm, $^1J(^{125}Te_t,^{19}F_{A,t})$ = 3501 Hz, $^1J(^{125}Te_t,^{19}F_{B,t})$ = 3768 Hz, $^5J(^{125}Te_t,^{19}F_{B,c})$ = 32 Hz.

NMR Spectra of $[NMe_4][Au(OTeF_5)_4]$

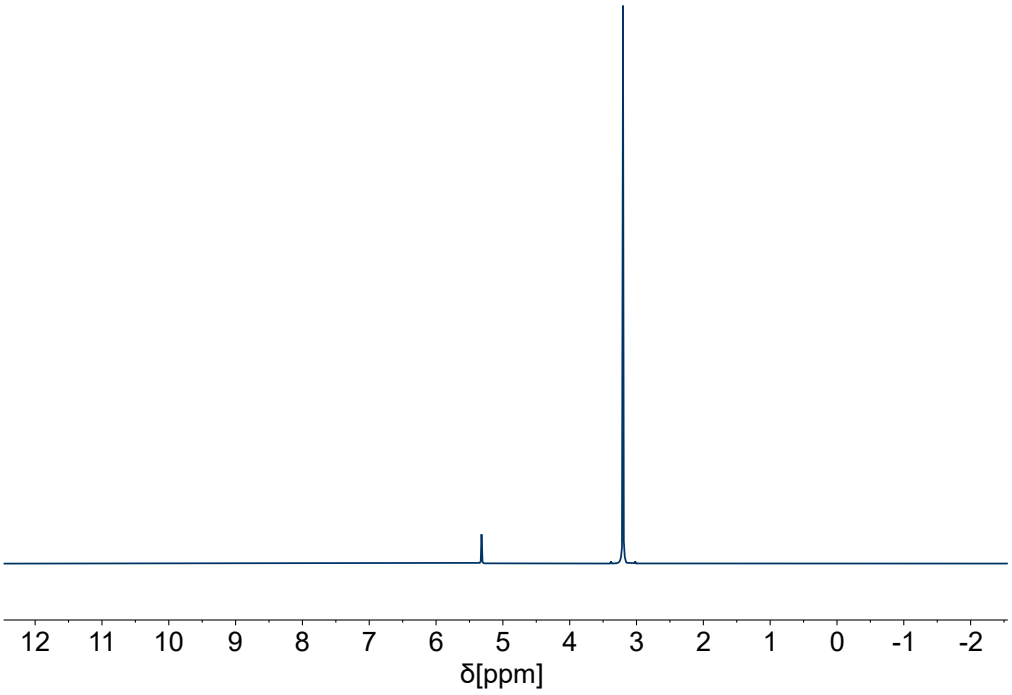

Figure S11: ^{1}H NMR spectrum (400 MHz, DCM-d_2, 19 °C) of $[NMe_4][Au(OTeF_5)_4]$.

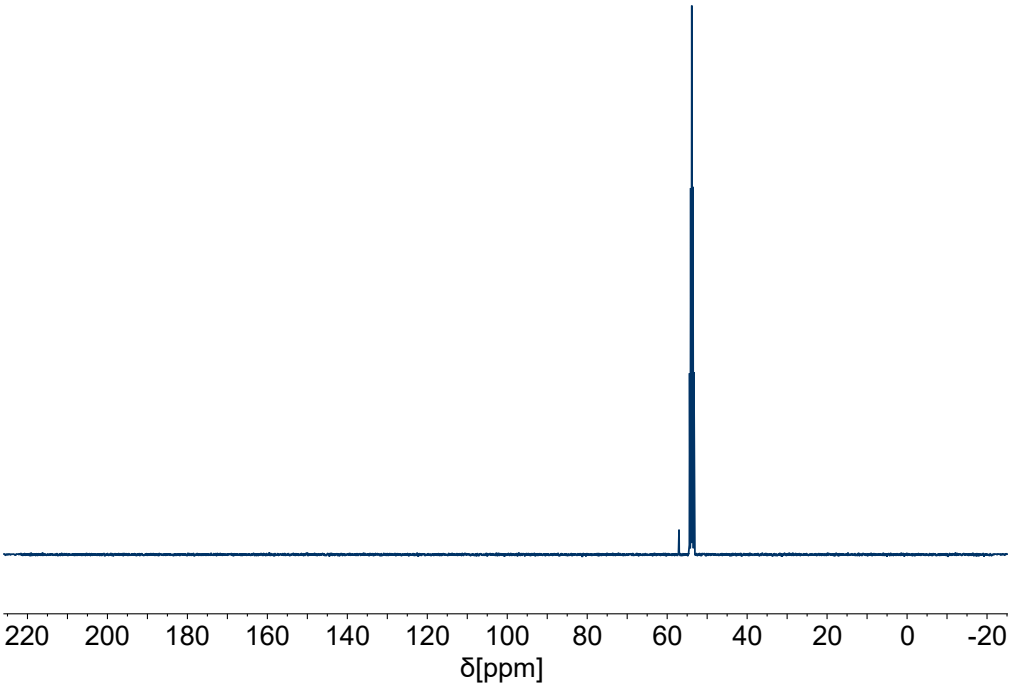

Figure S12: $^{13}C\{^{1}H\}$ NMR spectrum (101 MHz, DCM-d_2, 21 °C) of $[NMe_4][Au(OTeF_5)_4]$.

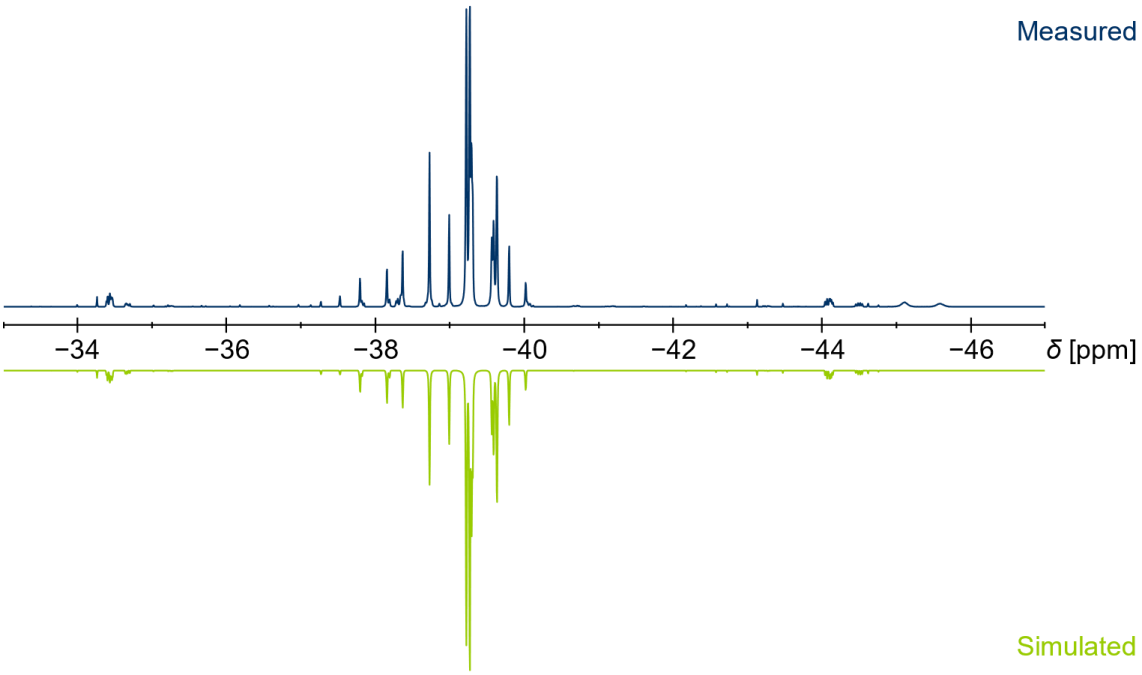

Figure S13: ^{19}F NMR spectrum (377 MHz, DCM-d_2, 20 °C) of [NMe_4][$Au(OTeF_5)_4$] (top, blue) compared to the simulated spectrum (bottom, green). NMR spectroscopical parameters used in the simulation: $\delta(F_A)$ = −38.4 ppm, $\delta(F_B)$ = −39.4 ppm, $^2J(^{19}F,^{19}F)$ = 183 Hz, $^1J(^{19}F_A,^{125}Te)$ = 3282 Hz, $^1J(^{19}F_B,^{125}Te)$ = 3663 Hz.

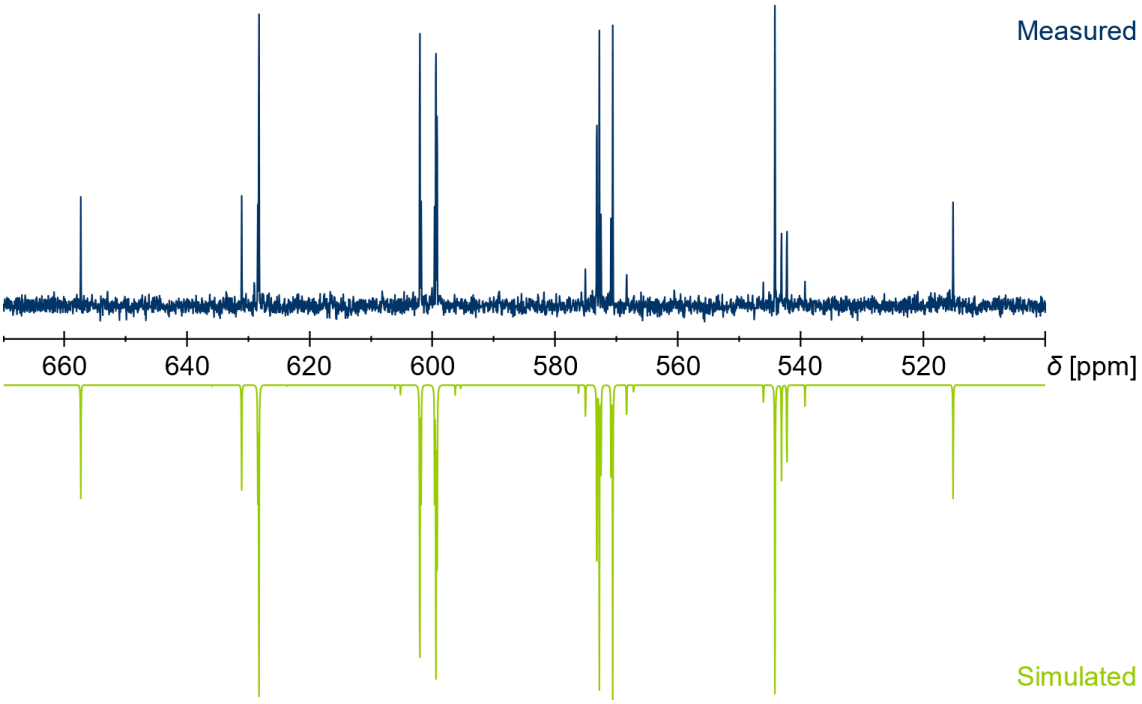

Figure S14: ^{125}Te NMR spectrum (126 MHz, DCM-d_2, 19 °C) of [NMe_4][$Au(OTeF_5)_4$] (top, blue) compared to the simulated spectrum (bottom, green). NMR spectroscopical parameters used in the simulation: δ(Te) = 586 ppm, $^1J(^{125}Te,^{19}F_A)$ = 3282 Hz, $^1J(^{125}Te,^{19}F_B)$ = 3663 Hz.

NMR Spectra of $[NEt_3Me][Au(OTeF_5)_4]$

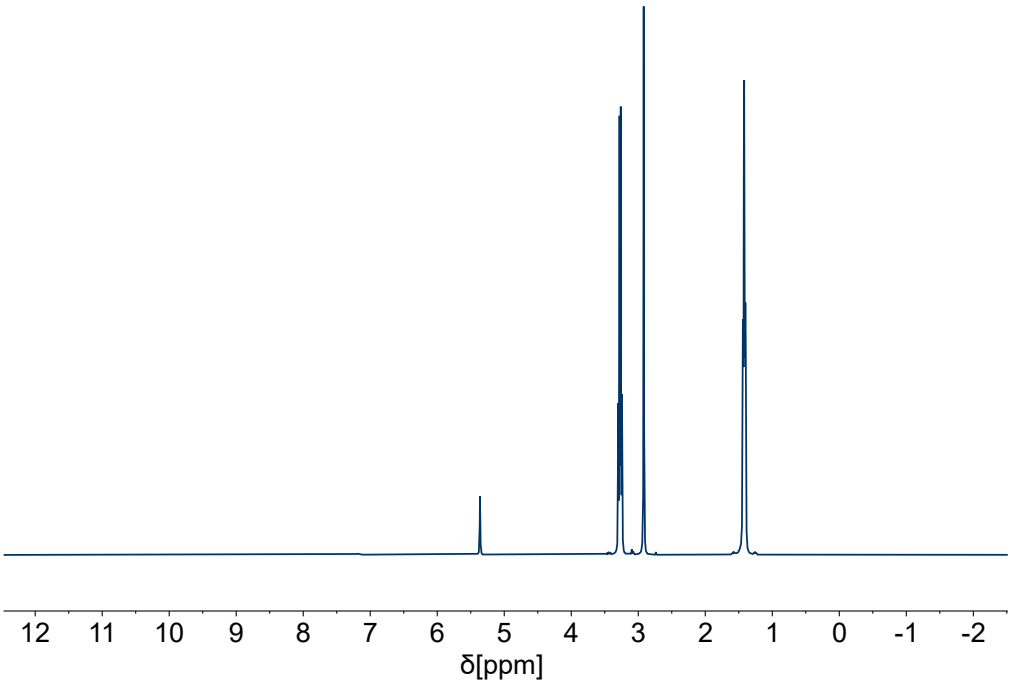

Figure S15: ^{1}H NMR spectrum (400 MHz, DCM-d_2, 18 °C) of $[NEt_3Me][Au(OTeF_5)_4]$.

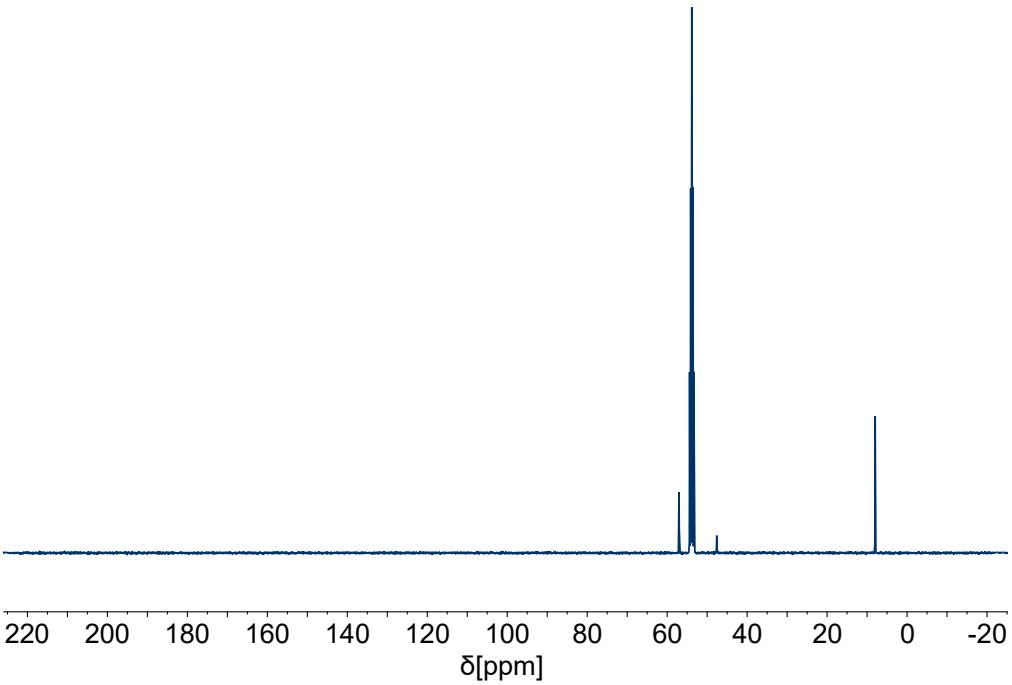

Figure S16: $^{13}C\{^{1}H\}$ NMR spectrum (101 MHz, DCM-d_2, 19 °C) of $[NEt_3Me][Au(OTeF_5)_4]$.

NMR Spectra of $Cs[Au(OTeF_5)_4]$

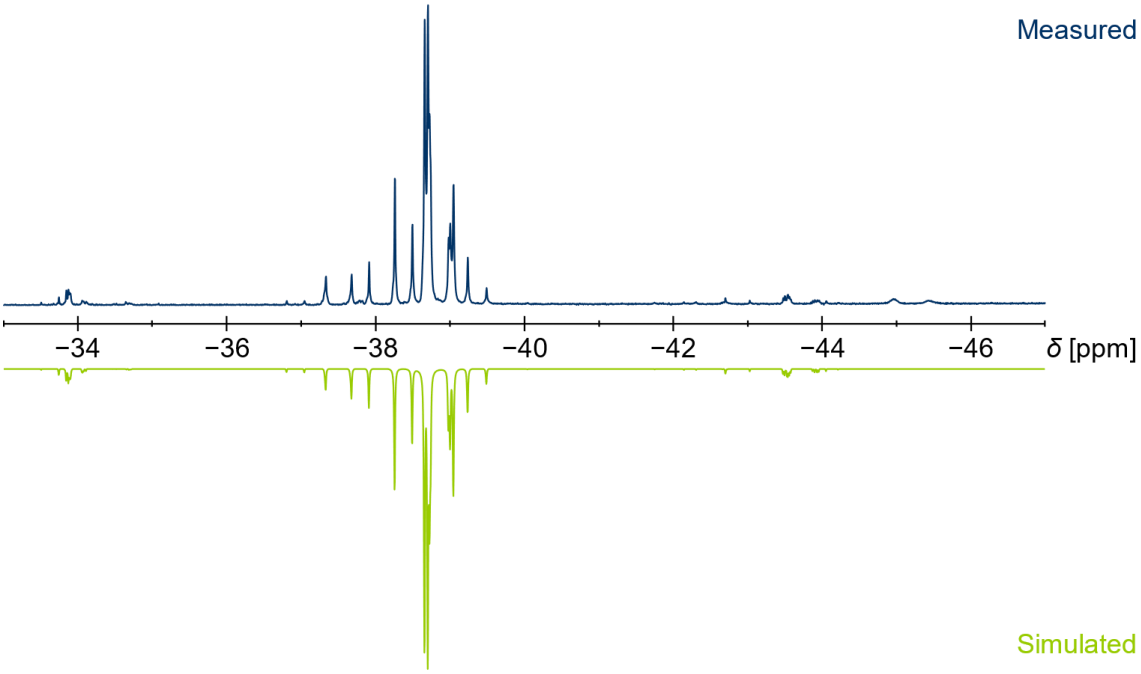

Figure S17: ^{19}F NMR spectrum (377 MHz, DCM-d_2, 19 °C) of $Cs[Au(OTeF_5)_4]$ (top, blue) compared to the simulated spectrum (bottom, green). NMR spectroscopical parameters used in the simulation: $\delta(F_A)$ = −37.9 ppm, $\delta(F_B)$ = −38.9 ppm, $^2J(^{19}F,^{19}F)$ = 183 Hz, $^1J(^{19}F_A,^{125}Te)$ = 3309 Hz, $^1J(^{19}F_B,^{125}Te)$ = 3662 Hz.

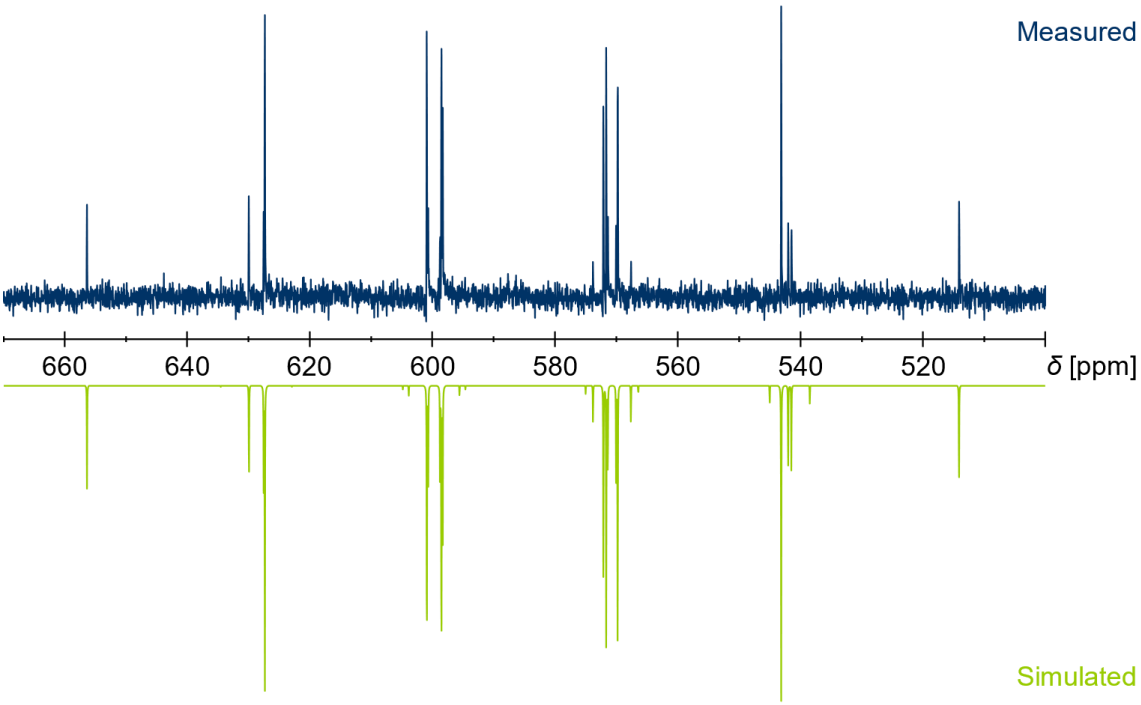

Figure S18: ^{125}Te NMR spectrum (126 MHz, DCM-d_2, 19 °C) of $Cs[Au(OTeF_5)_4]$ (top, blue) compared to the simulated spectrum (bottom, green). NMR spectroscopical parameters used in the simulation: δ(Te) = 585 ppm, $^1J(^{125}Te,^{19}F_A)$ = 3309 Hz, $^1J(^{125}Te,^{19}F_B)$ = 3662 Hz.

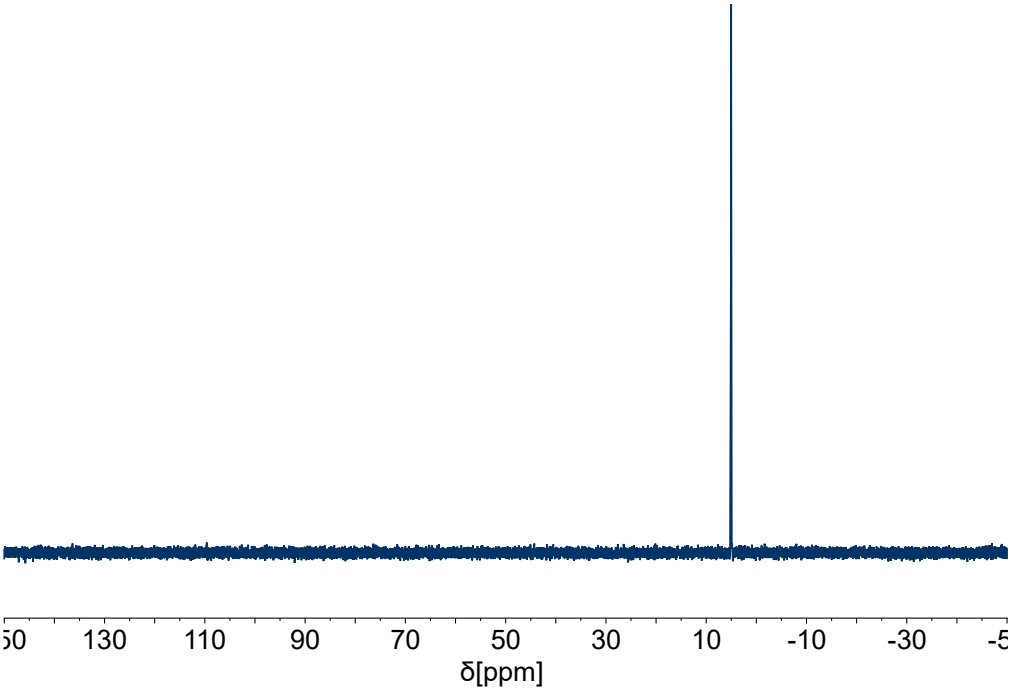

Figure S19: ^{133}Cs NMR spectrum (53 MHz, DCM-d_2, 19 °C) of $Cs[Au(OTeF_5)_4]$.

Vibrational Spectroscopy

Vibrational Spectra of $[Au_2(OTeF_5)_6]$

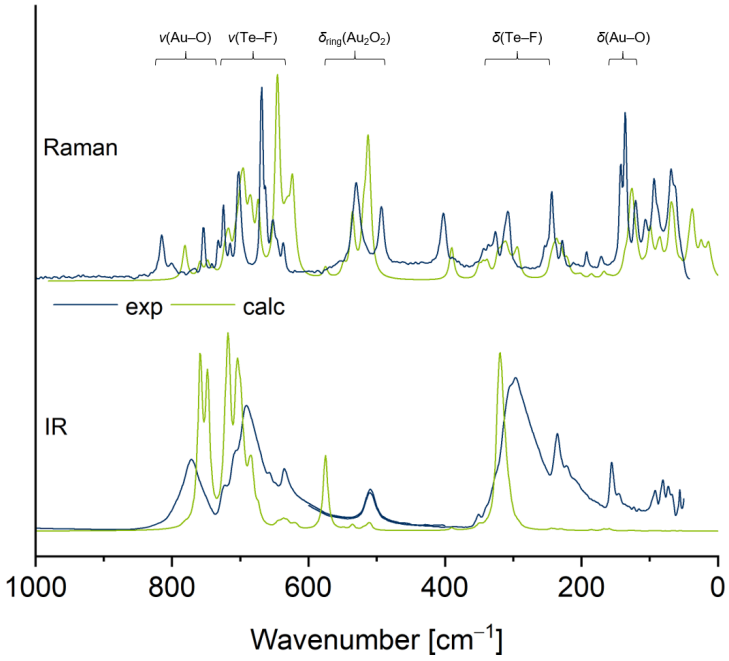

Figure S20: Raman (top) and IR (bottom) spectra of $[Au_2(OTeF_5)_6]$ recorded at room temperature (blue lines) compared to the respective calculated spectra at the RI-B3LYP-D3/def2-TZVPP level of theory (green lines). Note that the experimental IR spectrum consists of two spectra, one for the MIR region (4000 – 400 cm^{-1}) and one for the FIR region (650 – 50 cm^{-1}).

IR Spectrum of $[Au(CD_3CN)(OTeF_5)_3]$

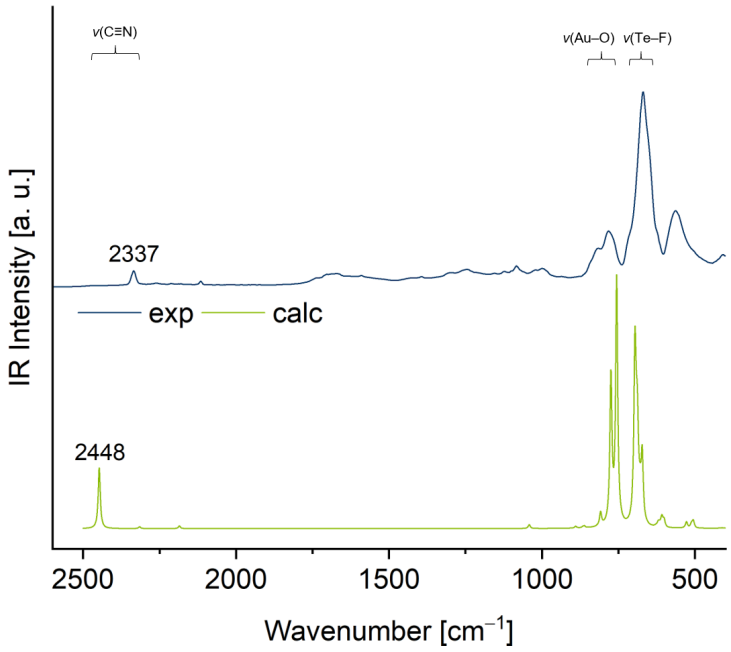

Figure S21: Experimental (top, blue line) and calculated (bottom, green line; RI-B3LYP/def2-TZVPP level) IR spectrum of $[Au(CD_3CN)(OTeF_5)_3]$, highlighting the wavenumber of the *ν*(C≡N) stretching vibration.

IR Spectra of $[Cat][Au(OTeF_5)_4]$ ($[Cat]^+ = [NMe_4]^+, [NEt_3Me]^+, Cs^+$)

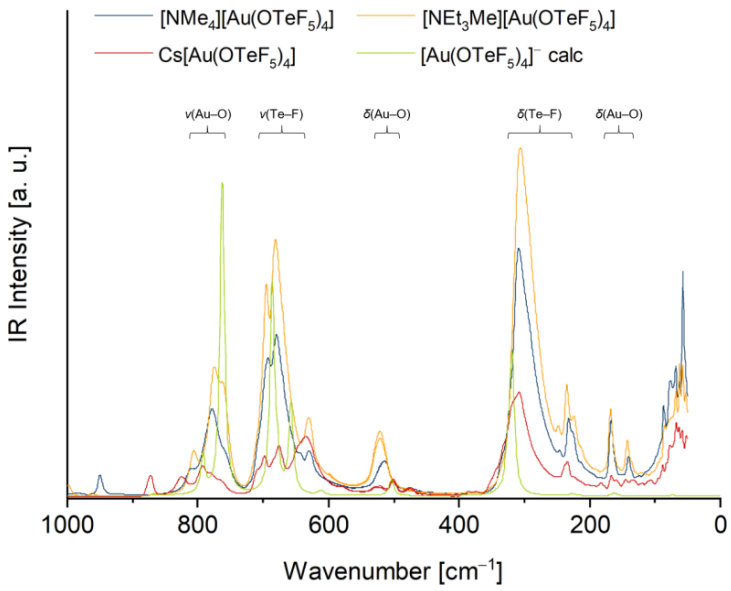

Figure S22: IR spectra of $[NMe_4][Au(OTeF_5)_4]$ (blue), $[NEt_3Me][Au(OTeF_5)_4]$ (orange) and $Cs[Au(OTeF_5)_4]$ (red) compared to the calculated Raman spectrum of the $[Au(OTeF_5)_4]^-$ anion (green; RI-B3LYP-D3/def2-TZVPP level). Note that the experimental IR spectra of each compound consist of two spectra, one for the MIR region (4000 – 400 cm^{-1}) and one for the FIR region (650 – 50 cm^{-1}).

Raman Spectra of $[Cat][Au(OTeF_5)_4]$ ($[Cat]^+ = [NMe_4]^+, [NEt_3Me]^+, Cs^+$)

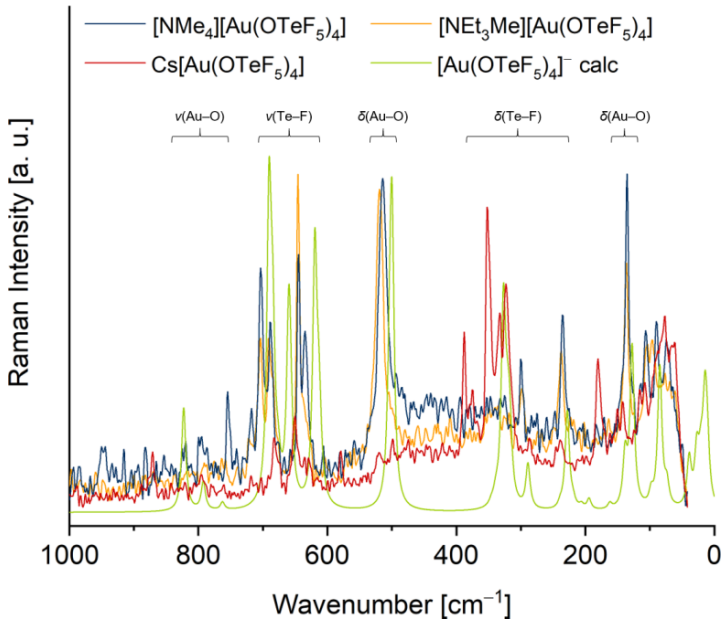

Figure S23: Raman spectra of $[NMe_4][Au(OTeF_5)_4]$ (blue), $[NEt_3Me][Au(OTeF_5)_4]$ (orange) and $Cs[Au(OTeF_5)_4]$ (red) compared to the calculated Raman spectrum of the $[Au(OTeF_5)_4]^-$ anion (green; RI-B3LYP-D3/def2-TZVPP level).

UV/Vis Spectroscopy

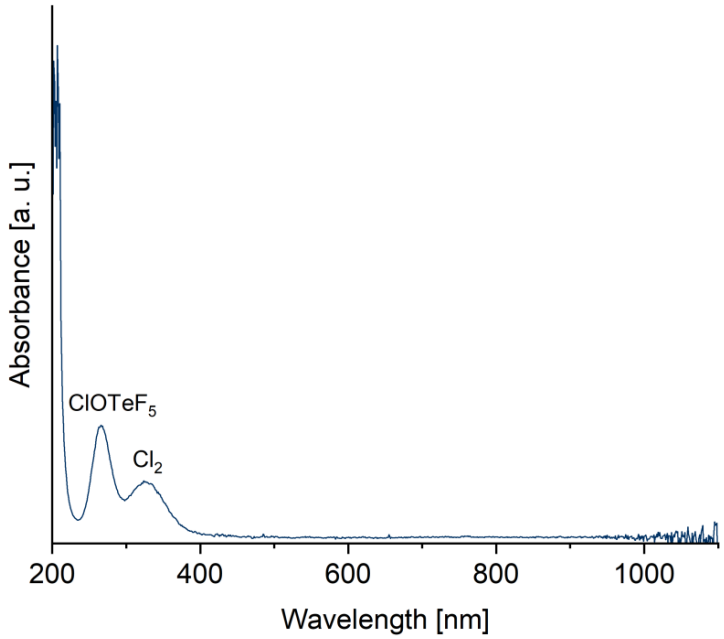

Figure S24: UV/Vis spectrum of the gas phase of the reaction between $AuCl_3$ and $ClOTeF_5$, showing the formation of gaseous chlorine.

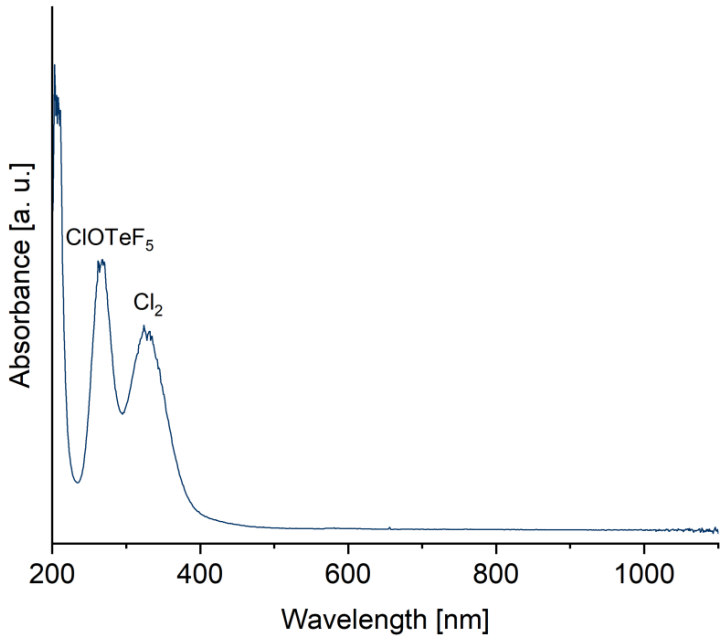

Figure S25: UV/Vis spectrum of the gas phase of the reaction between $[NEt_3Me][AuCl_4]$ and $ClOTeF_5$, showing the formation of gaseous chlorine.

Quantum-Chemical Calculations

Reactant Screening for the Pentafluoroorthotelluration of $[AuCl_4]^-$

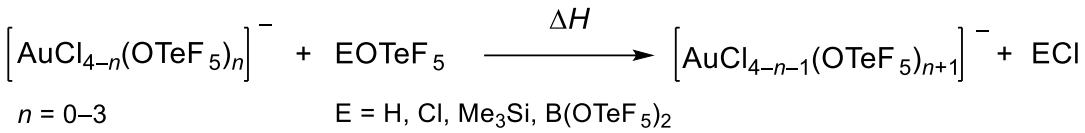

Scheme S1: Reaction scheme for the quantum chemical calculations of reaction enthalpies for the substitution of chloride ligands by teflate ligands with different teflate transfer reagents (cf. Table S2).

Table S2: Overview of the reaction enthalpies Δ*H* of the stepwise and complete substitution of the chloride ligands in the $[AuCl_4]^-$ anion by teflates (cf. Scheme S1) at the RI-B3LYP-D3/def2-TZVPP level of theory, values in kJ · mol^{-1}.

n \ E	H	Cl	Me_3Si	$B(OTeF_5)_2$
0	–5	–97	17	32
1	5	–87	27	42
2	23	–69	46	60
3	28	–64	51	65
Σ	**51**	**−317**	**141**	**199**

Optimized Structure of $[Au(OPPh_3)(OTeF_5)_3]$ on RI-B3LYP-D3/def2-TZVPP Level

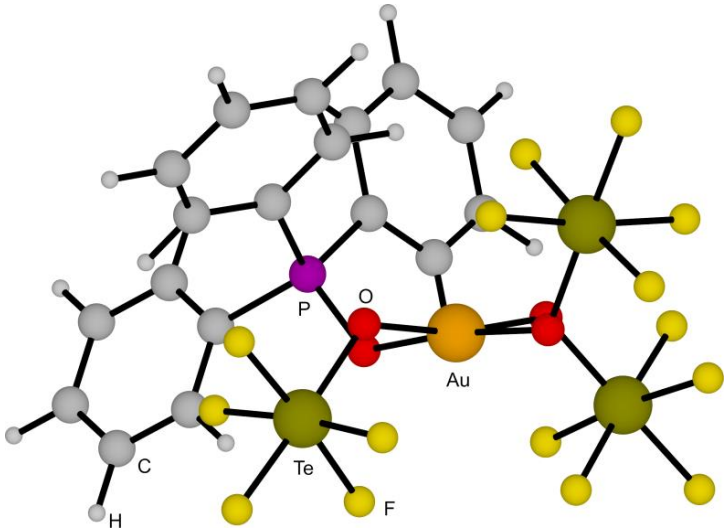

Figure S26: Optimized minimum structure of $[Au(OPPh_3)(OTeF_5)_3]$ on the RI-B3LYP-D3/def2-TZVPP level of theory.

Optimized Structure of $[Au(OTeF_5)_4]^-$ on RI-B3LYP-D3/def2-TZVPP Level

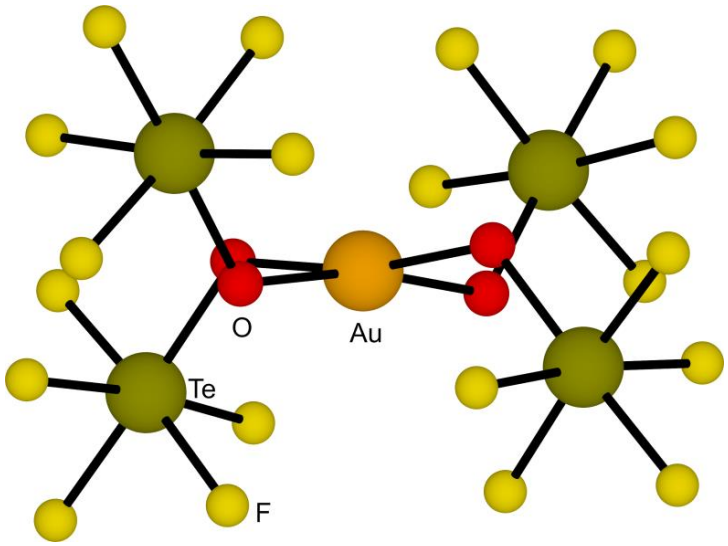

Figure S27: Optimized minimum structure of the $[Au(OTeF_5)_4]^-$ anion on the RI-B3LYP-D3/def2-TZVPP level of theory.

Coordinates of $[Au(OTeF_5)_3]$ on RI-BP86/def-SV(P) Level

xyz-Coordinates [Å] of the optimized minimum structure of $[Au(OTeF_5)_3]$.

22

O	0.0150844	0.8477828	1.0678960
Te	1.2417057	-0.2036679	2.2570106
F	2.3492078	-1.1007713	3.5283028
Au	-0.4285260	0.1087979	-0.7442126
O	-2.3918408	-0.1614936	-0.8820507
Te	-3.2787542	-1.7659937	-0.1414521
F	-4.1388245	-3.3153168	0.5745378
O	1.5328880	0.2445420	-1.1844363
Te	2.1167841	1.9385086	-2.0079949
F	2.6978647	3.5489332	-2.8595540
F	1.0040417	1.2912827	3.4368203
F	-0.2646766	-1.0915389	3.0555229
F	1.4138343	-1.6750207	1.0179734
F	2.8392040	0.5918099	1.5449381
F	3.8969097	1.2331729	-2.0548198
F	1.7575446	1.2418715	-3.7678437
F	0.2904601	2.6240953	-1.9709777
F	2.4480760	2.8113990	-0.3271730
F	-4.9859265	-1.0084467	-0.5636365
F	-3.2369173	-2.6233578	-1.8633110
F	-1.5608240	-2.5644167	0.2751739
F	-3.3173152	-0.9721715	1.6092865

Coordinates of $[Au_2(OTeF_5)_6]$ on RI-BP86/def-SV(P) Level

xyz-Coordinates [Å] of the optimized minimum structure of $[Au_2(OTeF_5)_6]$.

44
O -1.1032523 -0.1159469 0.7231356
Au -0.8530219 0.1131360 -1.3767433
Te -1.1768414 1.7319754 -4.3683142
F -1.9116225 2.5729199 -2.7837235
Au 0.9139746 0.0740576 1.3656487
O 0.4906185 -0.2986448 3.2874920
Te 0.7078865 -2.1942876 3.8456089
F 0.4111735 -1.6103946 5.6441981
Te -2.4790632 1.0755180 1.6541639
F -1.0493509 2.1487589 2.3716288
O 1.1219602 0.5178985 -0.7015989
Te 2.7015413 -0.2707820 -1.7339148
F 1.5445623 -1.5557602 -2.5800623
Te 3.5070858 1.6881389 2.8975092
F 1.7771394 2.5613250 2.8433398
O 2.8657343 0.1600903 1.8041469
F 0.8950376 -4.0080973 4.4198647
F 0.9719790 -2.7583057 2.0019119
F -1.1709427 -2.5494762 3.6375335
F 2.6114267 -2.0323780 4.0525039
F -2.5067856 2.2300940 0.1116074
F -3.7471739 2.2044947 2.5211719
F -3.8906194 0.0248042 0.9112601
F -2.4227183 -0.0613353 3.1891402
O -2.7812428 -0.1886023 -1.8280075
Te -3.2817732 -2.0565433 -2.2859546
F -1.6605579 -2.7336632 -1.4488828
O -0.4101368 0.2291891 -3.3227950
F -4.2146821 -2.2695258 -0.6204106
F -3.8071615 -3.8466341 -2.7021524
F -4.8724699 -1.3609432 -3.0924657
F -2.3622957 -2.0335823 -3.9756852
F 2.3751335 1.0000885 -3.1259975
F 4.1849056 -0.9697877 -2.7061037
F 3.8506047 0.9744894 -0.8486477
F 3.0021644 -1.5720014 -0.3476698
F 0.4097925 2.7918859 -4.1270738
F -1.8598240 3.1591115 -5.4415869
F -0.4010454 0.8973824 -5.9090402
F -2.8445532 0.8278827 -4.6795922
F 3.0343940 0.8644270 4.5682967
F 4.2127488 3.1381562 3.9247295
F 5.2125277 0.8156944 2.9015514
F 4.0047437 2.6851731 1.3299794

Coordinates of $[AuF(OTeF_5)_3]^-$ on RI-BP86/def-SV(P) Level

xyz-Coordinates [Å] of the optimized minimum structure of $[AuF(OTeF_5)_3]^-$.

```
23
O    -0.4881959   -1.0432467    1.9915545
Au   -0.3106076   -0.8925027   -0.0303935
F    -0.0453390   -2.8239300   -0.1562656
Te    1.0978453   -0.7838719    3.0637615
F     0.6249011    1.0110035    3.5982672
F     2.6310859   -0.5570498    4.2098335
F     0.1495546   -1.4705421    4.5950553
F     1.8108363   -2.5462196    2.7138340
F     2.1862397   -0.0757206    1.6226286
Te   -2.1634511    1.9618419    0.0899403
F    -2.3232936    2.0252229    2.0154243
O    -0.5186944   -0.7945548   -2.0522423
Te    1.0820366   -0.6936596   -3.1278077
F     1.1428770   -2.5888491   -3.5005101
O    -0.4163873    1.1387220    0.1064093
F    -3.8809318    2.8396253    0.0832725
F    -1.3424580    3.7053522    0.1097580
F    -2.2915722    2.0531431   -1.8371599
F    -3.1352873    0.2737547    0.0676825
F     2.6231629   -0.5702410   -4.2796376
F    -0.0149975   -0.4437744   -4.6915108
F     1.2678791    1.2205901   -2.9418185
F     2.3147974   -0.9450935   -1.6500756
```

Coordinates of Me_3SiF on RI-BP86/def-SV(P) Level

xyz-Coordinates [Å] of the optimized minimum structure of Me_3SiF.

```
14
Si   -0.0000000    0.0000000   -0.4278533
F    -0.0000000    0.0000000   -2.0836509
C    -0.9018412    1.5620348    0.1220598
C    -0.9018412   -1.5620348    0.1220598
C     1.8036824    0.0000000    0.1220598
H    -0.9437929    1.6346972    1.2323608
H    -0.3905686    2.4742217   -0.2586336
H    -1.9474546    1.5753532   -0.2586336
H    -0.9437929   -1.6346972    1.2323608
H    -1.9474546   -1.5753532   -0.2586336
H    -0.3905686   -2.4742217   -0.2586336
H     1.8875857    0.0000000    1.2323608
H     2.3380232   -0.8988685   -0.2586336
H     2.3380232    0.8988685   -0.2586336
```

Coordinates of Me_3Si^+ on RI-BP86/def-SV(P) Level

xyz-Coordinates [Å] of the optimized minimum structure of Me_3Si^+.

13
C 1.8470823 -0.0254680 -0.0023110
Si 0.0003329 0.0000930 -0.0005563
C -0.9018088 1.6089464 -0.0978702
C -0.9451280 -1.5834838 0.0997078
H 2.2712962 -1.0488962 0.0709779
H 2.2285057 0.4624713 -0.9324601
H 2.2343911 0.5942118 0.8428072
H -0.6730765 -2.1232264 1.0399465
H -2.0456014 -1.4393423 0.0700667
H -0.6396137 -2.2609896 -0.7343457
H -1.5816763 1.7141621 0.7825225
H -0.2261040 2.4888431 -0.1438265
H -1.5685996 1.6126787 -0.9946587

Coordinates of $[Au(CH_3CN)(OTeF_5)_3]$ on RI-BP86/def-SV(P) Level

xyz-Coordinates [Å] of the optimized minimum structure of $[Au(CH_3CN)(OTeF_5)_3]$.

28
O -0.6893830 0.0604346 1.9886849
Te 0.9171737 -0.1020402 3.0716672
F 2.0957271 0.1348451 1.5447831
Au -0.4546919 0.2027226 -0.0356696
O -0.3234548 2.1896774 0.1307748
Te -1.9971899 3.2036338 -0.0116877
F -3.0582535 1.5905192 -0.2531521
N -0.3500523 -1.8200528 -0.1229880
O -0.6228654 0.3774758 -2.0568105
Te 0.9908759 0.2229528 -3.1383159
F 1.8886493 -0.8906112 -1.8153096
F 1.0357697 1.7723422 3.4743336
F 2.4684259 -0.3486197 4.1684283
F -0.1923376 -0.3964792 4.6080382
F 1.0047327 -2.0238586 2.7603113
F -2.3438259 3.1023950 1.8799946
F -3.6012010 4.2420233 -0.1501261
F -0.9672892 4.7994543 0.2430220
F -1.8449203 3.3890502 -1.9206731
F 0.3165419 -1.3819638 -3.9703769
F 2.5439095 0.0248175 -4.2431332
F 0.1788375 1.2840730 -4.5121067
F 1.8395399 1.7710734 -2.3641582
C -0.0893377 -2.9464282 -0.0045688
C 0.2459483 -4.3466597 0.1491425
H -0.6638747 -4.9747163 0.0358495
H 0.9950716 -4.6378938 -0.6189223
H 0.6774740 -4.4981668 1.1629686

Coordinates of CH_3CN on RI-BP86/def-SV(P) Level

xyz-Coordinates [Å] of the optimized minimum structure of CH_3CN.

6
N -0.0000000 0.0000000 -0.9386084
C 0.0000000 0.0000000 -2.1245600
C -0.0000000 0.0000000 0.4788267
H 0.5215470 -0.9033458 0.8630656
H 0.5215470 0.9033458 0.8630656
H -1.0430939 0.0000000 0.8630656

Coordinates of [Au(OPEt$_3$)(OTeF$_5$)$_3$] on RI-BP86/def-SV(P) Level

xyz-Coordinates [Å] of the optimized minimum structure of [Au(OPEt$_3$)(OTeF$_5$)$_3$].

45

O	0.5952480	1.1261178	2.0251988
Te	2.1610983	1.2404879	3.1694284
F	3.3872832	1.5078842	1.6920460
Au	0.8730588	1.1853186	0.0119164
O	1.2361910	3.1775775	0.0982126
Te	-0.3394748	4.3016304	-0.1417200
F	-1.5402319	2.7697685	-0.3851078
O	0.6469961	-0.8581037	-0.0759092
O	0.7387576	1.2751841	-2.0136129
Te	2.3684972	1.0290391	-3.0431401
F	3.3648878	0.3232298	-1.5340237
F	2.0179229	3.1395068	3.4290719
F	3.6544866	1.2857351	4.3720223
F	1.0010104	0.9304086	4.6723829
F	2.4801475	-0.6710536	3.0428160
F	-0.7927922	4.2770603	1.7323829
F	-1.8735453	5.4312318	-0.3696571
F	0.7571248	5.8529595	0.1065951
F	-0.1301764	4.4213797	-2.0529897
F	1.8651717	-0.7823597	-3.5270193
F	3.9222629	0.7569218	-4.1331463
F	1.4396930	1.6775158	-4.5937957
F	3.0577261	2.7847743	-2.6641516
P	-0.8210716	-1.4851731	0.0097574
C	-0.5260354	-3.2751700	-0.2208606
C	-1.6210343	-1.1668495	1.6289480
C	-1.9305331	-0.8358611	-1.2996618
C	-1.7870336	-4.1522799	-0.1592408
H	-0.0015376	-3.3684160	-1.1974105
H	0.2142968	-3.5590571	0.5594110
H	-2.9586179	-1.1908813	-1.0567709
H	-1.9379474	0.2704178	-1.1613025
C	-1.5220964	-1.2055582	-2.7343285
H	-2.6716286	-1.5290141	1.5464411
C	-0.8956872	-1.7799547	2.8364909
H	-1.6689480	-0.0574981	1.7222554
H	-1.5040860	-5.2157774	-0.3131782
H	-2.2970854	-4.0860703	0.8259876
H	-2.5216509	-3.8884480	-0.9502674
H	-2.1898499	-0.6819390	-3.4510418
H	-0.4816444	-0.8935513	-2.9549278
H	-1.6149915	-2.2965018	-2.9256234
H	-1.3971724	-1.4510862	3.7712618
H	-0.9152870	-2.8910829	2.8159580
H	0.1582984	-1.4424621	2.8903030

Coordinates of Et_3PO on RI-BP86/def-SV(P) Level

xyz-Coordinates [Å] of the optimized minimum structure of Et_3PO.

23

O	0.1569474	0.0000004	0.1139275
P	0.0820610	-0.0000000	1.6317585
C	1.7669955	-0.0000005	2.4125609
C	-0.8210822	1.4665366	2.3215576
C	-0.8210826	-1.4665367	2.3215567
C	1.8617856	0.0000005	3.9443699
H	2.2823950	-0.8854444	1.9759170
H	2.2823960	0.8854422	1.9759158
H	-0.8073051	1.4354913	3.4351584
C	-0.2773453	2.7960813	1.7771709
H	-1.8812300	1.3295657	2.0076170
H	-0.8073067	-1.4354914	3.4351576
H	-1.8812302	-1.3295660	2.0076151
C	-0.2773451	-2.7960814	1.7771706
H	-0.9233586	-3.6467152	2.0871909
H	-0.2403610	-2.7698950	0.6670746
H	0.7510572	-3.0065915	2.1461827
H	-0.9233587	3.6467150	2.0871919
H	0.7510572	3.0065916	2.1461820
H	-0.2403624	2.7698949	0.6670749
H	2.9253599	0.0000002	4.2715062
H	1.3820300	0.8978859	4.3926585
H	1.3820290	-0.8978838	4.3926597

Coordinates of $[Au(OPPh_3)(OTeF_5)_3]$ on RI-BP86/def-SV(P) Level

xyz-Coordinates [Å] of the optimized minimum structure of $[Au(OPPh_3)(OTeF_5)_3]$.

57

O	1.1266651	1.3465269	1.9646340
Te	2.6625435	0.8207126	3.0210878
F	3.9083335	0.9730335	1.5421645
Au	1.3712714	1.6043412	-0.0425092
O	1.9654031	3.5137703	0.2854156
Te	0.5620959	4.8639536	0.2502910
F	-0.8370268	3.5848613	-0.2281265
O	0.9824151	-0.3861177	-0.3825802
O	1.2574418	1.9617572	-2.0432697
Te	2.8684978	1.7401236	-3.1063300
F	3.7567630	0.6394839	-1.7784664
F	3.0817952	2.6061213	3.6003302
F	4.1243651	0.2239892	4.1125713
F	1.5027539	0.5910862	4.5402775
F	2.4144675	-1.0627910	2.5900294
F	0.0871764	4.6012305	2.1037693
F	-0.7897894	6.2267858	0.2402518
F	1.8642772	6.1846718	0.7370020
F	0.8068810	5.2729736	-1.6170492
F	2.1614069	0.1353355	-3.9437275
F	4.4007559	1.4938976	-4.2339636
F	2.0613017	2.7835308	-4.5032454
F	3.7594400	3.2945116	-2.4010334
P	-0.4568607	-1.0498962	-0.1539343
C	-0.0766425	-2.8198696	-0.0169584
C	-1.2700883	-0.4356363	1.3428227
C	-1.5425666	-0.7553838	-1.5764017
C	-0.9904190	-3.7869546	-0.4919331
C	-0.6871517	-5.1505094	-0.3584943
C	0.5247048	-5.5490066	0.2338992
C	1.4374637	-4.5845477	0.6950777
C	1.1459376	-3.2167756	0.5714896
H	-1.9327458	-3.4788328	-0.9729969
H	-1.3990516	-5.9060966	-0.7282290
H	0.7620831	-6.6212624	0.3304431
H	2.3906635	-4.8955408	1.1522308
H	1.8610223	-2.4605697	0.9289549
C	-0.9534002	-0.4655479	-2.8269069
C	-1.7741060	-0.2906557	-3.9526178
C	-3.1696663	-0.4116875	-3.8387041
C	-3.7557204	-0.7026103	-2.5933893
C	-2.9475338	-0.8724773	-1.4582975
H	0.1371950	-0.3570327	-2.9226497
H	-1.3117873	-0.0505848	-4.9234252
H	-3.8084151	-0.2712967	-4.7261119
H	-4.8505958	-0.7889374	-2.5017484
H	-3.4126905	-1.0844438	-0.4814764
C	-1.9514496	0.8040451	1.2953121
C	-2.4456782	1.3691211	2.4796069
C	-2.2667176	0.7043566	3.7049262
C	-1.5919968	-0.5280129	3.7518767
C	-1.0895638	-1.1016631	2.5752688
H	-2.0804685	1.3424985	0.3427521
H	-2.9578403	2.3436534	2.4432870
H	-2.6479621	1.1567477	4.6349927
H	-1.4420962	-1.0404249	4.7153050
H	-0.5450902	-2.0579547	2.6185059

Coordinates of Ph_3PO on RI-BP86/def-SV(P) Level

xyz-Coordinates [Å] of the optimized minimum structure of Ph_3PO.

35

C	2.7832642	0.4129311	-1.1238425
C	1.7244123	-0.0235224	-0.2991238
C	1.9844198	-0.3798712	1.0408407
C	3.2877636	-0.2755312	1.5568479
C	4.3366404	0.1757657	0.7367072
C	4.0837765	0.5153498	-0.6042415
P	0.0660791	-0.1123788	-1.0941638
C	-0.8201036	-1.5169516	-0.2988475
C	-1.4791871	-1.4398376	0.9460929
C	-2.1273146	-2.5715175	1.4707633
C	-2.1277337	-3.7798781	0.7519494
C	-1.4867518	-3.8548765	-0.4975920
C	-0.8376849	-2.7268456	-1.0252106
O	0.1562247	-0.2670682	-2.6040675
C	-0.8319583	1.4173073	-0.5997375
C	-0.6497409	2.0839806	0.6300351
C	-1.3846024	3.2476796	0.9156386
C	-2.2967213	3.7540819	-0.0266729
C	-2.4681684	3.1010231	-1.2602859
C	-1.7360726	1.9383233	-1.5498635
H	-1.5080073	-0.4882602	1.5031290
H	-2.6440191	-2.5059473	2.4427473
H	-2.6399949	-4.6655292	1.1636513
H	-1.4990455	-4.7977522	-1.0693584
H	-0.3499425	-2.7619867	-2.0132932
H	0.0842919	1.7098386	1.3637038
H	-1.2359170	3.7682259	1.8764419
H	-2.8695141	4.6694843	0.1974235
H	-3.1726884	3.5049550	-2.0064115
H	-1.8418604	1.4271964	-2.5211358
H	1.1735705	-0.7620867	1.6836512
H	3.4870079	-0.5585763	2.6039845
H	5.3591445	0.2529920	1.1425771
H	4.9077997	0.8558929	-1.2532144
H	2.5726336	0.6533900	-2.1791226

Coordinates of $[Au(OTeF_5)_3]$ on RI-B3LYP-D3/def2-TZVPP Level

xyz-Coordinates [Å] of the optimized minimum structure of $[Au(OTeF_5)_3]$.

22
O 0.3969627 0.2874136 1.6370649
Te 0.9586506 -1.3789143 2.5629544
F 1.5450434 -2.9250343 3.5217812
Au 0.2066624 0.1596174 -0.3382585
O -1.6088355 -0.6547821 -0.0645508
Te -3.1240254 0.5773055 0.1797672
F -4.6336550 1.7342515 0.3877148
O 2.1154215 0.8320315 -0.7339224
Te 2.2460843 0.8021092 -2.6680164
F 1.9604622 0.6567820 -4.5515643
F 0.2156084 0.2318869 -2.4668253
F 1.1872211 -0.2879738 4.1207917
F -0.8333150 -1.8085360 3.1034682
F 0.7402450 -2.4566760 0.9651270
F 2.7979251 -1.1034218 2.0599633
F 4.0785530 1.2947383 -2.8160438
F 2.6682618 -1.0762512 -2.7367285
F 1.6684873 2.6272353 -2.8660132
F -4.2442166 -0.9581395 0.4209211
F -2.8640391 0.7337950 2.0790315
F -1.9800922 2.1303423 -0.0861288
F -3.4974102 0.5822204 -1.7105336

Coordinates of $[Au_2(OTeF_5)_6]$ on RI-B3LYP-D3/def2-TZVPP Level

xyz-Coordinates [Å] of the optimized minimum structure of $[Au_2(OTeF_5)_6]$.

```
44
O    -1.0417889    0.2656703    0.5905024
Au   -0.7092845    0.0129453   -1.4482672
Te   -0.9235498    0.5404549   -4.8066739
F    -1.8627165    1.7518645   -3.7370896
Au    0.9252583    0.0136212    1.2315580
O     0.3958829   -0.4599951    3.0539600
Te    0.0323364   -2.2810170    3.4838961
F     0.5133002   -1.9484415    5.2372041
Te   -2.2035191    1.6625063    1.3095009
F    -0.7428555    2.3956677    2.1905241
O     1.2203136    0.4751795   -0.7855790
Te    2.4434780    1.7896338   -1.5189299
F     2.5178700    0.8548532   -3.1054939
Te    3.8070191    0.5264539    2.9760910
F     2.4713403    1.8030729    3.2532340
O     2.8144831   -0.3279195    1.5944019
F    -0.3448925   -4.0350106    3.9245308
F    -0.4633694   -2.6547460    1.7153885
F    -1.7265943   -1.8596991    3.8854121
F     1.7598639   -2.8200277    3.0615028
F    -1.8030963    2.7105774   -0.1723526
F    -3.2665322    3.0076834    1.9780436
F    -3.6464867    0.9618732    0.4049018
F    -2.5694709    0.6098930    2.7729112
O    -2.5597206   -0.4831121   -1.8424575
Te   -3.1947636   -2.2258429   -1.4073756
F    -1.4563865   -2.8935392   -1.2073792
O    -0.1698980   -0.3398155   -3.2946930
F    -3.2082544   -1.8355085    0.4138428
F    -3.8655887   -3.8929035   -0.9750401
F    -4.9178557   -1.5763848   -1.5852432
F    -3.1875562   -2.7554646   -3.1807219
F     0.9773596    2.7433771   -2.1389924
F     3.5699963    3.0787416   -2.1921213
F     2.3540612    2.7078273    0.0927079
F     3.8826242    0.8226717   -0.8949689
F     0.4928191    1.7411108   -4.8791436
F    -1.6036934    1.3704178   -6.3134027
F     0.0248186   -0.6343517   -5.8773607
F    -2.4014762   -0.5766771   -4.8506319
F     3.0784960   -0.5325918    4.3141785
F     4.8297447    1.3410801    4.2842330
F     5.1459086   -0.7195030    2.6963645
F     4.6123757    1.6653745    1.7490283
```

Coordinates of $[AuF(OTeF_5)_3]^-$ on RI-B3LYP-D3/def2-TZVPP Level

xyz-Coordinates [Å] of the optimized minimum structure of $[AuF(OTeF_5)_3]^-$.

```
23
O    -0.3871548   -1.2325332    1.9721545
Au   -0.2697915   -1.0420291   -0.0121046
F    -0.0440000   -2.9403075   -0.1665414
Te    0.9916747   -0.8495812    3.1567985
F     0.5079236    0.9399342    3.3678097
F     2.3299198   -0.4987791    4.4132746
F    -0.1104204   -1.3101641    4.5902831
F     1.6656278   -2.5929342    3.1303147
F     2.2262469   -0.3648498    1.8331728
Te   -1.8781989    1.9621434    0.0510026
F    -2.0852842    2.0598401    1.9045387
O    -0.4882170   -0.9056210   -1.9906264
Te    0.9027547   -0.5988135   -3.1829418
F     1.0336862   -2.3974361   -3.6711303
O    -0.3239149    0.9527213    0.1537953
F    -3.4110064    3.0280472   -0.0364671
F    -0.8838104    3.5378806    0.0840961
F    -1.9001047    2.0137530   -1.8157017
F    -3.0242603    0.4736723    0.0126459
F     2.2489494   -0.3000963   -4.4439898
F    -0.3268672   -0.3317024   -4.5591660
F     0.9643928    1.2410970   -2.8748028
F     2.2618548   -0.8442417   -1.9164147
```

Coordinates of Me_3SiF on RI-B3LYP-D3/def2-TZVPP Level

xyz-Coordinates [Å] of the optimized minimum structure of Me_3SiF.

```
14
Si   -0.0000000    0.0000000   -0.4305173
F    -0.0000000    0.0000000   -2.0501619
C    -0.8921881    1.5453152    0.1194539
C    -0.8921881   -1.5453152    0.1194539
C     1.7843763    0.0000000    0.1194539
H    -0.9286159    1.6084099    1.2094073
H    -0.3895711    2.4407124   -0.2509914
H    -1.9189334    1.5577346   -0.2509914
H    -0.9286159   -1.6084099    1.2094073
H    -1.9189334   -1.5577346   -0.2509914
H    -0.3895711   -2.4407124   -0.2509914
H     1.8572318    0.0000000    1.2094073
H     2.3085045   -0.8829778   -0.2509914
H     2.3085045    0.8829778   -0.2509914
```

Coordinates of Me_3Si^+ on RI-B3LYP-D3/def2-TZVPP Level

xyz-Coordinates [Å] of the optimized minimum structure of Me_3Si^+.

```
13
C     1.8291696   -0.0256019   -0.0000883
Si    0.0003772    0.0007002   -0.0037049
C    -0.8929688    1.5952809   -0.0738610
C    -0.9356337   -1.5689792    0.0699906
H     2.2393595   -1.0234819    0.1474769
H     2.1917830    0.3691950   -0.9570432
H     2.2129660    0.6495236    0.7712916
H    -0.7326985   -2.0593592    1.0299441
H    -2.0103018   -1.4291494   -0.0353806
H    -0.5755826   -2.2560838   -0.7025728
H    -1.5109335    1.7008282    0.8256158
H    -0.2272690    2.4534191   -0.1516065
H    -1.5882674    1.5937084   -0.9200618
```

Coordinates of $[Au(CD_3CN)(OTeF_5)_3]$ on RI-B3LYP-D3/def2-TZVPP Level

xyz-Coordinates [Å] of the optimized minimum structure of $[Au(CD_3CN)(OTeF_5)_3]$.

```
28
O    -0.5796655    0.2506750    1.9490568
Te    0.7477930   -0.3043885    3.1420158
F     2.0411564   -0.4924995    1.7928730
Au   -0.3768512    0.3061585   -0.0384572
O    -0.3406317    2.2624810    0.0512545
Te   -1.9040387    3.3117587    0.0482567
F    -3.0234076    1.8055068    0.0372714
N    -0.1784294   -1.6761850   -0.1110067
O    -0.5259251    0.4259690   -2.0225774
Te    0.9153536    0.1628348   -3.1890113
F     2.1759473    0.1423242   -1.7990377
F     1.3344397    1.4224821    3.4823023
F     2.0229335   -0.8970471    4.3516606
F    -0.4683007   -0.2101640    4.5368996
F     0.3220766   -2.1216656    2.8853593
F    -1.9864720    3.3428577    1.9056529
F    -3.4180873    4.3804242    0.0502616
F    -0.8501699    4.8349530    0.0582288
F    -1.9793185    3.3599641   -1.8092706
F     0.7915022   -1.7054829   -3.0230600
F     2.3070310   -0.1423566   -4.3760996
F    -0.2589720    0.1170375   -4.6229063
F     1.1958907    1.9797827   -3.4355217
C     0.0794475   -2.7856318   -0.0571761
C     0.4235951   -4.1830133    0.0297914
H    -0.4644604   -4.7927381   -0.1364266
H     1.1744093   -4.4148309   -0.7260408
H     0.8231542   -4.3792057    1.0257073
```

Coordinates of $[Au(CH_3CN)(OTeF_5)_3]$ on RI-B3LYP-D3/def2-TZVPP Level

xyz-Coordinates [Å] of the optimized minimum structure of $[Au(CH_3CN)(OTeF_5)_3]$.

```
28
O    -0.5795346    0.2506886    1.9491550
Te    0.7480959   -0.3043321    3.1419513
F     2.0414047   -0.4919180    1.7926918
Au   -0.3769148    0.3062774   -0.0383604
O    -0.3407355    2.2625769    0.0515498
Te   -1.9042190    3.3116931    0.0481604
F    -3.0235576    1.8054111    0.0371464
N    -0.1785069   -1.6760972   -0.1109293
O    -0.5258555    0.4261643   -2.0224979
Te    0.9154496    0.1627598   -3.1888439
F     2.1758164    0.1416777   -1.7986850
F     1.3343103    1.4226385    3.4824277
F     2.0234726   -0.8968063    4.3514282
F    -0.4679229   -0.2106167    4.5369299
F     0.3228111   -2.1216674    2.8850740
F    -1.9868792    3.3429307    1.9055502
F    -3.4183145    4.3802658    0.0499607
F    -0.8504659    4.8349634    0.0581293
F    -1.9793403    3.3597943   -1.8093816
F     0.7909869   -1.7055330   -3.0231123
F     2.3071916   -0.1427317   -4.3757564
F    -0.2587053    0.1174966   -4.6228970
F     1.1965599    1.9796521   -3.4350427
C     0.0792922   -2.7855704   -0.0571634
C     0.4233250   -4.1829867    0.0296895
H    -0.4647239   -4.7926445   -0.1367981
H     1.1742784   -4.4147319   -0.7260235
H     0.8226814   -4.3793543    1.0256472
```

Coordinates of CH_3CN on RI-B3LYP-D3/def2-TZVPP Level

xyz-Coordinates [Å] of the optimized minimum structure of CH_3CN.

```
6
N     0.0000000    0.0000000   -0.9357327
C     0.0000000    0.0000000   -2.1004713
C    -0.0000000    0.0000000    0.4834238
H     0.5124462   -0.8875829    0.8525450
H     0.5124462    0.8875829    0.8525450
H    -1.0248924    0.0000000    0.8525450
```

Coordinates of [Au(OPEt$_3$)(OTeF$_5$)$_3$] on RI-B3LYP-D3/def2-TZVPP Level

xyz-Coordinates [Å] of the optimized minimum structure of [Au(OPEt$_3$)(OTeF$_5$)$_3$].

45

O	0.1335815	1.4739097	1.6946076
Te	1.1361576	1.6321771	3.2656925
F	2.3508291	2.8478350	2.5584669
Au	0.8920346	1.3048309	-0.1436193
O	1.2798535	3.2438161	-0.2234470
Te	-0.0768828	4.4973386	-0.5340501
F	-1.4003264	3.1731697	-0.7732620
O	0.6739319	-0.6819254	-0.0595852
O	1.2646936	1.2215809	-2.0982154
Te	2.4833847	0.1092768	-2.9718287
F	3.2958530	-0.4784166	-1.3932775
F	0.0556522	3.0032907	3.8913058
F	2.0737442	1.7165600	4.8644728
F	0.0058235	0.3929352	4.0984414
F	2.2762733	0.2287917	2.7690188
F	-0.5356859	4.5942042	1.2686508
F	-1.3970529	5.7681496	-0.8315875
F	1.1504509	5.8698219	-0.3183878
F	0.2055674	4.5048262	-2.3738755
F	1.3230423	-1.3694172	-2.9205429
F	3.6488524	-0.9964943	-3.9044977
F	1.7379792	0.6046094	-4.6000103
F	3.7581260	1.4512093	-3.1347958
P	-0.6739754	-1.4295635	0.1330340
C	-0.4654745	-3.0012865	-0.7292093
C	-1.0114748	-1.7182686	1.8802400
C	-2.0722867	-0.5085293	-0.5506836
C	-1.6556118	-3.9587005	-0.6140549
H	-0.2435661	-2.7452310	-1.7654940
H	0.4462679	-3.4430359	-0.3226486
H	-2.9724026	-1.0766353	-0.3016061
H	-2.1265139	0.4221670	0.0210202
C	-1.9868440	-0.2274744	-2.0557316
H	-1.9529577	-2.2686629	1.9472833
C	0.1250001	-2.4486764	2.6052434
H	-1.1787157	-0.7341170	2.3196036
H	-1.4468237	-4.8695553	-1.1738956
H	-1.8497481	-4.2454834	0.4195878
H	-2.5674568	-3.5240288	-1.0247226
H	-2.8479632	0.3645611	-2.3617199
H	-1.0915819	0.3344847	-2.3141026
H	-1.9861625	-1.1486316	-2.6375019
H	-0.0968306	-2.4994401	3.6695929
H	0.2508280	-3.4674420	2.2369113
H	1.0684111	-1.9185298	2.4891803

Coordinates of Et_3PO on RI-B3LYP-D3/def2-TZVPP Level

xyz-Coordinates [Å] of the optimized minimum structure of Et_3PO.

23

O	0.0908586	0.0001423	0.1030254
P	0.0459729	0.0000519	1.5893393
C	1.7175372	-0.0000632	2.3311631
C	-0.8276068	1.4407163	2.2961733
C	-0.8277235	-1.4406300	2.2959945
C	1.8077631	-0.0001500	3.8594007
H	2.2220340	-0.8716585	1.9086637
H	2.2221087	0.8715342	1.9087590
H	-0.8598950	1.3476154	3.3842161
C	-0.2170633	2.7785220	1.8678018
H	-1.8573013	1.3611737	1.9385704
H	-0.8604274	-1.3474226	3.3840158
H	-1.8572933	-1.3612301	1.9379996
C	-0.2168836	-2.7784160	1.8679829
H	-0.8292889	-3.6117015	2.2143164
H	-0.1421185	-2.8370888	0.7822804
H	0.7845013	-2.9124044	2.2811098
H	-0.8294081	3.6117800	2.2143073
H	0.7844735	2.9126394	2.2805171
H	-0.1427385	2.8371086	0.7820645
H	2.8498618	-0.0002354	4.1815571
H	1.3327495	0.8809810	4.2930044
H	1.3326336	-0.8812646	4.2929123

Coordinates of [Au(OPPh$_3$)(OTeF$_5$)$_3$] on RI-B3LYP-D3/def2-TZVPP Level

xyz-Coordinates [Å] of the optimized minimum structure of [Au(OPPh$_3$)(OTeF$_5$)$_3$]

57

O	1.2447613	1.3067488	1.9361357
Te	2.5962611	0.5851807	2.9940734
F	3.7463466	0.2732528	1.5474501
Au	1.3370581	1.5302003	-0.0427804
O	1.8603900	3.4279205	0.1966245
Te	0.5989289	4.7734064	0.5175540
F	-0.8752418	3.6481639	0.1760997
O	1.0205913	-0.4367538	-0.3009798
O	1.0702297	1.8277672	-1.9926472
Te	2.4515008	2.0223560	-3.2346507
F	3.8026641	1.7646250	-1.9672480
F	3.4061272	2.2292749	3.3027843
F	3.8920398	-0.1588652	4.0991402
F	1.5212772	0.7976803	4.4975211
F	1.9376051	-1.1639676	2.8007115
F	0.4477913	4.3572263	2.3288440
F	-0.6256005	6.1341475	0.8425486
F	1.9656074	5.9732655	0.8790462
F	0.5706282	5.3114930	-1.2619481
F	2.4732712	0.1819329	-3.5969960
F	3.7691625	2.1773809	-4.5332998
F	1.1773745	2.2408403	-4.5744030
F	2.5753275	3.8624946	-3.0222520
P	-0.3853583	-1.0927208	-0.1526483
C	-0.0612591	-2.8438942	0.0539018
C	-1.2587397	-0.4366707	1.2658971
C	-1.3550431	-0.8094456	-1.6323143
C	-1.0523933	-3.7776547	-0.2631902
C	-0.8126813	-5.1294968	-0.0626528
C	0.4136429	-5.5511159	0.4445817
C	1.4023676	-4.6224928	0.7514324
C	1.1709291	-3.2660684	0.5596399
H	-1.9999682	-3.4534015	-0.6727093
H	-1.5779773	-5.8532476	-0.3083060
H	0.5994028	-6.6063408	0.5953155
H	2.3564400	-4.9510294	1.1404937
H	1.9342948	-2.5417590	0.7999158
C	-0.6710957	-0.6523025	-2.8416455
C	-1.3837501	-0.4424107	-4.0135254
C	-2.7742990	-0.4053433	-3.9858551
C	-3.4582729	-0.5766756	-2.7856337
C	-2.7531155	-0.7749627	-1.6061065
H	0.4075889	-0.6725800	-2.8620713
H	-0.8499566	-0.2944159	-4.9420852
H	-3.3272037	-0.2352593	-4.9001819
H	-4.5391057	-0.5421637	-2.7656965
H	-3.2860575	-0.8847001	-0.6714195
C	-1.8469045	0.8313599	1.1712463
C	-2.3196849	1.4605047	2.3118835
C	-2.2212210	0.8252074	3.5457945
C	-1.6554039	-0.4419089	3.6410824
C	-1.1689249	-1.0744190	2.5060959
H	-1.9062782	1.3427826	0.2203458
H	-2.7419415	2.4527421	2.2373734
H	-2.5758987	1.3245163	4.4374636
H	-1.5701368	-0.9280389	4.6030517
H	-0.6960960	-2.0423651	2.5891983

Coordinates of Ph_3PO on RI-B3LYP-D3/def2-TZVPP Level

xyz-Coordinates [Å] of the optimized minimum structure of Ph_3PO.

35

C	2.7525841	0.4687526	-1.1035173
C	1.7013169	-0.0470394	-0.3412870
C	1.9428125	-0.4614866	0.9700064
C	3.2156658	-0.3454094	1.5174151
C	4.2557423	0.1793144	0.7572655
C	4.0237852	0.5820623	-0.5544433
P	0.0671871	-0.1211632	-1.1388434
C	-0.8209923	-1.4927908	-0.3383658
C	-1.5036041	-1.3701278	0.8737153
C	-2.1358266	-2.4736419	1.4355770
C	-2.0957528	-3.7041651	0.7877298
C	-1.4284273	-3.8291000	-0.4270928
C	-0.7940705	-2.7283665	-0.9900348
O	0.1527733	-0.2749497	-2.6138593
C	-0.8020604	1.3972978	-0.6382733
C	-0.5568267	2.0697960	0.5605641
C	-1.2816378	3.2115209	0.8832671
C	-2.2513589	3.6910885	0.0089695
C	-2.4917893	3.0315536	-1.1926390
C	-1.7696887	1.8899920	-1.5173340
H	-1.5572535	-0.4120143	1.3736990
H	-2.6656690	-2.3707034	2.3735998
H	-2.5910943	-4.5617004	1.2244324
H	-1.4063330	-4.7826037	-0.9384638
H	-0.2874864	-2.8100311	-1.9426932
H	0.2099015	1.7150443	1.2368686
H	-1.0831660	3.7306101	1.8119728
H	-2.8123938	4.5821536	0.2593585
H	-3.2380377	3.4096541	-1.8791909
H	-1.9360470	1.3800850	-2.4572859
H	1.1444396	-0.8894187	1.5618312
H	3.3964330	-0.6720398	2.5332933
H	5.2469017	0.2658965	1.1833402
H	4.8341888	0.9796276	-1.1513381
H	2.5657842	0.7623025	-2.1282434

Coordinates of $[Au(OTeF_5)_4]^-$ on RI-B3LYP-D3/def2-TZVPP Level

xyz-Coordinates [Å] of the optimized minimum structure of $[Au(OTeF_5)_4]^-$.

```
29
Au    0.000000    0.000000    0.000000   79
 O    0.562760   -1.902984    0.196978    8
 O    1.902984    0.562760   -0.196978    8
 O   -1.902984   -0.562760   -0.196978    8
 O   -0.562760    1.902984    0.196978    8
Te   -1.061784    3.012206   -1.212345   52
Te   -3.012206   -1.061784    1.212345   52
Te    1.061784   -3.012206   -1.212345   52
Te    3.012206    1.061784    1.212345   52
 F   -1.366607    4.402372   -0.010755    9
 F    0.673482    3.637411   -1.494355    9
 F   -0.793211    1.708331   -2.530890    9
 F   -2.862874    2.538154   -1.117157    9
 F   -1.569680    4.178944   -2.578152    9
 F   -4.402372   -1.366607    0.010755    9
 F   -2.538154   -2.862874    1.117157    9
 F   -1.708331   -0.793211    2.530890    9
 F   -3.637411    0.673482    1.494355    9
 F   -4.178944   -1.569680    2.578152    9
 F    1.366607   -4.402372   -0.010755    9
 F   -0.673482   -3.637411   -1.494355    9
 F    0.793211   -1.708331   -2.530890    9
 F    2.862874   -2.538154   -1.117157    9
 F    1.569680   -4.178944   -2.578152    9
 F    4.402372    1.366607    0.010755    9
 F    2.538154    2.862874    1.117157    9
 F    1.708331    0.793211    2.530890    9
 F    3.637411   -0.673482    1.494355    9
 F    4.178944    1.569680    2.578152    9
```

Coordinates of $[AuCl(OTeF_5)_3]^-$ on RI-B3LYP-D3/def2-TZVPP Level

xyz-Coordinates [Å] of the optimized minimum structure of $[AuCl(OTeF_5)_3]^-$.

```
23
 O    0.614384   -1.937511   -1.062437    8
Au   -0.242781   -0.129403   -1.042872   79
Te   -1.634922   -0.971885    1.996425   52
 F   -2.970994   -1.753976    3.047683    9
Te    2.425990   -2.253240   -0.794171   52
 F    2.258865   -2.435718    1.054039    9
 F    4.234015   -2.652528   -0.537420    9
 F    2.139012   -4.085521   -0.995544    9
 F    2.851117   -2.134484   -2.610328    9
 F    2.881296   -0.448806   -0.576439    9
 O   -1.388766    1.510187   -1.014180    8
 O   -0.289599   -0.184891    0.998737    8
Cl    0.011001    0.056118   -3.292160   17
 F   -0.757289   -0.549917    3.588235    9
 F   -2.642755    0.596023    2.134316    9
 F   -2.657068   -1.478356    0.501594    9
 F   -0.836450   -2.662206    2.005031    9
Te   -0.777129    3.224849   -0.638432   52
 F   -2.524516    3.871418   -0.735657    9
 F   -0.950264    3.039880    1.208551    9
 F    1.027991    2.736909   -0.517779    9
 F   -0.531192    3.664488   -2.438335    9
 F   -0.239947    4.978572   -0.278858    9
```

Coordinates of *cis*-$[AuCl_2(OTeF_5)_2]^-$ on RI-B3LYP-D3/def2-TZVPP Level

xyz-Coordinates [Å] of the optimized minimum structure of *cis*-$[AuCl_2(OTeF_5)_2]^-$.

17

O	0.571832	-0.570434	-1.244019	8
Te	2.376590	-0.554561	-0.854571	52
F	4.211721	-0.599880	-0.475977	9
Au	-0.639200	1.087486	-1.287906	79
Cl	-2.146447	2.794579	-1.296612	17
O	-0.789270	0.949554	0.754467	8
Cl	-0.265157	1.310666	-3.522590	17
F	2.469473	-2.415440	-1.005319	9
F	2.907336	-0.400042	-2.644566	9
F	2.498505	1.311909	-0.666728	9
F	2.143807	-0.720057	0.992667	9
Te	-1.970221	-0.137300	1.666636	52
F	-1.240095	0.379085	3.308199	9
F	-3.276358	1.191751	1.853965	9
F	-2.844263	-0.774248	0.128481	9
F	-0.859123	-1.640234	1.644375	9
F	-3.149129	-1.212833	2.649498	9

Coordinates of *trans*-$[AuCl_2(OTeF_5)_2]^-$ on RI-B3LYP-D3/def2-TZVPP Level

xyz-Coordinates [Å] of the optimized minimum structure of *trans*-$[AuCl_2(OTeF_5)_2]^-$.

17

O	1.321037	-1.514782	-0.043532	8
Te	3.163087	-1.319568	0.023951	52
F	5.031486	-1.212305	0.087265	9
Au	0.000208	-0.000642	-0.044943	79
O	-1.320485	1.513774	-0.058578	8
Cl	-0.010225	0.001626	2.270195	17
Cl	0.010801	-0.002841	-2.359733	17
F	3.370076	-3.168684	-0.146345	9
F	3.364478	-1.141633	-1.825476	9
F	3.148367	0.548372	0.196868	9
F	3.260959	-1.498967	1.881591	9
Te	-3.163152	1.319726	-0.006065	52
F	-3.367328	3.168886	-0.179294	9
F	-3.350014	1.140589	-1.856856	9
F	-3.151133	-0.548090	0.168229	9
F	-3.275996	1.500379	1.850490	9
F	-5.032166	1.214160	0.042232	9

Coordinates of $[AuCl_3(OTeF_5)]^-$ on RI-B3LYP-D3/def2-TZVPP Level

xyz-Coordinates [Å] of the optimized minimum structure of $[AuCl_3(OTeF_5)]^-$.

11

Au	-1.931485	0.794474	-0.029836	79
Cl	-1.782962	0.940060	2.284041	17
Cl	-2.010942	0.593397	-2.342548	17
Cl	-3.548319	2.410171	-0.074733	17
O	-0.599961	-0.786239	0.013464	8
Te	1.236673	-0.665046	0.023979	52
F	1.401545	-2.524576	-0.144232	9
F	1.409319	-0.499614	-1.834483	9
F	1.314913	1.205159	0.186978	9
F	1.396777	-0.844914	1.881986	9
F	3.114443	-0.622871	0.035385	9

Coordinates of $[AuCl_4]^-$ on RI-B3LYP-D3/def2-TZVPP Level

xyz-Coordinates [Å] of the optimized minimum structure of $[AuCl_4]^-$.

```
5
Au    0.000000    0.000000    0.000000    79
Cl    1.652814   -1.652814    0.000000    17
Cl    1.652814    1.652814    0.000000    17
Cl   -1.652814   -1.652814    0.000000    17
Cl   -1.652814    1.652814    0.000000    17
```

Coordinates of $ClOTeF_5$ on RI-B3LYP-D3/def2-TZVPP Level

xyz-Coordinates [Å] of the optimized minimum structure of $ClOTeF_5$.

```
8
 O    0.085493   -0.201997   -1.593052     8
Te    0.128390   -0.105062    0.347467    52
 F    0.236591   -0.087311    2.191533     9
 F    1.980842   -0.071628    0.258947     9
 F    0.085760    1.752936    0.357457     9
 F   -1.724691   -0.145360    0.483072     9
 F    0.184042   -1.958539    0.380967     9
Cl   -0.976426    0.816961   -2.426392    17
```

Coordinates of Cl_2 on RI-B3LYP-D3/def2-TZVPP Level

xyz-Coordinates [Å] of the optimized minimum structure of Cl_2.

```
2
Cl    0.000000    0.000000   -0.017213    17
Cl    0.000000    0.000000    1.997213    17
```

Coordinates of $HOTeF_5$ on RI-B3LYP-D3/def2-TZVPP Level

xyz-Coordinates [Å] of the optimized minimum structure of $HOTeF_5$.

```
8
 O    0.181897    1.621651   -0.000000     8
Te    0.103998   -0.267790    0.000000    52
 F    0.054307   -2.118172   -0.000000     9
 F    1.952133   -0.314097   -0.000000     9
 F    0.092279   -0.340442    1.855943     9
 F   -1.763670   -0.230776   -0.000000     9
 F    0.092279   -0.340442   -1.855943     9
 H   -0.713224    1.990067   -0.000000     1
```

Coordinates of HCl on RI-B3LYP-D3/def2-TZVPP Level

xyz-Coordinates [Å] of the optimized minimum structure of HCl.

```
2
 H    0.000000    0.000000   -0.640329     1
Cl    0.000000    0.000000    0.640329    17
```

Coordinates of $TMSOTeF_5$ on RI-B3LYP-D3/def2-TZVPP Level

xyz-Coordinates [Å] of the optimized minimum structure of $TMSOTeF_5$.

20

C	0.005851	-0.086718	-2.521046	6
Si	0.201117	0.369050	-0.724791	14
O	-0.536348	-0.962000	0.065895	8
Te	-0.793024	-1.442157	1.839366	52
F	-1.067450	-1.954135	3.602108	9
C	1.983369	0.442440	-0.188844	6
C	-0.745821	1.905802	-0.266144	6
F	-1.530648	-3.059111	1.312475	9
F	0.888976	-2.232870	1.948833	9
F	-0.065671	0.152928	2.493689	9
F	-2.484652	-0.667690	1.877229	9
H	-1.047277	-0.193936	-2.784690	1
H	0.437946	0.688971	-3.157474	1
H	0.510313	-1.028148	-2.743470	1
H	2.063870	0.647470	0.879637	1
H	2.493828	-0.500335	-0.392653	1
H	2.511807	1.234941	-0.723428	1
H	-0.659449	2.114801	0.800976	1
H	-0.361874	2.771444	-0.810606	1
H	-1.804864	1.799253	-0.507063	1

Coordinates of TMSCl on RI-B3LYP-D3/def2-TZVPP Level

xyz-Coordinates [Å] of the optimized minimum structure of TMSCl.

14

Si	0.000000	0.000000	-0.405535	14
Cl	0.000000	0.000000	-2.500499	17
C	-0.891982	1.544959	0.153264	6
C	-0.891982	-1.544959	0.153264	6
C	1.783965	0.000000	0.153264	6
H	-0.920752	-1.594789	1.244519	1
H	-1.918855	-1.557428	-0.214553	1
H	-0.389344	-2.440491	-0.214553	1
H	-0.920752	1.594789	1.244519	1
H	-0.389344	2.440491	-0.214553	1
H	-1.918855	1.557428	-0.214553	1
H	1.841503	0.000000	1.244519	1
H	2.308199	-0.883063	-0.214553	1
H	2.308199	0.883063	-0.214553	1

Coordinates of [B(OTeF$_5$)$_3$] on RI-B3LYP-D3/def2-TZVPP Level

xyz-Coordinates [Å] of the optimized minimum structure of [B(OTeF$_5$)$_3$].

22

B	0.000000	0.000000	0.000000	5
O	-0.041472	-1.368989	0.000000	8
O	1.206315	0.648579	0.000000	8
O	-1.164843	0.720410	0.000000	8
Te	2.993890	0.003355	0.000000	52
Te	-1.499851	2.591107	0.000000	52
Te	-1.494040	-2.594463	0.000000	52
F	-0.625547	-3.571559	1.304987	9
F	-2.389813	-1.643406	1.314768	9
F	-2.389813	-1.643406	-1.314768	9
F	-0.625547	-3.571559	-1.304987	9
F	-2.861329	-3.836915	0.000000	9
F	-2.780287	2.327519	1.304987	9
F	-0.228325	2.891342	1.314768	9
F	-0.228325	2.891342	-1.314768	9
F	-2.780287	2.327519	-1.304987	9
F	-1.892202	4.396442	0.000000	9
F	3.405835	1.244040	1.304987	9
F	2.618138	-1.247936	1.314768	9
F	2.618138	-1.247936	-1.314768	9
F	3.405835	1.244040	-1.304987	9
F	4.753531	-0.559526	0.000000	9

Coordinates of [BCl(OTeF$_5$)$_2$] on RI-B3LYP-D3/def2-TZVPP Level

xyz-Coordinates [Å] of the optimized minimum structure of [BCl(OTeF$_5$)$_2$].

16

O	-1.228120	1.422983	-0.018539	8
Te	-1.000304	1.494511	1.870779	52
F	-0.828889	1.627993	3.705812	9
B	-0.660644	0.603996	-0.960103	6
O	0.207659	-0.367138	-0.544945	8
Te	1.256101	-1.713741	-1.374287	52
F	2.301863	-3.044163	-2.116998	9
F	0.685039	-2.903753	-0.082325	9
F	-0.144971	-2.238187	-2.467868	9
F	1.857445	-0.544894	-2.680359	9
F	2.672357	-1.226229	-0.293894	9
F	-0.833799	3.331541	1.744241	9
F	-2.831066	1.677084	2.050639	9
F	-1.173555	-0.343463	2.049079	9
F	0.842419	1.325117	1.741360	9
Cl	-1.121532	0.898343	-2.622592	17

Coordinates of $[BCl_2(OTeF_5)]$ on RI-B3LYP-D3/def2-TZVPP Level

xyz-Coordinates [Å] of the optimized minimum structure of $[BCl_2(OTeF_5)]$.

```
10
 B    0.731996   -0.959343    1.556520    5
Cl    0.273050   -1.818698    3.013278   17
Cl    2.419945   -0.737786    1.149210   17
 O   -0.308557   -0.499011    0.799253    8
Te   -0.474169    0.498921   -0.812394   52
 F   -1.760981    1.540053    0.012565    9
 F    0.827712    1.716658   -0.300418    9
 F    0.801338   -0.524180   -1.687854    9
 F   -1.788128   -0.681058   -1.360529    9
 F   -0.722207    1.464444   -2.369631    9
```

Coordinates of $[BCl_3]$ on RI-B3LYP-D3/def2-TZVPP Level

xyz-Coordinates [Å] of the optimized minimum structure of $[BCl_3]$.

```
4
 B    0.000000    0.000000    0.000000    5
Cl    0.874573   -1.514804    0.000000   17
Cl    0.874573    1.514804    0.000000   17
Cl   -1.749145    0.000000    0.000000   17
```

Literature

[1] P. Huppmann, H. Hartl, K. Seppelt, *Z. Anorg. Allg. Chem.* **1985**, *524*, 26.